HYDRODYNAMIC FORCES ON RECTANGULAR CYLINDERS OF VARIOUS ASPECT RATIOS IMMERSED IN DIFFERENT FLOWS

DJAMEL HAMEL-DEROUICH, B.Sc., M.Sc.

SUBMITTED AS A THESIS
FOR THE DEGREE OF DOCTOR OF PHILOSOPHY
IN ENGINEERING

DEPARTMENT OF NAVAL ARCHITECTURE AND OCEAN ENGINEERING
UNIVERSITY OF GLASGOW

ProQuest LLC.
789 East Eisenhower Parkway
P.O. Box 1346
Ann Arbor, MI 48106 – 1346

To my mother who died on the 7th January 1992 from Alzheimer disease, aged 58.

TABLE OF CONTENTS

Notation

A	Cross-sectional area of cylinder
C_A	Added mass coefficient
C_D	Drag coefficient
$C_{D_{LS}}$	Drag coefficient by least squares method
C_{Dx}	Horizontal drag coefficient
C_{Dy}	Vertical drag coefficient
C_F	Force coefficient
C_{Fmax}	Maximum measured force per unit length coefficient
C_{Frms}	Root mean square of measured force per unit length
C_{Fxmax}	Maximum measured horizontal force per unit length coefficient
C_{Fymax}	Maximum measured vertical force per unit length coefficient
C_{Fxrms}	Root mean square of measured horizontal force per unit length coefficient
C_{Fyrms}	Root mean square of measured vertical force per unit length coefficient
C_L	Lift coefficient
C_{Lmax}	Maximum lift force coefficient
C_{Lrms}	Root mean square of lift force coefficient
C_{Lurms}	Root mean square of lift force coefficient
C_M	Inertia coefficient
$C_{M_{LS}}$	Inertia coefficient by least squares method
C_{Mx}	Horizontal inertia coefficient
C_{My}	Vertical inertia coefficient
D	Cylinder section width normal to the flow
d	Cylinder section height parallel to the flow
d/D	Cylinder aspect ratio
ds	section length increment
E	Ellipticity of the path, or error between measured and computed forces
ESDU	Engineering Science Data Unit
F	Force per unit length
F_A	Added mass force
F_D	Drag force term
F_I	Inertia force term
F_K	Froude-Krylov force

F_{max}	Maximum measured in-line force per unit length
f_o	Frequency of vortex shedding
F_x	Total measured horizontal force per unit length
F_y	Total measured Vertical force per unit length
g	Acceleration of gravity
H	Wave height
KC	Keulegan-Carpenter number
k	Wave number
L/D	Cylinder length to width ratio
r	Cylinder corner radius
Re	Reynolds number
S	Strouhal number
T	Wave period
t	Time
u	Water particle instantaneous velocity
$\dot{u}$	Water particle instantaneous acceleration
u_b	Velocity of the incremental section of structural member
$\dot{u}_b$	Acceleration of the incremental section of structural member
u_m	Water particle maximum velocity
u_x	Water particle instantaneous horizontal velocity
$\dot{u}_x$	Water particle instantaneous horizontal acceleration
u_y	Water particle instantaneous vertical velocity
$\dot{u}_y$	Water particle instantaneous vertical acceleration
V	Volume, or velocity of ambient flow, or towing tank carriage speed
V_C	Current velocity
VR	Reduced velocity
y	Depth of cylinder in water
β	Frequency parameter
λ	Wave length
η	Wave amplitude
ω	Angular wave frequency
ν	Kinematic viscosity
ρ	Water density
θ	$2\pi t/T$

List of figures page no.

List of tables page no.

Table no.

Acknowledgements

This thesis is based on a research carried out at the Hydrodynamics Laboratory of the Department of Naval Architecture and Ocean Engineering at the University of Glasgow during the period of December 1988 to August 1992 before the author joined ABB Vetco Gray UK Ltd, Aberdeen.

Being a newcomer to the field of Offshore Engineering after finishing an M.Sc. in Ship Design, I was inspired by my supervisor Dr. A. Incecik who introduced me to this field and helped me to achieve a modest understanding of this vast and still unexplored field. Throughout the research Dr. A. Incecik provided me with a methodical approach, precious advice and valuable support and to whom I am ever grateful.

The author wishes to express his gratitude to Professor D. Faulkner, head of Department of Naval Architecture and Ocean Engineering, for his interest, valuable help and continuous encouragement he demonstrated throughout the research.

The author would like also to thank the academic staff of the Department of Naval Architecture and Ocean Engineering, and particularly Dr. R. M. Cameron and Dr. K. Varyani for their lasting and appreciated friendships.

The author would like to expand his gratitude to the technical staff at the Hydrodynamics Laboratory for their assistance and patience during the experiments.

Special thanks are made to my girlfriend Alison Kershaw for her ever lasting encouragement, her great support during difficult moments and for her remarkable patience, and to Mr B. Hamoudi for his excellent friendship and for those nice years spent sharing the same office.

The author would like to thank his colleagues at R. & D. Department, ABB Vetco Gray UK Ltd. for their help and support. Their friendship is greatly appreciated.

Finally, the author is greatly indebted to the Algerian Government who through the Ministry of High Education provided the financial support to carry out this research.

Declaration

Except where reference is made, this thesis is believed to be original.

SUMMARY

Previous studies of fluid loading on rectangular and circular cylinders are critically reviewed in this study. This review revealed that whilst comprehensive experimental data on circular cylindrical forms have been accumulated over the past 30 years or so, comparatively little experimental data on rectangular cylinders exist particularly in wavy flow and in combined wavy and steady flows. Experiments were therefore carried out at the Hydrodynamics Laboratory of the Department of Naval Architecture and Ocean Engineering at the University of Glasgow. Rectangular cylinders of various cross-sectional aspect ratios were constructed and tested vertically, as surface piercing, and horizontally, with their axes parallel to wave crests, in steady flow, wavy flow and a combination of the two flows to simulate the presence of currents along with waves. Force measuring systems were designed and incorporated into the test section of each cylinder. In-line and transverse forces were measured for the surface piercing vertical cylinders and in-line and vertical forces were measured for the horizontally submerged cylinders.

This thesis presents the results of experiments conducted on sharp-edged rectangular cylinders in terms of hydrodynamic coefficients of inertia C_M, drag C_D and lift C_L coefficients as well as in terms of the maximum C_{Fmax} and the r.m.s. value C_{Frms} of the measured forces.

In steady flow, the drag coefficients measured were smaller than those measured earlier by other investigators who conducted experiments in two dimensional flow using cylinders with a very high length to width L/D ratio spanning the entire height of a wind tunnel or by testing cylinders mounted between end plates.

In wavy flow, the inertia coefficients of the cylinders of aspect ratios 1 and 2 horizontally submerged in regular waves decreased rapidly with increasing KC number. The inertia coefficients of the horizontal cylinders were found to be smaller than those of the vertical cylinders. The drag coefficients for the different cylinders were found to have high values as the KC number approached zero and to decrease sharply with increasing KC number. The lift coefficients for the different vertical cylinders were found to have high values as the KC number approached zero and to decrease rapidly as the KC number increased. These coefficients were also found to be affected by

variations in the cylinder's aspect ratio. The variations of C_M and C_D coefficients with the KC number in wavy flow were generally found to be different from those in planar oscillatory flow.

The various hydrodynamic force coefficients measured in combined wavy and steady flows were found to be smaller than those measured in wavy flow. At very low KC numbers, the presence of currents was found to be most important and caused significant reduction in the drag coefficient.

In wavy flow, the Morison equation using measured C_M and C_D coefficients was found to predict the measured forces well. In combined wavy and steady flows, the modified Morison equation using measured C_M and C_D coefficients under these flow conditions was found to predict the measured forces well. However, when using measured C_M and C_D coefficients, obtained in wavy flow, in combined wavy and steady flow conditions, the modified Morison equation was found to overestimate the measured forces.

The measured inertia coefficients for the square cylinder were found to be higher than those predicted by the potential flow theory. For the cylinders with aspect ratios of 0.5 and 2, however, the measured inertia coefficients were found to be only slightly higher than those predicted by the potential flow theory. In terms of forces, the theory was found to underestimate the total forces for the square cylinder. However, good agreement was found between the measured and predicted forces on the cylinders with aspect ratios of 0.5 and 2.

CHAPTER 1

INTRODUCTION

1.1 REVIEW OF THE PROBLEM

Since the fifteenth century, the pace of ocean transportation and deep water fishing has gradually increased but man's utilisation of the oceans has still been restricted to these two activities.

Over the last five decades, however, traditional uses of the oceans have expanded to include the exploitation of hydrocarbons below the sea bed and the potential of large-scale mineral gathering and energy extraction. Since the early 1960s exploitation of oil and gas reserves from hydrocarbon reservoirs below the sea bed has increased rapidly and in doing so has stimulated a wide-ranging base of theoretical analysis, model testing and practical experience in the scientific disciplines that contribute to the design and operation of offshore structures. These disciplines are, however, spread out over the traditional boundaries of the established physical sciences. The design, construction and operation of fixed and floating offshore structures require expertise in subject areas ranging from meteorology, oceanography, hydrodynamics, naval architecture, structural and fatigue analysis, corrosion metallurgy, petroleum engineering, geology, sea bed soil mechanics, mechanical and process engineering, diving physiology and even marine biology. These disciplines are often combined within the descriptive title of 'ocean engineering'.

The design of offshore structures used for oil and gas production poses technically challenging problems for scientists and engineers in the development of materials, structures and equipment for use in the harsh environment of the oceans. At the same time the physical processes that govern interactions between the atmosphere and the ocean surface, and the effects of the structure on the fluid around it and on the behaviour of the sea bed foundation are not completely understood in scientific terms. These problems are compounded by the uncertainties of predicting the most extreme environment likely to be encountered by the structure over its lifetime, which is measured in decades. All these interacting problems offer unique challenges for advanced scientific analysis and engineering design.

There is a large variety of marine structures used by the industry for exploration

and production of oil and gas. The primary objective of the structural design is to fulfil some functional and economical criteria for the platform that support the top side facilities for oil operations. It is essential that the structure has a high reliability against failure. Human lives and enormous economical investments are at risk when the structure is exposed to the tremendous environmental forces during a storm.

A structure used for offshore oil drilling and production will be exposed to a variety of loads during its life cycle. The loads are commonly classified as follows.

Normal functional loads

-dead loads;

-live loads.

Environmental loads

-sea loads;

-wind loads;

-seismic loads.

Accidental loads.

The waves and current are considered the most important source of environment loads for fixed structures. Moored floating structures will also be sensitive to wind loading. Wind forces on offshore structures account for approximately 15% of the total forces from waves, current and winds acting on the structure.

Offshore structures are subjected to both steady and time dependent forces due to the action of winds, current and waves. Winds exert predominantly steady forces on the exposed parts of offshore structures, although there are significant gust or turbulence components in winds which induce high, unsteady, local forces on structural components as well as a low frequency total force on the whole structure. Ocean currents also exert largely steady forces on submerged structures, although the localized effects of vortex shedding induce unsteady force components on structural members. However, gravity waves are by far the largest force on most structures. The applied force is periodic in nature, although non-linear wave properties give rise to mean and low-frequency drift forces. Non-linearities in the wave loading mechanism can also induce superharmonic force components. Both these secondary forces can be significant if they excite resonance in a compliant structure.

In general, an air or water flow incident on an offshore structure will exert forces that arise from two primary mechanisms. A steady or unsteady flow will directly exert a corresponding steady or unsteady force with a line of action that is parallel to the

incident flow direction. Such forces are called 'in-line' forces. However, the localized interaction of steady or unsteady flow with a structural member will also cause vortices to be shed in the flow and will induce unsteady transverse or 'lift' forces with lines of action that are perpendicular to the incident flow direction.

The design of offshore structures requires calculation methods to translate a definition of environmental conditions into the resultant steady and time dependent forces exerted on the structure. Therefore, the industry has, during the years, devoted much effort to improving design criteria, calculation procedures and construction methods to refine the balance between economical investment and structural safety.

The technical evolution of the modern offshore industry can be measured by the depth at which it has been able to carry out exploration drilling and by the structures that have made such drilling possible.

Initially, exploration drilling was carried out from shallow water fixed platforms which were piled to the sea bed. The water depth capability of drilling has gradually increased to enable exploration of fields in deeper waters by the use of floating and compliant structures. The water depths at which exploration drilling is carried out is a *barometer* of future requirements for oil production. In drilling programmes where significant discoveries of hydrocarbons are made, a decision on oil production is dependent upon the prevailing price of oil and the economics of platform construction and operation. Therefore with the necessity of reducing the capital cost in exploring and exploiting marginal fields, new generations of semi-submersible drilling rigs and tension-leg platforms whose hulls and legs conform to rectangular cross-section geometry are emerging nowadays. Such designs are considered to be economically more viable than the conventional designs with circular cylindrical sections. However, most of the research on fluid loading has concentrated on circular cross-section cylinders with data accumulated over the years and a limited amount of research has been carried out with regard to other geometries such as rectangular cross-section cylinders.

1.1.1 FLUID LOADING

1.1.1.1 Vortex formation, drag and lift forces

The relative velocity between a flow field and a solid body is governed by the boundary condition that the fluid layer immediately adjacent to the body does not move relative to the body. This is often called the 'no-slip' boundary condition. For flows

around streamlined bodies or upstream segments of flow around bluff bodies, the no-slip boundary condition gives rise to a thin layer of fluid adjacent to the surface where the flow velocity relative to the surface increases rapidly from zero at the surface to the local stream velocity at the outer edge of the layer. Such a thin sheared layer is appropriately called the boundary layer. Hence, the velocity gradients within the boundary layer in a direction perpendicular to the surface are very large in comparison to velocity gradients parallel to the surface. The former velocity gradients induce large shear stresses from the action of viscosity within the boundary layer fluid.

Within the boundary layer and wake, the rates of shear strain are high so that the effects of viscosity and the associated shear stresses must be accounted for. The value of this shear stress at the body surface contributes to a frictional or viscous drag force. The shearing of the flow along the boundary with a member applies a direct shear force on the surface of the member. More importantly the shearing imparts a rotation to the flow leading to the formation of vortices. These become detached from the member and are carried downstream as a 'vortex street' in the wake of the member. The boundary layer is then said to separate. At and after this separation point, the boundary layer appears to move away from the surface, with a large eddy forming between it and the surface. Such eddies are unstable and tend to move downstream from the surface with new eddies forming to replace them. The wake behind the body is then filled with a stream of vortices. The energy dissipated in these vortices results in a reduction of pressure which produces a pressure drag force in the direction of the flow. Therefore the boundary layer has a substantial effect on the bulk of the flow around the body and on the forces experienced by the body. Boundary layer separation and the formation of a thick wake are a characteristic feature of flow around bluff bodies typically used as members of offshore structures.

Any lack of symmetry in the flow, i.e. asymmetry of the vortex shedding from the sides of the body, also produces a lift force at right angles to the flow. This particular component of the total force cannot be ignored for several reasons. Firstly, its amplitude could, under certain circumstances, be as large as that of the in-line force (drag and inertia forces). Secondly, the transverse force could give rise to fluid-elastic oscillations in wavy flows and to fatigue failure. Thirdly, even the small transverse oscillations of the body distinctly regularise the wake motion, alter the spanwise correlation, and change drastically the magnitude of both the in-line and transverse forces.

The forces induced by vortex shedding are usually assumed to be proportional to velocity squared and are given by empirical equations of common forms.

Time average drag force per unit length = $0.5\, C_D\, \rho\, D\, U^2$. (1.1)

Time average lift force per unit length = $0.5\, C_L\, \rho\, D\, U^2$. (1.2)

Because of the irregular nature of vortex shedding, the lift force is generally irregular, and alternative equations are used to determine the lift coefficient C_L.

Root mean square (rms) lift force per unit length = $0.5\, C_L(\text{rms})\, \rho\, D\, U^2(\text{max})$, (1.3)
(Sarpkaya (1976a)).

Root mean square (rms) lift force per unit length = $0.5\, C_L'(\text{rms})\, \rho\, D\, U^2(\text{rms})$, (1.4)
(Bearman et al. (1985a)).

Maximum lift force per unit length = $0.5\, C_L(\text{max})\, \rho\, D\, U^2(\text{max})$, (1.5)
(Sarpkaya (1976a)).

1.1.1.2 Inertia forces

A member in a uniformly accelerating flow is subject to an inertia force which may be calculated from the potential flow theory, see for example Sarpkaya and Isaacson (1981). It is convenient to consider the force as having two components.

The Froude-Krylov component of the inertia force

An accelerating fluid contains a pressure gradient equal to $\rho \dot{U}$. If the presence of a member in an accelerating fluid did not affect the pressure distribution then the force on a member of volume V would be

$$F_K = \rho V \dot{U}, \quad (1.6)$$

referred as the Froude-Krylov force. Therefore the Froude-Krylov force is the force that the fluid would exert on the body, had the presence of the body not disturbed the flow. It is a dynamic equivalent of the buoyancy force in Archimedes' principle where the force field inducing acceleration is replaced by a gravitational force field (i.e. $\rho V g$).

The added mass component of the inertia force

The added mass concept arises from the tendency of a submerged body moving with an acceleration relative to the surrounding fluid to induce accelerations to the fluid. These fluid accelerations require forces which are exerted by the body through a pressure distribution of the fluid on the body. Since the submerged body, in effect, imparts an acceleration to some of the surrounding fluid, this phenomenon can be equated to the body having an added mass of fluid attached to its own physical mass.

Hence, an additional force

$$F_A = C_a \rho V \dot{U} \qquad (1.7)$$

$F_A = C_a \rho V \dot{U}$

occurs, where C_a is known as the added mass coefficient.

The two forces added together form the inertia force given as

$$F_I = F_K + F_A = (1+C_a)\rho V \dot{U} = C_M \rho V \dot{U}, \qquad (1.8)$$

where

$$C_M = 1 + C_a \qquad (1.9)$$

is the inertia coefficient.

1.1.1.3 The Morison equation

The most widely accepted approach to the calculation of wave forces on a rigid body is the Morison equation. It is based on the assumption that the total in-line wave force can be expressed as the linear sum of a drag force, due to the velocity of the water particles flowing past the body, and an inertia force, due to the acceleration of the water particles.

The equation developed by Morison, O'Brien, Johnston and Schaaf (1950), to name all its contributors, in describing the horizontal wave forces acting on a vertical pile which extends from the bottom through the free surface, gives the in-line force per unit length as

$$F = \frac{1}{2}\rho D C_D |u|u + \rho A C_M \dot{u}. \qquad (1.10)$$

Since its introduction more than forty years ago, the Morison equation has been extensively used to determine the wave forces and several experimental results have shown that it has enough accuracy for practical applications.

There are, however, a number of assumptions that are implicit in the use of the Morison equation, which must be satisfied before its use is valid.

These may be summarised in four groups as follows.

(1) The water particle kinematics, e.g. instantaneous velocities and accelerations, must be found from some wave theories which assume that the wave characteristics are unaffected by the presence of the structure. This puts a limitation on the size of the structure for which Morison's equation is applicable. The generally accepted limit is $D/\lambda < 0.2$, though for rectangular cylinders this limit can be lower.

(2) The two hydrodynamic coefficients C_M and C_D must be determined experimentally. It should be noted that any different structural shape or configuration, for which values of C_M and C_D coefficients are not available, must be subject to

extensive experimental tests and analysis in order to determine their C_M and C_D values. Extrapolation from existing data may be very misleading. Since the particle velocities and accelerations are dependent on the wave theories used, it follows that values of C_M and C_D coefficients are only strictly valid when used with the wave theory for which they were selected. If using another wave theory, C_M and C_D coefficients should be used with great care allowing a factor of safety.

(3) The standard form of Morison's equation assumes that the structure, which is experiencing the forces, is rigid. However, if the structure has a dynamic response or is part of a floating body, its induced motions may be significant when compared with the water particle velocities and accelerations. In this case the dynamic form of the equation must be used.

$$dF=\frac{1}{2}C_D\rho D|(u-u_b)|(u-u_b)ds+C_M\rho A(\dot{u}-\dot{u}_b)ds+(\rho Ads-M)\dot{u}_b, \qquad (1.11)$$

(Hallam et al. (1978)),

where u_b is the velocity of the incremental section of the structural member,

$\dot{u}_b$ is the corresponding acceleration of the section, and

M is the mass of the section.

(4) The Morison equation, using values of C_D coefficient quoted, can only give the forces normal to the longitudinal axis of the structural member and therefore is only applicable to members that have small skin friction values. This is true for most structural components with clean exteriors, but the accumulation of marine growth or the incorporation of external structural parts, i.e. pile guides, stiffeners, etc, may invalidate this assumption. In this case the forces along the member must be evaluated and in many cases the most economical method will be by experimental means, or by assumed values of skin friction coefficient, which will be of the order of a tenth of the drag coefficient.

In spite of the wide experience gained from the use of Morison's equation, there are still questions and uncertainties about its applicability as a tool for prediction, and on the reliability of the coefficients to be used with it. One of the problems arises from the fact that the coefficients for full scale use cannot be obtained from laboratory tests, as these are usually at lower Reynolds numbers. In addition, the incident flow during laboratory tests is not usually representative of real sea conditions as these tests are commonly done in regular waves or in planar oscillatory flow. Oscillatory flow represents a simpler case where the orbit of water particles is flat as opposed to elliptical

or circular in waves. Field tests are carried out to determine these coefficients and not surprisingly the data exhibit considerable scatter. Examples of these can be found in Wiegel et al. (1957), Wiegel (1964), Borgman and Yfantis (1979), Heideman et al. (1979), Bishop (1984) and Bishop (1987) for smooth and roughened vertical and horizontal circular cylinders.

Furthermore, other factors such as irregularity of the incident wave, three dimensionality of the flow and different spanwise correlation all contribute to the scatter in field data. The methods used in data analysis, both in field tests and laboratory studies could also induce scatter in the available data. This is particularly relevant to experiments where water particle velocities and accelerations are calculated from measurements of surface elevations coupled with some wave theory. The accuracy of the data thus obtained will depend on the choice of the wave theory (Dean (1970)), and even if the best available wave theory is used, there is no guarantee that the wave structure will be the same from one cycle to another, especially in field tests.

1.1.2 WAVE LOADING FLOW REGIMES

The wave loading flow regimes may be broadly classified under the headings of, pure reflection, diffraction, inertia, and drag. There are no distinct boundaries separating these loading regimes and quite often a structure experiences loads of different types. However, within certain ranges of flow conditions one type of loading may prevail over another.

The procedure for calculating wave forces on offshore structures can be split up into fundamentally different approaches depending on the size of the structural member and the height and wavelength of incident waves. These parameters can be written in the form of two ratios: structural member diameter (or size) to wavelength (D/λ) and wave height to structural member diameter (H/D).

For small circular structural members where $D/\lambda<0.2$, the Morison equation is used to estimate forces due to wave action with the implicit assumption that the diameter of the member is small enough in relation to the wavelength so as not to alter incident wave characteristics to any significant extent. On the other hand, for larger structural members with $D/\lambda>0.2$, the employment of a diffraction theory is necessary to account for the reflection and radiation of waves from structural members. Potential flow methods, however, cannot account for viscous drag forces. Pure reflection of waves

occur when $D/\lambda>1$, and is of more significance in the design of coastal structures such as sea walls and breakwaters rather than in the design of offshore structures.

The second parameter of interest is the ratio H/D. Its importance is based on the fact that drag forces on structures in an oscillatory wave flow are dominated by the separation of flow behind the cylinder and the formation of large vortices. For a small H/D ratio ($H/D<1.5$), the wave height and thus the orbital diameter of fluid particle motions does not remain unidirectional long enough for the flow to initiate separation and develop or shed vortices. In this case, drag forces are very small and acceleration dependent inertia forces dominate and hence the potential flow diffraction theory can be used to predict wave forces with confidence. For an intermediate region, where the ratio $1.5<H/D<8$, the drag effect becomes significant and the complete Morison equation is required to compute the total force. At the other extreme, for approximately $H/D>8$, the wave flow will have been unidirectional long enough for a substantial vortex flow to develop. Drag forces will then be large and the Morison equation, which accounts for these, must be used.

The drag/inertia regime is very important as different offshore structures operate in this fluid loading region. Considerable attention and studies have been focused on fluid loading and prediction methods in this regime. However, there is still no clear understanding of the fluid mechanics associated with flow reversal. Further problems arise because of the cylinder orientation, and variation of flow conditions along the length of the cylinder.

The limits of flow regimes in terms of D/λ and H/D discussed above are based on preceding experience with vertical circular cylinders. For rectangular cylinders these limits can be expected to be lower. Figure 1.1 illustrates the above flow regime limits.

1.2 PREVIOUS WORK

1.2.1 STEADY FLOW

The main feature of a flow past a body is the phenomenon of flow separation from the body surface and the resulting formation of a large wake behind the body. The presence of the wake alters the flow and the pressure distribution on the body resulting in a deficit of pressure on the downstream side, the rear side, of the body and an excess on the upstream side, the front side, of the body. This difference of pressure between

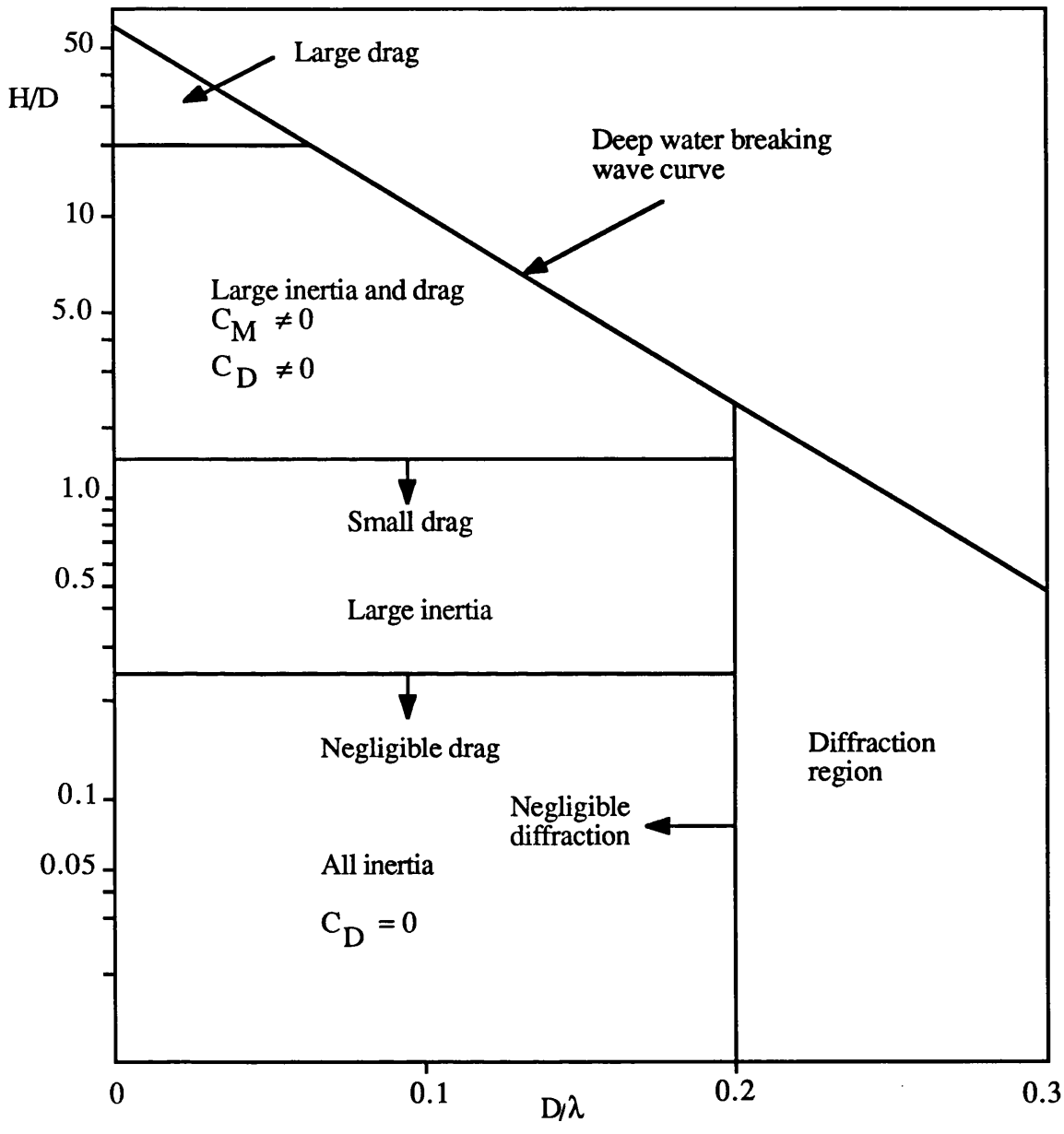

Fig. 1.1 Regions of influence of drag, inertia and diffraction effects

the front and the back of the body gives rise to a force, the pressure drag.

1.2.1.1 Smooth circular cross-section cylinders

The variation of flow patterns around a smooth circular cylinder with Reynolds numbers was investigated using wind tunnels through measurements and flow visualisations by many researchers, among the pioneers were Delaney and Sorensen (1953), Roshko (1961), and Roshko and Fiszdon (1969). Roshko and Fiszdon have shown that when the Reynolds number was between about 1 and 50, the entire flow was steady and laminar. In the range of Reynolds number from about 50 and 200, the flow still retained its laminar character but the near wake became unstable and oscillated periodically. At Reynolds numbers below 1500, turbulence set in and spread downstream. In the region between about 1500 and $2x10^5$, the transition and turbulence gradually moved upstream along the free shear layers and the wake became increasingly irregular. When the transition coincided with the separation point at the Reynolds number of about $5x10^5$, there was first a laminar separation followed by reattachment to the cylinder, and then a turbulent separation occurred forming a narrower wake. This resulted in a large fall in the drag coefficient, phenomenon known as the 'drag crisis'. The transition in the drag coefficient between Reynolds numbers of about $5x10^5$ and $7x10^5$ was interpreted as the transition of the separated boundary layer to a turbulent state, the formation of a separation bubble, reattachment of the rapidly spreading turbulent free shear layer, and finally separation of the turbulent boundary layer at a position further downstream from the first point of laminar separation. The reduction of the wake size as a consequence of the retreat of the separation points then resulted in a smaller form drag. The subsequent increase in the drag coefficient between Reynolds numbers of about 10^6 and 10^7 was then interpreted to be a consequence of the transition to a turbulent state of the attached portion of the boundary layer. At very high Reynolds numbers several orders of magnitude larger than 10^7, drastic changes are not likely to occur in the boundary layers and the drag coefficient is not expected to be too much affected. Figure 1.2 illustrates the different aforementioned stages of the flow patterns from subcritical to post critical Reynolds numbers.

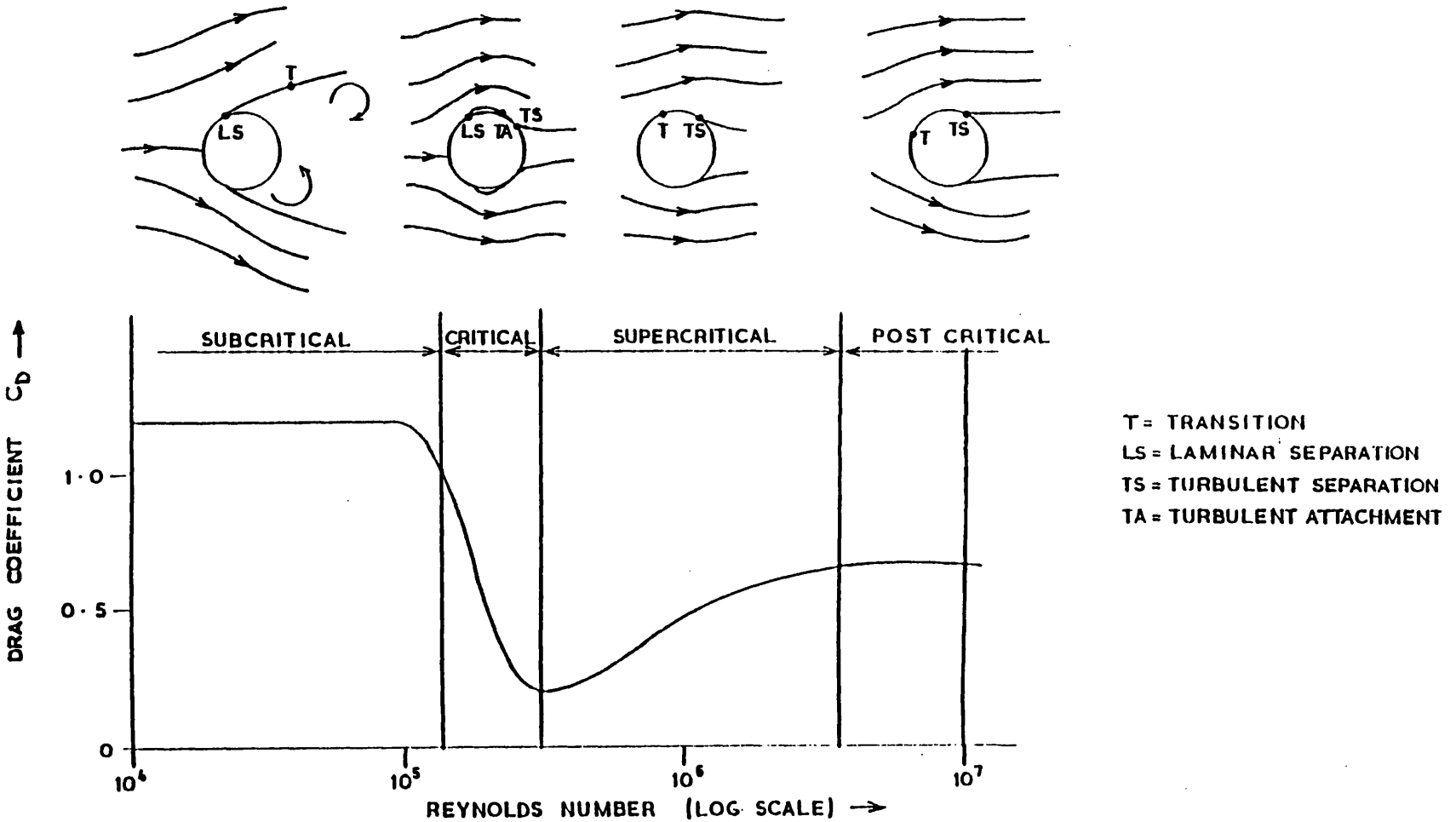

Fig. 1.2 The different two dimensional flow regimes over a smooth circular cylinder (based upon diagram by Scruton (1981))

1.2.1.2 Smooth rectangular cross-section cylinders

Wakes behind bluff bodies, such as rectangular cylinders, are so frequently encountered in engineering applications that research studies have been conducted in large numbers and massive data accumulated. In particular, since von Kármán elucidated theoretically the vortex street formed behind a body, numerous investigations have been carried out on theoretical and experimental aspects of the vortex street, including collapse (Taneda (1959)), stability (Taneda (1963)), and formation mechanism (Nishioka and Sato (1978)). Furthermore, detailed information regarding flows around rectangular cylinders in a uniform flow is of special interest for the basic understanding of aerodynamics, and is of great importance in the study of aeroelastic instability.

Various investigations with reliable results have been carried out in this field, for example Delany and Sorensen (1953), Parkinson and Brooks (1961), Vickery (1966), Nakaguchi, Hashimoto and Muto (1968), Bearman and Trueman (1972), Bostock and Mair (1972), Novak (1972), Otsuki et al. (1974), Laneville et al. (1975), Lee (1975), Nakamura and Mizota (1975b), Courchesne and Laneville (1979), Okajima (1982), Laneville and Yong (1983), and Okajima, Mizota and Tanida (1983).

At extremely low Reynolds numbers, the separation of flow around smooth rectangular cylinders is known to occur at the trailing edges rather than the leading edges where the separation is indiscernible owing to immediate reattachment. As the Reynolds number increases, the flow separation at the leading edges will develop and the steady reattachment becomes impossible. At sufficiently high Reynolds numbers a complicated vortex system is formed behind the bodies. This vortex system determines the hydrodynamic (or aerodynamic) forces acting on these bluff bodies. In steady flow, the character of the vortices shed immediately behind the cylinder and in the wake further downstream is strongly dependent of the Reynolds number. The shedding frequency f_0 is given in the dimensionless form, $S=f_0D/V$ called the Strouhal number, where D is the body diameter (or size) and V is the velocity of the ambient flow. The Strouhal number characterised somewhat the periodic behaviour showed by the fluctuation of the flow in the wake behind the cylinder. Roshko (1955) pointed out that for bodies having the same frontal area, e.g. a circular cylinder, a 90^0 wedge and a flat plate, the bluffer the body tended to be, the larger was the wake created behind it, the lower the Strouhal number was obtained and the higher was the drag force. Gerrard (1966) provided a good discussion on the subject of the formation region of vortices.

Delany and Sorensen, investigating the effect of the aspect ratio at rather large Reynolds

numbers between $1.1x10^3$ and $2.3x10^6$, found that as the aspect ratio (height to width ratio, d/D) was increased from 0.5 to 2, the drag coefficient decreased from 2.2 to 1.4. They also measured the effect of corner radius and found that the drag coefficient of sharp-edged cylinders reduced significantly when the corners were rounded. For example for a square cylinder with r/D=0.167 (r is the corner radius), they reported a drag coefficient of 1.2 at a Reynolds number of $2x10^5$ compared with a value of 2 found with a sharp-edged square cylinder. Vickery measured the fluctuating loads on a long square cylinder, and showed that the presence of a large-scale turbulence in the stream had a marked influence on both the steady and the fluctuating forces, and presented that spanwise correlation was quite different between smooth and turbulent stream. Laneville et al. found that the square-section cylinder was extremely sensitive to upstream turbulence level and showed that a free stream turbulence level of 10% can reduce the drag coefficient from 2.2 to about 1.5. The presence of free stream turbulence seems to accelerate the growth of the separated shear layers to such an extent that some reattachment, or at least some interference between the shear layers and the rear edges takes place, and thus results in a drag coefficient smaller than that for smooth flow. Nakaguchi et al. and Bearman and Trueman found that the aspect ratio of rectangular cylinders was one of the major contributing factors to the flow characteristics around the cylinders. The flow was found to be affected by the behaviour of the shear layers which, in turn, were affected by the afterbody length d. Thus the aspect ratio has been found to influence the wake shape and size, and the distribution of pressure on the downstream face of the cylinder (the base pressure), and hence the values of drag forces. Using flow visualisations, Nakaguchi et al. found that there was a direct relationship between the base pressure and the curvature of the streamlines in the base region. They showed that as the cylinder ratio d/D increased from zero, the base pressure decreased rapidly to a critical minimum at a ratio just beyond 0.6. They found that the decrease in base pressure for cylinders shorter than the critical is associated with an increased curvature of the shear layer and high drag. Bearman and Trueman confirmed the correlation between the curvature of the shear layer and the drag coefficient. They suggested that for small values of d/D, the effect of the body downstream of separation is to reduce the size of the separated wake cavity, thus leading to a decrease in base pressure and an increase in drag. In the case of d/D>0.6, they suggested that the vortices were forced to form further downstream because of the influence of the trailing edge corners, thus occasioning a reduction in drag. Therefore,

the further the vortices can be persuaded to form away from the body the higher was the base pressure and hence the lower was the drag. They observed that cylinders with d/D=0.62 had non-uniform base pressure distributions while cylinders with d/D=0.2 and 1 had uniform distributions. Bostock and Mair, and Laneville and Yong found that the pressure distribution on the upstream face was of similar form for the whole range of d/D. On the downstream face, however, they found that the base pressure distribution was not uniform. Nakaguchi et al., Nakamura, Mizota and Yoshimura, (1973) and Nakamura and Mizota (1975a) divided the flow patterns roughly into two types. For a rectangular cylinder with $d/D \leq 2.8$, the flow around the cylinder separated at the corners of the frontal side forming a dead air region without reattachment of the shear layers to the sides parallel to the flow. However, for a rectangular cylinder with $d/D > 2.8$, the shear layers of the flow reattach somewhere to form separation bubbles on the sides parallel to the flow. Laneville and Yong using flow visualisations found that as the wake vortices were forming closer to the base area, they induced lower base pressures and consequently an increase in drag. To describe the effect of the aspect ratio, they defined four types of regime associated with $0<d/D<0.5$, $0.5<d/D<1$, $1<d/D<3$ and $d/D>3$. Detailed discussion of these regimes are given in Laneville and Yong (1983). Okajima et al. carried out flow visualisations in a wind tunnel at rather lower Reynolds numbers between 0.7×10^4 and 1×10^4. They found that for d/D of 1 and 2 shear layers separated at the leading edges of the cylinders never reattached on the surfaces and fully detached themselves. For d/D of 3, however, they found that the flow was characterised by an occurrence of not a stationary reattachment but a periodic one. They explained that the separated shear layer instantaneously reattached on the surface and detached itself from the surface and this pattern repeated with a period of a shedding vortex street. Around cylinders with large d/D of 8 they found that the shear layer before going downstream always reattached on the surface which resulted in the formation of a separation bubble followed by a turbulent boundary layer and a shedding of a vortex street behind the cylinders. In other words cylinders with long afterbodies had shear layers which reattached after separation and their resulting wake expanded considerably less than that of cylinders with short afterbodies.

The change of flow pattern has been found to have a direct link with the variation of the Strouhal number S. Nakaguchi et al., Bearman and Trueman, and Xuejian (1985) measured the variation of the Strouhal number with d/D. They found that the Strouhal number decreased with increasing d/D and then rose sharply as d/D approached

a critical value of 2.8. The jump of the Strouhal number at d/D=2.8 was interpreted as a result from the reattachment of the separated shear layers to the sides of the cylinder. Nakaguchi et al. found no sudden change of the drag coefficient when there was a sharp increase of the Strouhal number.

Okajima, and Okajima et al., using flow visualisation techniques. found that changes of flow patterns coincided with the discontinuities in the Strouhal number curves (the Strouhal number versus the Reynolds number). Okajima investigated this using cylinders of different aspect ratios d/D of 1 (square cylinder), 2, 3 and 4. He found that the region of the Reynolds number where the discontinuity occurred in the Strouhal number curve was strongly dependent on the d/D ratio of the rectangular cylinders. His report is summarised as fellows. With a square cylinder, the variation of the Strouhal number with the Reynolds number showed slight and continuous change around a constant value in the range of Reynolds numbers between 10^2 and $2.0x10^4$. The average value of the Strouhal number was near 0.13, a value found in most literature. With a cylinder of d/D=2, the Strouhal number increased with increasing Reynolds number reaching a value of 0.18 and then a striking discontinuity occurred at a Reynolds number of about 500 where the Strouhal number sharply decreased. Beyond Reynolds number of 500 the Strouhal number gradually increased before reaching a constant value of about 0.08-0.09 when $Re>5x10^3$, a constant value consistent with that found by Nakaguchi et al. With a cylinder of d/D=3, the variation of the Strouhal number with the Reynolds number was similar though the Strouhal number was generally found to have higher values and the discontinuity, which occurred at higher Reynolds numbers of 10^3-$3x10^3$, was less profound. Finally with the cylinder of d/D=4, the Strouhal number was found to be practically independent of the Reynolds number. Okajima found that the discontinuity of the Strouhal number was related to the sudden changes in the flow patterns. He pointed out that with cylinders with d/D of 2 or more, the variation of the flow pattern depended entirely upon the Reynolds numbers. At extremely Low Reynolds numbers, there was a steady reattachment just behind the leading edges, and the flow separated at the trailing edges. At moderate Reynolds numbers, the flow separation at the leading edges was developed and the separated flows could not detach themselves fully from the cylinder but reattached on either the upper or the lower surface during a period of vortex shedding. Further increase of the Reynolds number made the separated flows detach themselves suddenly from the surfaces, which resulted in a widening of the wake, accompanied by the discontinuous

change of the Strouhal number. With the cylinder of d/D=3, the critical Reynolds number was delayed until about 10^3-$3x10^3$. Okajima suggested that the bigger d/D, the higher was the critical value since the increase in the length of the afterbody of the cylinder tended to prevent the separated flows from expanding and to keep themselves attached to the side surfaces. With cylinders of d/D of 4 or more, the flow separated at the leading edges remained reattached to the upper and lower surfaces, and no drastic change in the Strouhal number occurred. Okajima et al. using flow visualisation verified early findings and went further investigating the flow around cylinders with higher aspect ratios d/D. They found in addition to the critical d/D of 2.8 another critical d/D of 6 where the Strouhal number suddenly decreased at a relatively higher Reynolds number of about 10^4.

The ESDU (Engineering Science Data Unit) data sheet 71016 (1971) provides comprehensive descriptions of the effects of the Reynolds number, aspect ratio, turbulence and flow direction on the forces acting on isolated rectangular blocks.

Figure 1.3 illustrates the effect of the aspect ratio on the drag coefficient from the findings of some of the authors mentioned above. The results clearly show that a peak value of the drag coefficient of about 2.9 occurs when the aspect ratio d/D approached 0.6.

1.2.2 PERIODIC FLOW

1.2.2.1 Circular cross-section cylinders

The circular cylinder has dominated fluid loading experiments and over the years comprehensive data have been accumulated. Tests were performed in different flow conditions, e.g. accelerating flow, planar oscillating flow, simulated waves, laboratory waves, and sea waves.

The inertia force on a circular cylinder in an inviscid, irrotational, accelerating flow may be calculated from the potential flow theory which gives C_M coefficient a value of 2.

Sarpkaya and Garrison (1963) measured the forces on a circular cylinder in a flow accelerated uniformly from zero velocity. The C_M and C_D coefficients were found to be close to 2 and 0, respectively, as the flow started to accelerate. After the fluid had displaced by about 3 cylinder diameters, C_M and C_D coefficients had fluctuating values of about 1.25. Wolfram and Theophanatos (1985) estimated the added mass C_A and

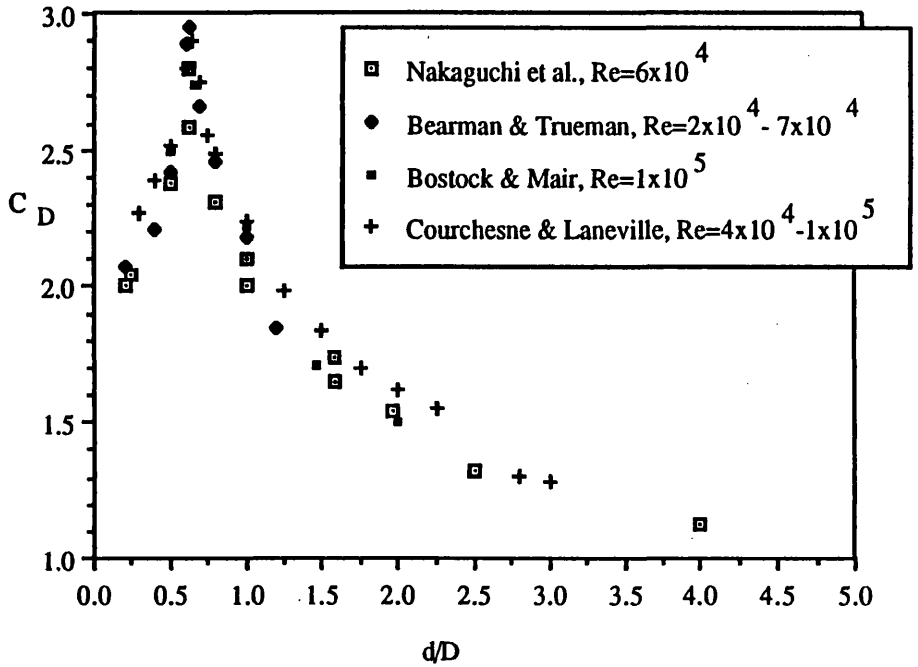

Fig. 1.3 Variation of C_D with the aspect ratio d/D

drag C_D coefficients of smooth and roughened circular cylinders and found that these coefficients depended on the roughness of the cylinders.

Sarpkaya (1976 a,b) has produced large amount of data on smooth and roughened circular cylinders in planar oscillating flow generated by a large U-shaped water oscillating tunnel. Using this apparatus it is possible to study drag, inertia and lift forces at a wide range of Reynolds and KC numbers, though the type of flow it generates is only found near the sea bed in shallow water waves.

For smooth circular cylinders and for $Re<10^5$, C_D coefficient was found to be higher than the steady flow value and C_M coefficient lower than the potential flow value of 2. In the range of $Re>10^5$ and KC>20, the value of C_D coefficient was found similar to the post supercritical steady flow value of 0.68. For KC=20 and $Re>10^5$, C_M coefficient was found to have a value of about 1.75. Sarpkaya found that C_M, C_D and C_L coefficients were dependent on the KC and Reynolds numbers and the roughness of the cylinders. He then introduced a new parameter called the frequency parameter β defined as $Re/KC=D^2/\nu T$ to eliminate the maximum water particle velocity u_m appearing on both Re and KC numbers and correlated all his data with the KC number for fixed values of β. It is a convenient parameter for periodic flows since, for a given model size and fluid, β parameter depends only on the flow frequency, whereas the Reynolds number depends on both the flow frequency and amplitude of oscillation. Further details of the results of smooth and roughened circular cylinders are given in Sarpkaya (1976 a,b).

The hydrodynamic coefficients obtained from such experiments have been widely used to predict forces on bodies immersed in different flows, e.g. in wavy flow. In recent years, attention has been paid to the question of the applicability of these coefficients such as Sarpkaya's data to predict forces induced by waves.

It is suggested that the flow parallel to the axis of a cylinder does not influence the loading normal to the member. This would suggest that the oscillating flow results should also be applicable to vertical cylinders in regular waves with elliptical orbits (shallow water).

Chakrabarti et al. (1976) and Chakrabarti (1980) measured the wave forces on vertical circular cylinders in shallow water conditions and found that the drag and inertia coefficients agreed well with those of Sarpkaya. However, in the range of KC number up to about 300, Sarpkaya's measurements had led to higher forces than those measured on structures in deep water waves. Ramberg & Niedzwecki (1979), Ramberg (1981),

Stansby et al. (1983), Dawson (1984) and Heideman and Sarpkaya (1985) found that Sarpkaya's data gave considerable overestimation of the total measured forces on fixed vertical circular cylinders in deep water waves. The total measured forces were found to be overestimated by approximately 30 to 50%. Maull & Norman (1979) and Ikeda et al. (1988) also found that for a horizontal circular cylinder deeply submerged in regular waves the forces estimated with Sarpkaya's C_M and C_D coefficients were higher than the measured forces. Ikeda et al. found that the wave forces were twice or more as high as the measured forces when estimated using hydrodynamic coefficients of plane oscillatory flow.

These discrepancies between measured forces and predicted forces using coefficients such as those of Sarpkaya may be caused by the re-encounter with the cylinders own wake which occurs repeatedly in Sarpkaya's tunnel but occurs less frequently in real seas because of the effects of currents and random seas. The water particle orbital eccentricities of the wave induced flow are the other reasons for the discrepancies. While under shallow water conditions the fluid particle orbits are almost flat like those of planar oscillatory flow, under deep water conditions they are approximately circular. The effect of water particles orbital ellipticity were investigated by Maull and Norman (1979). They reported that the orbital ellipticity influence the values of the coefficients of drag, inertia and transverse forces and the ways in which they vary with such parameters as KC and Re numbers.

The difficulties of achieving high Re numbers in laboratory waves have led researchers to simulate wavy flow by orbiting cylinders in initially stationary flow. The flow generated around an orbiting cylinder is similar to the orbital flow of a wave about a horizontal cylinder. However, the inertia force acting on the orbiting cylinder is only the added mass force. The Froude-Krylov force, which is associated with the acceleration of the flow, does not occur. This force can, however, be estimated and the inertia coefficient can be adjusted.

In simulated waves, Holmes and Chaplin (1978), Chaplin (1981), Grass et al. (1984), Chaplin (1985 a,b) and Chaplin (1988 b) performed experiments in which a smooth circular cylinder was driven around an elliptical path in a tank of water initially at rest. The ellipticity E of the path was varied from 0 (planar oscillating flow) to 1 (circular orbital flow corresponding to a horizontal cylinder parallel to the crest of a deep water wave). When the ellipticity was zero, Chaplin (1985 b) and Chaplin (1988 b) found values of C_M and C_D coefficients similar to those obtained by Sarpkaya. As the

ellipticity of the flow was increased C_M coefficient was found to decrease, typically from 1.8 at E=0 to about 1 or less at E=0.9. The C_D coefficient was also found to decrease as E increased. Chaplin suggested that the fall of C_M coefficient from its planar oscillatory flow value to about unity for circular orbital flow was due to the generation of circulation around the cylinder which induced a lift force acting in the opposite direction to the inertia force. Grass et al. also found that C_M and C_D coefficients reduced as the ellipticity of the flow increased. Grass et al. made an alternative suggestion that the reduction of the inertia force was caused by the drag force being imperfectly in phase with the velocity of the cylinder, and cancelling part of the inertia force. On the reduction of C_D coefficient with increasing E, Chaplin suggested that was probably caused by the stirring effect of the cylinder rotating in the fluid.

In laboratory waves, many researchers have carried out experiments on vertical and to a lesser extent on horizontal circular cylinders. Chakrabarti et al. (1976), Gaston and Ohmart (1979), Pearcey (1979), Chakrabarti (1980), Bearman et al. (1985a) and Pearcey et al. (1985) measured forces on vertical cylinders and C_M and C_D coefficients were determined. Bearman et al. using the large Delta flume at the Delft Hydraulics Laboratory achieved post-supercritical flows where the Reynolds number was in the range of 1.46×10^5 to 5.05×10^5 and the KC number varied from 4 to 20. Keulegan and Carpenter (1958) (horizontal cylinder placed in the node of a standing wave), Maull and Norman (1979), Bearman et al. (1985a), Pearcey et al. (1985), Teng and Nath (1985) and Ikeda et al. (1988) measured forces on horizontal cylinders and C_M and C_D coefficients were determined.

Numerous experiments have been carried out in the sea, for example the Ocean Test Structure experiments, the Eugene Island experiments, both conducted in the Gulf of Mexico, the Forties Field experiments, the Christchurch Bay experiments, conducted in the sea off Southern England. The Ocean Test Structure experiments were performed with smooth and roughened vertical circular cylinders. For further details, see Borgman and Yfantis (1979), and Heideman et al. (1979). Most of the Christchurch Bay experiment were performed with smooth and roughened vertical circular cylinders and some with smooth and roughened horizontal circular cylinders. For further details, see Bishop (1984) for smooth cylinders and Bishop (1987) for roughened cylinders. For details about the Forties Field and the Eugene Island experiments, see Atkins (1979) and Ohmart and Gratz (1979) respectively.

The fluid loading on a vertical cylinder is profoundly different from that on a

horizontal cylinder fully submerged with its axis parallel to the wave crests. The orientation of a member affects the values of inertia and drag coefficients. Pearcey (1978) reviewed some fundamental features of wave loading on vertical and horizontal circular cylinders. For a vertical cylinder in idealised regular, deep water waves and piercing the free surface, the water-particle circular orbits are co-planar with the axis of the cylinder and the velocity vector which is constant in magnitude has components normal and parallel to the axis of the cylinder. The position of flow separation and the vortex shedding would be dependent only on the normal component and the parallel component would not be expected to influence the flow phenomena external to the cylinder. The periodic motion is thus similar to the planar oscillatory motion with the stagnation point on the cylinder switching from fore to aft of the cylinder and then back once in each cycle. Therefore, the whole flow field in the plane normal to the cylinder's axis, generated by the cylinder, in response to the particle motions, accelerates from rest and decelerates again in each half cycle before reversing in the next. The vortices shed by the cylinder in one half cycle and the velocity deficit of its wake are periodically swept back past the cylinder strongly influencing the flow induced loading. Large transverse forces associated with the vortex shedding are usually found for vertical cylinders which indicate that the vortices have a significant coherence along the length of the cylinder in spite of the decay of orbital motions with depth.

On the other hand, for a horizontal cylinder fully submerged in idealised regular, deep water waves with its axis parallel to the wave crests, the plane of the water particles circular orbits is normal to the axis of the cylinder with no axial component of velocity, and also no variation in phase along the length of the cylinder, and no depth dependence. The forces associated with vortex shedding are now co-planar with the orbits and hence there is no force transverse to the plane of the orbits. The velocity vector constant in magnitude has therefore vertical and horizontal components both normal to the axis of the cylinder and with associated forces having vertical and horizontal periodic components. The more fundamental differences from the vertical cylinder can be seen better by considering, for the idealised circular orbit, the tangential and radial elements of the kinematics and forces before resolution into horizontal and vertical components. Then, there is a constant tangential velocity, and a constant centripetal acceleration, and therefore the flow itself is not inherently time-dependent, except for the influence of vortex shedding. The stagnation point 'precesses' round the cylinder, and the wake sweeps some cylindrical volume co-axial with the cylinder. Any

vortices that are shed also lie within a co-axial volume. The forces will have the following principal elements.

(a) A tangential drag element associated with the tangential velocity and influenced by the separated flow and vortex shedding in much the same way as the drag in uniform incident flow;

(b) a vortex-induced element normal to the tangential drag element and therefore radial; and

(c) a radial inertia element associated with the Froude-Krylov force and the virtual added mass, the later being influenced by the viscous flow.

Each of these elements will have horizontal and vertical components.

The resulting total horizontal and vertical force components do not differ from one another in principle, but are of course orthogonal in phase. Each force component has a resolved part of each of the three principal elements described above. The resolved parts of the tangential drag and radial inertia will be periodic with the wave motion. The magnitude of the resolved part of the radial vortex element will also vary cyclically, but there could be an additional frequency superimposed on this because the vortex shedding itself will not necessarily be related to wave frequency but rather to something analogous to the Strouhal frequency.

For waves with elliptical orbital motions instead of circular (waves in finite water depth), the tangential and perpendicular elements of the forces would themselves vary periodically, with the vortex shedding subject to some modulation both in intensity and frequency which now responds to wave frequency. As the orbits become progressively more elliptical, the flow and forces would presumably become progressively more similar in nature to those for the vertical cylinder in waves, and cylinder in planar oscillatory incident flow. Chaplin (1984 a,b) reported that the wave forces acting on a circular cylinder horizontally submerged decrease with increasing KC at a low KC number range, and suggested that this is caused by the non-linear effect of oscillatory boundary layer due to viscosity. Inoue et al. (1984) measured the wave forces acting on circular and lowerhull cylinders horizontally submerged in waves, and showed that these forces are much smaller than the potential values at comparatively high wave height. Grass et al. (1984) measured hydrodynamic forces acting on a circular cylinder moving with circular or elliptical orbital motion in still water, and also suggested that the wave forces estimated by the potential flow theory may be possibly overestimated when it is applied to the particular case of horizontal structural members. Chaplin (1987)

pointed out that for a horizontal cylinder parallel to wave crests, the wave flow is predominantly in the plane normal to the cylinder's axis, and is more uniform, and better correlated in the axial direction. He suggests that when the cylinder encounters its own wake, it is likely to experience a reduction in incident velocity rather than the increase which occurs in the case of a vertical cylinder.

In summary, when the cylinder is orientated vertically, it will be subjected to different flow conditions including a spanwise velocity component if it is long enough because for deep water waves the orbit is near-circular towards the surface and elliptical lower down. Regardless of the orbit, the wake will be swept back against the cylinder. When the cylinder is submerged horizontally, it may have the same incident flow along its span but the wake interaction would be different to that of a vertical cylinder unless the orbit is flat. The wake will in general follow the orbital path, and depending on the orbit the vortices shed from the previous half cycle may be swept far enough away from the cylinder, so that when the flow reverses they may not significantly affect the forces on the cylinder.

The difference in flow described above between that of vertical and horizontal cylinders in waves would be expected to influence the values of the hydrodynamic drag, and inertia coefficients and hence the values of wave forces, and the way in which the coefficients vary with such parameters as KC and Re numbers. Generally, the inertia and drag coefficients of vertical cylinders have been found higher than those of horizontal cylinders with their axis parallel to wave crests. Bishop (1987), analysing the data from experiments carried out in sea waves at the Christchurch Bay, found that C_M and C_D coefficients of roughened vertical circular cylinders were 37% and 14% higher than those of roughened horizontal circular cylinders respectively.

1.2.2.2.Rectangular cross-section cylinders

As mentioned earlier, new generations of semi-submersible drilling rigs and tension-leg platforms with rectangular cross-section members are emerging nowadays. The incentive of such new designs is the reduced capital cost in exploring and exploiting marginal fields in harsher and deeper waters. However, a limited amount of investigation regarding wave loading on non-circular sections exist in the literature.

Keulegan and Carpenter (1958) investigated the loading on submerged horizontal circular cylinders and flat plates placed in the node of a standing wave. They generated curves giving C_M and C_D coefficients which they successfully correlated with a period

parameter defined as $u_m T/D$ (referred as the Keulegan-Carpenter KC number) but they did not find any significant dependence of these coefficients on the Reynolds number. The Physical meaning of the KC number is the ratio of wave particle displacement in one direction in one wave period multiplied by π to the cylinder diameter, i.e. when the particle maximum displacement equals the cylinder diameter, $KC=\pi$. They found that the variation of C_M and C_D coefficients of flat plates with the KC number was very different from that of circular cylinders. The C_M coefficient was found to increase then decrease before increasing again to a value of about 5 at KC numbers near 120. The most remarkable behaviour was found with the variation of C_D coefficient. The drag coefficient was found to follow an asymptotic trend with large values at small KC numbers then a sharp fall as the KC number increased within a small range and finally a gradual decrease with increasing KC number. The largest value of C_D coefficient measured was 11.55 at KC number of 1.7. Keulegan and Carpenter observed that for a small value of the KC number, eddies were formed almost simultaneously at the upper and lower edges of the plates and were concentrated near the edges. These authors questioned whether the large values of C_D coefficient for small KC numbers were associated with the behaviour of the eddies.

Paape and Breusers (1967) considered the wave force on square pipes but did not derive any C_M and C_D coefficients. Bearman et al. (1978) carried out experiments in a U-tube water tunnel generating a planar oscillatory flow past a circular cylinder, flat plates, a square cross-section cylinder and a diamond cylinder (a square cylinder with a diagonal in-line with the flow). They found that the circular cylinder experienced the lowest hydrodynamic forces. The body shape was found to have a strong effect on the value of C_D coefficient at small KC numbers and they suggested this was associated with flow separation and the first appearance of vortices. They found that at small KC numbers, C_D coefficient of a circular cylinder approached zero whereas that of flat plates attained very high value following an asymptotic trend similar to that found by Keulegan and Carpenter. The second highest value of C_D coefficient was found with the diamond cylinder. The variation of C_M coefficient with the KC number showed different behaviour from that of the other shapes. At low KC numbers, the square cylinder showed the highest value of C_M coefficient approaching the potential flow value of 2.78 (area of the square cylinder considered being $\pi D^2/4$ instead of D^2). Bearman et al. also measured a force coefficient derived from the Morison equation in terms of non dimensionalised root mean square force during a cycle. The variation of this force

coefficient with the KC number showed the same behaviour for all the body shapes. At small KC numbers the force coefficient had a high value and then decreased gradually as the KC number increased before becoming constant. The flat plates and the square cylinder had the largest value of the force coefficient, particularly at low KC numbers. From flow visualisation, Bearman et al. observed that intense discrete vortices, which dominate the flow around a body, were visible in the case of the sharp-edged bodies at the lowest KC number. Below a KC number of about 15, they found that only two main vortices were formed per half cycle and one appeared to grow more rapidly then the other. At flow reversal, the large vortex passed rapidly over one side of the body where it became of opposite sign to the vorticity being generated there. The induced flow of the reversed vortex helped to generate rapidly a second large vortex of opposite sign. When the two vortices were of roughly the same strength, the pair was carried away from the cylinder. In the mean time the other shear layer rolled up to form a large vortex ready to initiate a similar process on the other side of the body at the next flow reversal. It was only at KC number in excess of 20 or 30 that the semblance of a vortex street was formed during each half cycle.

Singh (1979) carried out experiments with a circular, square and a diamond cylinders and three flat plates in a planar oscillatory flow as part of a Ph.D. research. From flow visualisation, he observed similar flow patterns on all the sections with the exception of the square cylinder which resulted in the in-line force being similar on these sections. Large vortices were formed for KC numbers between 10 and 25. For KC numbers less than 5, the pattern on all the sections was more or less symmetrical, and on the flat plate and diamond section weak vortices were observed which resulted in a drag force still important at low KC numbers. On the circular cylinder the flow remained attached over most of its surface, and on the square section the flow separated on the front face and weak recirculation was observed on the upper and lower surfaces. Singh concluded that of the four sections, the flat plates experienced the largest forces and the circular cylinder would be the best shape for the design purpose as it experienced the smallest in-line forces. Comparing results of the circular cylinder with previous results, inertia and drag C_M and C_D coefficients obtained by Singh revealed considerable amount of disagreement particularly when comparison is made to Sarpkaya's data for KC numbers between 10 and 20. Singh found no obvious explanation for this difference and suggested that this might be due to different data analysis techniques and to the manner in which the oscillations in the U-tube were produced. Again large discrepancies in C_M

and particularly C_D coefficients throughout the KC number range were found for flat plates when Singh compared his results to those of Keulegan and Carpenter (1958). The C_M and C_D coefficients measured by Singh were found to be lower than those measured by Keulegan and Carpenter. The largest discrepancy was found for C_D coefficient at low KC numbers where the drag coefficient measured by Keulegan and Carpenter was considerably larger than that measured by Singh.

Isaacson (1979a) conducted experiments on large vertical square cross-section cylinders in waves. Tests were carried out with an isolated cylinder at various orientations with respect to the wave propagation and with a pair of cylinders at different orientations and separating distances to study the effect of interference. The experiments were conducted in diffraction regime conditions and the results were given in terms of a force coefficient versus diffraction parameter $2\pi D/\lambda$ for various orientations.

Graham (1978) and Graham (1980) conducted a theoretical analysis of the forces induced by separation and vortex shedding from sharp-edged bodies in oscillatory flow at low Keulegan-Carpenter numbers. The theory was based on the assumption that at low KC numbers vortices were not convected by the oscillatory flow far from their point of origin. He derived theoretical expressions for inertia and drag coefficients of a circular cylinder, a flat plate, a diamond and a square cylinders and compared them with experimental C_M and C_D coefficients (obtained from Keulegan and Carpenter, and Singh). He found that the theoretical values of the different body shapes did agree with the trends of the measured data for KC numbers less than 10 but the agreement deteriorated for KC numbers over 10.

Tanaka et al. (1982) carried out experiments with rectangular cylinders oscillating horizontally in still water to measure drag and added mass coefficients. The aspect ratio and the corner radius of the cylinders were systematically varied for various angles of flow attack to determine the effects on C_A and C_D coefficients. For a square cylinder (aspect ratio of 1), Tanaka et al. found no significant dependence of C_A and C_D coefficients on the Reynolds number (the range considered was up to $10x10^4$). However, a dependence on the KC number was found to exist for all cylinders. On the effect of corner radii, C_A and C_D coefficients were found to decrease for increasing corner radii. For cylinders with a small corner radius C_D coefficient decreased rapidly as the KC number increased in the region of low KC numbers, and became constant for higher KC numbers. As the corner radius became smaller, the decrease of C_D coefficient was more gradual. On the effect of the aspect ratio, C_A and C_D coefficients

were found to increase as the aspect ratio was reduced below 1.

Shankar et al. (1983) carried out a numerical analysis of wave forces on large vertical surface piercing cylinders of square and rectangular cross-sections. The study was mainly concerned with such structures as the gravity type of concrete platform and oil storage tank causing significant scattering or diffraction to waves acting upon them due to the effect of the large size of the structure. They used the diffraction theory based on a finite element approach. They derived non dimensionalised forces and moments for varying angles of incidence, aspect ratio d/D, relative depth y/D and diffraction parameter $2\pi D/\lambda$. They also computed the diffraction coefficient and an equivalent inertia coefficient. They found that the non-dimensionalised horizontal force and moment about the sea bed followed the same trend, increasing up to a certain value with an increasing diffraction parameter and then decreasing with a further increase of the diffraction parameter. On the effect of the relative depth, the non-dimensionalised force and moment were found to increase for an increasing relative depth at small values of the diffraction parameter. The diffraction and the equivalent inertia coefficients were found to increase up to certain values with an increasing diffraction parameter and then to decrease with a further increase of the diffraction parameter. The numerical result of the equivalent inertia coefficient was compared with the theoretical result for large vertical rectangular cylinders in waves obtained by Isaacson (1978b) and based on Green's function and with the experimental result of Isaacson (1979). The comparison found good agreement.

Bearman (1984) conducted experiments in planar oscillatory flow with circular, square and diamond cylinders and investigated the effects of the corner radius on the hydrodynamic forces in the KC number range from 1 to 100 and the Reynolds number range from 200 to $2x10^4$. For both the square and diamond cylinders, they found that C_D coefficient decreased with increasing corner radius. The reduction of C_D coefficient caused by the rounding of corners was more marked at low KC numbers. When measuring the drag coefficient of a circular cylinder, they found that this shape did not give the lowest drag over the whole range of the KC number. They found that at KC=90, the sharp-edged square cylinder had a C_D coefficient of 1.9, a circular cylinder had C_D coefficient of 1.15 and a rounded square cylinder with r/D=0.265 (r is the radius) had C_D coefficient of only 0.65. They concluded that there was an optimum corner radius $0.265<r/D<0.5$ giving minimum drag force. The inertia coefficient of the

square cylinder decreased with increasing corner radius only when the KC number was between 10 and 50. Outwith this range of KC, the effect of corner radiusing was small. The circular cylinder gave lower C_M values than the rounded square cylinder over the whole range of the KC number. However, C_M coefficient of the diamond cylinder was found to be lower than that of the circular cylinder for KC numbers up to 20. Comparing the effect of corner radius on C_D coefficient of the square cylinder in oscillatory flow with that investigated by Delaney and Sorensen (1953) in steady flow, Bearman et al. found that C_D coefficient at high KC numbers decreased more rapidly with an increasing corner radius in the former flow than the latter at subcritical Reynolds numbers. The authors suggested that the drag coefficient was more sensitive to corner radius in oscillatory flow because the turbulence in the ambient flow caused flow separation to be delayed and to occur further downstream and this resulted in a larger reduction in drag coefficient.

Bearman et al. (1985b) carried out experiments at low KC numbers on circular, square and diamond cylinders and a flat plate horizontally mounted in a U-shaped water tank generating a planar oscillatory flow. They also conducted an inviscid theoretical analysis to compare theoretical values of inertia C_M and drag C_D coefficients with those obtained experimentally. This theory is claimed to be valid for KC numbers less than about 3. They found that in the case of the flat plate, theoretical predictions of inertia and drag coefficients were good. However, in the case of the square and diamond cylinders, the theory overpredicted the magnitude of the drag coefficients by about 20% though the measured drag coefficients followed the predicted trends. The prediction of the inertia coefficient was reasonable in the case of the square cylinder, but less in the case of the diamond cylinder. When the KC number exceeded 3, the measured drag coefficients for all three sharp-edges cylinders were found to vary similarly with the KC number suggesting that all the cylinders may have a similar vortex shedding pattern.

Lian (1988) used a numerical model based on a thin free shear layer method to study separated flow around a flat plate and a mid-ship cross section with bilge keels in harmonically oscillating flow. He calculated the in-line force and determined drag and inertia coefficients at moderate KC numbers. The calculated C_D coefficient for the flat plate was found to be lower than that measured by Keulegan and Carpenter for KC numbers below 8 and the agreement was good for higher KC numbers. The calculated C_M coefficient for the flat plate was found to be in good agreement with that measured by Keulegan and Carpenter for KC numbers up to 4 and the agreement deteriorated for

higher KC numbers where the calculated C_M coefficient was found to be much higher than that measured. However, when comparing the total force with the force obtained by Morison's equation using numerically determined C_M and C_D coefficients at KC =1, Lian found good agreement with respect to amplitude and phase.

Ikeda et al. (1988) carried out experiments on cylinders of different shapes horizontally submerged in regular waves at low KC numbers. The cylinders investigated were a circular cylinder, a square cylinder and a diamond cylinder and a flat plate. For a flat plate, Ikeda et al. found that C_M and C_D coefficients measured in waves were lower than those measured in oscillatory flow (Tanaka et al. (1980)). From flow visualisations, they observed that the behaviour of vortices around the plate was very different from that in plane oscillatory flow. A circulating flow round the plate was also observed in regular waves but not as strong as the flow around circular cylinders. They suggested that the decrease of C_M coefficient with increasing KC numbers was due to this circulation. They also pointed out that the behaviour of vortex shedding in regular waves was different from that in oscillatory flow. This phenomenon explained the difference in C_D coefficient found with wavy and oscillatory flows. For a square cylinder, C_M coefficient decreased rapidly with increasing KC numbers, similar to the case of a circular cylinder, reached a minimum value at about KC=4, and then increased. Again the variation of C_M coefficient with the KC number was found to be different from that in oscillatory flow (Tanaka et al. (1982), Bearman et al. (1984)) where C_M coefficient showed less variation with the KC number. The C_D coefficient was also found to be different from that measured in oscillatory flow. For KC numbers less than about 2, C_D coefficient measured in regular waves gave higher values than in oscillatory flow, and vice versa for KC numbers exceeding 2. From flow visualisation, Ikeda et al. observed a strong circulation as in the case of a circular cylinder. In the case of a circular cylinder, they observed two anti-clockwise vortices released in one wave cycle, but in the case of the square cylinder, four vortices one at each corner were observed. As with the square cylinder, the diamond cylinder in waves had different C_M and C_D coefficients from those measured in oscillatory flow (Bearman et al. (1984)). Ikeda et al. again observed a strong circulation which was created due to clockwise vortices round the cylinder, and as in the case of the square cylinder, four anti-clockwise vortices were released at each corner one after another.

Therefore, when the KC number is very small, curves showing the variations of C_D coefficient with the KC number show a different pattern for different geometrical shapes. The two extreme cases found are the circular cylinder and the flat plate. While for a circular cylinder $C_D \rightarrow 0$ as $KC \rightarrow 0$, for a flat plate $C_D \rightarrow \infty$ as $KC \rightarrow 0$. The reason for this is that sharp-edged cylinders shed vortices in oscillatory flow even at very low KC numbers, and it is believed that the large values of C_D coefficient are associated with the behaviour of these vortices.

It is believed that the differences in flow pattern between a vertical and a horizontal circular cylinder, as discussed above, would not necessarily be similar to those between a vertical and a horizontal rectangular cylinder. One reason is that the rotating wake about a horizontal sharp-edged rectangular cylinder would give rise to four new and essentially different separated regions and bring closer to the cylinder the effects of secondary separations and interesting vortex motions. This is not the case with a horizontal circular cylinder where the wake just rotates at some distance away from the cylinder. In addition, flow separation on a rectangular cylinder occurs earlier, and the aspect ratio would have an influence on the wake field. Indeed, one would expect that the flow would be dominated by separation and vortex shedding from successive corners of the cylinder as the stagnation point processes around the cylinder. Therefore, the time intervals and spacing between successive vortices would be a feature and would vary with the aspect ratio of the cylinder. However, it is expected that the steady streaming on a horizontal circular cylinder in waves would also be present for say a square cylinder. Furthermore, as in the case of a circular cylinder, the main differences between a vertical and a horizontal rectangular cylinder are associated with the difference in the span-wise correlation and effect of the orbit on the cylinder.

Nevertheless, this problem is still not clarified and needs to be investigated using, for instance, flow visualisation techniques to determine the complicated vortex structure on rectangular cylinders and to study the effect of varying the aspect ratio on the flow separation and the wake field.

1.2.3 PRESENCE OF A CURRENT WITH WAVES

The presence of current in the ocean waves is a common occurrence. Several offshore platforms operate in areas where waves propagate on currents. These currents are generated by tidal forces, ocean circulation, difference of density at depths and wind

at the water surface. Currents in coastal waters influence wave properties significantly because of high velocity and strong current shear. In shallow waters where relatively strong currents are encountered (e.g. North Sea), wave-current interactions are most significant. The interaction of waves and currents and the resulting effect on the response of the structure must be considered for the design of an offshore structure. In the design of marine structures and performing stability analysis of submarine pipelines it is crucial to accurately compute the total water particle velocities of the combined wave -current flow field. Drag and lift forces exerted on those marine systems are proportional to the square of this total fluid velocity. In shallow waters there are a variety of design conditions in which both drag and lift forces dominate over the inertia forces. In addition, design procedures that consider vortex-induced oscillations of structures are becoming more critical as oil exploration is extended into areas where significant currents exist. Presence of shear in currents can have a significant effect on the lengthwise coherence of vortex shedding which might enhance the fluid-induced forces. Hence, knowledge of possible modification of the ambient current shear by surface waves is required. However, little information exists on the effect of waves and current interaction on the hydrodynamic loading of offshore structures. The difficulty in finding an analytical approach to describe the interaction and the uncertainties over how the Morison equation can predict the wave-current induced forces and the fact that waves and currents are omnidirectional and that the directional distribution of energy is anisotropic are examples of the complexity of the problem. Furthermore, an experimental investigation of the problem in the practically significant range of Reynolds numbers, Keulegan-Carpenter numbers, relative current velocity, and suitably defined current gradient is practically impossible.

The existence of currents will change the wave parameters such as wave height, wave length, wave period and the wave kinematic field as compared with waves in still water. For example, if the current is in the direction of wave propagation, the wave amplitude decreases and its length increases. If the current opposes the wave, the wave becomes steeper and shorter. Therefore, when the Morison equation is used, the values of wave height, wave length and wave period (or frequency) should be taken as the values of waves in current. A technique which has been in use in the oil industry to include current in wave force calculations is linear superposition. Once a design wave is chosen, its kinematics are calculated via irrotational wave theories with the assumption of still water. Then, the design current profile is added linearly to the wave velocity

field generated in the absence of a current in order to calculate the total fluid-induced force.

Among the first to perform substantial controlled experiments of this nature on circular cylinders was Sarpkaya (1955). He carried out measurements of wave-phase velocity, amplitude, wave length, and shape of ascending and descending waves in a long wave-current flume and determined the neutral stability conditions for waves propagating with constant amplitude. Dalrymple and Dean (1975) following the simple superposition principle, related waves of maximum height on currents to equivalent waves in still water. Their procedure, however, did not address the problem of waves-current interaction. Moe and Verley (1980) found that inertia and drag coefficients of circular cylinders at low KC numbers were affected when waves and currents were present together. Ismail (1983) carried out a study of the effects of waves and current interaction on the design of marine structures by heading a steady turbulent jet directly into surface waves generated in a water tank. He found that the mean velocity profiles of the currents in shallow water are modified by the action of surface gravity waves. In the case of following waves to the currents, the mean velocity of the currents increased, and in the case of opposing waves to the currents, the mean velocity of the current near the bed decreased. Kato et al. (1983), when measuring the drag forces of circular cylinders oscillating in uniform flow, found that C_D coefficient decreased as the current velocity increased at low KC numbers. Sarpkaya et al. (1984) and Sarpkaya and Storm (1985) using a U-tube to oscillate water and moving the cylinders at a constant velocity found that current influenced the values of inertia and drag coefficients. In the drag/inertia dominated regime ($7<KC<15$), the drag coefficient was found to decrease with increasing current velocity and the inertia coefficient was found to increase up to a certain current velocity. For lower KC numbers both C_M and C_D coefficients were found to decrease with increasing current velocity. Teng and Nath (1985) towed a smooth and a roughened circular cylinder in waves to simulate the waves-current flow field in a region where the drag force was dominant. They found that C_D coefficient decreased slowly with increasing reduced velocity VR ($VR=VcT/D$, where Vc is the current velocity). Ikeda et al. (1990) carried out an experimental investigation on a horizontal cylinder towed in head and following waves generated in a towing tank. They found that the wave forces decreased in the low KC number region whether the cylinder was stationary or moving at steady speed. The inertia coefficient was found to be very sensitive to the steady motion of the cylinder, and was found to be different

between the two cases of following sea and head sea. Malleswara-Rao and Narasimham (1990) developed a numerical method to compute forces on circular cylinders in waves and current for two cases, following waves and opposing waves to the current. They plotted C_M and C_D coefficients against the phase angle, however, it is not clear what ranges of the KC number and VR were so that the change in the coefficients induced by the current could be assessed. Most recently Li and Kang (1992) carried out model tests on a circular single pile subjected to waves-current coexisting field. They found that both inertia and drag coefficients were affected by the presence of the current with waves. The drag coefficient was found to decrease and the inertia coefficient was found to increase very slightly.

It is believed that there are no previous data giving explicit values of hydrodynamic coefficients for rectangular cylinders in combined wave and current flow. It is anticipated in this study that the presence of currents may be more important for rectangular-shaped bodies than for bodies with no sharp corners (e.g. circular cylinders).

1.3 AIMS OF THE PRESENT RESEARCH

From the foregoing discussion, it is clear that further experiments involving rectangular cross-sectional cylinders particularly in wavy flow are necessary to provide data for design purposes. Regarding sharp-edged cylinders, very few experiments (most of them performed in planar oscillatory flow) were carried out with square and diamond sections and flat plates, and practically no results are available for rectangular cylinders with an aspect ratio (height to width) other than 1. Furthermore, data obtained at very low KC numbers with rectangular cylinders in wavy flow are almost non-existent. Finally, the author is not aware of any experiments conducted with rectangular cylinders studying the effects of a current flow when interacting with a wavy flow.

Therefore, the first aim of this research was to carry out extensive experiments involving rectangular cylinders of different aspect ratios and different sizes immersed in different flow conditions in order to measure hydrodynamic coefficients such as drag, inertia, lift and non dimensionalised root mean square and maximum force coefficients. The different flows simulated were the steady flow, the wavy flow and a combination of the two flows to simulate the presence of a current in waves. Some flow visualisation was made with the help of video films to examine the flow development and the

formation and shedding of vortices around vertical cylinders immersed in the different flows.

The second aim was to study the effect of varying the aspect ratio on the forces experienced by the cylinders in the three different flows. This was done by keeping one side of the cylinder constant and varying the other side.

The third aim was to compare the forces on vertical surface piercing cylinders with those on the same cylinders but submerged horizontally in flow with their axes parallel to wave crests (in periodic flows).

The fourth aim was the examination of the effect of the presence of a current along with waves on C_M and C_D coefficients. This was carried out by comparing the coefficients measured in waves only with those measured in waves and currents of different velocities for identical values of KC and β numbers. Therefore, the effects of the current reduced velocity were examined.

Finally, the fifth aim of this research was the assessment of the Morison equation at low KC numbers for the rectangular geometry. This was achieved by comparing the measured in-line forces in waves with the predicted forces calculated from Morison's equation through the use of measured C_M and C_D coefficients for identical values of KC and β numbers. Further comparisons were also made between the root mean square of the measured in-line forces with the calculated root mean square of the in-line forces given by Morison's equation. Similar comparisons were made for waves and current flow using a modified Morison equation with measured C_M and C_D coefficients to assess its validity to predict in-line forces when a current is present. The experimental data were examined using different analysis techniques. A brief theoretical study was also carried out to show the limitations of the potential flow theory to predict wave forces on these sharp edged cylinders.

The results obtained from the measurements were plotted against Reynolds numbers for the steady flow and against KC numbers for the periodic flows.

Because of the large size of the towing tank and test models, and the non-availability of relevant equipment when the experiments were conducted, detailed flow visualisation was not possible. However, an attempt to visualise the flow around vertical cylinders with the help of video films was made and the formation and shedding of vortices in the different flows simulated were observed. Flow visualisation with submerged horizontal cylinders was not possible due to the non availability of suitable underwater cameras.

1.4 STRUCTURE OF THESIS

Chapter 2 gives a description of the towing tank with its facilities. The different configurations of the test models and a description of the rig for force measurements are also included in this Chapter.

The data analysis techniques used in this study to determine inertia and drag coefficients measured in the different flow conditions are given in Chapter 3. Other formulations giving various in-line and transverse force coefficients are also included in this Chapter.

Chapter 4 gives the results obtained in this study from the different flow conditions simulated.

Chapter 5 gives a review on flow visualisation and discusses the present flow visualisations carried out in steady flow and in wavy flow.

Chapter 6 is devoted to a discussion of the results obtained in the different flow conditions and discusses the limitation of the potential flow theory. It also provide an assessment of the Morison equation in wavy flow and in combined wavy and steady flows.

Finally, Chapter 7 gives the overall conclusions of this study with recommendations for future work.

CHAPTER 2

EXPERIMENTAL EQUIPMENT AND TEST MODELS

2.1 THE TOWING TANK

The experiments were carried out in the towing tank of the Hydrodynamic Laboratory of the Department of Naval Architecture and Ocean Engineering at the University of Glasgow. The tank is 77 metres long, 4.6 metres wide and 2.7 metres deep with a 2.4 metres water depth. The tank is equipped with an electro-hydraulic plunger type wave-maker fitted across the width at one end of the tank which generates regular waves in the frequency range of 0.4-1.4 Hertz. The maximum wave height generated is 22 cm. At the other end of the tank, an inclined mesh beach is fitted to absorb the energy of the oncoming waves. The tank is also equipped with an electronically controlled towing carriage, with an observation platform, capable of travelling up to 6.4 m/sec.

In order to measure the undisturbed wave heights, three resistance type wave probes fixed to a bridge were placed across the tank width at a distance of about 15 metres in front of the wave-maker. These wave probes induced electrical signals whose strength varied with the varying wave height. The electrical signals were amplified and recorded by a micro computer and a chart recorder for analysis. The calibration of the wave probes was carried out by lifting the wave probes bridge 5 cm and recording the corresponding analogue and digital signals on the chart recorder and the micro computer respectively.

On the observation platform of the towing carriage, several facilities are provided. During experimental runs the output from the model load cells was first filtered and then amplified before it was recorded on a computer IBM PC, later during the research replaced by a Macintosh IIci computer. The test output was then transferred to a VAX 11/730, later during the research replaced by a VAX station 3100, for subsequent analysis. Also fitted in the towing carriage beside the test model a wave probe, similar to those measuring the undisturbed wave heights, for the purpose of measuring wave phase angles. Another chart recorder was also available on the carriage to record test output for cross-checking purposes only.

2.2 THE TEST MODELS

The test models, manufactured from PVC, were constructed in the workshop of the Hydrodynamic Laboratory and were constructed to test two different sets of cylinders.

The first set comprised four rectangular cylinders of 2 metres long all having one common side of 40 cm. The other side was varied from 40 cm to 10 cm with a step of 10 cm, giving four cylinders with cross-sections of 40 cm x 40 cm (square cylinder), 40 cm x 30 cm, 40 cm x 20 cm and 40 cm x 10 cm. This would enable the study of the effect of varying the aspect ratio. At the mid-length of each model a test section of 10 cm long was constructed where all force measurements were taken. At each test section, four waterproof strain gauge type load cells were mounted inside, one load cell attached to each face to measure the total forces applied on that face during test runs. Therefore, each rectangular cylinder was made of three hollow pieces connected by an inner continuous rectangular beam. When joined together, the three pieces formed a continuous 2 metres long sealed smooth sharp-edged rectangular cylinder.

These cylinders were tested in steady flow and in wavy flow. The relatively large size of the cylinders was chosen in order to conduct experiments at high Reynolds numbers in the case of steady flow and at very low Keulegan-Carpenter numbers in the case of wavy flow.

The second set comprised two rectangular cylinders of 1.3 metres long with cross-sections of 10 cm x 10 cm (square cylinder) and 10 cm x 20 cm. The different cross-sections used during the tests enabled the examination of aspect ratio variations. Similar to the first set of cylinders, a 15 cm long test section was constructed at the mid-length of each cylinder where force measurements were taken. At each test section, two waterproof strain gauge type load cells were mounted inside, one load cell was attached to the front face and the other to the side face to measure the in-line and transverse forces applied during test runs. As with the first set of cylinders, each cylinder was made of three hollow pieces connected by a continuous inner rectangular beam and when joined together, the three pieces formed a continuous 1.3 metres long sealed smooth sharp-edged rectangular cylinder. When a cylinder was tested vertically, a further four load cells were mounted on the frame supporting the cylinder above the water, two on the front and two on the side to measure the total in-line and transverse forces applied on the whole length of the cylinder to check and validate the force measurements located in the

test section.

These cylinders were tested in wavy flow, and in a combination of wavy and steady flows to simulate the presence of currents with waves. The size of the second set was made smaller in order to carry out experiments at low and moderate Keulegan-Carpenter numbers.

The aspect ratio was defined as d/D, where d was the cylinder section depth parallel to the flow generated, and D was the cylinder section width normal to the flow. With the first set of cylinders, experiments were carried out for five different aspect ratios d/D of 0.25, 0.5, 0.75, 1 and 2. These corresponded to the cylinders with d=10 cm and D=40 cm, d=20 cm and D=40 cm, d=30 cm and D=40 cm, d=40 cm and D=40 cm, and d=40 cm and D=20 cm.

With the second set of cylinders, experiments were carried out for three different aspect ratios d/D of 0.5, 1 and 2. These corresponded to the cylinders with d=10 cm and D=20 cm, d=10 cm and D=10 cm, and d=20 cm and D=10 cm.

Care was taken to provide a small gap (of the order of few millimetre) between the faces of each test section in order to avoid any interference between them.

Each cylinder from both sets was tested vertically as surface piercing and horizontally submerged with its axis parallel to the wave crests. When a cylinder was positioned vertically, the top end of the inner beam above water was fixed to the towing carriage. Figures 2.1a and 2.1b illustrate the set-up of a vertical cylinder from the first and second sets respectively. When a cylinder was positioned horizontally below water, each end of the inner beam was fixed to a vertical beam which was fixed to the towing carriage. Figures 2.2a and 2.2b illustrate the set-up of a horizontal cylinder from the first and second sets respectively.

2.3 THE SIMULATED FLOWS

The steady flow was produced by towing a cylinder in calm water along the middle of the tank for different speeds, each representing a different Reynolds number. During a test run, a cylinder was towed at a maintained constant speed and the data were collected for 10 or 15 seconds depending on the magnitude of the speed. The subsequent test was run only after the water was completely at rest. The Reynolds number attained was up to 8×10^5.

The wavy flow was simulated by the wave-maker generating regular waves with

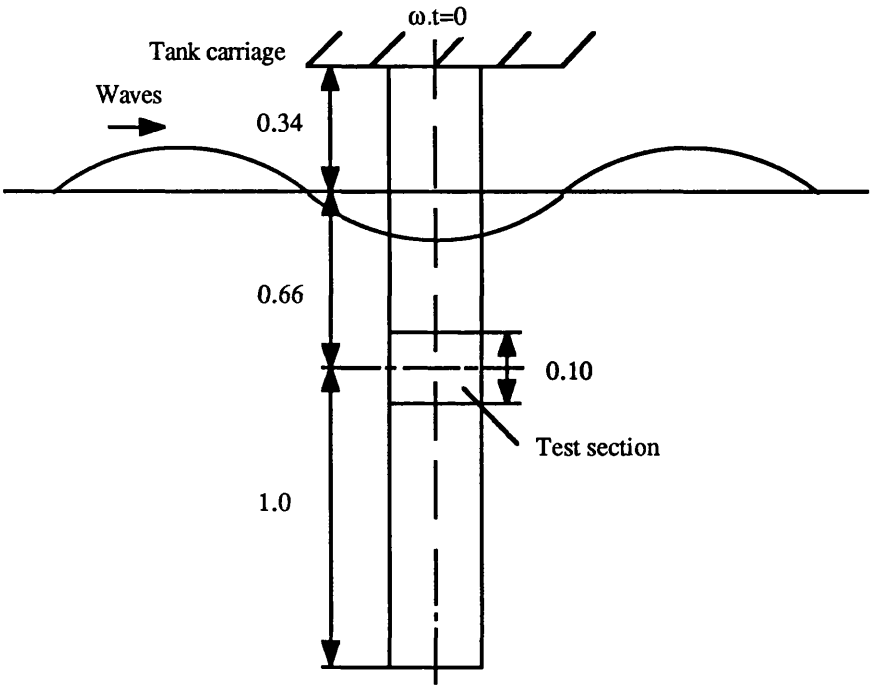

Figure 2.1a Set-up of a vertical cylinder from the 1st set

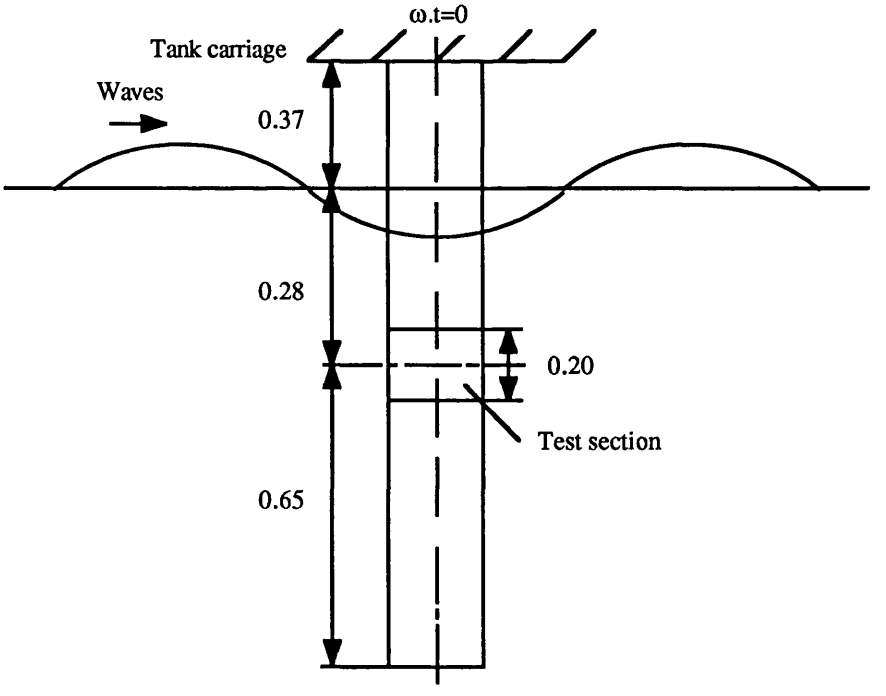

Figure 2.1b Set-up of a vertical cylinder from the 2nd set

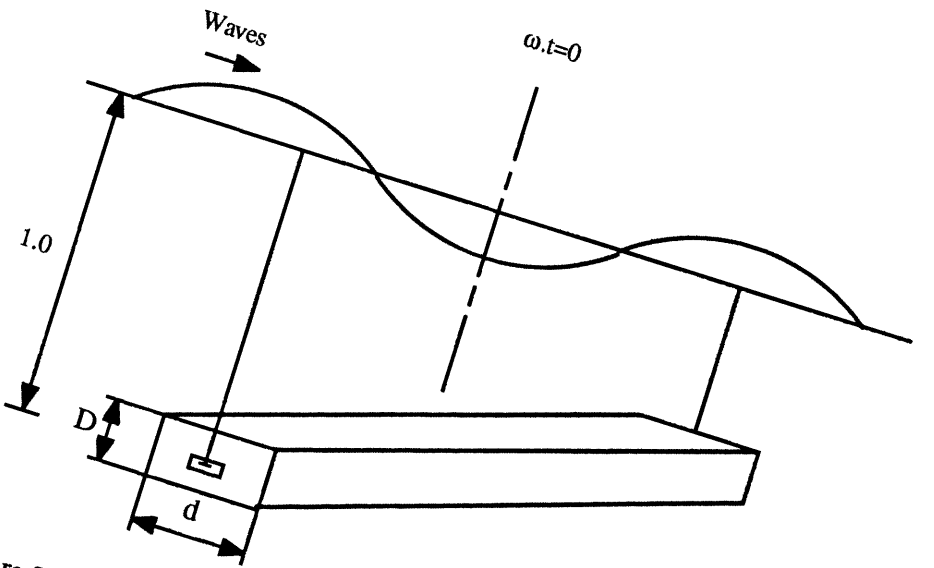

Figure 2.2a Set-up of a horizontal cylinder from the 1st set

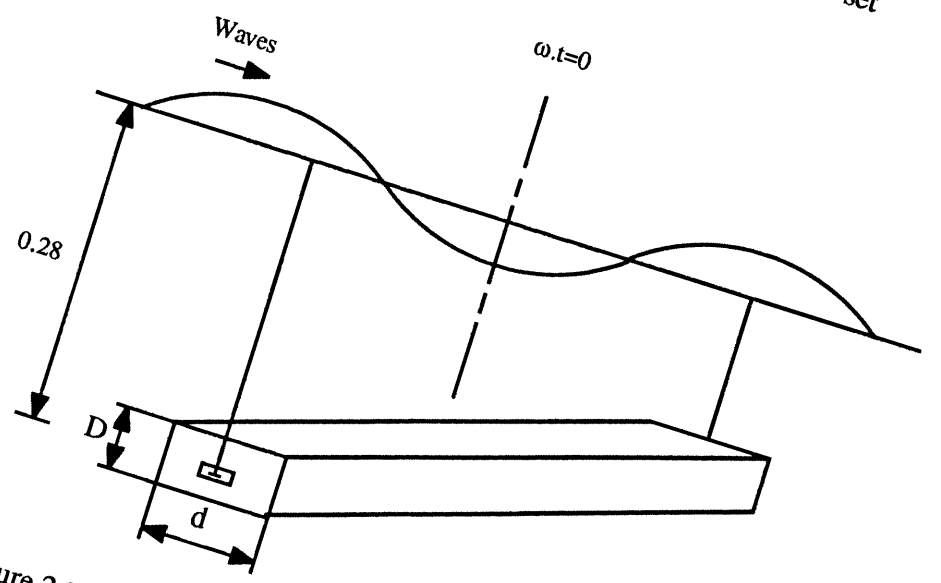

Figure 2.2b Set-up of a horizontal cylinder from the 2nd set

the cylinder to be tested being stationary and placed about 20 metres ahead of the wave-maker.

With the first set of cylinders, each cylinder was tested for two different wave periods of 1.67 and 2.5 seconds (equivalent to frequencies of 0.6 and 0.4 Hertz). Thus, every cylinder was tested for two fixed values of the frequency parameter β. The KC number was varied with the variation of the wave height for a fixed wave period. This was done by varying the voltage from the input signal of the wave-maker while keeping the wave period constant. The range of the KC number was up to 1.2 and the maximum Reynolds number attained was 6.4×10^4. The data were collected for 20-25 seconds.

With the second set of cylinders, each cylinder was tested for two different wave periods of 1.25 and 1.67 seconds (equivalent to frequencies of 0.8 and 0.6 Hertz) giving therefore two fixed values of β number. Similarly, the KC number was varied with the variation of the wave height for a fixed wave period. The range of the KC number was up to 4.5 and the maximum Reynolds number attained was 4.2×10^4.

The presence of currents with waves was simulated by towing the cylinders along the middle of the tank through oncoming regular waves at various constant speeds, each giving a different current reduced velocity. Each cylinder was tested for three different current reduced velocities for a fixed wave period and for several wave heights. The regular wave periods generated were 1.25 and 1.67 seconds giving therefore two fixed values of β number for every cylinder. The range of the KC number was up to 4 and the maximum Reynolds number attained was 4.2×10^4. The data were collected for 20-25 seconds.

2.4 TESTS MEASUREMENT EQUIPMENT

The strain gauge type load cells used were RDP model 31 with 2.54 cm (an inch) diameter and a height of 1.32 cm (0.52 inches) and a nominal capacity of 22.7 kg (50 lbs) and a resistance of 350 ohms. The load cell had a threaded stud on the base which was threaded into the test cylinder's inner beam flange at the height of the test section during assembly, and an active threaded stud which was threaded to one plate of the test section covering it and forming one face of the test section. The other faces of the test section were assembled in the same manner. The model 31 load cell was waterproof and had two welded stainless steel diaphragms on the top and bottom sides of the active

element to protect the load cell from the effects of off axis loading. After assembly inside the test section to the flanges and before being threaded to the faces of the test section, a silicone rubber was applied to the flanges and their bolts to seal them. The load cells were then connected to an amplifier one load cell per channel with their cables running inside the test cylinder through a small PVC tube which ran from the test section to one end of the test cylinder leaving the exterior of the cylinder perfectly smooth. The signals of the load cells, in the order of millivolts, were fed to the input of an amplifier of high impedance differential stage and high common mode rejection ratio of 120 dB. This allowed the amplifier to amplify only the signals from the load cells and to ignore any common mode signals. The amplifier sensitivity was set at 10 millivolts. This sensitivity achieved a highly accurate representation of the loads on the load cells. The signals from the amplifier were then taken to a low pass filter designed for a cut off frequency of 5 Hertz which removed any noise in the signals. The filter was a Sallen-Key 2 poles Butterworth filter and had an attenuation of 40 dB at 50 Hertz, thus filtering out any mains hum on the signals.

The load cells were individually calibrated first in air before assembly by applying different weights and checking that they behaved similarly. Once the load cells were built into the test section and fixed to its faces and the test model positioned in the desired orientation in water prior to test runs, they were carefully aligned and then calibrated in water for tension and compression through the use of a system comprising a frictionless pulley mounted on a vertical traverse and a set of weights. Adjusting the traverse, a horizontal load was applied to the face of the test section and hence to the load cell built in it. The same operation was repeated for each face of the test section. Therefore, the calibration was carried out for both in-line and transverse forces. Then a calibration factor was determined for each load cell and used later in the computer program analysis to convert output data into forces. For the first set of cylinders, when calibrating the front or rear face of the test section the response signal of the opposite face was taken into account in the calibration factor as an induced force.

Each load cell was connected to an amplifier with one channel per load cell to form a full bridge. Other channels were connected to wave probes for measuring wave phase angles, and when necessary for measuring wave heights.

Figures 2.3 and 2.4 illustrate the electronic equipment on the observation platform and a vertical cylinder during the tests respectively.

Because of the large size of the towing tank section compared to that of the test models,

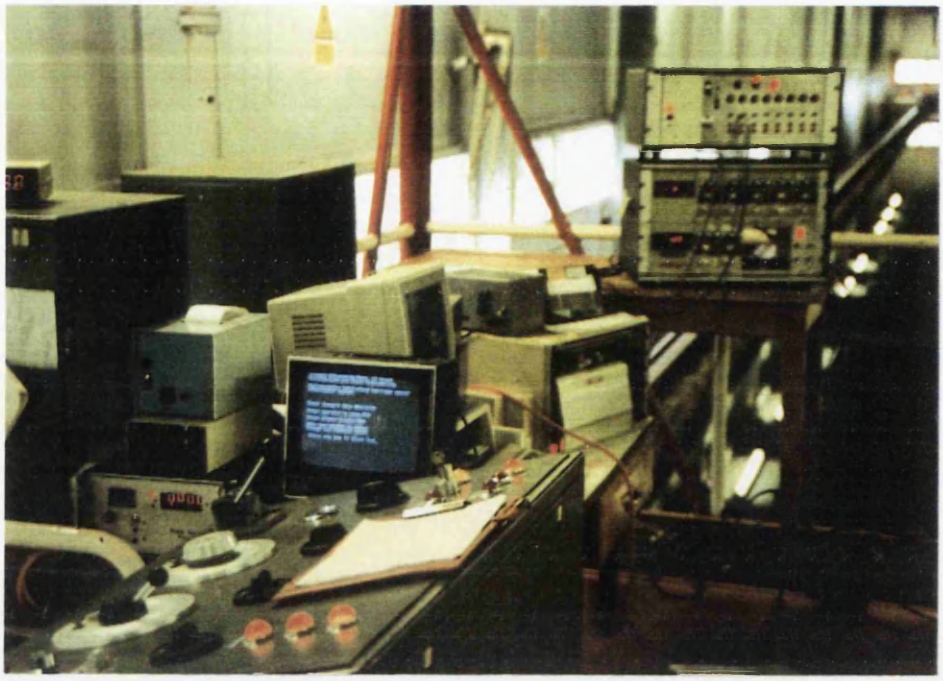

Figure 2.3 Electronic equipment on the observation platform

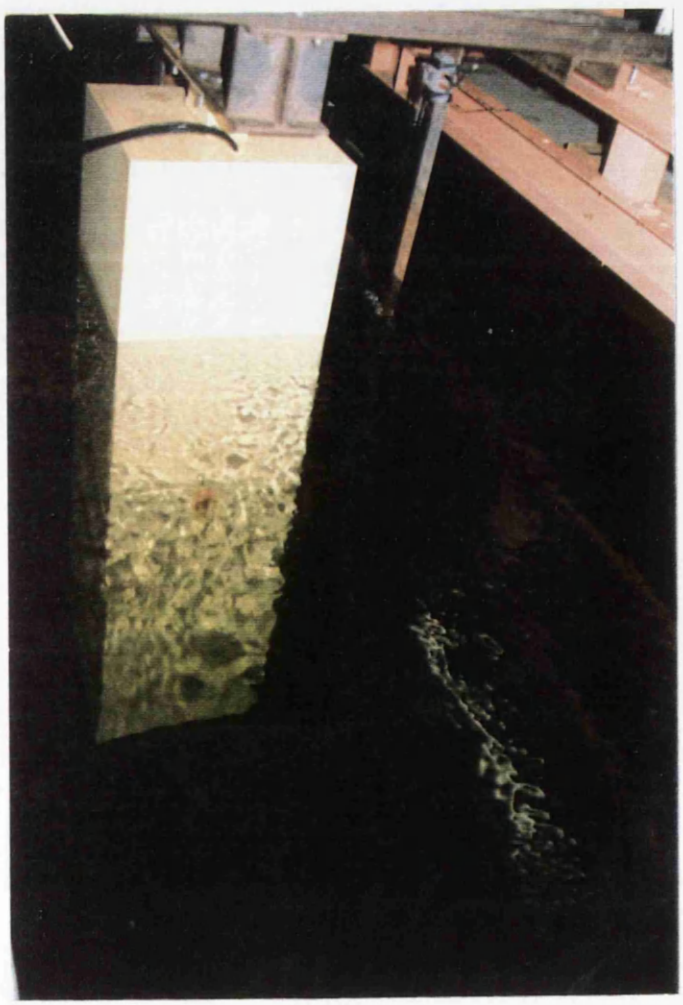

Figure 2.4 A vertical square cylinder during tests

no correction for blockage effects was necessary. The sampling rate was 100 samples per second per channel.

CHAPTER 3

DATA ANALYSIS TECHNIQUES

3.1 STEADY FLOW

In steady flow, the drag coefficient C_D was calculated as

$$C_D = \frac{F}{0.5\rho DV^2}, \tag{3.1}$$

where F is the measured drag force per unit length,

V is the towing tank carriage speed,

D is the test model section side normal to the stream, and

ρ is the tank water density.

The force F and the speed V used to determine C_D coefficient were taken as the average values of the force and speed records measured during the data collection.

3.2 WAVY FLOW

3.2.1 WAVE KINEMATICS

The simplest and most useful of all wave theories is the linear or Airy wave theory. Despite its simplicity, it offers a powerful analytical solution for gravity waves. However, the following assumptions have to be invoked.

(1) The wave height is small compared with the wavelength or water depth. This assumption allows the free surface boundary conditions to be linearised by neglecting wave height terms which are beyond the first order. This assumption also allows the free surface conditions to be satisfied at the mean water level, rather than at the oscillating free surface.

(2) The water is of uniform density with constant water depth.

(3) Viscosity and surface tension effects are negligible.

(4) The wave motion is irrotational.

More details about the linear wave theory and other wave theories can be found in Wiegel (1964), Myers et al. (1969), Sarpkaya and Isaacson (1981), Chakrabarti (1987), Patel (1989) and Barltrop et al. (1990). On the stretching techniques used at the free

surface, Swan (1990) investigated the wave kinematics of three wave forms throughout the crest to trough region to measure the maximum horizontal velocity component occurring beneath the wave crest and trough. He found no evidence to suggest that the steady wave theories overestimate the positive velocities occurring beneath the wave crest and underestimate the negative velocities occurring beneath the wave trough because of the free surface boundary layer.

The linear wave theory has been chosen in this study to compute the wave kinematics for its simplicity and also because the towing tank satisfies at least the first two conditions.

The linear wave theory gives the sinusoidal velocity and acceleration of the wave water as

$$u=-u_m\cos\theta \tag{3.2}$$

and

$$\dot{u}=u_m\frac{2\pi}{T}\sin\theta, \tag{3.3}$$

where $\theta = 2\pi t/T$,

t is the time,

T is the wave period, and

where the water particle maximum velocity u_m at the centre of the test section is given by

$$u_m=\frac{H}{2}\frac{2\pi}{T}e^{-ky}, \tag{3.4}$$

where H is the wave height,

k is the wave number given by $k=\omega^2/g$,

ω is the angular frequency given by $\omega=2\pi/T$,

g is the acceleration of gravity, and

y is the depth of the test section in water.

With regard to wave phases, t=0 is defined as the moment when a wave trough coincides with the cylinder's axis (see Figures 2.1a,b).

In the case of a horizontally submerged cylinder in waves, the kinematics of water particle will consist of a vertical and a horizontal component. The vertical and horizontal velocities are given as

$$u_x=-u_m\cos\theta \tag{3.5}$$

$$u_y=u_m\sin\theta \tag{3.6}$$

respectively, where x refers to horizontal direction and y to vertical direction.

Because the towing tank satisfies the deep waves condition (depth/wave length>0.5), the water particle maximum velocity u_m (eq. 3.4) at the centre of the test section is assumed in this study to be the same in either directions.

The vertical water particle acceleration is thus given as

$$\dot{u}_y = u_m \frac{2\pi}{T} \cos\theta. \tag{3.7}$$

3.2.2 FORCE COEFFICIENTS

The force per unit length acting on a vertical cylinder can be represented by

$F = f(t, T, u_m, D, \rho, \nu)$

and on the basis of dimensional analysis, the non-dimensional force is given by

$$C_F = \frac{F}{0.5\rho u_m^2 D} = f\left(\frac{t}{T}, \frac{u_m T}{D}, \frac{u_m D}{\nu}\right) \tag{3.8}$$

or replacing t/T by θ

$$C_F = f\left(\theta, \frac{u_m T}{D}, \frac{u_m D}{\nu}\right) \tag{3.9}$$

where $u_m T/D$ is the Keulegan-Carpenter KC number, and $u_m D/\nu$ is the Reynolds number.

The KC number can be written as $KC = 2\pi\eta e^{-ky}/D$ where η is the wave amplitude. This parameter expresses the ratio of the diameter of orbital wave motion at the depth of the cylinder centre to the diameter of the cylinder. If for instance $KC = \pi$, the diameter of the orbital motion is equal to that of the cylinder.

Substituting u and $\dot{u}$ in the Morison equation (eq. 1.10) by their expressions in (eq. 3.2) and (eq. 3.3), the non-dimensionalised Morison equation becomes

$$C_F = \frac{F}{0.5\rho u_m^2 D} = 4\pi C_M \frac{A}{D^2} \frac{D}{u_m T} \sin\theta - C_D \cos\theta |\cos\theta| \tag{3.10}$$

where A=Dxd is the cross-section area of the cylinders.

Representing the measured force by a Fourier series and comparing with (eq. 3.10) will yield expressions for inertia and drag C_M and C_D coefficients. This analysis was first carried out by Keulegan and Carpenter (1958). The method is shown in details in Appendix 1.

From Fourier analysis, C_M and C_D coefficients are found as

$$C_M = \frac{D^2}{2A\pi^2} \frac{u_m T}{D} \int_0^{2\pi} \frac{F \sin\theta}{\rho u_m^2 D} d\theta \tag{3.11}$$

and

$$C_D = -\frac{3}{4}\int_0^{2\pi} \frac{F\cos\theta}{\rho u_m{}^2 D} d\theta \qquad (3.12)$$

where F is the measured force per unit length.

These coefficients are obtained from the first term of series solutions giving C_M and C_D coefficients respectively, thus neglecting their variation with θ. The C_M and C_D coefficients are therefore assumed to be constant over a wave cycle. In this study, only constant averaged values of these coefficients are presented.

Another common method of obtaining C_M and C_D coefficients is the least squares technique. This has a more general application and can be used in cases where the water particle kinematics are not necessarily sinusoidal, e.g. in random waves. The technique is based on the minimisation of the error between the measured force and that predicted by Morison's equation in a least square sense. Therefore, if E is the error between the measured force per unit length (F) and computed force per unit length (F_c), one has

$$E = F - F_c . \qquad (3.13)$$

Then, C_M and C_D coefficients are calculated such that the quantity $\int_0^T E^2 dt$ is at a minimum. This results in

$$\int_0^T E\frac{\partial E}{\partial C_M} = 0 \qquad (3.14)$$

and

$$\int_0^T E\frac{\partial E}{\partial C_D} = 0. \qquad (3.15)$$

The above equations yield

$$C_{M_{LS}} = \frac{D^2}{2A\pi^2}\frac{u_m T}{D}\int_0^{2\pi} \frac{F\sin\theta}{\rho u_m{}^2 D} d\theta = C_M \qquad (3.16)$$

and

$$C_{D_{LS}} = -\frac{8}{3\pi}\int_0^{2\pi} \frac{F\cos\theta|\cos\theta|}{\rho u_m{}^2 D} d\theta \qquad (3.17)$$

where the subscript 'LS' refers to least squares. The Fourier averaging technique and the least squares method yield identical inertia coefficient values.

A third method occasionally used is wave by wave basis analysis (Davies et al. (1990)). This method is particularly useful when analysing random signals over a long sample of data. However, most of the research on fluid loading in regular waves is based on

Fourier analysis when C_M and C_D coefficients are obtained from the experiments. In this study, Fourier analysis was used and C_M and C_D coefficients were obtained from (eq. 3.11) and (eq. 3.12) respectively. In order to compare the values of C_D coefficient obtained using Fourier analysis method (eq. 3.12) with those obtained using the least squares method (eq. 3.17), the drag coefficients of the second set of cylinders in regular waves were derived using both techniques. The comparison is given in Chapter 4.

For a horizontally submerged cylinder in waves, the total horizontal and vertical force components per unit length are given as

$$F_x = \frac{1}{2}\rho D C_{Dx} u_x \sqrt{u_x^2+u_y^2} + \rho A C_{Mx} \dot{u}_x \tag{3.18}$$

and

$$F_y = \frac{1}{2}\rho d C_{Dy} u_y \sqrt{u_x^2+u_y^2} + \rho A C_{My} \dot{u}_y \tag{3.19}$$

respectively, where d is the other side length of the rectangular cylinder normal to the vertical water particle velocity. Replacing u_x and u_y by their expressions, the forces become

$$F_x = -\frac{1}{2}\rho D C_{Dx} u_m^2 \cos\theta + \rho A C_{Mx} u_m \frac{2\pi}{T}\sin\theta \tag{3.20}$$

and

$$F_y = \frac{1}{2}\rho d C_{Dy} u_m^2 \sin\theta + \rho A C_{My} u_m \frac{2\pi}{T}\cos\theta. \tag{3.21}$$

The determination on the horizontal and vertical inertia and drag coefficients C_{Mx}, C_{Dx} and C_{My}, C_{Dy} is carried out by multiplying F_x and F_y once by $\cos\theta$ and once by $\sin\theta$ and integrating between 0 and 2π (steps similar to those for the case of vertical cylinders, see Appendix 1).

Bearing in mind that

$$\int_0^{2\pi} \sin^2\theta\, d\theta = \int_0^{2\pi} \cos^2\theta\, d\theta = \pi$$

and

$$\int_0^{2\pi} \sin\theta\cos\theta\, d\theta = 0$$

the vertical and horizontal C_D coefficients are obtained as

$$C_{Dx} = -\frac{2}{\pi}\int_0^{2\pi} \frac{F_x \cos\theta}{\rho u_m^2 D} d\theta, \tag{3.22}$$

and

$$C_{Dy}=\frac{2}{\pi}\int_0^{2\pi}\frac{F_y\sin\theta}{\rho u_m{}^2 d}d\theta, \tag{3.23}$$

and the vertical and horizontal C_M coefficients are obtained as

$$C_{Mx}=\frac{T}{2\pi^2\rho A u_m}\int_0^{2\pi}F_x\sin\theta d\theta=\frac{D^2}{2A\pi^2}\frac{u_m T}{D}\int_0^{2\pi}\frac{F_x\sin\theta}{\rho u_m{}^2 D}d\theta, \tag{3.24}$$

and

$$C_{My}=\frac{T}{2\pi^2\rho A u_m}\int_0^{2\pi}F_y\cos\theta d\theta=\frac{d^2}{2A\pi^2}\frac{u_m T}{d}\int_0^{2\pi}\frac{F_y\cos\theta}{\rho u_m{}^2 d}d\theta. \tag{3.25}$$

The measured force per unit length can also be represented in terms of the maximum measured force during a wave cycle. The non-dimensionalised maximum force coefficient is given by

$$C_{F\max}=\frac{F_{MAX}}{0.5\rho D u_m{}^2} \tag{3.26}$$

where F_{MAX} is the maximum measured force per unit length in a cycle.

In addition to this force coefficient, the measured force per unit length can also be represented in terms of its non- dimensionalised root mean square value given by

$$C_{Frms}=\sqrt{\frac{1}{T}\int_0^T\frac{F^2}{(0.5\rho u_m{}^2 D)^2}dt} \tag{3.27}$$

This coefficient was calculated from the measured force in this study by numerically evaluating the integral. The Morison equation gives the calculated root mean square force coefficient as

$$C_{Frms}=\sqrt{\frac{1}{2}\left(\frac{3}{4}C_D{}^2+\frac{16d^2\pi^2}{u_m{}^2T^2}C_M{}^2\right)}. \tag{3.28}$$

The method of determining this coefficient is given in Appendix 2.

In this study the measured and calculated root mean square force coefficients were evaluated and compared for identical values of the governing parameters.

The lift or transverse force is in nature irregular and its description presents a problem. However, it is usually represented in terms of the maximum measured force during a cycle and in terms of its root mean square value of the entire record of data. In this study, two root mean square force coefficients were determined in addition to the maximum force coefficient.

The first coefficient of the lift force is defined in this study as a function of the maximum

peak of the lift force recorded in a cycle. It is given by

$$C_{L\max} = \frac{\text{maximum peak of the transverse force per unit length in a cycle}}{0.5\rho u_m^2 D}. \tag{3.29}$$

The first rms lift force coefficient is defined as a function of the maximum water particle velocity u_m as

$$C_{Lrms} = \sqrt{\frac{1}{T}\int_0^T \frac{(\text{measured transverse force per unit length})^2}{(0.5\rho u_m^2 D)^2} dt}. \tag{3.30}$$

The second rms lift force coefficient is defined as a function of the root mean square value of the square of the instantaneous water particle velocity as

$$C_{Lurms} = \frac{\text{rms value of transverse force per unit length}}{0.5\rho D u^2(\text{rms})} \tag{3.31}$$

which yields

$$C_{Lurms} = \frac{\sqrt{\frac{1}{T}\int_0^T \frac{(\text{measured transverse force per unit length})^2}{(0.5\rho D)^2} dt}}{\sqrt{\frac{1}{T}\int_0^T (u^2)^2 dt}}. \tag{3.32}$$

The inertia C_M and drag C_D coefficients were used in this study to describe the in-line forces on the first set of cylinders. For the second set of cylinders where the range of KC number is higher, C_M, C_D, C_{Fmax}, C_{Frms}, C_{Lmax}, C_{Lrms} and C_{Lurms} were used to describe the in-line and transverse forces.

These coefficients were obtained by running the computer program repeatedly over a record of data of different numbers of wave cycles from about 20 cycles (20 cycles corresponded to about the maximum number of cycles recorded during the experiments in wavy flow), each time cutting down the number of cycles, up to a record of data of one cycle. Individual cycles were also examined to determine these coefficients. The above coefficients presented in this study were the average values of the coefficients obtained for different records of data.

3.3 COMBINED WAVY AND STEADY FLOWS

The Morison equation can be modified to take into account the presence of a current with the waves. It is generally written to express the in-line force per unit length as

$$F=\frac{1}{2}\rho D C_D(V_C+u)|V_C+u|+\rho A C_M \dot{u} \tag{3.33}$$

where C_M and C_D are inertia and drag coefficients in the presence of a current and are different from those of the no current case. V_C is the current velocity.

For a horizontal cylinder in waves and current, the in-line force per unit length is expressed as

$$F=\frac{1}{2}\rho D C_D(V_C+u_x)|V_C+u|+\rho A C_M \dot{u}_x \tag{3.34}$$

where $u = u_x + u_y$. (3.35)

Note that if V_C is zero, (eq. 3.33 and 3.34) would be identical to those in wavy flow.

This method of determining the hydrodynamic forces acting on a cylinder in a combination of wavy and steady flows assumes that the effects of the current are considered by linear superposition of the current velocity on the wave velocity field generated in the absence of the current, and that the current is collinear with the wave propagation.

Replacing the wave particle velocity and acceleration in (eq. 3.33) by their expressions given in (eq. 3.2) and (eq. 3.3), (eq. 3.33) becomes

$$F=\frac{1}{2}\rho D C_D(V_C-u_m\cos\theta)|V_C-u_m\cos\theta|+\rho A C_M \frac{2\pi}{T}u_m\sin\theta. \tag{3.36}$$

The method of determining C_M and C_D coefficients is similar to that in wavy flow which is based on the Fourier averaging technique (Sarpkaya et al. (1984), Sarpkaya and Storm (1985) and Chakrabarti (1987)). This method is shown in appendix 3. The inertia coefficient is found as

$$C_M=\frac{D^2}{2A\pi^2}\frac{u_m T}{D}\int_0^{2\pi}\frac{F\sin\theta}{\rho u_m{}^2 D}d\theta \tag{3.37}$$

which is similar to that of wavy flow since V_C, which does not appear explicitly, is assumed to be time invariant.

The drag coefficient is found as

$$C_D=\frac{\int_0^{2\pi} F\cos\theta}{\pi\rho D u_m V_C}d\theta \tag{3.38}$$

where $V_C/u_m \geq 1$, which is the case in this study.

The expression giving C_D coefficient for $V_C/u_m < 1$ is given in Appendix 3.

Other force coefficients were generated in this study to describe the in-line and transverse forces due to waves and currents.

The first coefficient is expressed in terms of the maximum in-line force recorded in a cycle as

$$C_{F\max} = \frac{F_{MAX}}{0.5\rho D(u_m + V_C)^2} \tag{3.39}$$

where F_{MAX} is the maximum measured in-line force per unit length recorded in a cycle.

The second coefficient is defined in terms of the root mean square value of the in-line force as

$$C_{Frms} = \sqrt{\frac{1}{T}\int_0^T \frac{F^2}{(0.5\rho(u_m + V_C)^2 D)^2}dt}. \tag{3.40}$$

The transverse force is described in this study with two coefficients as a function of the maximum and of the root mean square of the transverse force. They are given as

$$C_{L\max} = \frac{\text{maximum peak of the transverse force per unit length in a cycle}}{0.5\rho(u_m + V_C)^2 D}. \tag{3.41}$$

and

$$C_{Lrms} = \sqrt{\frac{1}{T}\int_0^T \frac{(\text{measured transverse force per unit length})^2}{(0.5\rho(u_m + V_C)^2 D)^2}dt} \tag{3.42}$$

The above six coefficients, C_M, C_D, C_{Fmax}, C_{Frms}, C_{Lmax} and C_{Lrms} were used to describe the in-line and transverse forces measured in waves and currents.

As in the case of wavy flow, these coefficients were obtained by analysing records of data of various numbers of wave cycles from about 25 cycles (25 cycles corresponded to about the maximum number of cycles recorded during the experiments in combined wavy and steady flows) up to a record of data of one cycle. Individual cycles were also analysed to determine these coefficients. The above coefficients presented in this study were the average values of the coefficients obtained for different records of data.

During the experiments, the data collection started only after few waves passed the cylinder and care was taken to select the appropriate time collection before any wave had returned.

CHAPTER 4

RESULTS OF FORCE MEASUREMENTS

This Chapter gives the results of steady flow, wavy flow and combined wavy and steady flows experiments without providing substantial discussion. The results are discussed in the next Chapter.

4.1 STEADY FLOW RESULTS

The steady drag forces were measured using the force measuring system described in Chapter 2. The drag coefficients were calculated from the average of the measured forces during the test run time of 20-25 seconds with 100 samples taken per second.

4.1.1 VERTICAL CYLINDERS

The drag coefficients C_D of vertical cylinders are plotted against Reynolds numbers for different aspect ratios in Figures 4.1 through 4.5.

Figure 4.1 shows the variation of C_D coefficient with Reynolds number for the square cross-sectional cylinder. The C_D coefficient was found to have a mean value of 1.03 with a standard deviation of 0.03. When the aspect ratio was reduced from unity to 0.75, Figure 4.2, C_D coefficient remained practically unchanged with a mean value of 1 and with the same standard deviation. When the aspect ratio was further reduced to 0.5, Figure 4.3, C_D coefficient decreased to a mean value of 0.75, a 27% reduction from that of the square cylinder, and with a standard deviation of 0.02. However, when the aspect ratio was reduced to 0.25, Figure 4.4, C_D coefficient increased to a mean value of 1.15, 12% higher than that of the square cylinder, and with a standard deviation of 0.08. Finally, when the aspect ratio was increased from unity to 2, Figure 4.5, C_D coefficient decreased by about 9% to a mean value of 0.94, and with a standard deviation of 0.06.

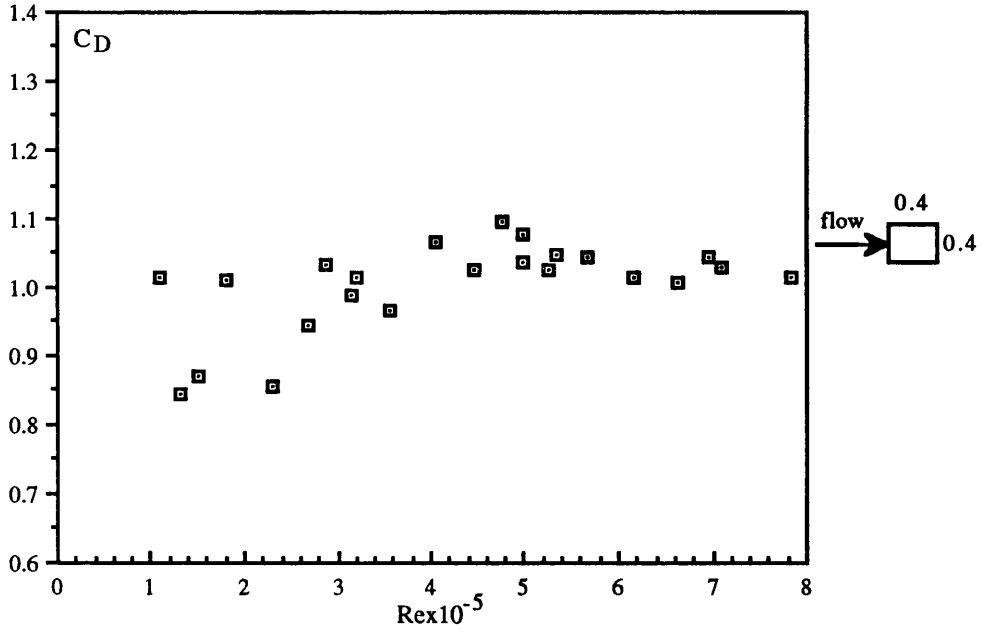

Fig. 4.1 C_D versus Re for a vertical cylinder with d/D=1 in steady flow

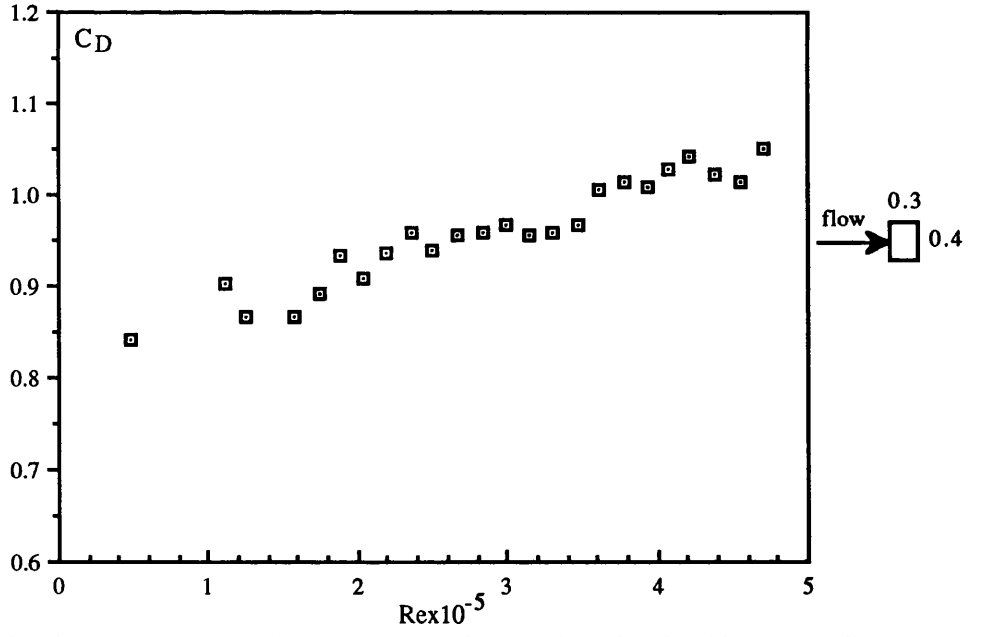

Fig. 4.2 C_D versus Re for a vertical cylinder with d/D=0.75 in steady flow

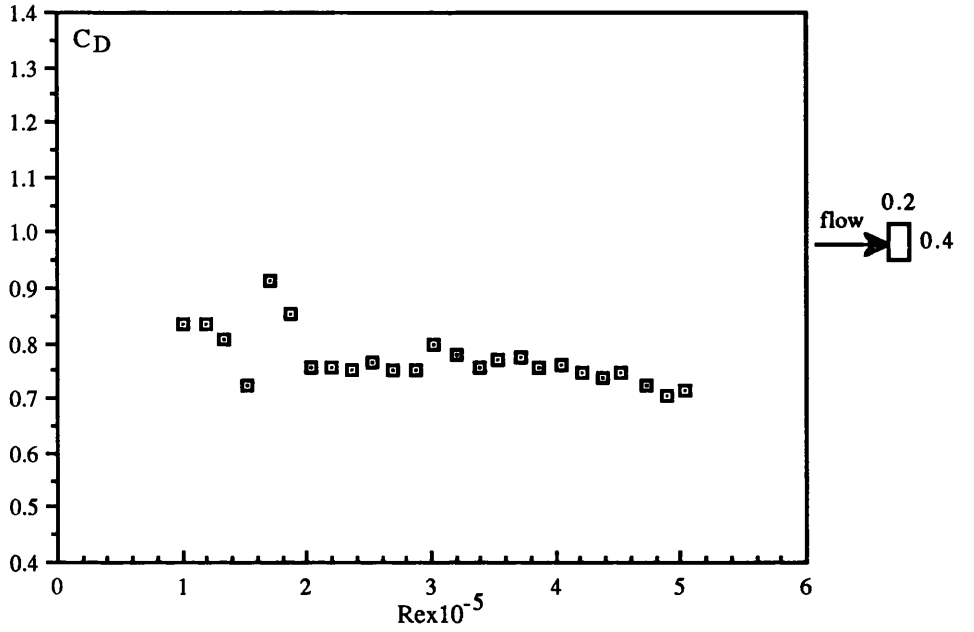

Fig. 4.3 C_D versus Re for a vertical cylinder with d/D=0.5 in steady flow

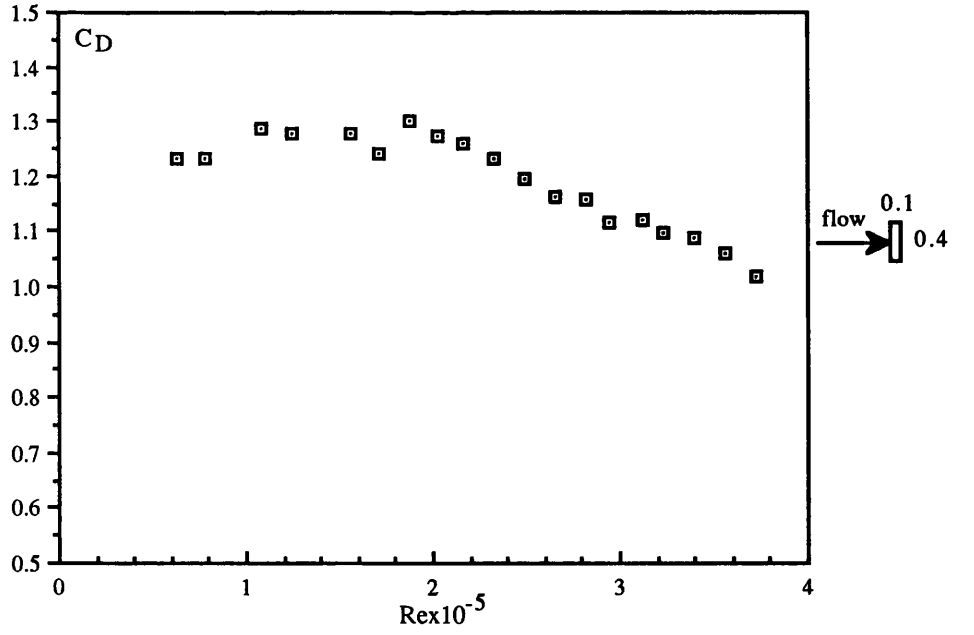

Fig. 4.4 C_D versus Re for a vertical cylinder with d/D=0.25 in steady low

4.1.2 HORIZONTAL CYLINDERS

The cylinders discussed in the previous section were also tested horizontally and C_D coefficients obtained are plotted against Reynolds numbers in Figures 4.6 through 4.10.

With the square cross-sectional cylinder, Figure 4.6, C_D coefficient was found to have a mean value of 0.95, about 8% less than that of the vertical cylinder. The standard deviation was 0.03. When the aspect ratio was reduced to 0.75, Figure 4.7, C_D coefficient increased by about 32% to a mean value of 1.25, and with a standard deviation of 0.02. On the effect of the cylinder's orientation, C_D coefficient of this cylinder was found to be 25 % higher than when tested vertically. When the aspect ratio was further reduced to 0.5, Figure 4.8, C_D coefficient decreased to a mean value of 0.87, 8% smaller than that of the square cylinder, and with a standard deviation of 0.01. When the orientation of this cylinder changed from vertical to horizontal, C_D coefficient increased by 16%. When the aspect ratio was reduced to 0.25, Figure 4.9, C_D coefficient increased to a mean value of 1.5, 58% higher than that of the square cylinder, and with a standard deviation of 0.07. With this cylinder, C_D coefficient increased by 30% when its orientation changed from vertical to horizontal. Finally, when the aspect ratio increased from unity to 2, Figure 4.10, C_D coefficient decreased by 13% to a mean value of 0.83, and with a standard deviation of 0.03. As with the square cylinder, C_D coefficient of this cylinder decreased by 12% when its orientation changed from vertical to horizontal.

Little scatter was found with the different results given above and this is shown by the small values of the standard deviations found with the different cylinders tested vertically and horizontally. The drag coefficients were found to be practically independent of the Reynolds number above about $2x10^5$ with most cylinders.

Figure 4.11 summarises the effects of varying the aspect ratio and orientation of the different cylinders on C_D coefficients at a Reynolds number of $2x10^5$. The results were compared with those of the Engineering Science Data Unit (1971) obtained mainly from wind tunnel experiments using cylinders with a length to width L/D ratio of 5 which corresponds to the ratio of most cylinders discussed above (L/D=2/0.4=5). There was some disagreement between the present results and those obtained from the ESDU. The results of the ESDU were obtained with long cylinders mounted between end plates,

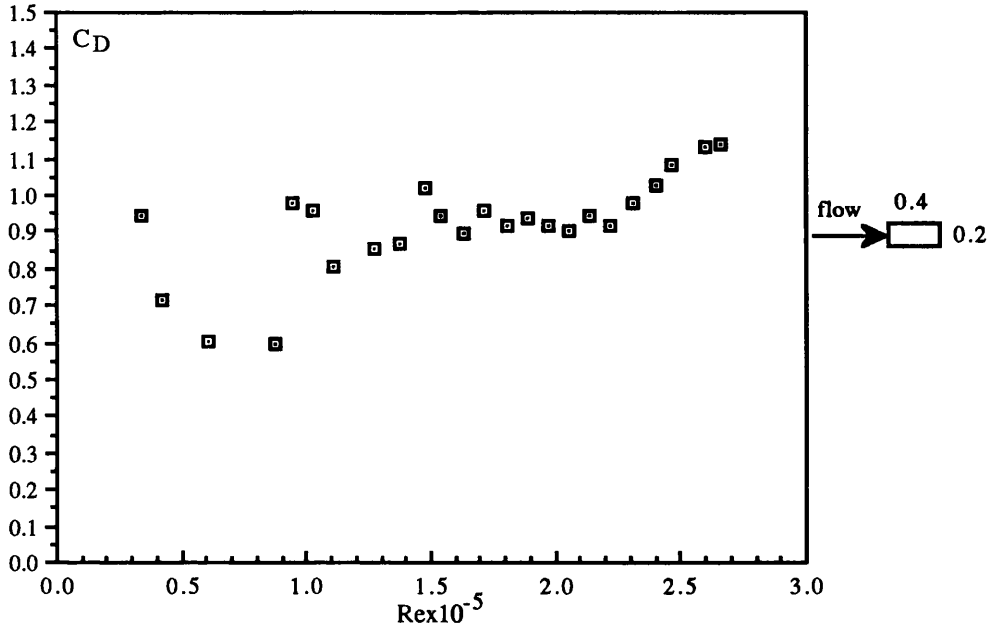

Fig. 4.5 C_D versus Re for a vertical cylinder with d/D=2 in steady flow

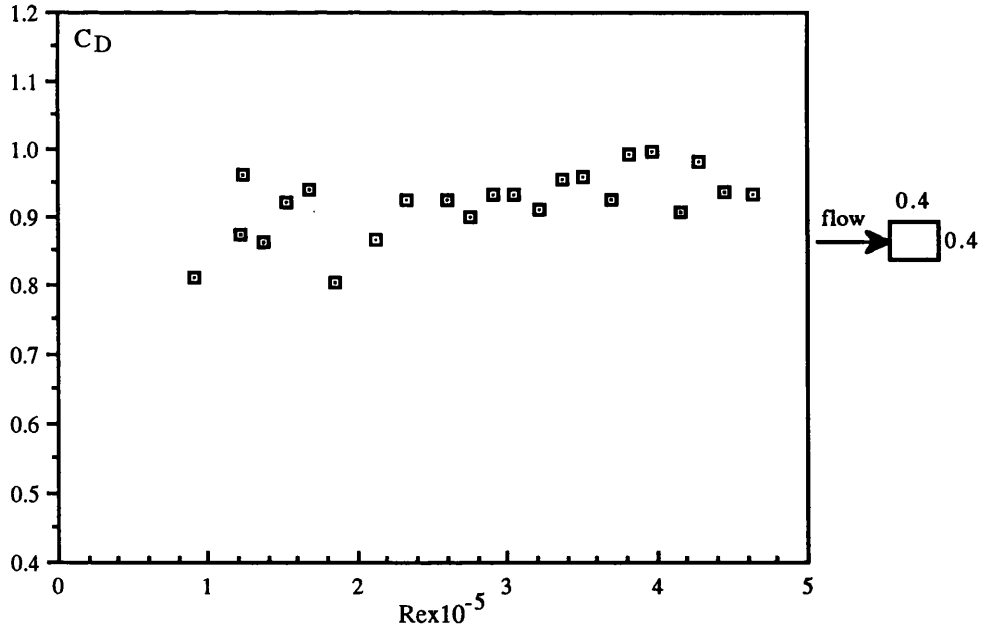

Fig. 4.6 C_D versus Re for a horizontal cylinder with d/D=1 in steady flow

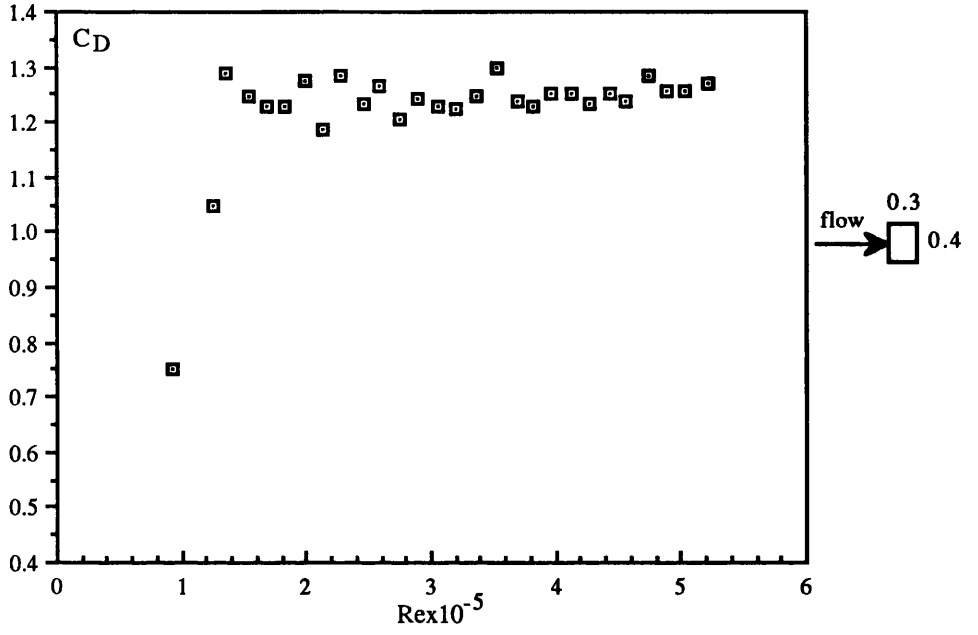

Fig. 4.7 C_D versus Re for a horizontal cylinder with d/D=0.75 in steady flow

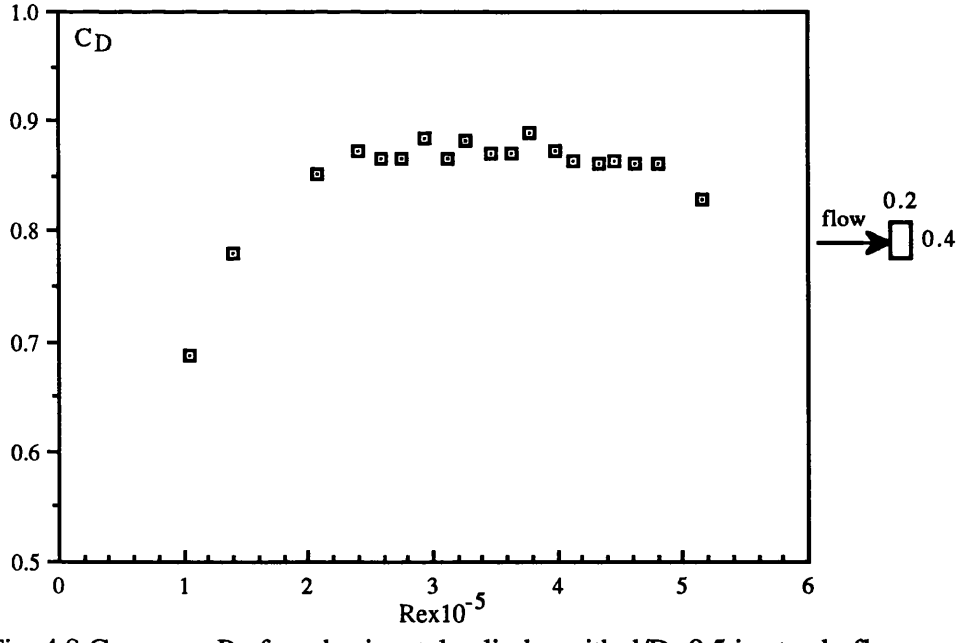

Fig. 4.8 C_D versus Re for a horizontal cylinder with d/D=0.5 in steady flow

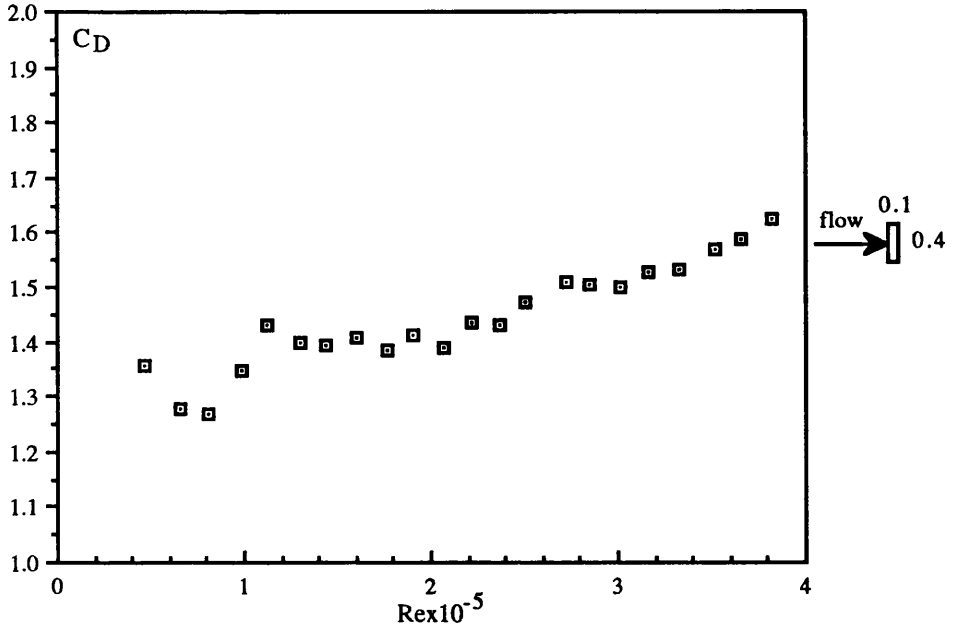

Fig. 4.9 C_D versus Re for a horizontal cylinder with d/D=0.25 in steady flow

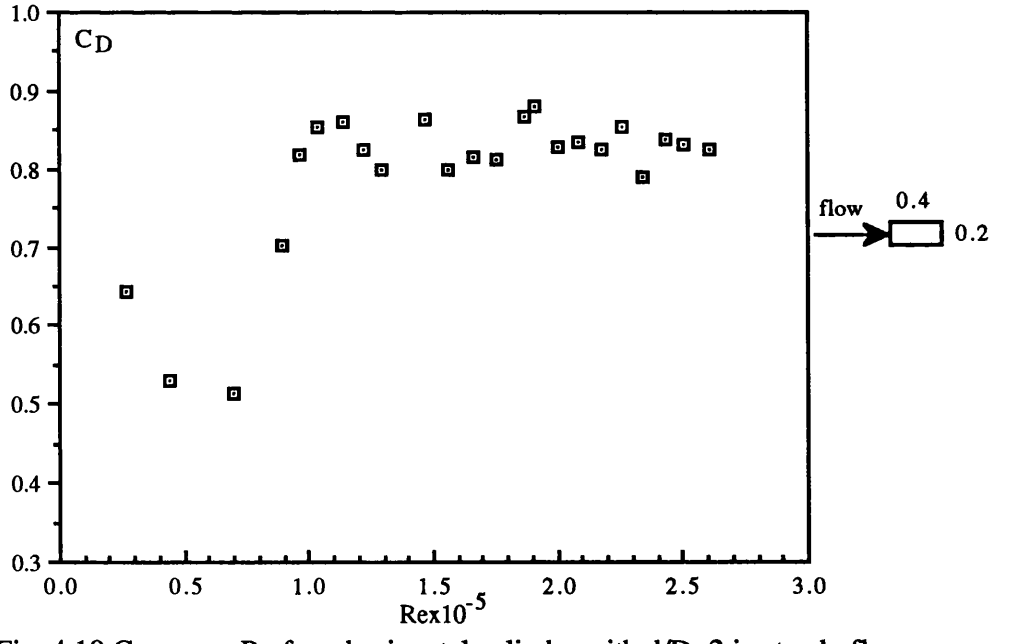

Fig. 4.10 C_D versus Re for a horizontal cylinder with d/D=2 in steady flow

and hence tested in an unbounded flow. In the present tests, the free surface and end effects inducing a cross flow could be the main reason for the discrepancy. An other reason may be attributed to the difference in Reynolds numbers at which measurements reported by the ESDU and the present measurements were conducted. The results of the ESDU are given for a wide range of Reynolds numbers between 10^4 and 10^6.

When the length to width L/D ratio is increased considerably the flow becomes two-dimensional with no free end or free surface to distort it when it passes a cylinder. The results shown in Figure 1.3 were obtained in such conditions from experiments carried out in wind tunnels where the models were either very tall spanning the whole height of the tunnel or very tall and mounted between end plates ensuring therefore the uniformity of the flow. As the L/D decreases the flow past the cylinders becomes less two-dimensional and C_D coefficient becomes further reduced. Under these conditions, the effect of varying the aspect ratio on C_D coefficient was found to be less important than when the cylinders were tested in a two-dimensional flow (see Figure 1.3). More detailed data on the effects of d/D on C_D coefficient for various values of L/D can be found in the ESDU (1976) publication no 71016.

4.1.3 VERTICAL ROUNDED CYLINDERS

The effect of rounding the corners of the cylinders was examined by measuring the drag coefficients of vertical corner-rounded cylinders and comparing them with those of vertical sharp edged cylinders.

Four aspect ratios d/D namely, 0.5, 0.75, 1 and 2 were investigated. As shown in Figures 4.12 through 4.15, the effect of corner radiusing on C_D coefficients for each cylinder was found to be small for the values of r/D considered (r is corner radius).

The author believes that the effect of rounding the corners of a cylinder in steady flow is minimised by the cross flow induced by the three dimensionality of the flow as it is thought to be the case in this study. When the flow is two-dimensional, rounding the corners of a cylinder has the immediate effect of reducing the drag coefficient as confirmed by Delany and Sorensen (1953).

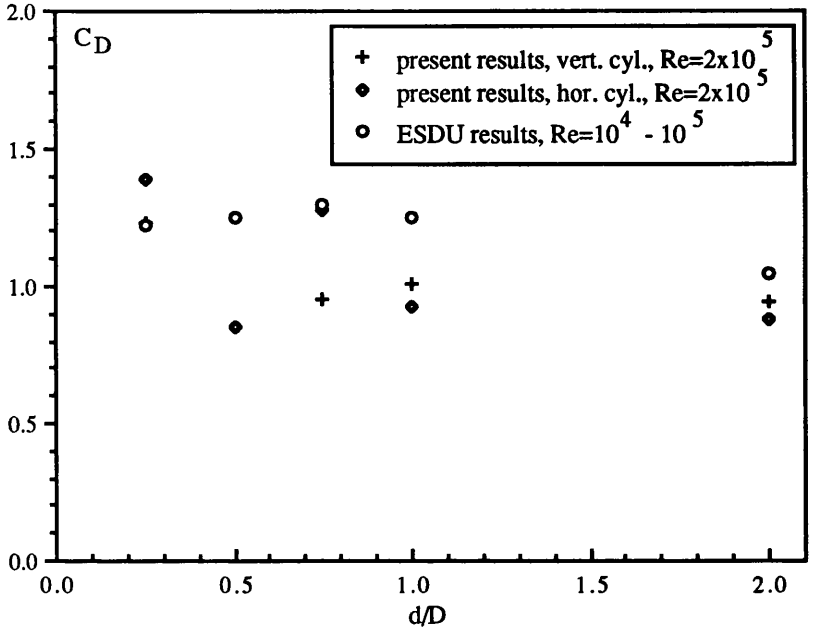

Fig. 4.11 C_D versus d/D for a steady flow

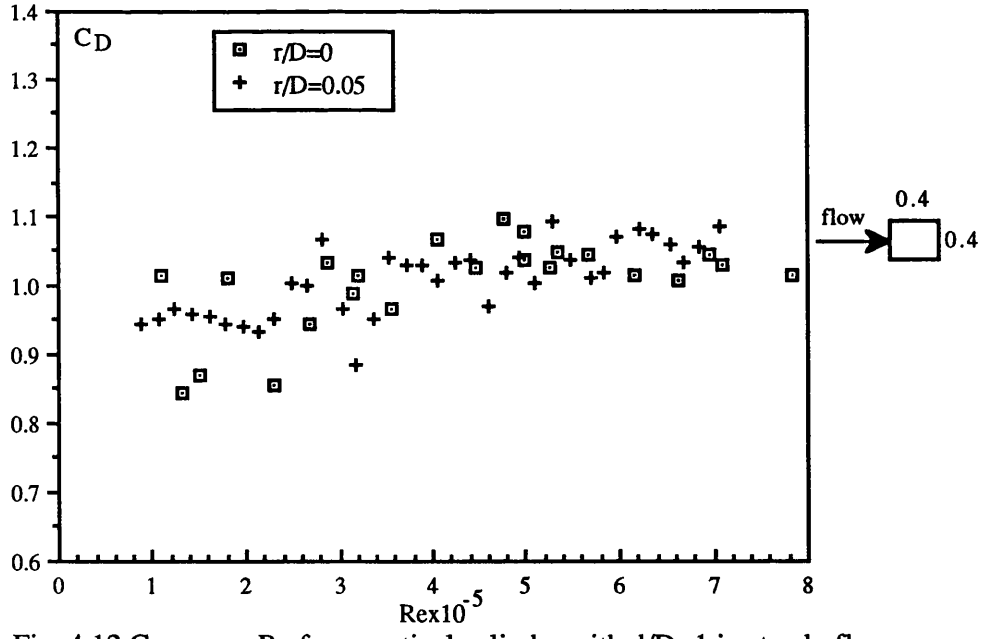

Fig. 4.12 C_D versus Re for a vertical cylinder with d/D=1 in steady flow

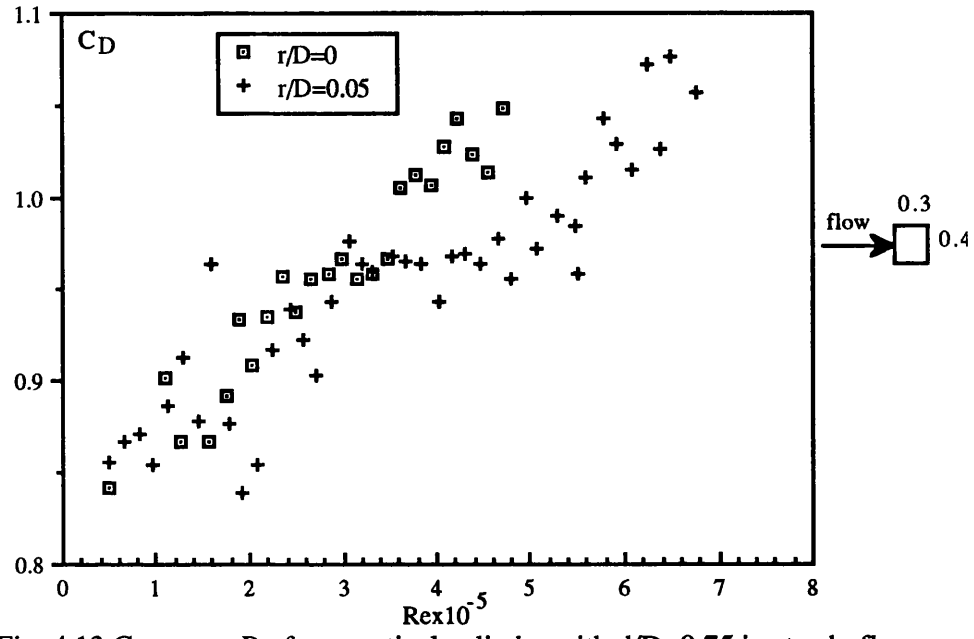

Fig. 4.13 C_D versus Re for a vertical cylinder with d/D=0.75 in steady flow

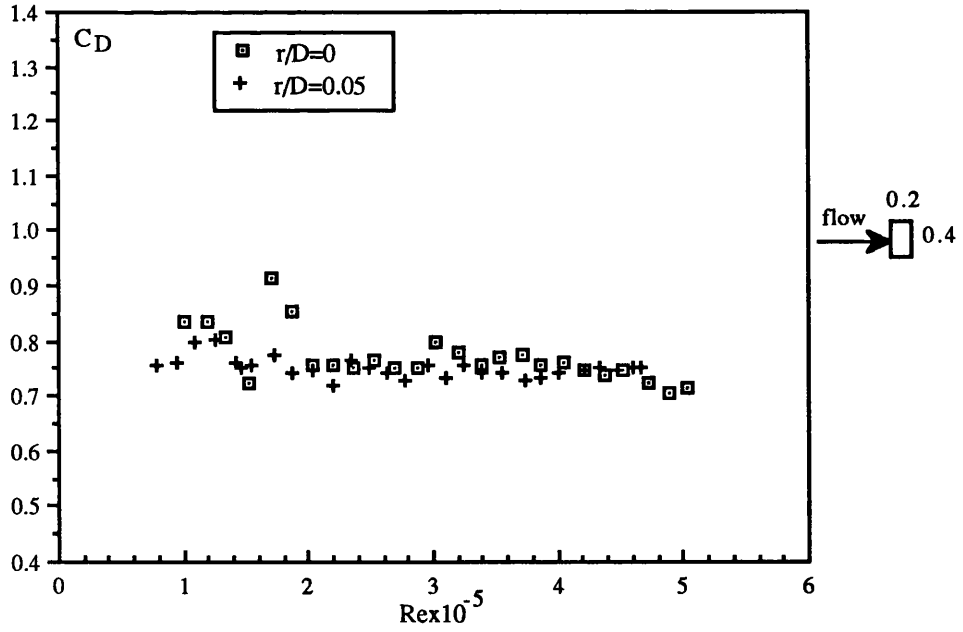

Fig. 4.14 C_D versus Re for a vertical cylinder with d/D=0.5 in steady flow

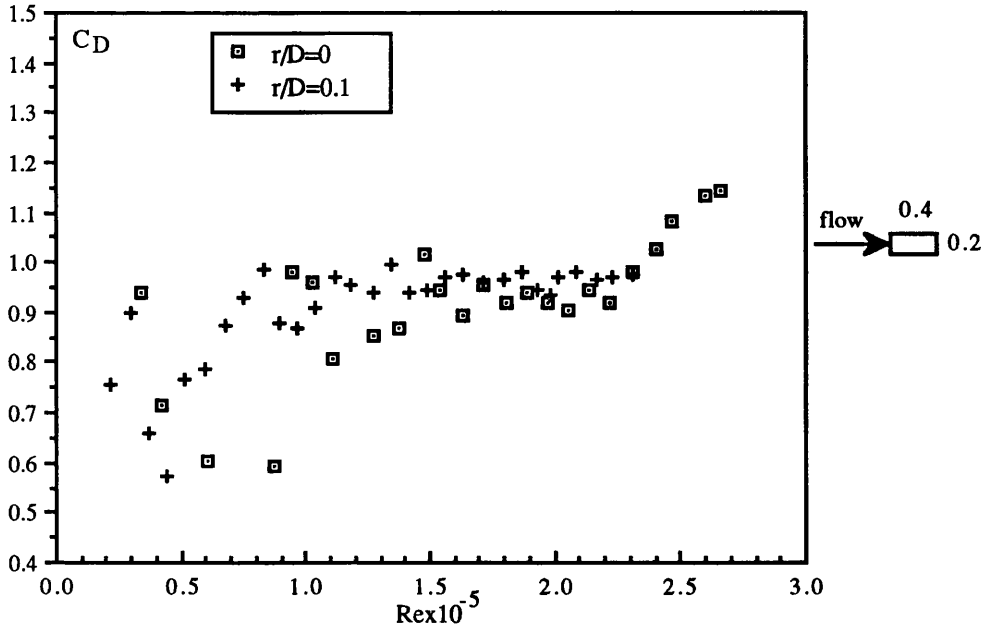

Fig. 4.15 C_D versus Re for a vertical cylinder with d/D=2 in steady flow

4.2 WAVY FLOW AT VERY LOW KEULEGAN-CARPENTER NUMBERS

The first set of cylinders tested in steady flow were also tested vertically and horizontally in regular waves. The forces were measured using the same force measuring system as for the steady flow. The force coefficients presented below were obtained from averaging the force coefficients measured for different wave cycles.

4.2.1 VERTICAL CYLINDERS

The drag and inertia coefficients of the vertical cylinders of different aspect ratios are plotted against the Keulegan-Carpenter KC number for constant values of the frequency parameter β. The Reynolds number if desired can easily be calculated from the relationship Re= βxKC. The results are shown in Figures 4.16 through 4.25. Figures 4.16 and 4.17 show C_M and C_D coefficients for the square cylinder. The variation of C_D coefficient with the KC number was found to have an asymptotic trend.

A large C_D coefficient was found when the KC number approached zero. As the KC number increased within a small range, C_D coefficient fell sharply. This behaviour of C_D coefficient was found with all cylinders. When the aspect ratio was reduced to 0.75, Figures 4.18 and 4.19, C_M coefficient decreased by more than 50%, and C_D coefficient was not found to be too much affected. When the aspect ratio was further reduced to 0.5, Figures 4.20 and 4.21, both C_M and C_D coefficients, particularly C_D values, decreased significantly. Both C_M and C_D coefficients increased when the aspect ratio was reduced from 0.5 to 0.25, Figure 4.22 and 4.23. With the cylinder of this aspect ratio, C_M coefficient was found to have the highest values. When the aspect ratio was increased from unity to 2, Figures 4.24 and 4.25, both C_M and C_D coefficients decreased significantly. However, attention should be paid to the fact that the results in Figures 4.24 and 4.25 were obtained at much smaller values of β.

4.2.2 HORIZONTAL CYLINDERS

The cylinders referred to in the previous section were also tested horizontally with their axes parallel to wave crests. The results of C_M and C_D coefficients are plotted against the KC number for constant values of the frequency parameter β in Figures 4.26 through 4.33.

Figures 4.26 and 4.27 show the variations of C_M and C_D coefficients with the KC number for the square cylinder. Both C_M and C_D coefficients were found to be much smaller than those of the same cylinder in the vertical orientation. When the aspect ratio was reduced from unity to 0.75, Figures 4.28 and 4.29, C_M coefficient increased slightly but the major effect was found in C_D coefficient which was found to be much smaller than that of the square cylinder particularly at the lower end of KC number range. On the effect of the cylinder's orientation, both C_M and C_D coefficients were found to be significantly smaller than those of the vertical cylinder, with C_M coefficient reduced by 50%. When the aspect ratio was further reduced from 0.75 to 0.5, Figures 4.30 and 4.31, both C_M and C_D coefficients increased slightly. Changing the orientation of this cylinder from vertical to horizontal had the opposite trend of increasing both C_M and C_D coefficients, though the increase in C_D coefficient was not significant. Finally, when the aspect ratio increased from unity to 2, Figures 4.32 and 4.33, C_D coefficient decreased significantly. On the effect of the cylinder's orientation, the variation of C_M coefficient with the KC number followed an opposite trend from that

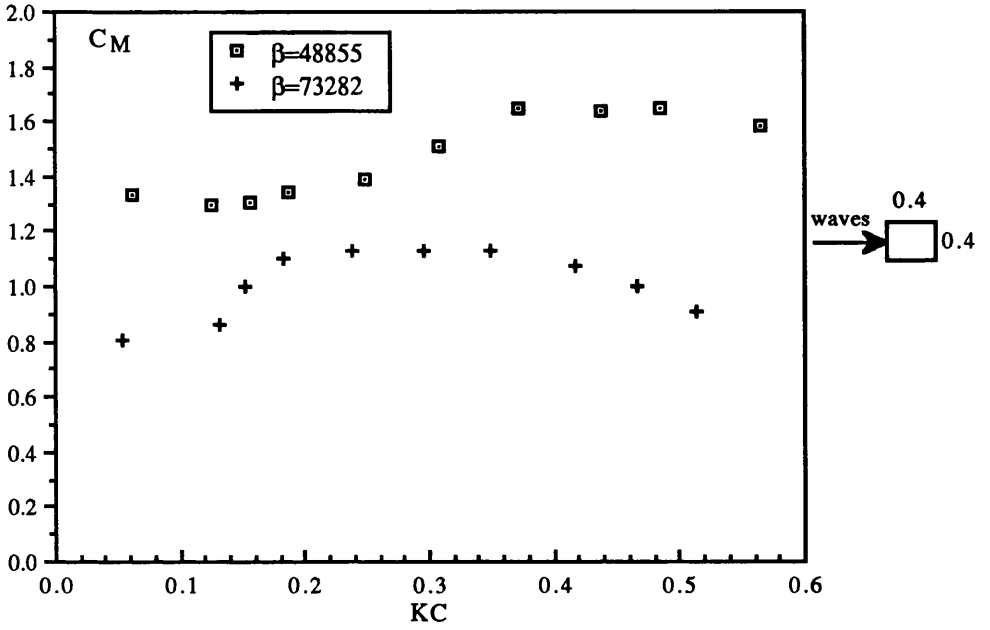

Fig. 4.16 C_M versus KC for a vertical cylinder with d/D=1 in waves

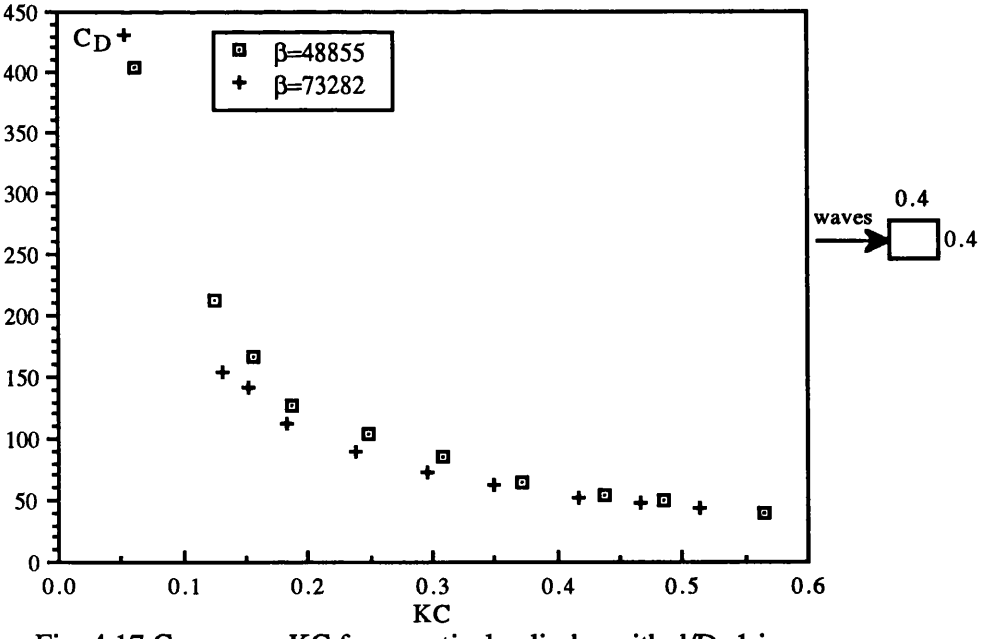

Fig. 4.17 C_D versus KC for a vertical cylinder with d/D=1 in waves

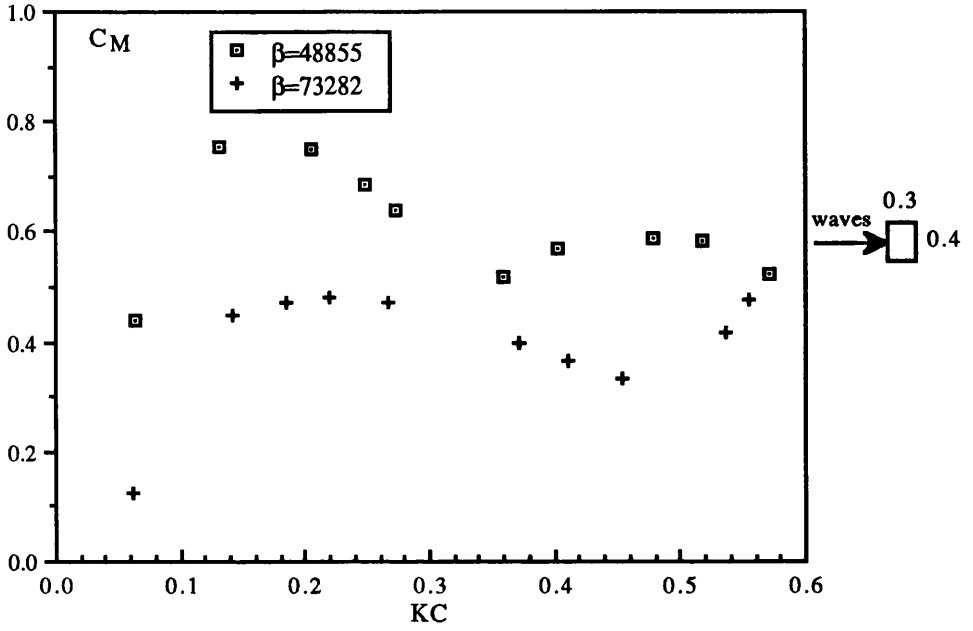

Fig. 4.18 C_M versus KC for a vertical cylinder with d/D=0.75 in waves

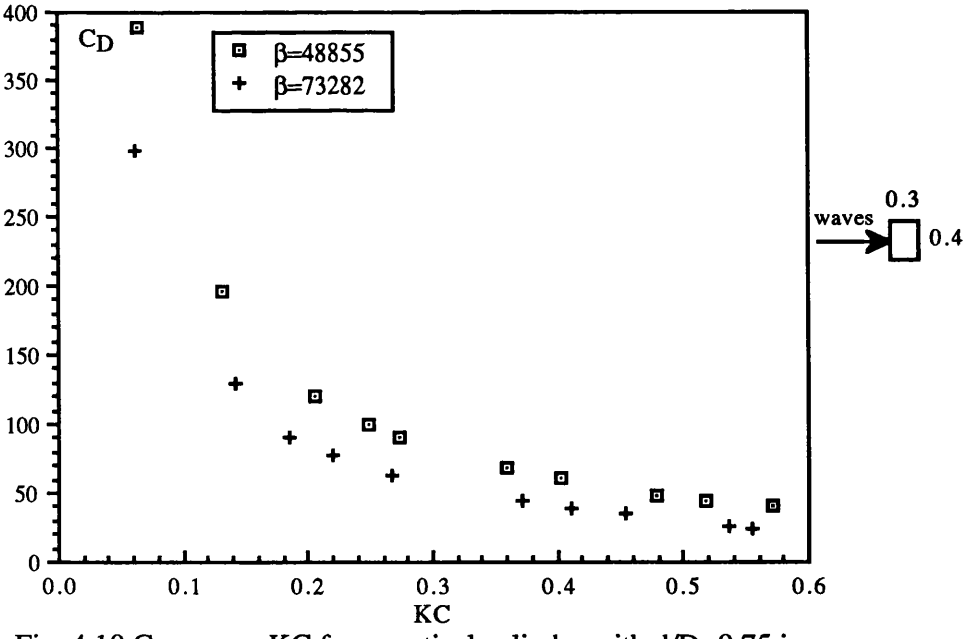

Fig. 4.19 C_D versus KC for a vertical cylinder with d/D=0.75 in waves

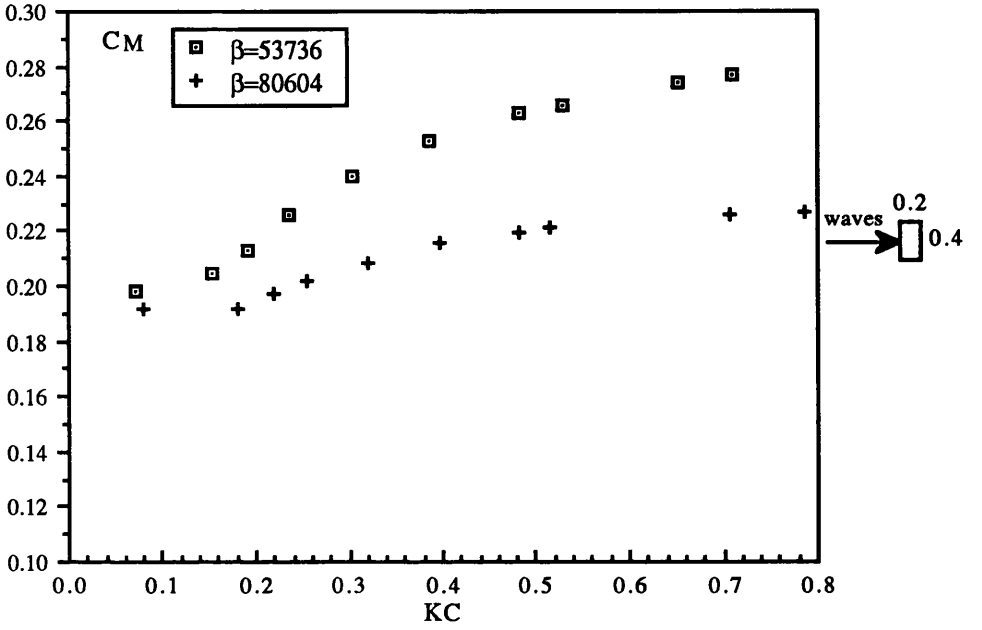

Fig. 4.20 C_M versus KC for a vertical cylinder with d/D=0.5 in waves

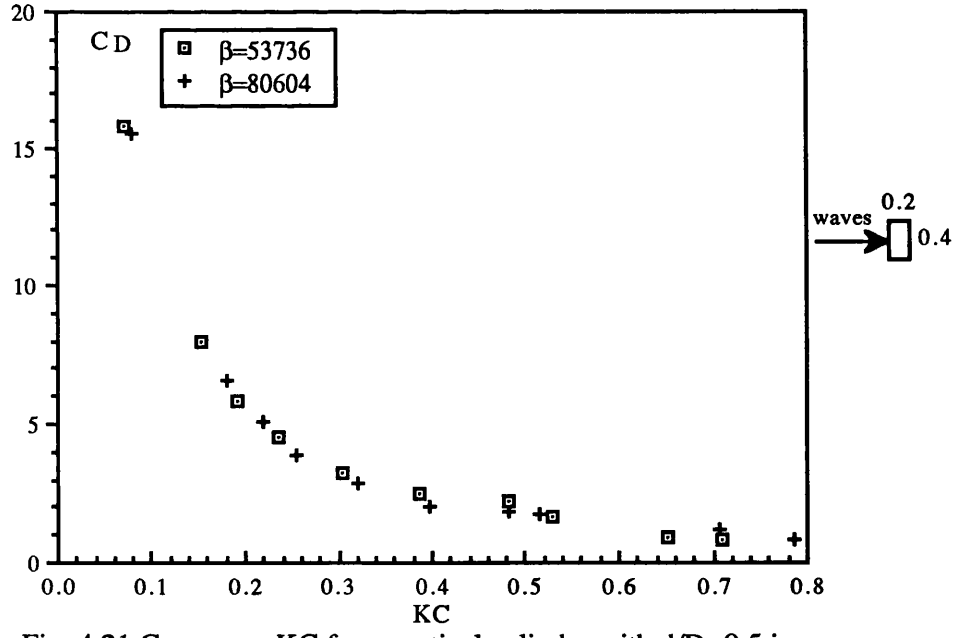

Fig. 4.21 C_D versus KC for a vertical cylinder with d/D=0.5 in waves

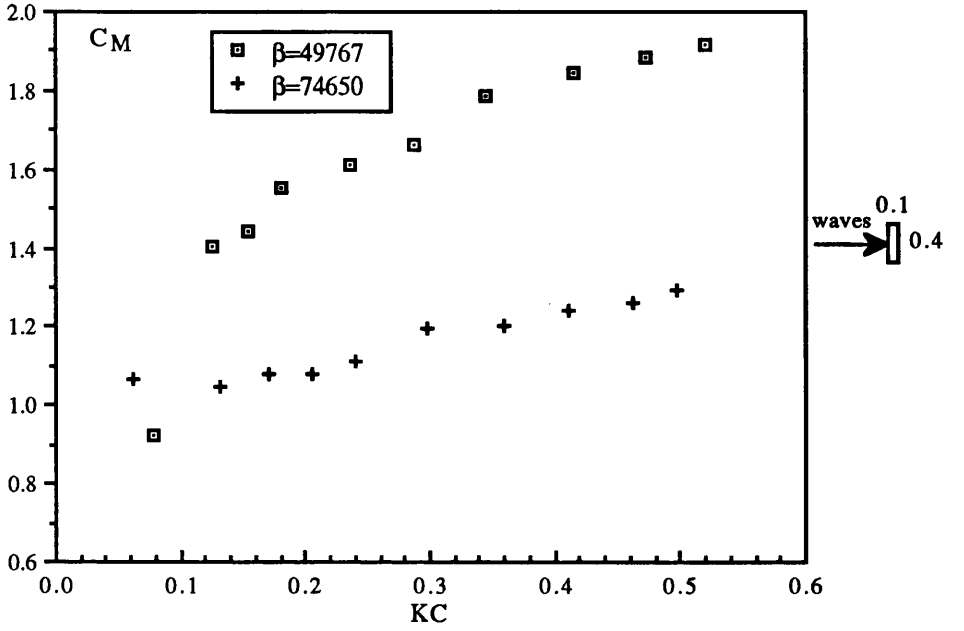

Fig. 4.22 C_M versus KC for a vertical cylinder with d/D=0.25 in waves

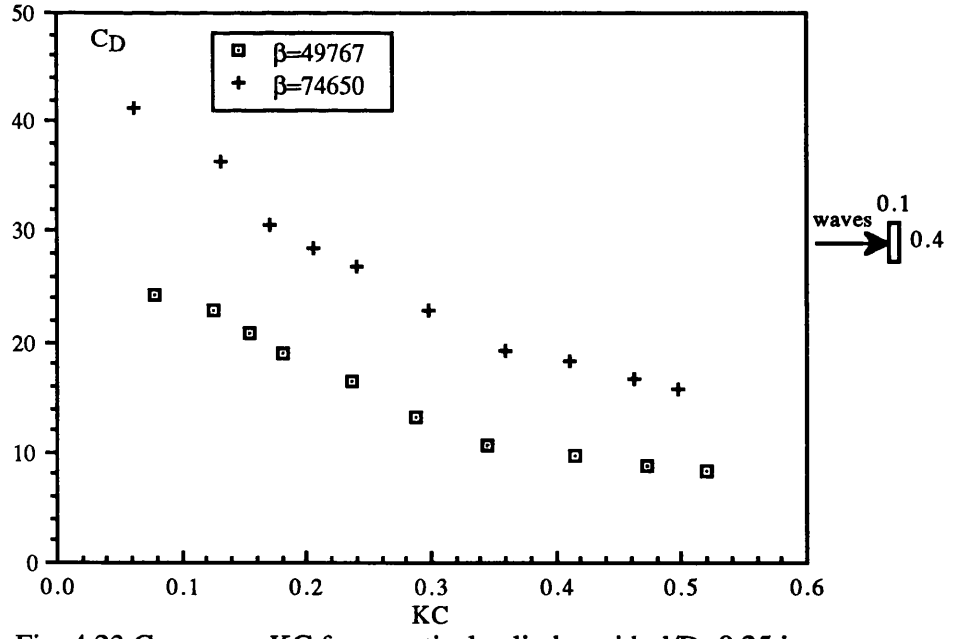

Fig. 4.23 C_D versus KC for a vertical cylinder with d/D=0.25 in waves

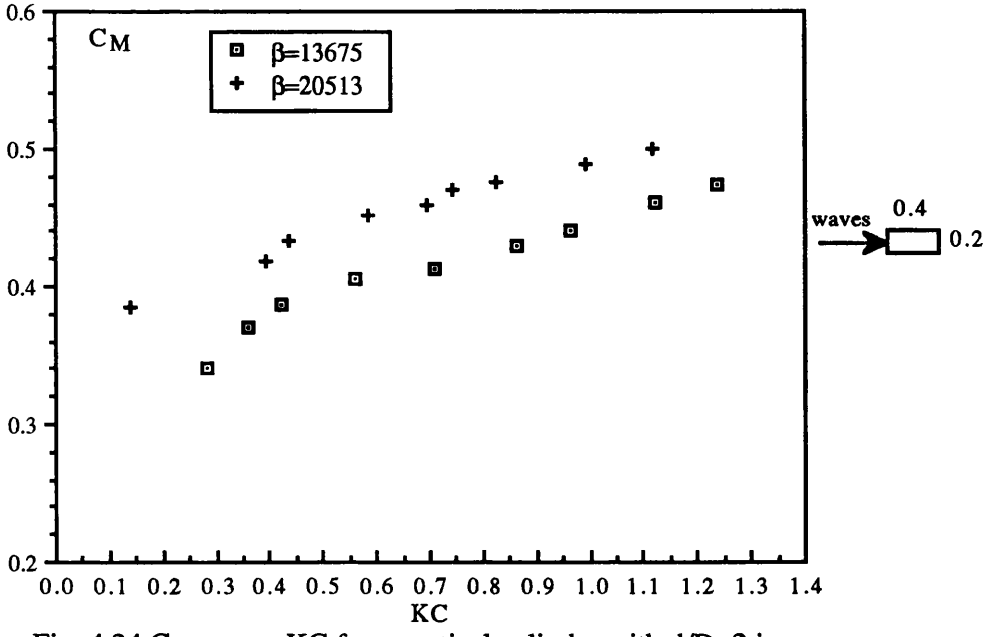

Fig. 4.24 C_M versus KC for a vertical cylinder with d/D=2 in waves

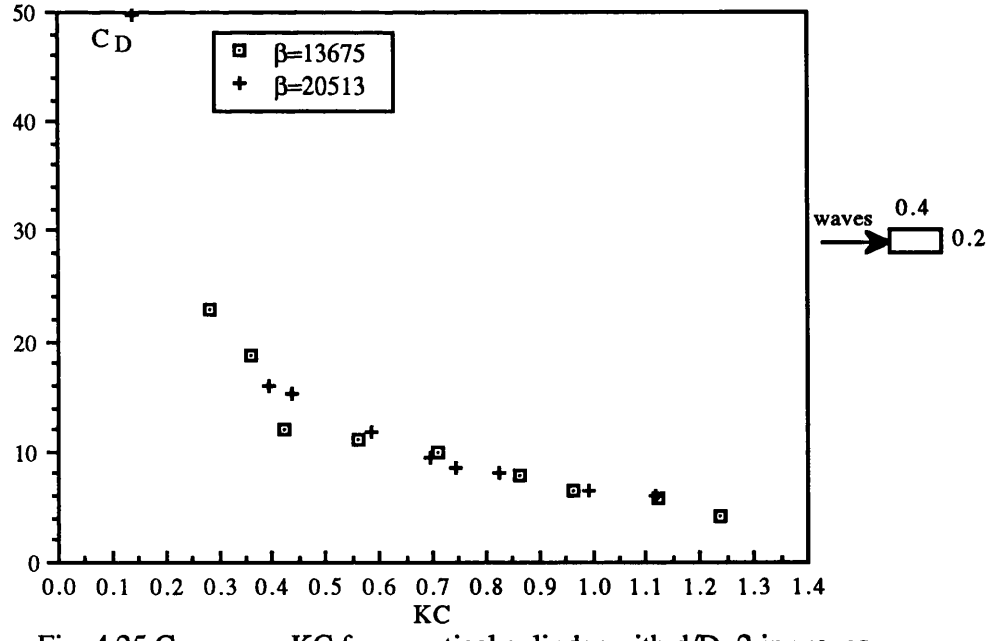

Fig. 4.25 C_D versus KC for a vertical cylinder with d/D=2 in waves

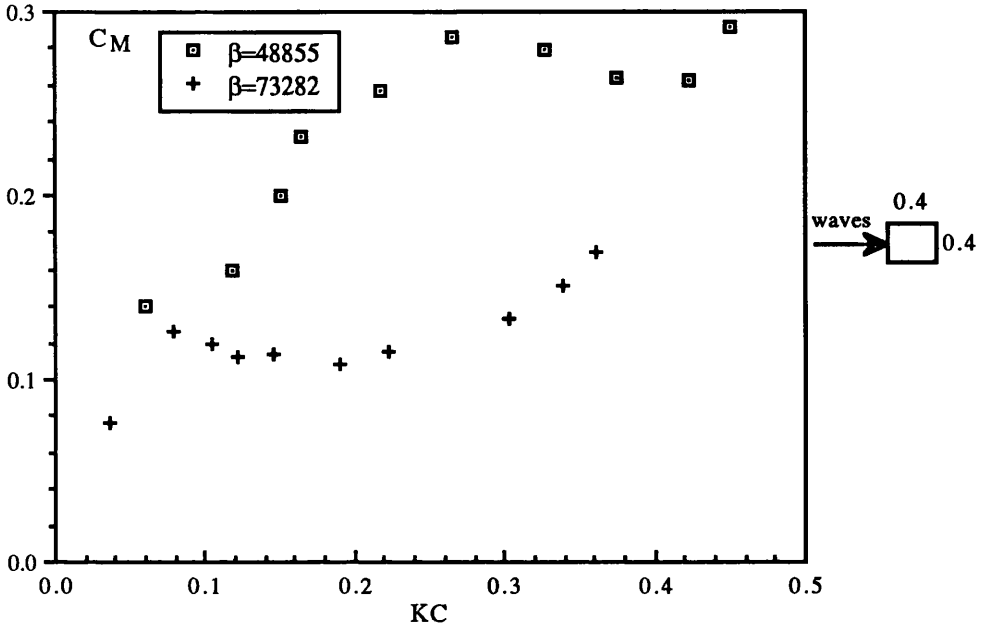

Fig. 4.26 C_M versus KC for a horizontal cylinder wih d/D=1 in waves

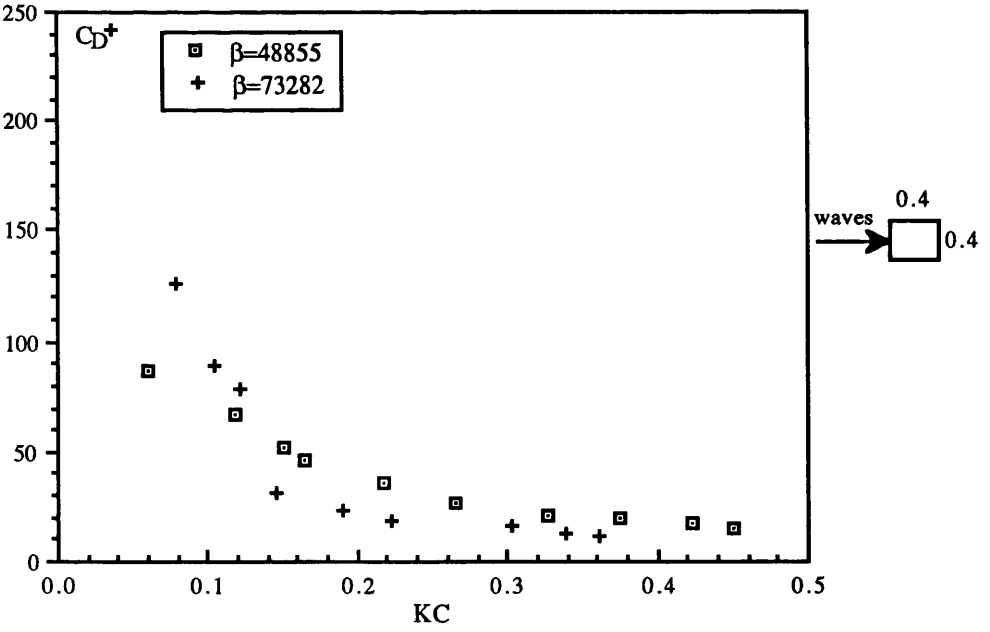

Fig. 4.27 C_D versus KC for a horizontal cylinder with d/D=1 in waves

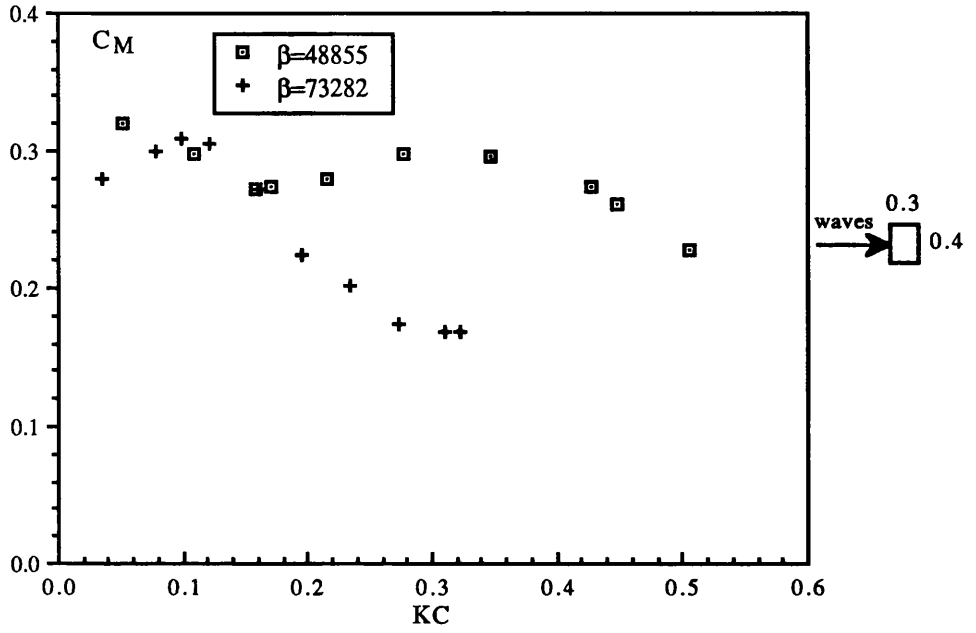

Fig. 4.28 C_M versus KC for a horizontal cylinder with d/D=0.75 in waves

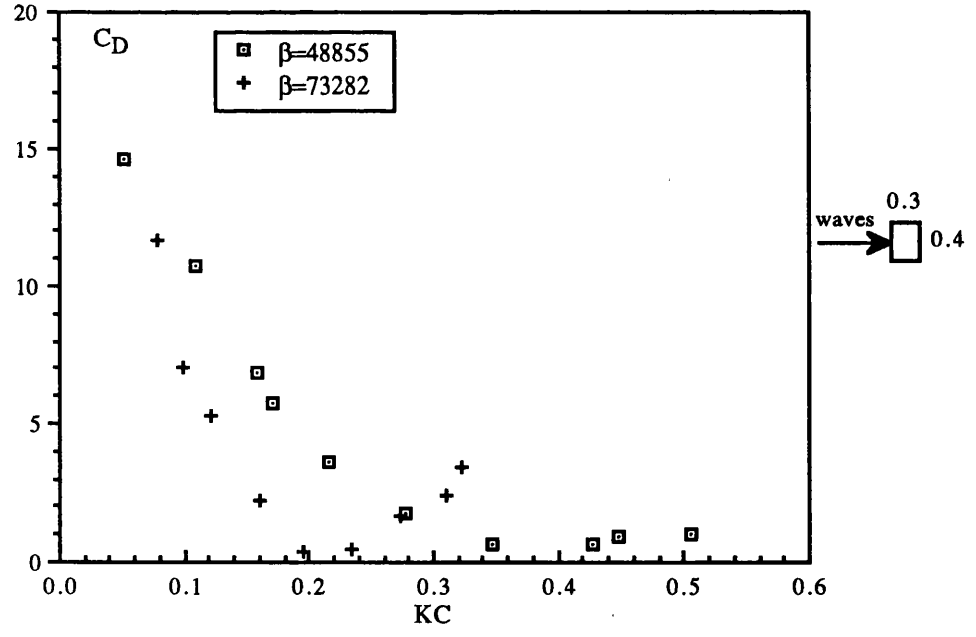

Fig. 4.29 C_D versus KC for a horizontal cylinder with d/D=0.75 in waves

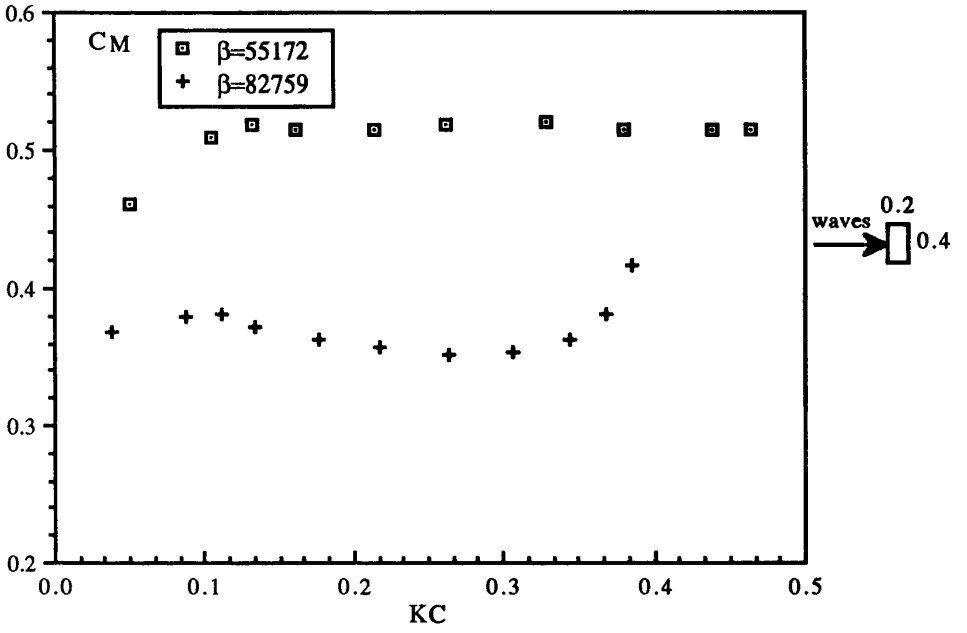

Fig. 4.30 C_M versus KC for a horizontal cylinder with d/D=0.5 in waves

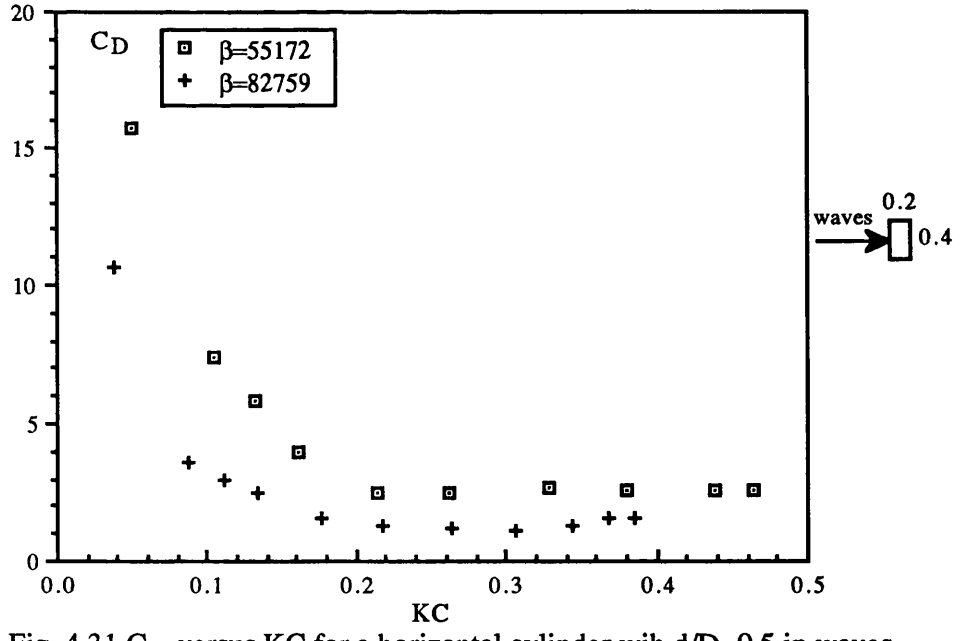

Fig. 4.31 C_D versus KC for a horizontal cylinder wih d/D=0.5 in waves

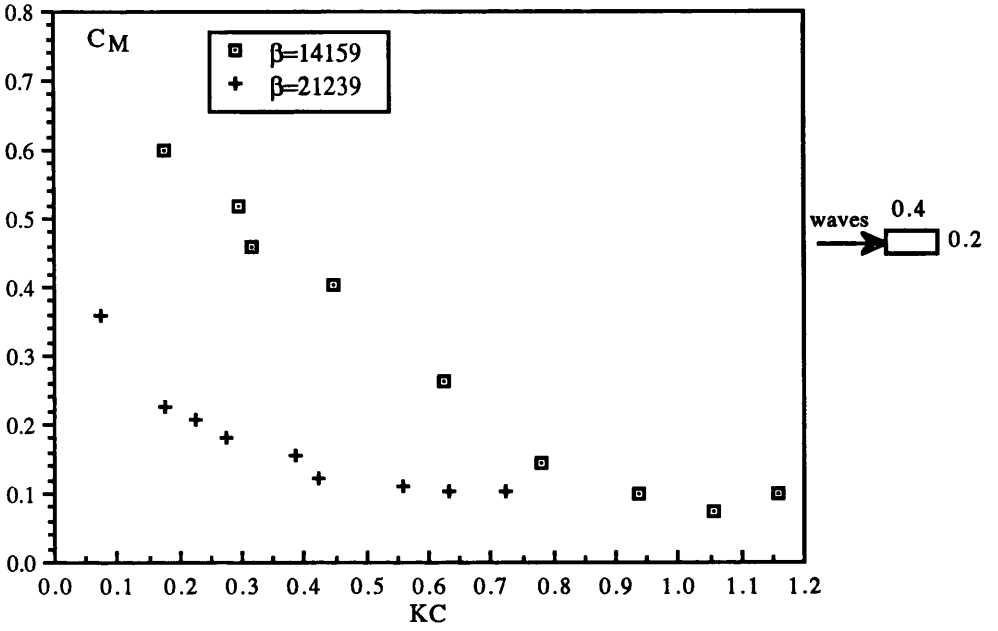

Fig. 4.32 C_M versus KC for a horizontal cylinder with d/D=2 in waves

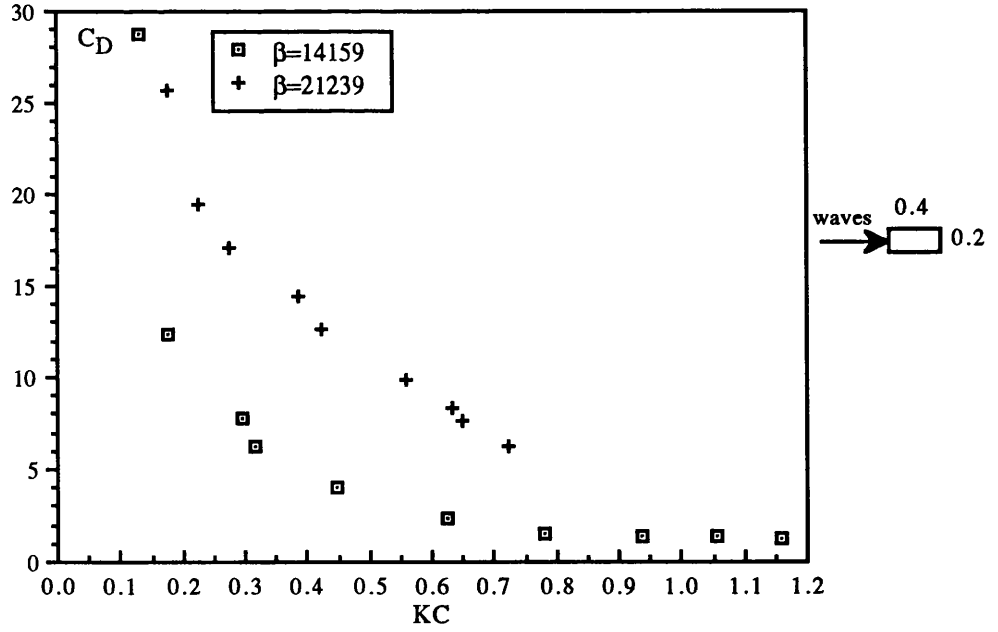

Fig. 4.33 C_D versus KC for a horizontal cylinder with d/D=2 in waves

of the vertical cylinder. The C_D coefficient was found to be smaller for this horizontal cylinder than for the vertical cylinder.

The above results obtained with vertical and horizontal cylinders were plotted without any comparison with other data since at these very low KC numbers there are not any published results for rectangular cylinders tested in wavy flow.

4.3 WAVY FLOW AT MODERATE KEULEGAN-CARPENTER NUMBERS

The second set of cylinders with smaller sizes were also tested vertically and horizontally in wavy flow in order to measure the in-line and transverse forces for the vertical cylinders and to measure the in-line and vertical forces for the horizontal cylinders at higher KC numbers than those at which the first set of cylinders were tested. These cylinders which had three different aspect ratios were tested vertically in regular waves as surface piercing and horizontally submerged with their axes parallel to wave crests.

The wave forces were measured using the different force measuring system described in Chapter 2.

As in the case of the first set of cylinders, the force coefficients presented here were obtained from averaging the force coefficients measured for different wave cycles. The equations giving the inertia C_M, drag C_D, maximum and root mean square force coefficients C_{Fmax} and C_{Frms} coefficients as well as the lift C_L (C_{Lmax}, C_{Lrms} and C_{Lurms}) coefficients are given in Chapter 3.

4.3.1 VERTICAL CYLINDERS

The different force coefficients of vertical cylinders are plotted against Keulegan-Carpenter KC number for constant values of the frequency parameter β. The results are shown in Figures 4.34 through 4.60.

4.3.1.1 In-line force coefficients

Figures 4.34 and 4.35 show the variations of C_M and C_D coefficients with the KC number for the square cross-sectional cylinder.

The C_M coefficient increased from about 2.6 at a low KC number, reached a high value of about 3.4 at a KC number of 2 and then decreased to 2.9 as the KC number approached 4. The present results showed that the variation of C_M coefficient with the KC number in waves is different from that in planar oscillatory flow as measured by Bearman et al. (1984). The inertia coefficient measured in waves was found to be higher than that measured in planar oscillatory flow for $1<KC<3.5$. The values of C_M coefficient measured by Bearman et al. and plotted in Figure 4.34 were corrected to take into account the actual cross-section of the square cylinder DxD instead of $\pi D^2/4$ used in the inertia term of the Morison equation.

The C_D coefficient was found to have large values at small KC numbers and to decrease rapidly as the KC number increased. This behaviour of C_D coefficient was found with all the cylinders whether tested vertically or horizontally. A value of C_D coefficient of 5 was found at a KC number of 4. As with the inertia coefficient, the drag coefficient measured in waves was found to be higher that that measured in planar oscillatory flow by Bearman et al.

Other in-line force coefficients in terms of the maximum force during a wave cycle C_{Fmax} and the root mean square force value C_{Frms} for the square cylinder are shown in Figures 4.36 and 4.37. The C_{Fmax} and C_{Frms} coefficients were found to follow the same trend of variation with the KC number as that of C_D coefficient. Large values of these coefficients, measured at a low KC number, decreased very rapidly as the KC number increased. This behaviour of the two force coefficients was also found with all the cylinders.

Using measured C_M and C_D coefficients in the Morison equation the r.m.s. of the horizontal force coefficient was calculated (eq. 3.28). This calculated coefficient was then compared to the measured r.m.s. of the horizontal force coefficient as shown in Figures 4.38 and 4.39. A comparison between the measured and the calculated r.m.s. force coefficients was made for identical values of KC and β numbers. The agreement between the two coefficients was found to be good.

The variations of C_M and C_D coefficients with the KC number for the cylinder with an aspect ratio of 2 are shown in Figures 4.40 and 4.41.

The C_M coefficient of this cylinder was found to be smaller than that of the square cylinder. The C_M coefficient had an average value between 1.9 and 2 at KC numbers between 1.5 and 4.5, after increasing from about 1.6 at a low KC number. At a KC number of 2, for example, C_M coefficient decreased by about 41% when the aspect ratio

increased from unity to 2. At the extreme KC numbers of 0.4 and 4, C_M coefficient decreased by about 36% and 31% respectively as the aspect ratio increased.

The C_D coefficient, however, was found to be influenced less by the increase in the aspect ratio. The same order of magnitude of C_D coefficient was found for both cylinders. For this cylinder, the drag coefficient measured in waves agreed quite well with that measured in planar oscillatory flow by Heideman and Sarpkaya (1985) despite the difference in β numbers at which measurements were carried out and the different nature of the two flows.

The other force coefficients C_{Fmax} and C_{Frms} were found to be higher with this cylinder than those of the square cylinder, Figures 4.42 and 4.43. For example, at a KC number just over 1 C_{Fmax} and C_{Frms} increased by 13% and 17% respectively when the aspect ratio increased from unity to 2. At a higher KC number just below 4, C_{Fmax} and C_{Frms} increased by 19% and 25% respectively.

Again comparison, for identical values of KC and β numbers, was made between the measured r.m.s. force coefficient and the calculated r.m.s. force coefficient from the Morison equation using measured C_M and C_D coefficients, Figures 4.44 and 4.45. The calculated r.m.s. force was also found to correlate well with the measured force.

Figures 4.46 and 4.47 show the variations of C_M and C_D coefficients with the KC number for the cylinder with the smallest aspect ratio of 0.5.

The C_M coefficient of this cylinder was found to follow the same variation with the KC number as that of the cylinder with an aspect ratio of 2. However, the values of C_M coefficient were found to be higher. The C_M coefficient was found to have an average value of 3.6 at KC numbers between 1 and 2, after increasing from about 3.1 at a low KC number. On the effect of varying the aspect ratio, C_M coefficient increased when the aspect ratio reduced from unity to 0.5. At KC numbers of 0.4 and 2, for example, C_M coefficient increased by 19% and 8% respectively, when the aspect ratio reduced from unity to 0.5.

The C_D coefficient, on the other hand, did not vary much as the aspect ratio was reduced. Again the same order of magnitude of C_D coefficient as that of the square cylinder was found. The inertia and drag coefficient for this cylinder are plotted on their own because there are no previous data for a cylinder with this aspect ratio and at this range of KC numbers.

The other in-line force coefficients C_{Fmax} and C_{Frms} were found to be smaller than those of the square cylinder, Figures 4.48 and 4.49. For example, at a KC number just

above 1 C_{Fmax} and C_{Frms} decreased by 24% and 37% respectively when the aspect ratio reduced from unity to 0.5. At a higher KC number approaching 2, C_{Fmax} and C_{Frms} decreased by 32% and 36% respectively. However, attention should be paid to the fact that values of β numbers for the cylinder with an aspect ratio of 0.5 are much higher than those of the other two cylinders. With the cylinders with aspect ratios of 1 and 2 the same dimension of 10 cm faced the waves whereas with the cylinder with an aspect ratio of 0.5 the dimension of 20 cm faced the waves and that explained the difference in β numbers since this parameter is a function of the cylinder's side facing the waves.

Comparison, for identical values of KC and β numbers, was also made between the measured r.m.s. force coefficient and the calculated r.m.s. force coefficient from the Morison equation through the use of measured C_M and C_D coefficients, Figures 4.50 and 4.51. The agreement between the measured and calculated r.m.s. force was also found to be good.

4.3.1.2 Transverse (lift) force coefficients

As mentioned earlier transverse forces are irregular in nature and pose certain problems to measure them. To overcome this difficulty the root mean squares of the forces are usually used as one way of dealing with the random nature of these forces. The other method of representing these forces is by measuring the maximum transverse force occurring in a wave cycle.

These forces were measured in this study with the cylinders discussed above and expressed in terms of the maximum force coefficient during a wave cycle C_{Lmax} (eq. 3.29) and in terms of two different r.m.s. force coefficients. The first r.m.s. force coefficient C_{Lrms} expresses the r.m.s. of the transverse force non dimensionalised using the maximum wave particle velocity (eq. 3.30). The second r.m.s. force coefficient C_{Lurms} expresses the r.m.s. of the transverse force non dimensionalised using the r.m.s. value of the square of the instantaneous wave particle velocity (eq. 3.31, eq. 3.32).

Figures 4.52 through 4.54 show the variations of C_{Lmax}, C_{Lrms} and C_{Lurms} coefficients with the KC number for the square cross-sectional cylinder.

The variations of these coefficients with the KC number were found to follow the same trend as that of C_D, C_{Fmax} and C_{Frms} coefficients. The values of C_{Lurms} coefficient were found to be nearly twice as high as those of C_{Lrms} coefficient at corresponding

KC numbers. In theory and for a perfect sinusoidal variation of the wave particle velocity u, $u^2(rms)=0.5x\sqrt{3/2}u^2(max)$, therfore $C_{Lurms}=1.63\ C_{Lrms}$. The values of C_{Lmax} coefficient were found to be 61% to 115% higher than those of C_{Lrms} coefficient at corresponding KC numbers.

The variations of C_{Lmax}, C_{Lrms} and C_{Lurms} coefficients with the KC number for the cylinder with an aspect ratio of 2 are shown in Figures 4.55 through 4.57.
As with the square cylinder, these coefficients decreased rapidly as the KC number increased. At corresponding KC numbers, the values of C_{Lurms} coefficient were found to be about 65% higher than those of C_{Lrms} coefficient and the values of C_{Lmax} coefficient were found to be about twice as high as those of C_{Lrms} coefficient.
The lift coefficients of this cylinder were found to be lower than those of the square cylinder. For example, at KC=1.3 and β number of about 7000, C_{Lmax} and C_{Lrms} coefficients decreased by 11% and 15% respectively when the aspect ratio increased from unity to 2. At a higher KC number approaching 3, C_{Lmax} and C_{Lrms} coefficients decreased by 28% and 20% respectively.

The variations of C_{Lmax}, C_{Lrms} and C_{Lurms} coefficients with the KC number for the cylinder with the smallest aspect ratio of 0.5 are shown in Figures 4.58 through 4.60.
As with the other cylinders, the same trend of variation of these coefficients with the KC number was found. As in the case of the square cylinder, the values of C_{Lurms} coefficient were found to be nearly twice as high as those of C_{Lrms} coefficient at corresponding KC numbers. The values of C_{Lmax} coefficient were found to be 60% to 75% higher than those of C_{Lrms} coefficient. Again the lift coefficients of this cylinder were found to be lower than those of the square cylinder, though the results of these two cylinders were plotted for very different β numbers. For example at a KC number of about 1, C_{Lmax} and C_{Lrms} coefficients decreased by 50% and 46% respectively when the aspect ratio reduced from unity to 0.5. At a higher KC number approaching 2, C_{Lmax} and C_{Lrms} decreased by 60% and 54% respectively.

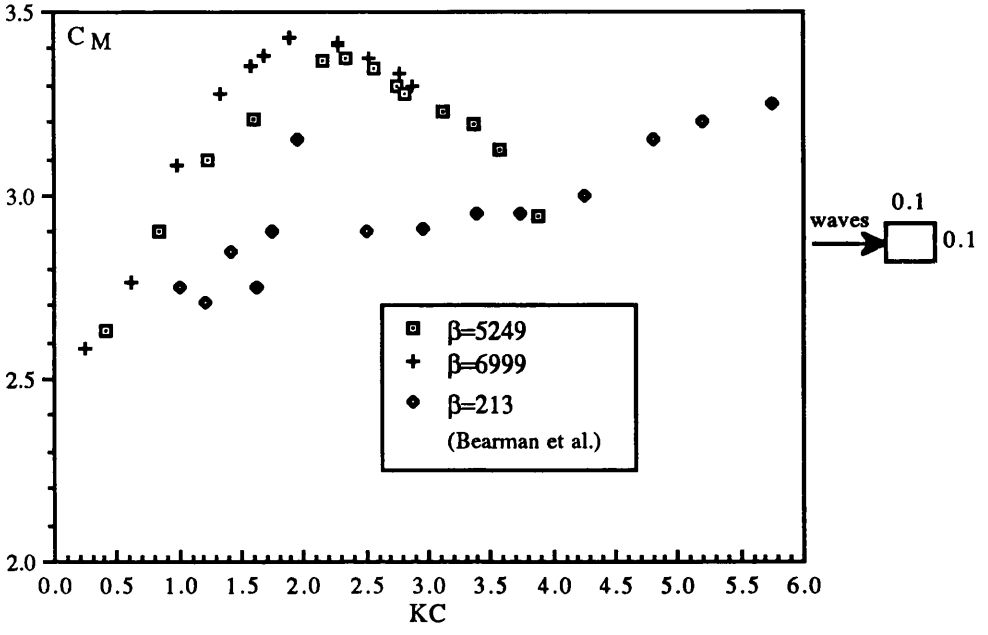

Fig. 4.34 C_M versus KC for a vertical cylinder with d/D=1 in waves

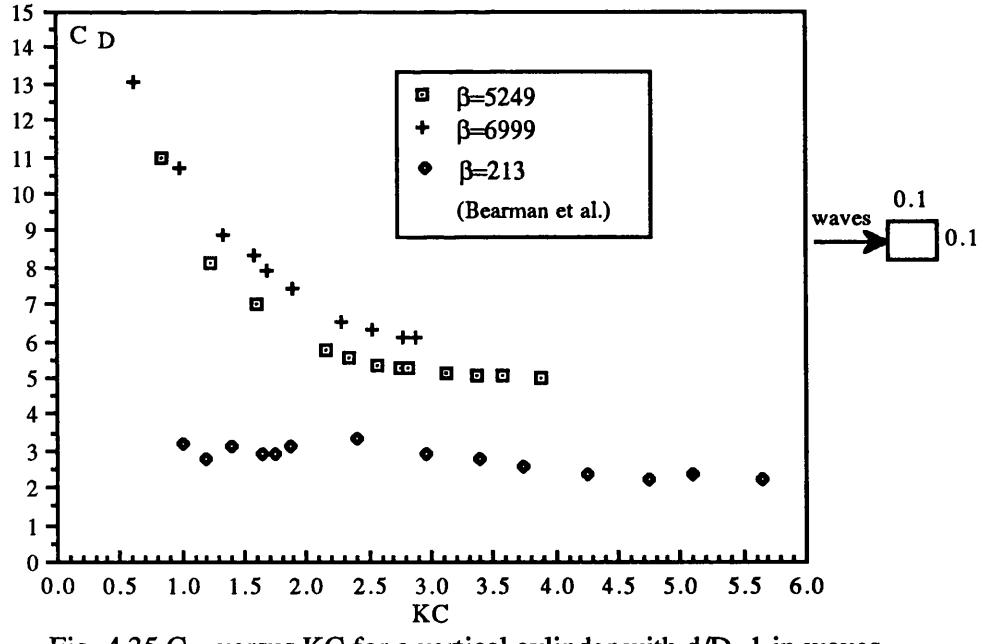

Fig. 4.35 C_D versus KC for a vertical cylinder with d/D=1 in waves

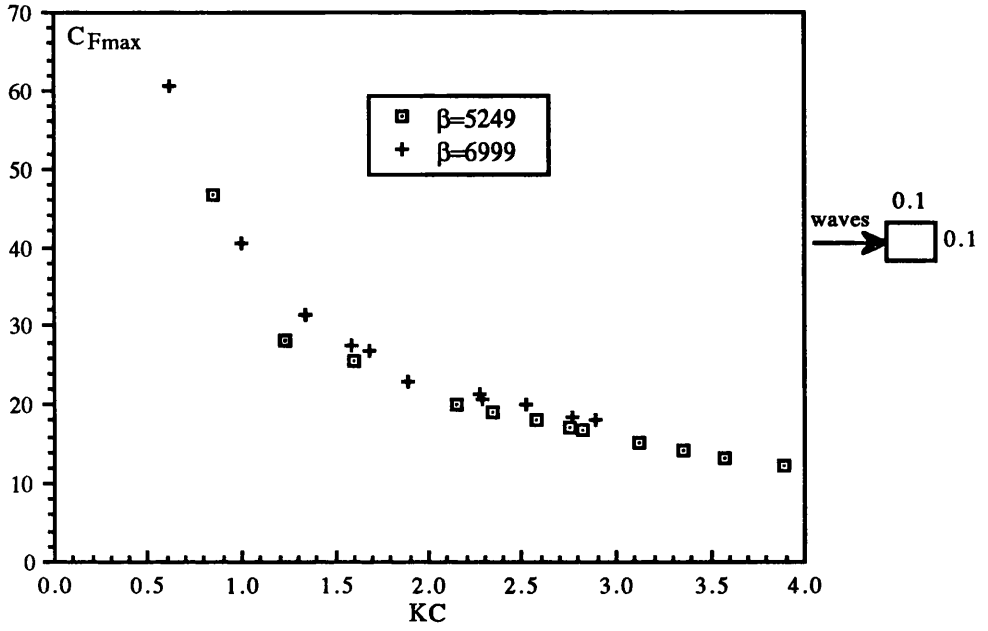

Fig. 4.36 C_{Fmax} versus KC for a vertical cylinder with d/D=1 in waves

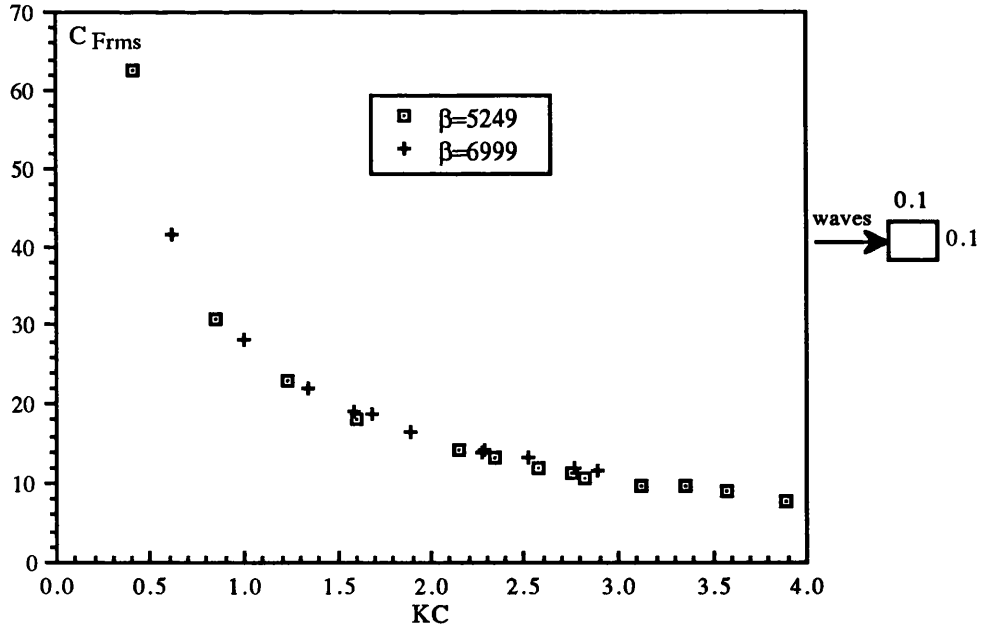

Fig. 4.37 C_{Frms} versus KC for a vertical cylinder with d/D=1 in waves

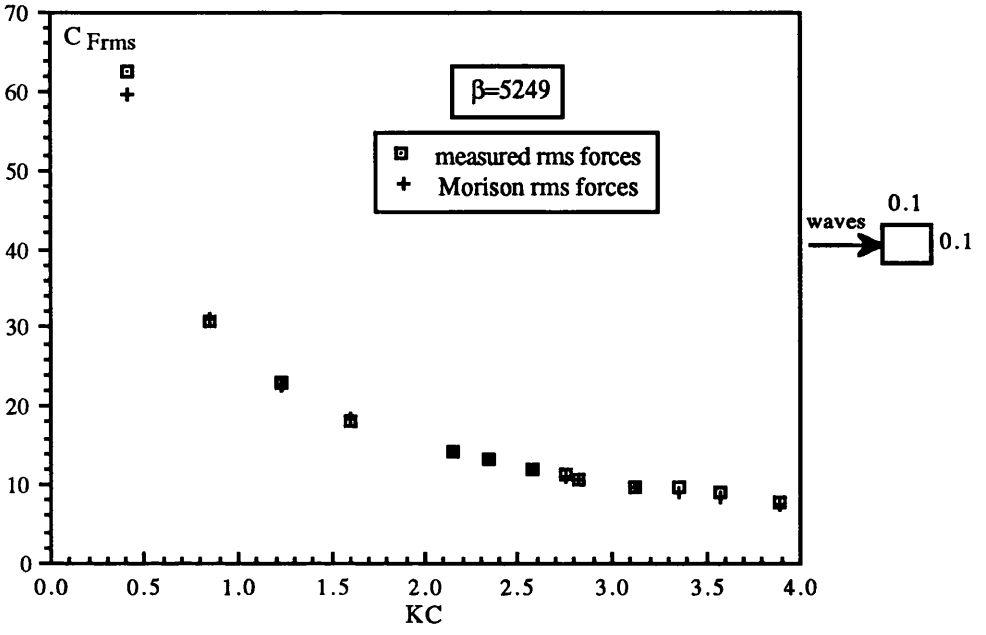

Fig. 4.38 C_{Frms} versus KC for a vertical cylinder with d/D=1 in waves

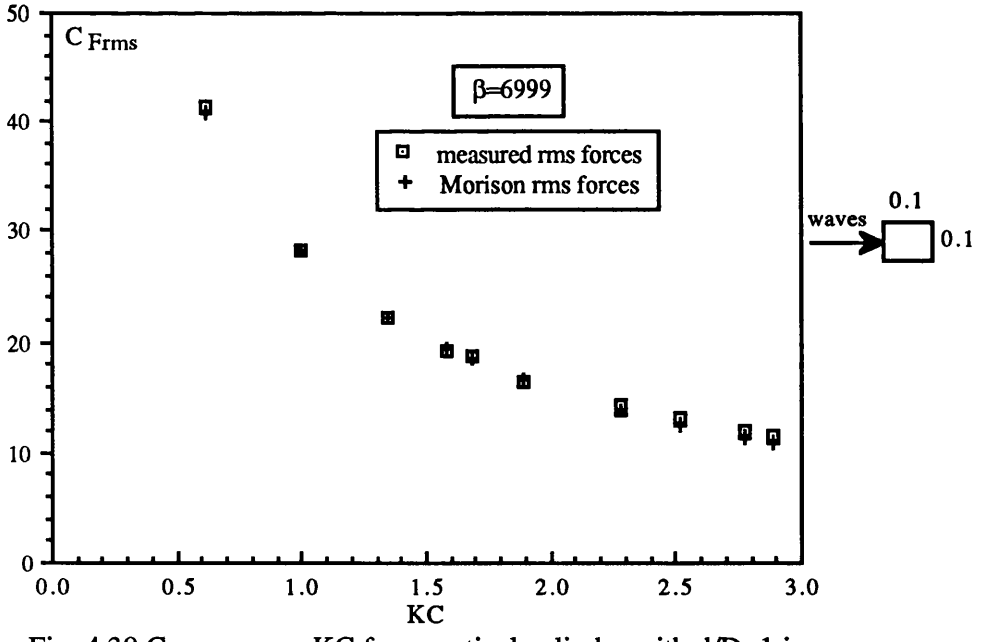

Fig. 4.39 C_{Frms} versus KC for a vertical cylinder with d/D=1 in waves

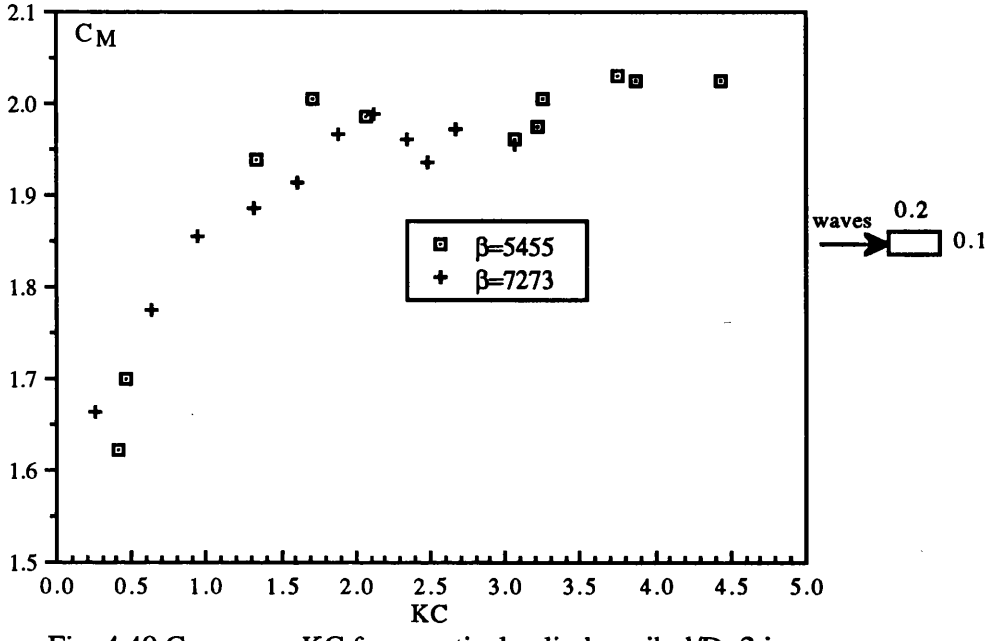

Fig. 4.40 C_M versus KC for a vertical cylinder wih d/D=2 in waves

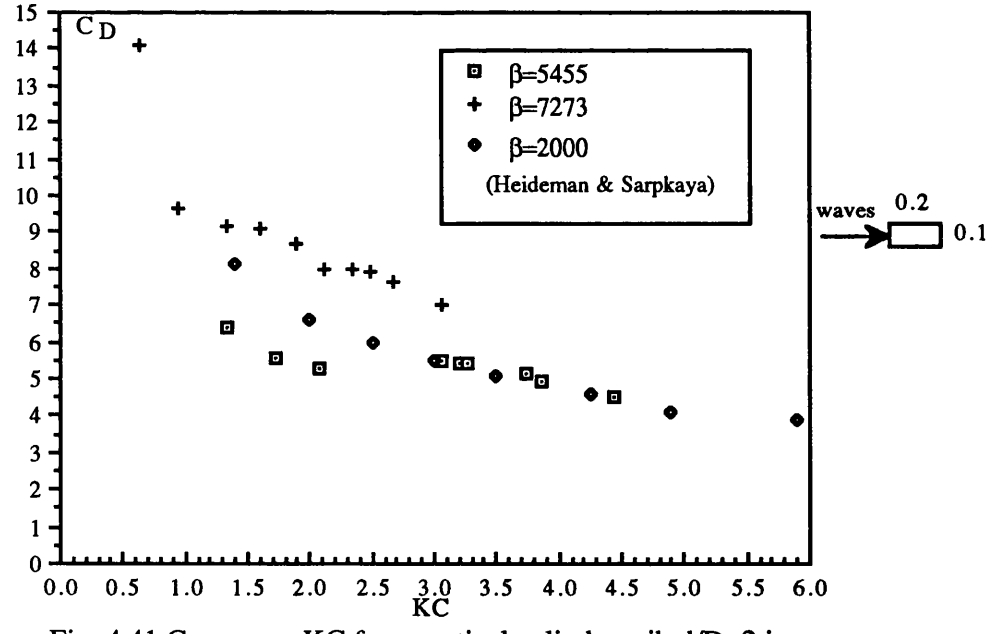

Fig. 4.41 C_D versus KC for a vertical cylinder wih d/D=2 in waves

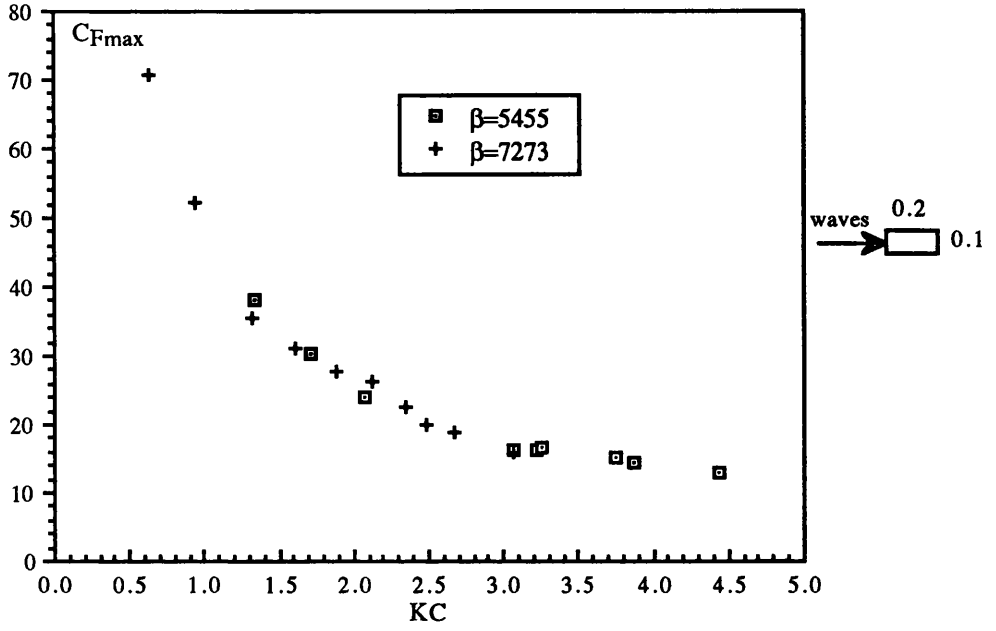

Fig. 4.42 C_{Fmax} versus KC for a vertical cylinder wih d/D=2 in waves

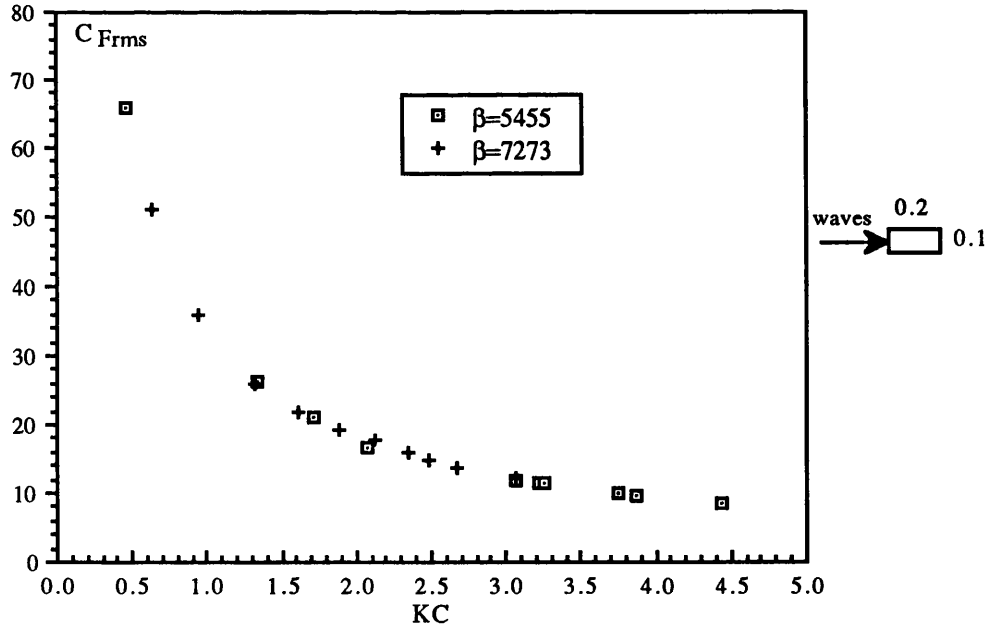

Fig. 4.43 C_{Frms} versus KC for a vertical cylinder wih d/D=2 in waves

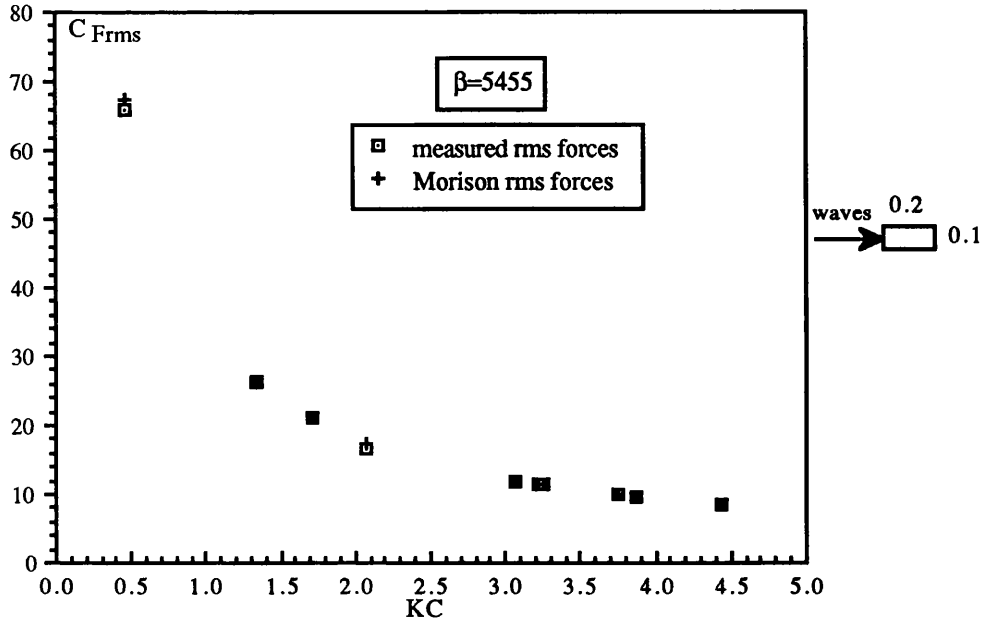

Fig. 4.44 C_{Frms} versus KC for a vertical cylinder wih d/D=2 in waves

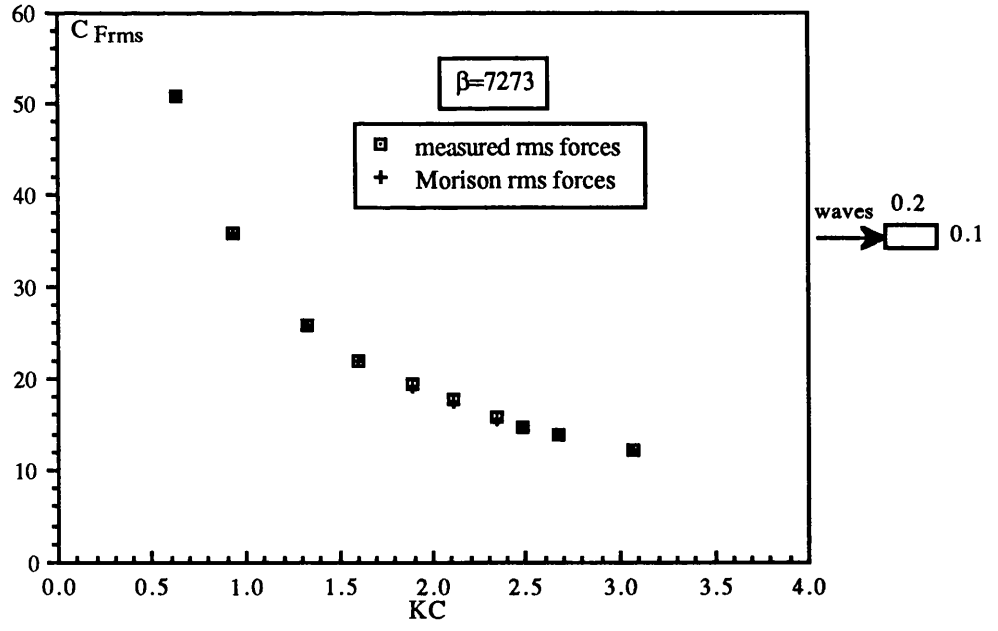

Fig. 4.45 C_{Frms} versus KC for a vertical cylinder wih d/D=2 in waves

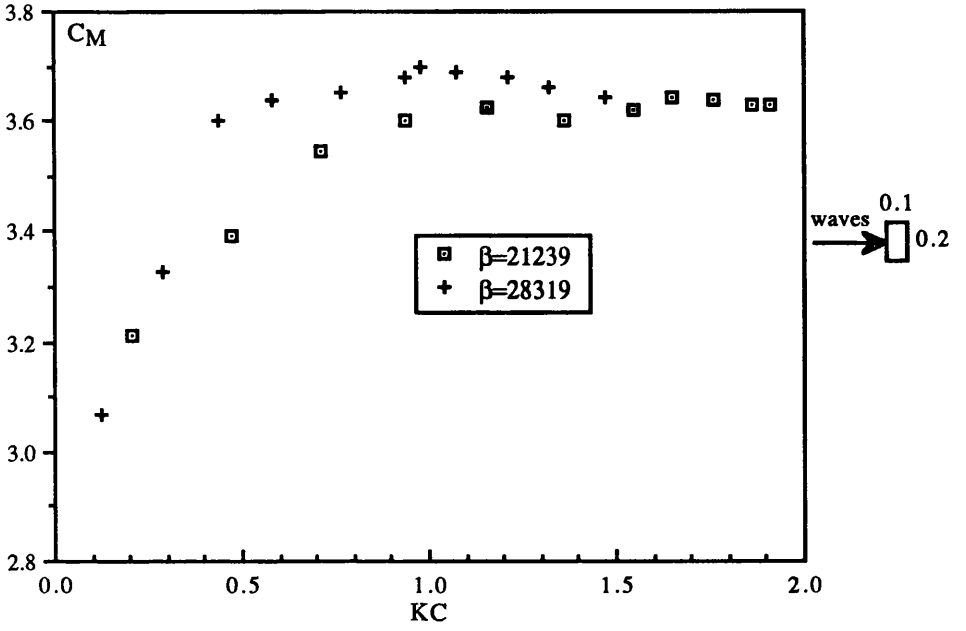

Fig. 4.46 C_M versus KC for a vertical cylinder with d/D=0.5 in waves

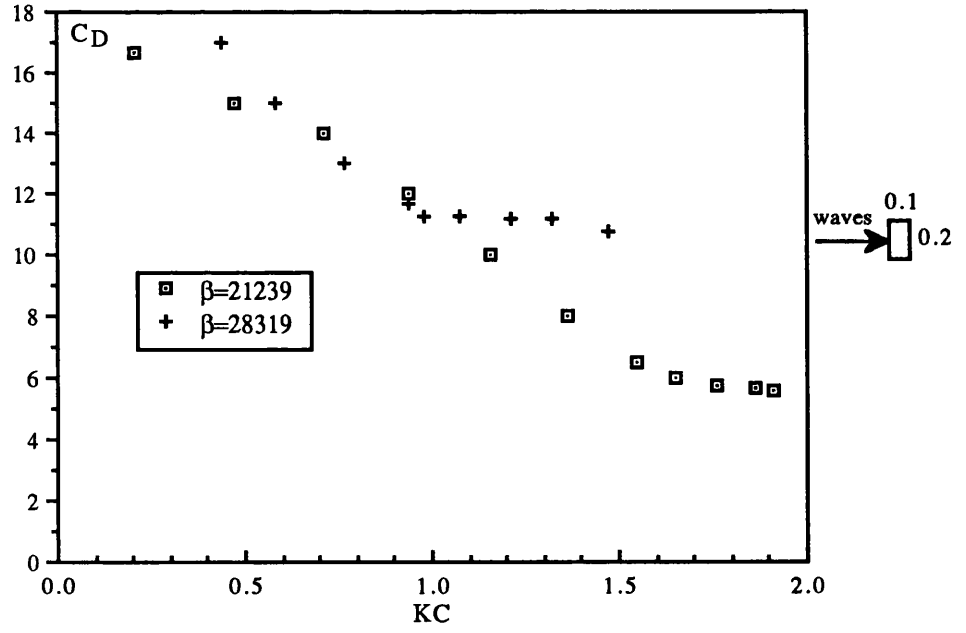

Fig. 4.47 C_D versus KC for a vertical cylinder with d/D=0.5 in waves

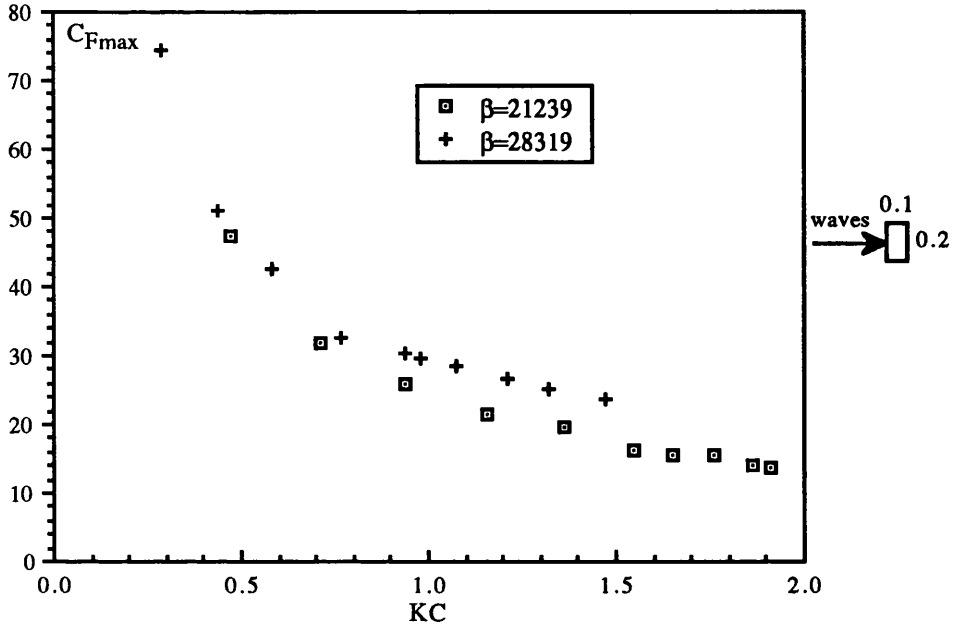

Fig. 4.48 C_{Fmax} versus KC for a vertical cylinder with d/D=0.5 in waves

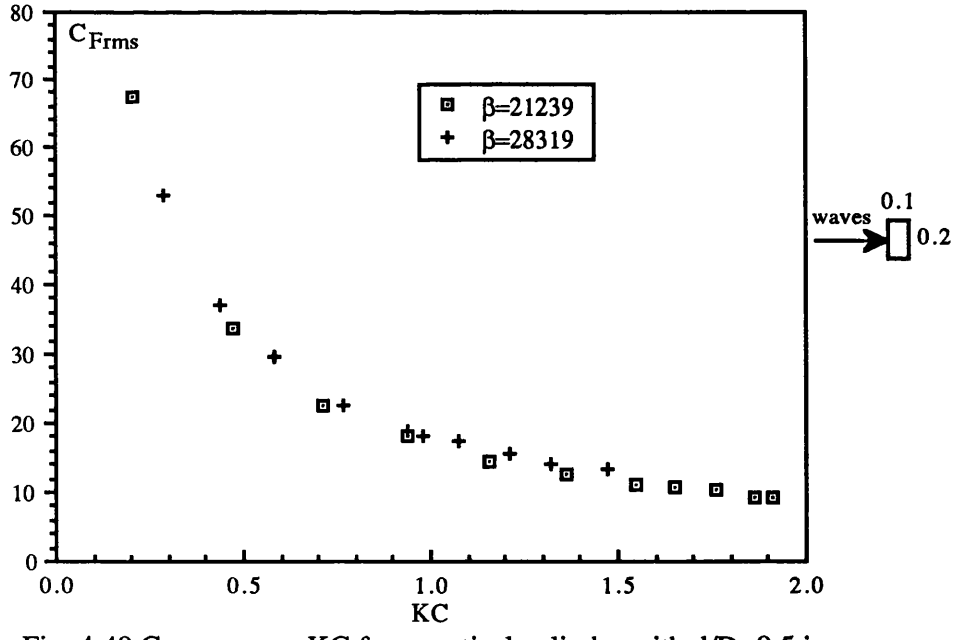

Fig. 4.49 C_{Frms} versus KC for a vertical cylinder with d/D=0.5 in waves

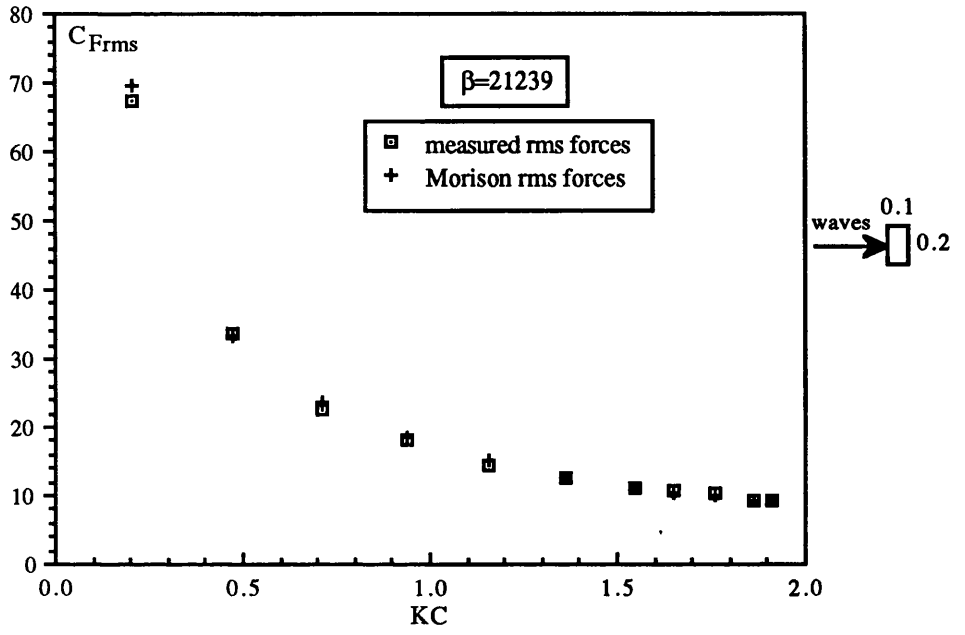

Fig. 4.50 C_{Frms} versus KC for a vertical cylinder with d/D=0.5 in waves

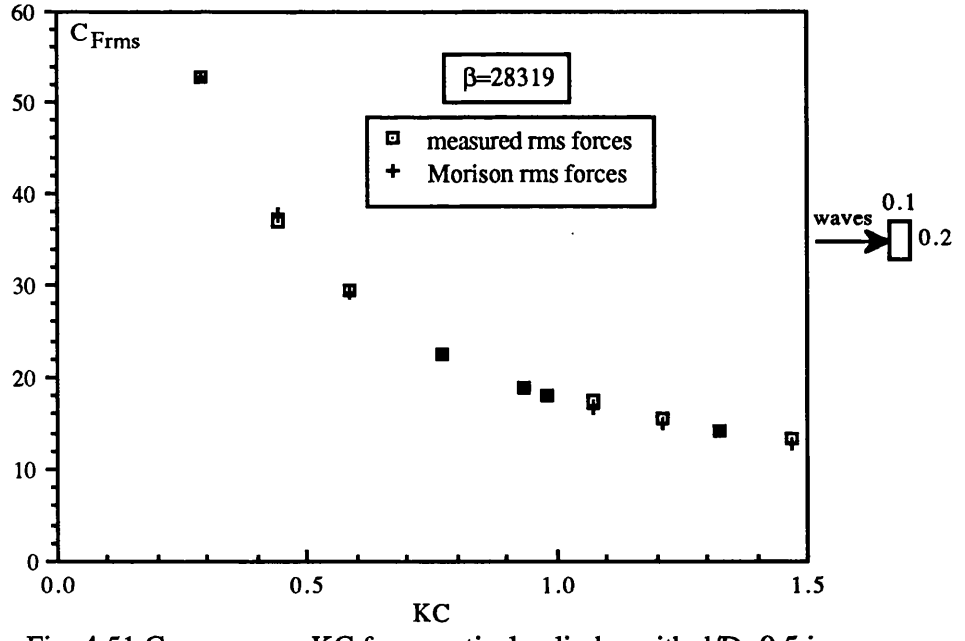

Fig. 4.51 C_{Frms} versus KC for a vertical cylinder with d/D=0.5 in waves

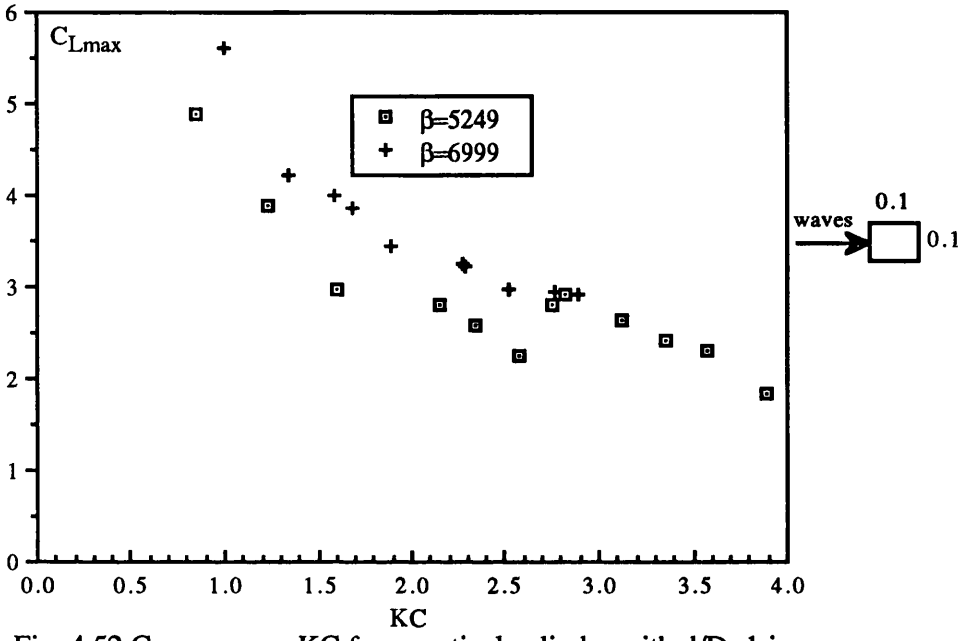

Fig. 4.52 C_{Lmax} versus KC for a vertical cylinder with d/D=1 in waves

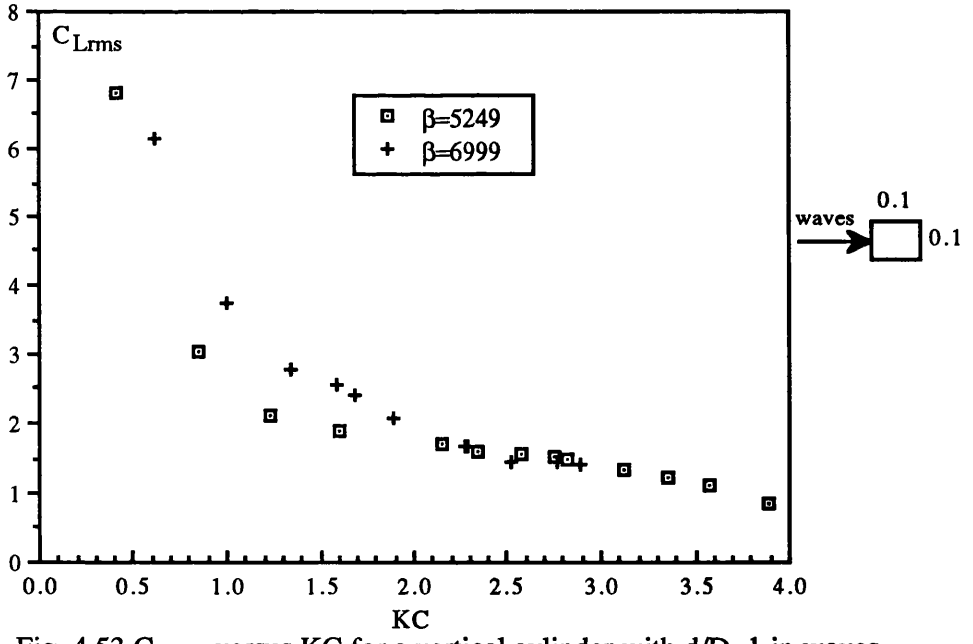

Fig. 4.53 C_{Lrms} versus KC for a vertical cylinder with d/D=1 in waves

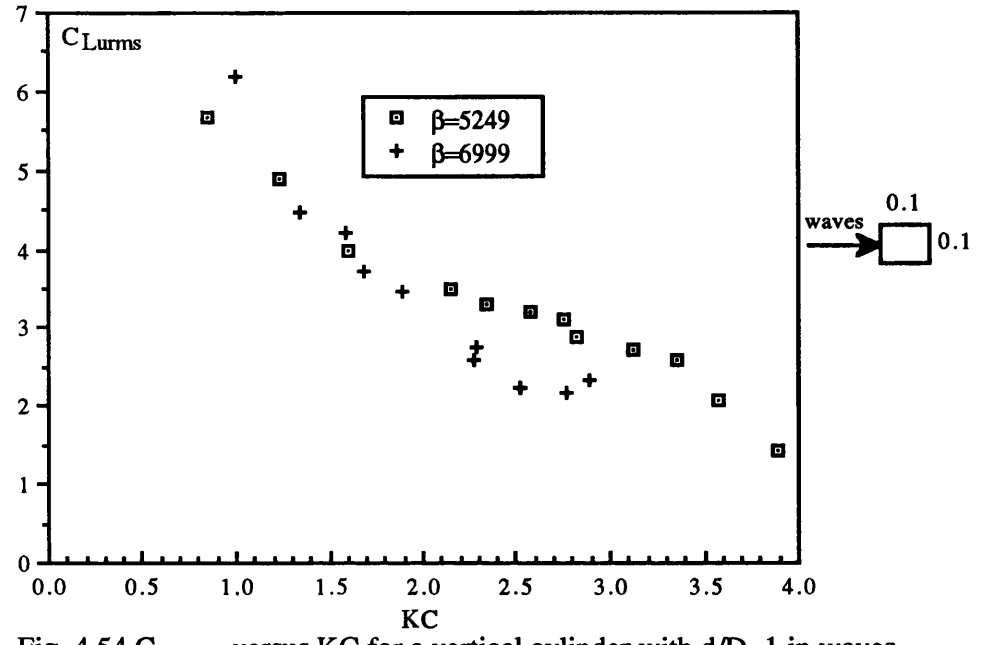

Fig. 4.54 C_{Lurms} versus KC for a vertical cylinder with d/D=1 in waves

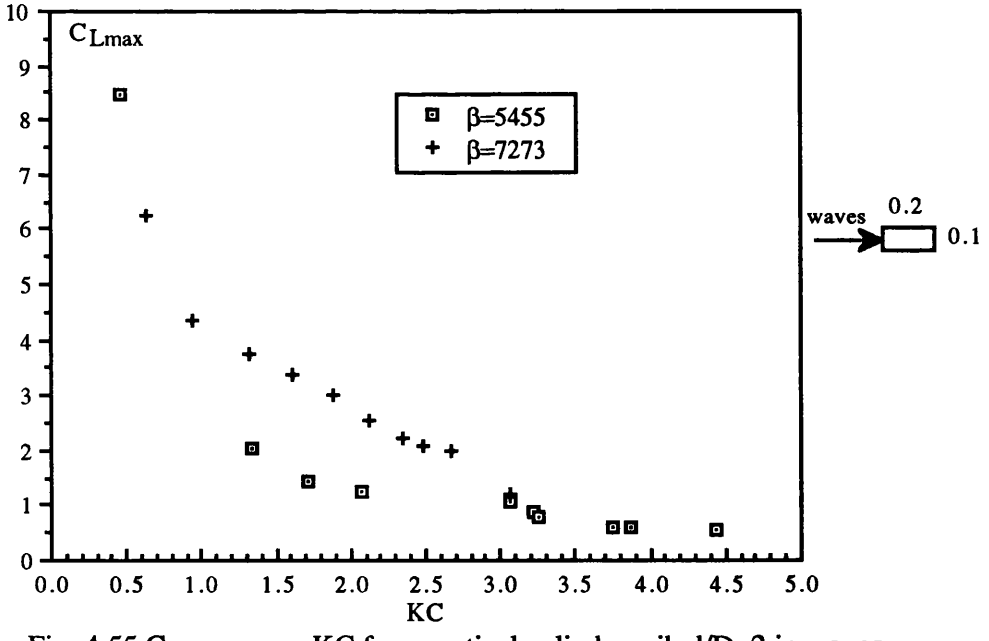

Fig. 4.55 C_{Lmax} versus KC for a vertical cylinder wih d/D=2 in waves

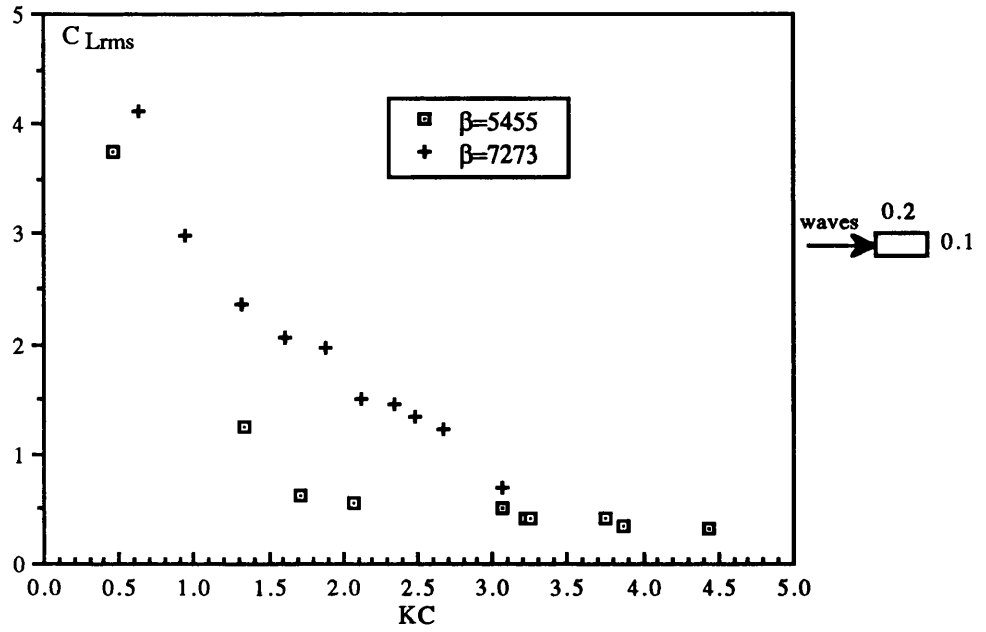

Fig. 4.56 C_{Lrms} versus KC for a vertical cylinder wih d/D=2 in waves

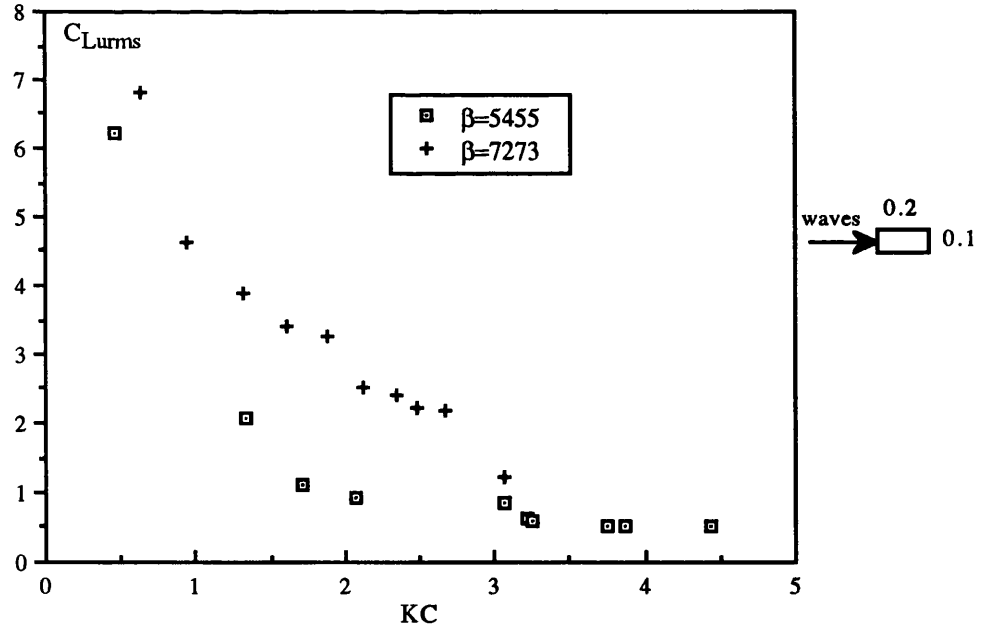

Fig. 4.57 C_{Lurms} versus KC for a vertical cylinder wih d/D=2 in waves

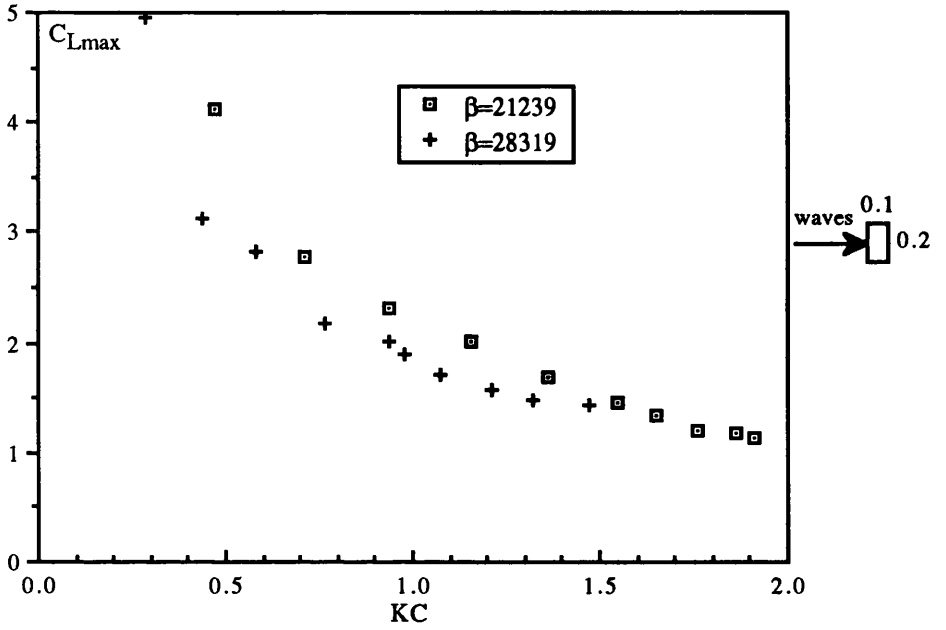

Fig. 4.58 C_{Lmax} versus KC for a vertical cylinder with d/D=0.5 in waves

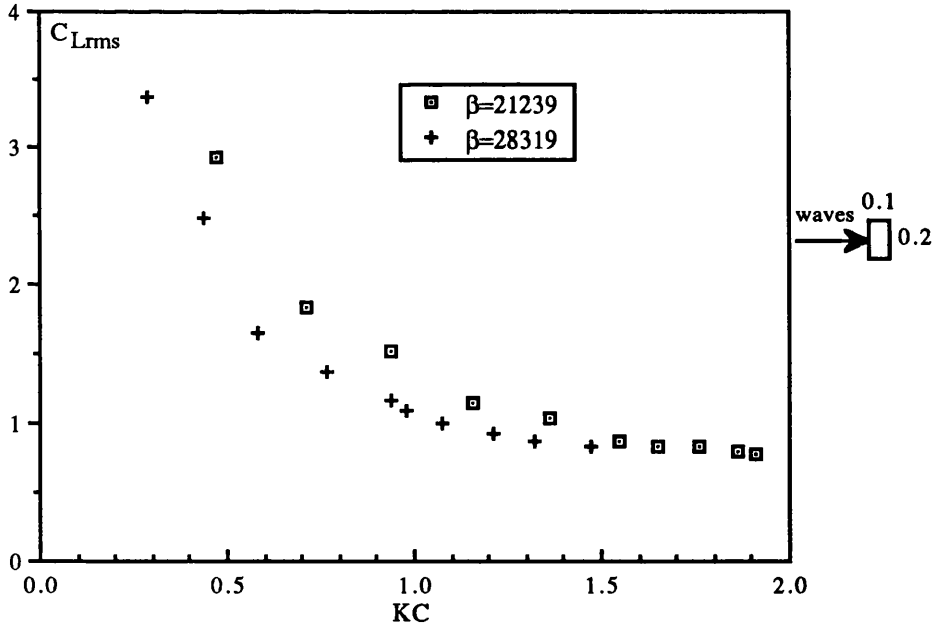

Fig. 4.59 C_{Lrms} versus KC for a vertical cylinder with d/D=0.5 in waves

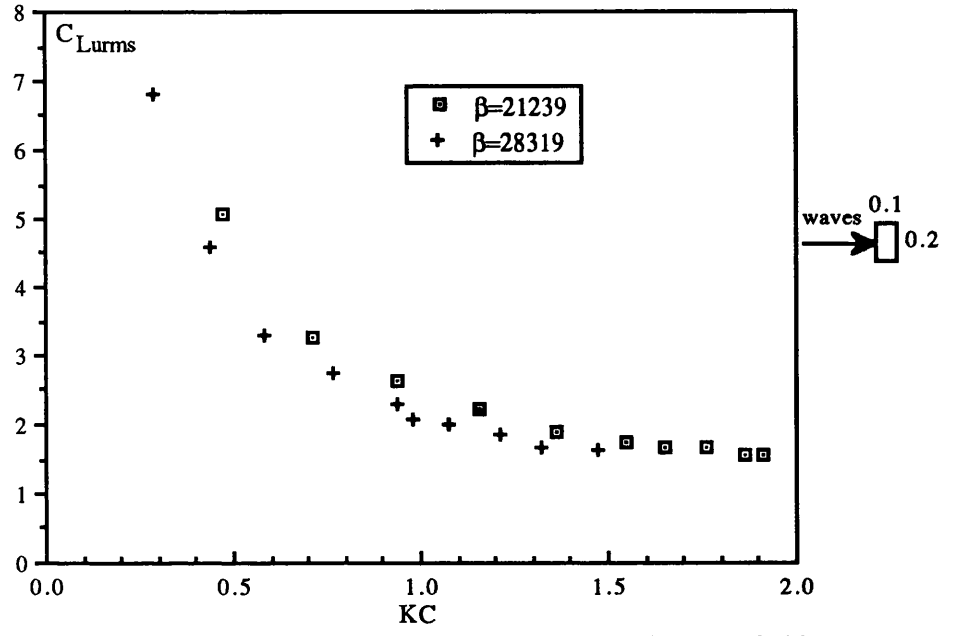

Fig. 4.60 C_{Lurms} versus KC for a vertical cylinder with d/D=0.5 in waves

4.3.2 HORIZONTAL CYLINDERS

The different cylinders discussed above were tested horizontally with their axes parallel to waves crests to measure the different wave coefficients.

The drag and inertia coefficients and maximum and r.m.s. force coefficients of measured horizontal forces (C_{Mx}, C_{Dx}, C_{Fxmax} and C_{Fxrms}) and of measured vertical forces (C_{My}, C_{Dy}, C_{Fymax} and C_{Fyrms}) are plotted against the Keulegan-Carpenter KC number for constant values of the frequency parameter β in Figures 4.61 through 4.96.

Figures 4.61 and 4.62 show the variations of C_{Mx} and C_{My} coefficients with the KC number for the square cross-sectional cylinder.

Both coefficients were found to follow the same trend of variation against the KC number and of similar values at corresponding KC numbers. As the KC number increased to about 3 C_M coefficient decreased to about 1.65. The present inertia coefficients agreed well with those measured by Ikeda et al. (1988) for a horizontal square cylinder in regular waves at rather lower β numbers. However, discrepancies were found in the variation of C_M coefficient with the KC number in waves and under planar oscillatory flow (Bearman et al. (1984)).

The variations of C_{Dx} and C_{Dy} coefficients with the KC number for this cylinder are shown in Figures 4.63 and 4.64. At corresponding KC numbers, the two drag coefficients had similar values. As in the case of vertical cylinders the drag coefficient was found to have large values at very low KC numbers and to decrease rapidly as the KC number increased. This behaviour of the drag coefficient was found with all horizontal cylinders. A value of C_D coefficient of 4 was found at a KC number of 2.8. Good agreement was also found between present C_D coefficients and those measured by Ikeda et al. (1988) in waves, though at much smaller β numbers. However, the drag coefficient measured by Bearman et al. in planar oscillatory flow was again smaller than the present results, though the comparison was made at very different β numbers.

The maximum horizontal force coefficient C_{Fxmax} during a wave cycle and the root mean square force coefficient of the horizontal force C_{Fxrms}, and the corresponding force coefficients C_{Fymax} and C_{Fyrms} of the vertical force for the square cylinder are shown in Figures 4.65 through 4.68. At corresponding KC numbers, the coefficients of the horizontal force had similar values to those of corresponding coefficients of the vertical force. As in the case of vertical cylinders, these coefficients were found to have large values at very low KC numbers and to decrease rapidly as the KC number increased. Again this behaviour by these coefficients was found with all horizontal cylinders. Comparisons between the measured r.m.s. of the horizontal and vertical force coefficients and the calculated r.m.s. of the horizontal and vertical force coefficients from the Morison equation using measured C_{Mx} and C_{Dx}, and C_{My} and C_{Dy} coefficients (eq. 3.28) are shown in Figures 4.69 through 4.72. The comparisons between the measured and calculated r.m.s. force coefficients were made for identical values of KC and β numbers. The correlation between the measured and the predicted force coefficients was found to be good.

The variations of C_{Mx} and C_{My} coefficients with the KC number for the cylinder with an aspect ratio of 2 are shown in Figures 4.73 and 4.74.

The C_{My} coefficient was found to have higher values than those of C_{Mx} coefficient. Both coefficients were found to have the same trend of variation with the KC number as that of the square cylinder. However, smaller values of C_{Mx} coefficient were found for this cylinder than those of the square cylinder. C_{Mx} and C_{My} coefficients were found to have values between 1.6 and 1.2, and 3.1 and 2 respectively when the KC number varied up to 4. At KC numbers of 0.4 and 2.8, for example, C_{Mx} coefficient decreased by 42% and 20% respectively, when the aspect ratio increased from unity to 2.

Figures 4.75 and 4.76 show the variations of C_{Dx} and C_{Dy} coefficients with the KC number for this cylinder. The C_{Dy} coefficient was found to have slightly higher values than C_{Dx} coefficient. As the KC number increased from about 1 to 4, C_D coefficient (both C_{Dx} and C_{Dy}) decreased from a high value of about 8 to 5. Unlike the case of vertical cylinders, increasing the aspect ratio from unity to 2 for horizontal cylinders had a greater influence on the value of the drag coefficient. Indeed, at a KC number of 2.5, for example, C_{Dx} increased by 33% when the aspect ratio increased from unity to 2.

The variations of C_{Fxmax}, C_{Fymax}, and C_{Fxrms}, C_{Fyrms} coefficients with the KC number are shown in Figures 4.77 through 4.80. At corresponding KC numbers and as in the case of the square cylinder, the horizontal force coefficients had similar values with corresponding ones of the vertical force. On the effect of changing the aspect ratio from unity to 2, at a KC number just below 1, C_{Fxmax} and C_{Fxrms} coefficients were found to remain almost constant. At a higher KC number of 2.5, however, C_{Fxmax} and C_{Fxrms} coefficients increased by 33% and 37% respectively when increasing the aspect ratio from unity to 2.

Figures 4.81 through 4.84 show comparisons between the measured r.m.s. of the horizontal and vertical force coefficients and the calculated r.m.s. of the horizontal and vertical force coefficients from the Morison equation using measured C_{Mx} and C_{Dx}, and C_{My} and C_{Dy} coefficients. Comparisons between the measured and calculated r.m.s. force coefficients were made for identical values of KC and β numbers. The predicted force coefficients agreed well with the measured forces.

The variations of C_{Mx} and C_{My} coefficients with the KC number for the cylinder with the smallest aspect ratio of 0.5 are shown in Figures 4.85 and 4.86.

With this cylinder, C_{Mx} coefficient was found to have higher values than those of C_{My} coefficient. When the KC number varied from a very low value of 0.15 to 2, C_{Mx} and C_{My} coefficients had an average value of 3.2 and 1.6 respectively. The in-line inertia coefficient C_{Mx} measured for this aspect ratio was found to be the highest of the three aspect ratios investigated. For example, at KC numbers of 0.4 and 2, C_{Mx} coefficient increased by 22% and 43% respectively, when the aspect ratio was reduced from unity to 0.5.

Figures 4.87 and 4.88 show the variations of C_{Dx} and C_{Dy} coefficients for this cylinder with the KC number. The two drag coefficients were found to have similar values at corresponding KC numbers. As the KC number increased from a very low value of 0.5 to 2, C_{Dx} coefficient decreased from a high value of about 15 to 5. Unlike the inertia

coefficient, reducing the aspect ratio from unity to 0.5 decreased the drag coefficient. For example, at KC numbers of 1.2 and 2, C_D coefficient decreased by 21% and 7% respectively when the aspect ratio reduced.

The variations of C_{Fxmax}, C_{Fymax}, and C_{Fxrms}, C_{Fyrms} coefficients with the KC number are shown in Figures 4.89 through 4.92. As with other cylinders, the horizontal force coefficients were similar to the vertical force coefficients at corresponding KC numbers. At KC=1.2, C_{Fxmax} and C_{Fxrms} coefficients decreased by 26% and 23% respectively when the aspect ratio was reduced from unity to 0.5. At a higher KC number of 2, C_{Fxmax} and C_{Fxrms} coefficients decreased by 29% and 21% respectively. Again, attention should be paid to the fact that comparisons were made between the square cylinder and the cylinder with aspect ratio of 0.5 at much different values of β numbers.

Comparisons between the measured r.m.s. force coefficient and the calculated r.m.s. force coefficient from the Morison equation using measured C_M and C_D coefficients are shown in Figures 4.93 through 4.96. Comparisons between the measured and calculated r.m.s. force coefficients were made for identical values of KC and β numbers. Again the agreement between the measured and predicted force coefficients was good.

4.3.3 EFFECT OF CYLINDER'S ORIENTATION

On the effect of the cylinder's orientation, the force coefficients of vertical cylinders were in general found to be higher than those of the corresponding horizontal cylinders for identical governing parameters.

With the square cylinder, at a low KC number of about 0.8, the in-line C_M and C_D coefficients decreased by 7% and 1% respectively when the orientation of the cylinder was changed from vertical to horizontal (compare Figures 4.34, 4.35 with 4.61, 4.63). At a higher KC number of about 2.8, the in-line C_M and C_D coefficients decreased by 49% and 24% respectively. At a KC number of about 0.8, C_{Fmax} and C_{Frms} coefficients of the vertical square cylinder had practically identical values with the corresponding in-line coefficients of the horizontal square cylinder (compare Figures 4.36, 4.37 with 4.65, 4.67). However, at a higher KC number of about 2.8, C_{Fmax} and C_{Frms} coefficients decreased by 43% and 45% respectively when the orientation of the cylinder was changed from vertical to horizontal.

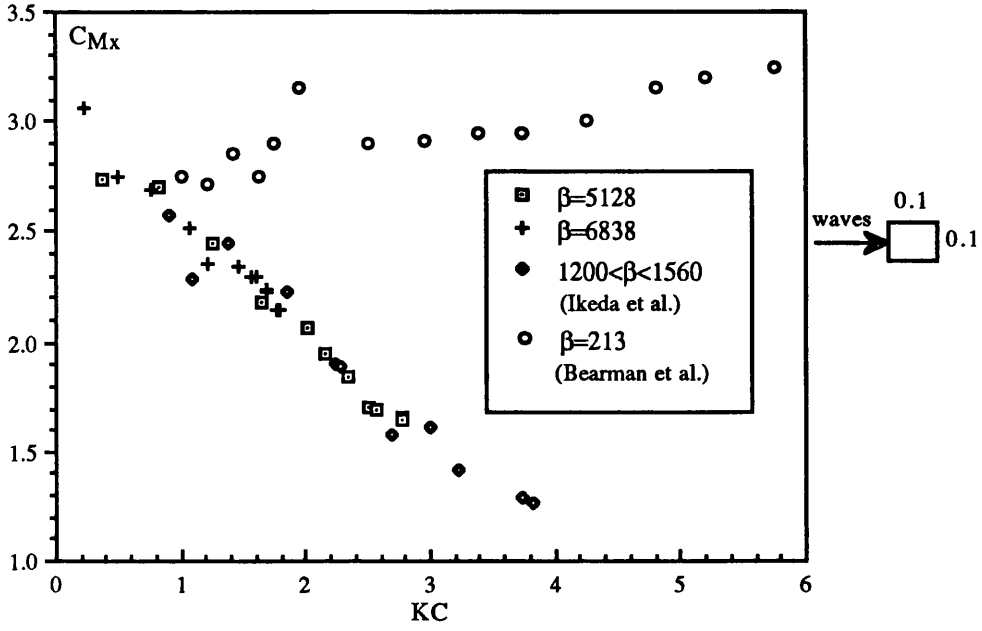

Fig. 4.61 C_{Mx} versus KC for a horizontal cylinder with d/D=1 in waves

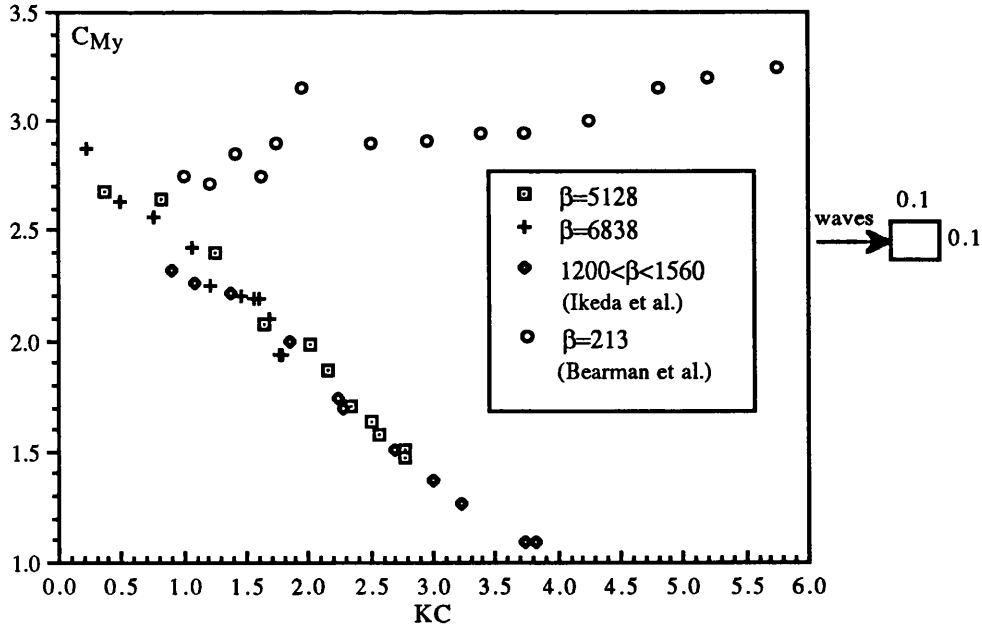

Fig. 4.62 C_{My} versus KC for a horizontal cylinder with d/D=1 in waves

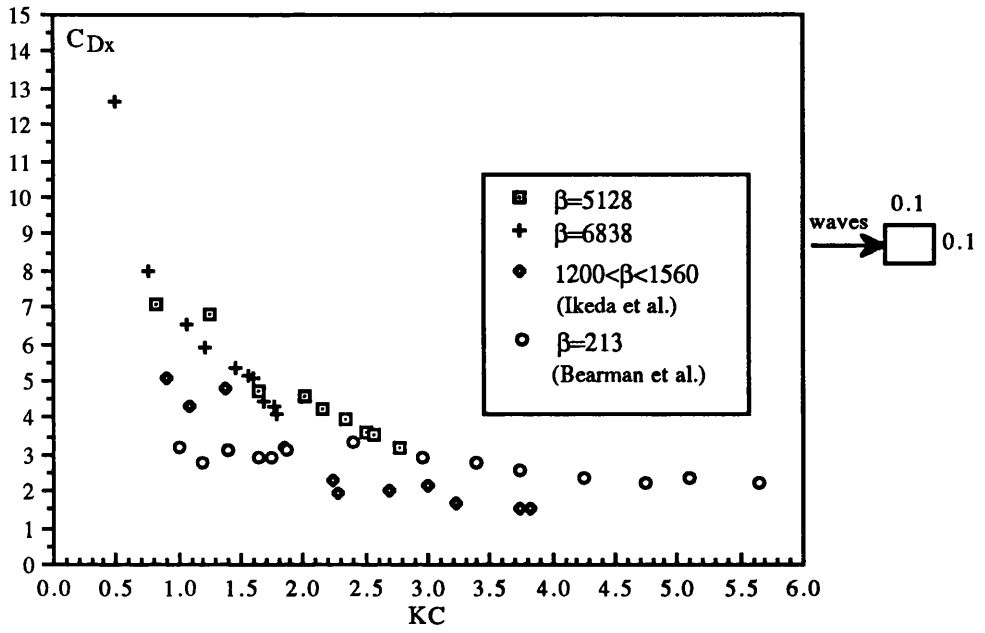

Fig. 4.63 C_{Dx} versus KC for a horizontal cylinder with d/D=1 in waves

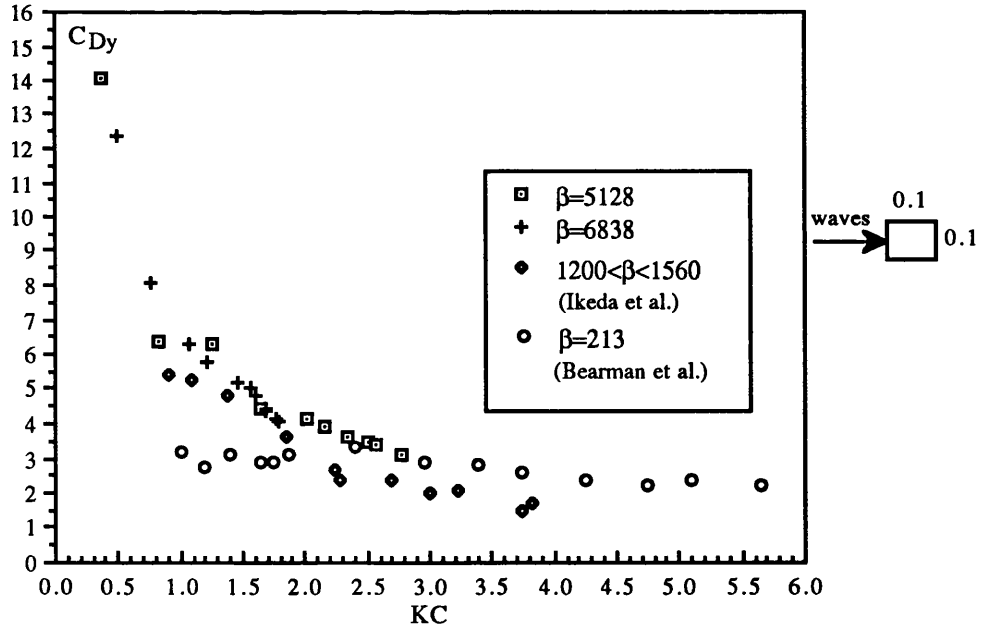

Fig. 4.64 C_{Dy} versus KC for a horizontal cylinder with d/D=1 in waves

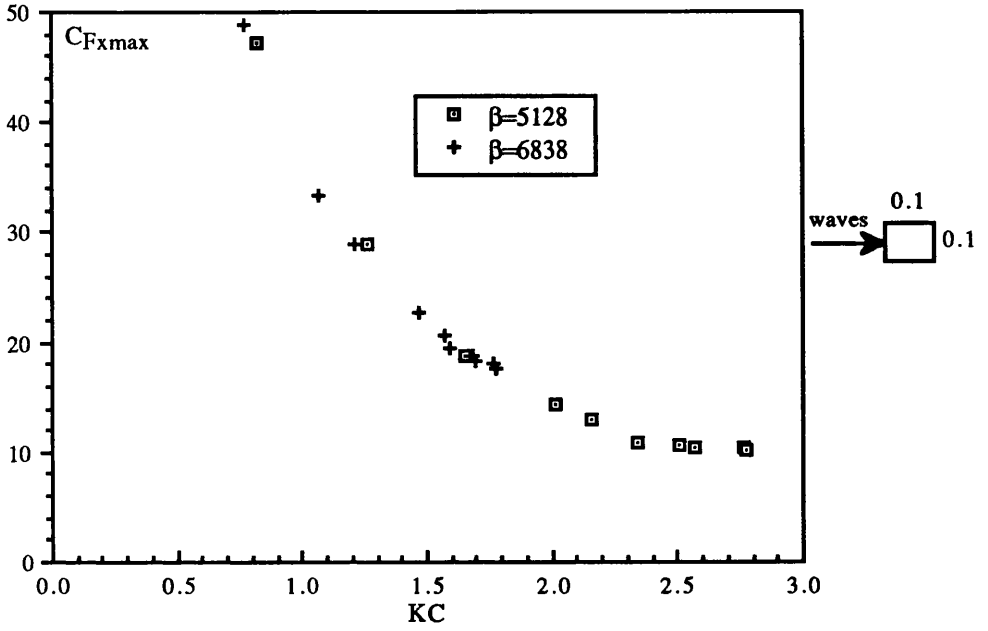

Fig. 4.65 C_{Fxmax} versus KC for a horizontal cylinder with d/D=1 in waves

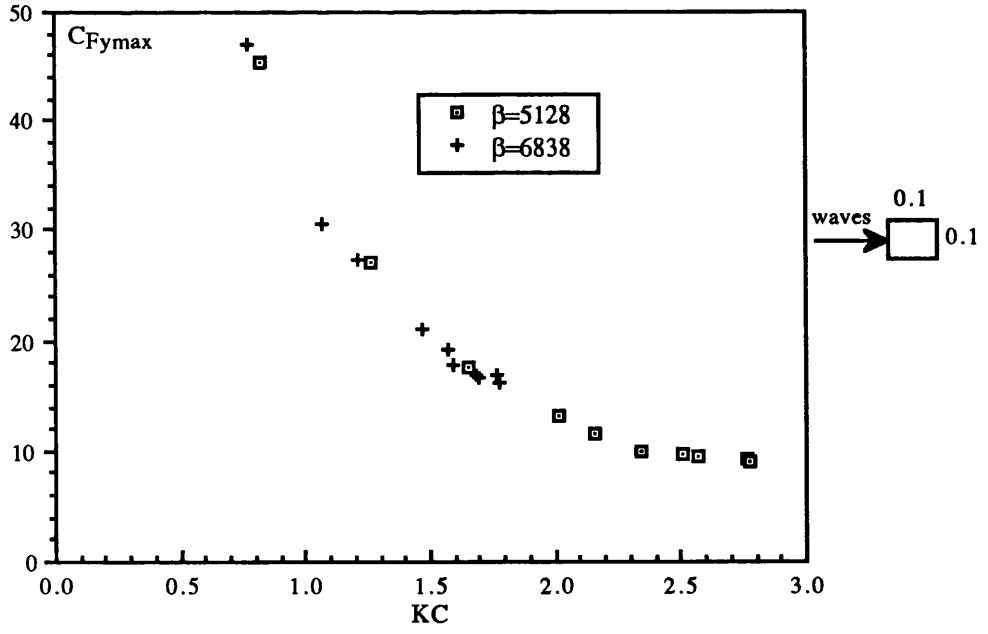

Fig. 4.66 C_{Fymax} versus KC for a horizontal cylinder with d/D=1 in waves

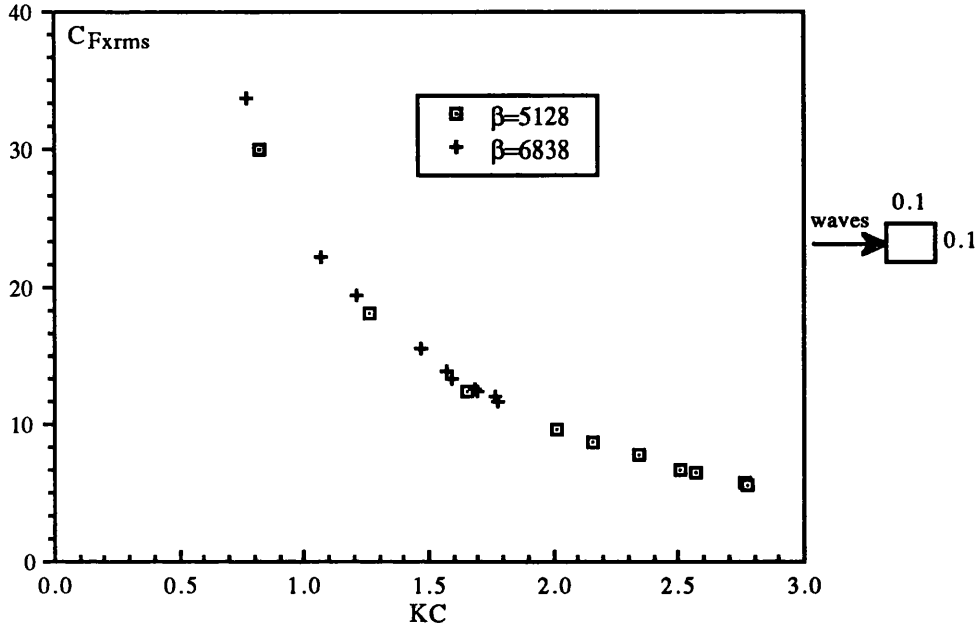

Fig. 4.67 C_{Fxrms} versus KC for a horizontal cylinder with d/D=1 in waves

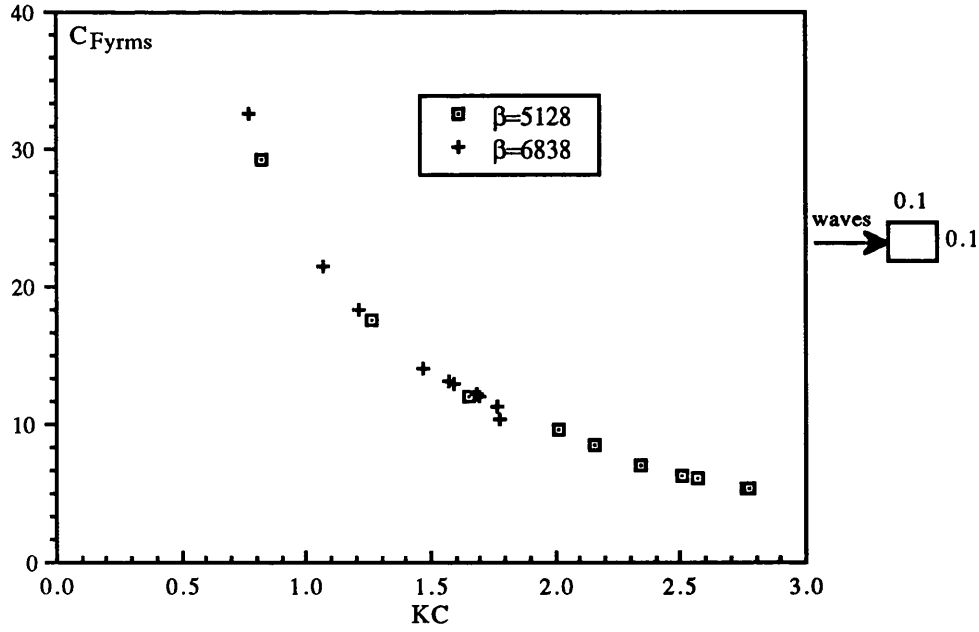

Fig. 4.68 C_{Fyrms} versus KC for a horizontal cylinder with d/D=1 in waves

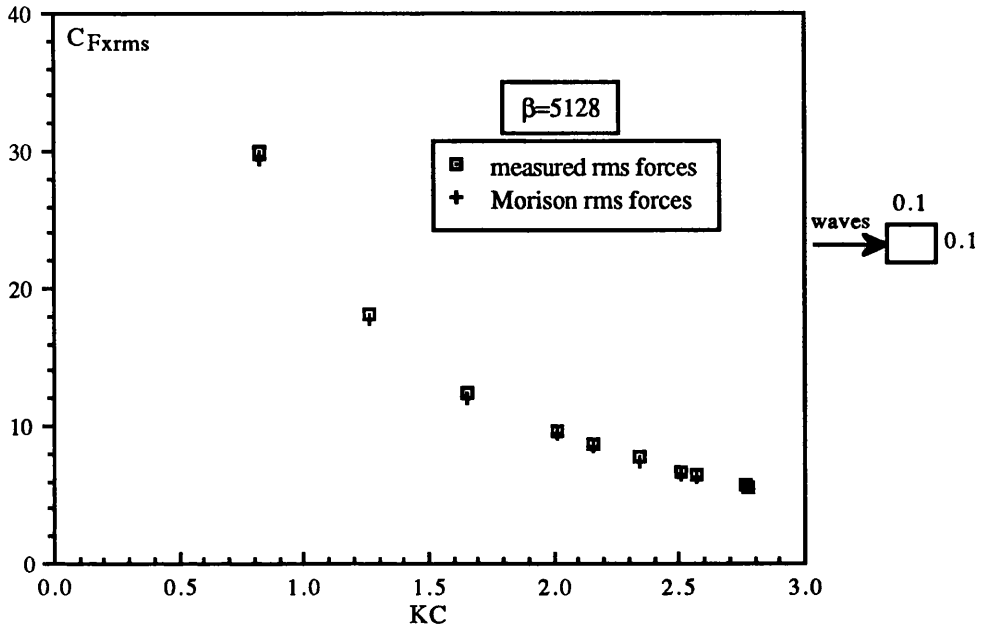

Fig. 4.69 C_{Fxrms} versus KC for a horizontal cylinder with d/D=1 in waves

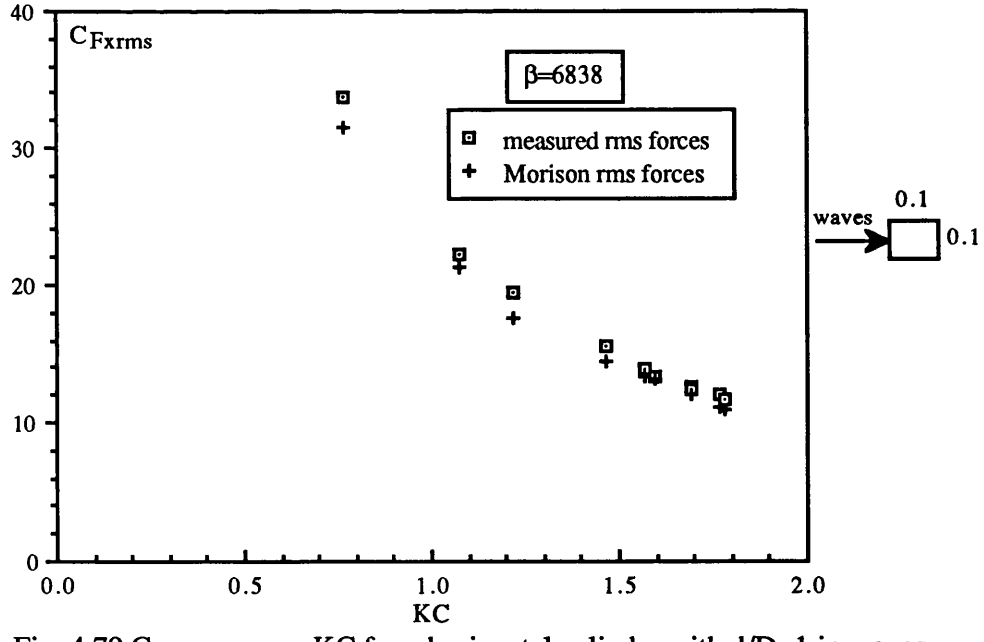

Fig. 4.70 C_{Fxrms} versus KC for a horizontal cylinder with d/D=1 in waves

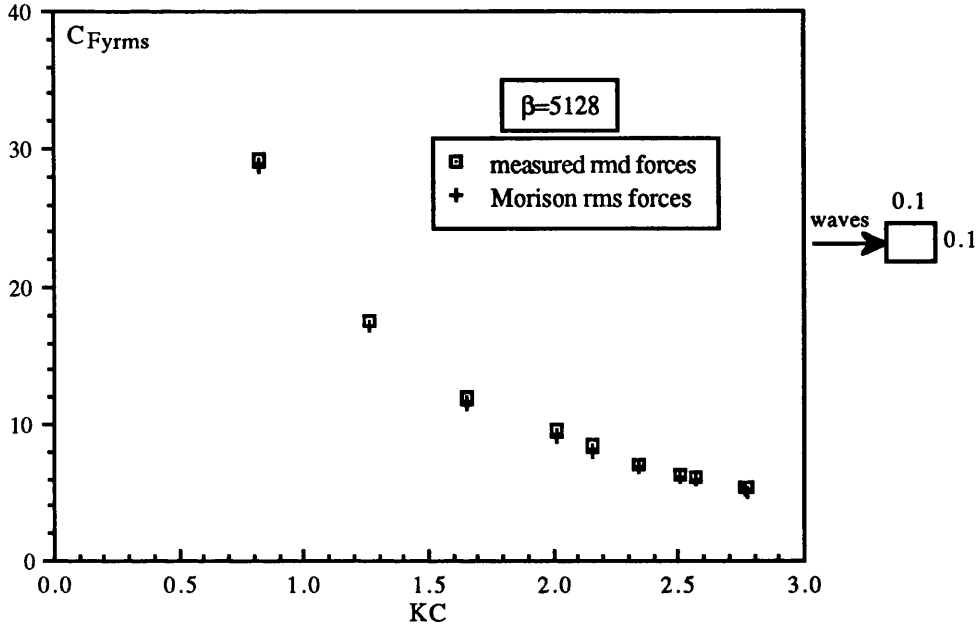

Fig. 4.71 C_{Fyrms} versus KC for a horizontal cylinder with d/D=1 in waves

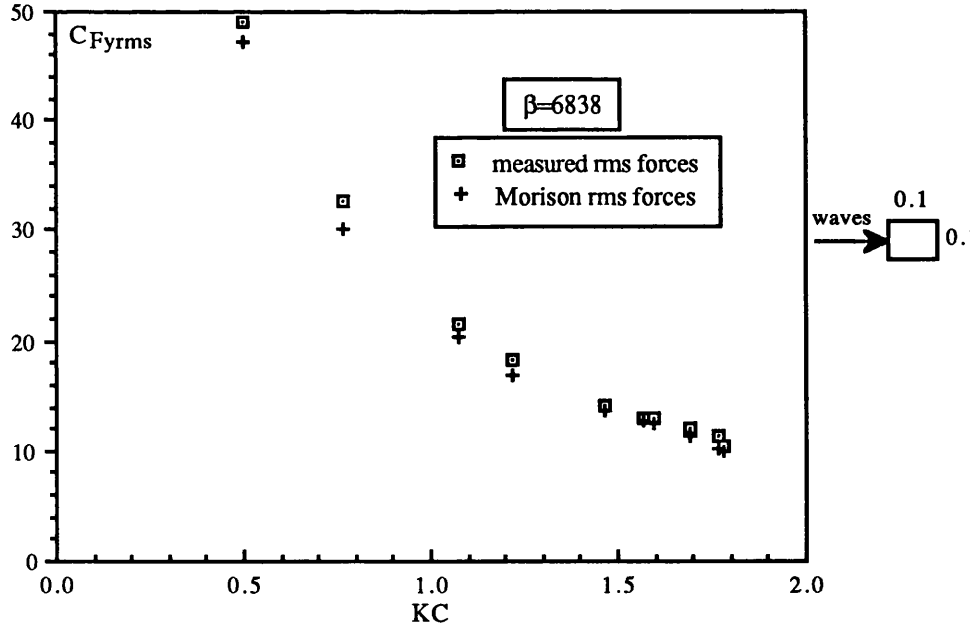

Fig. 4.72 C_{Fyrms} versus KC for a horizontal cylinder with d/D=1 in waves

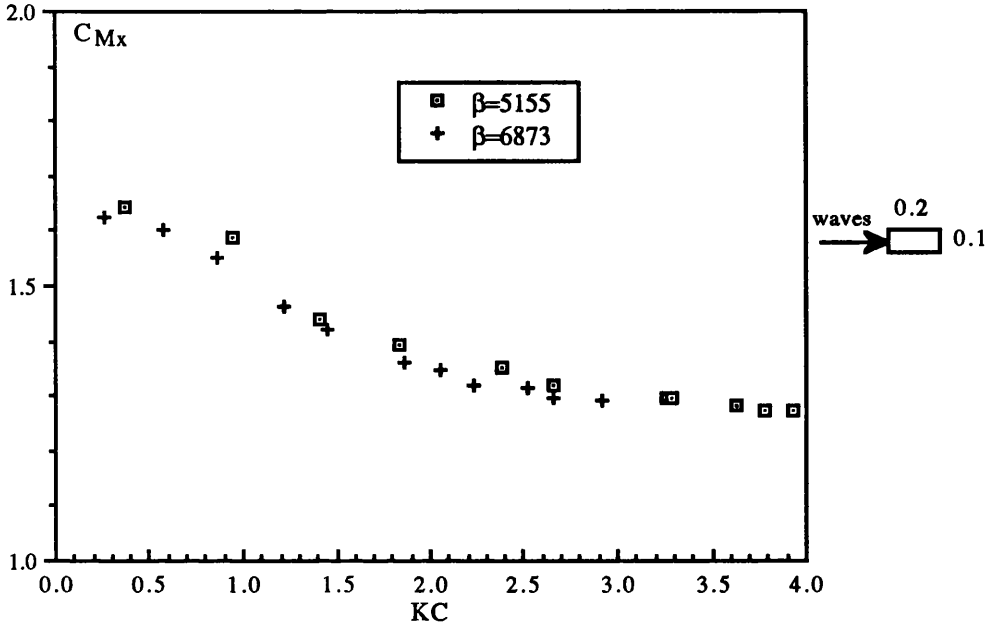

Fig. 4.73 C_{Mx} versus KC for a horizontal cylinder wih d/D=2 in waves

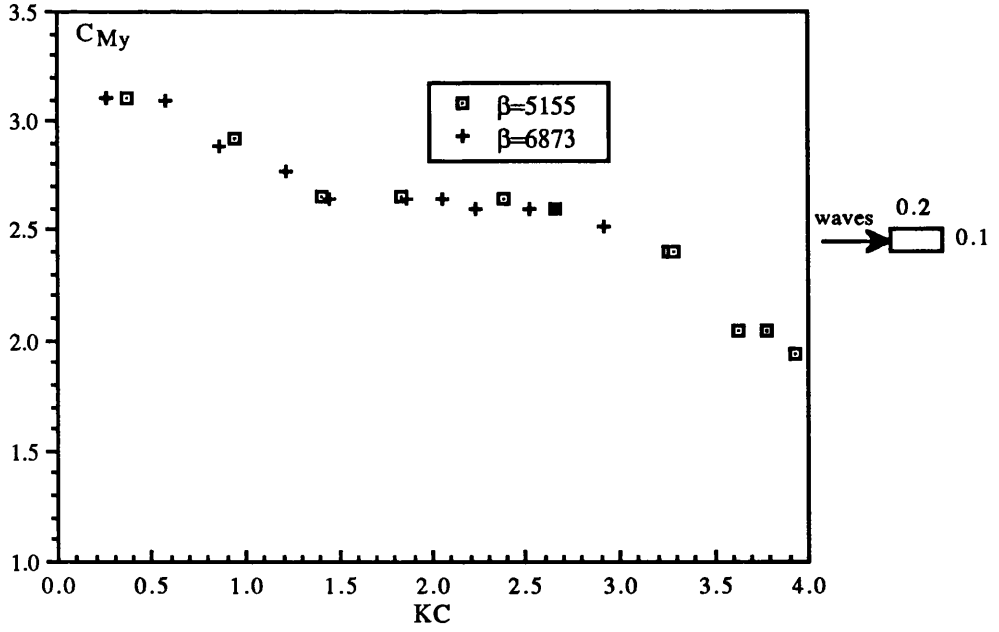

Fig. 4.74 C_{My} versus KC for a horizontal cylinder wih d/D=2 in waves

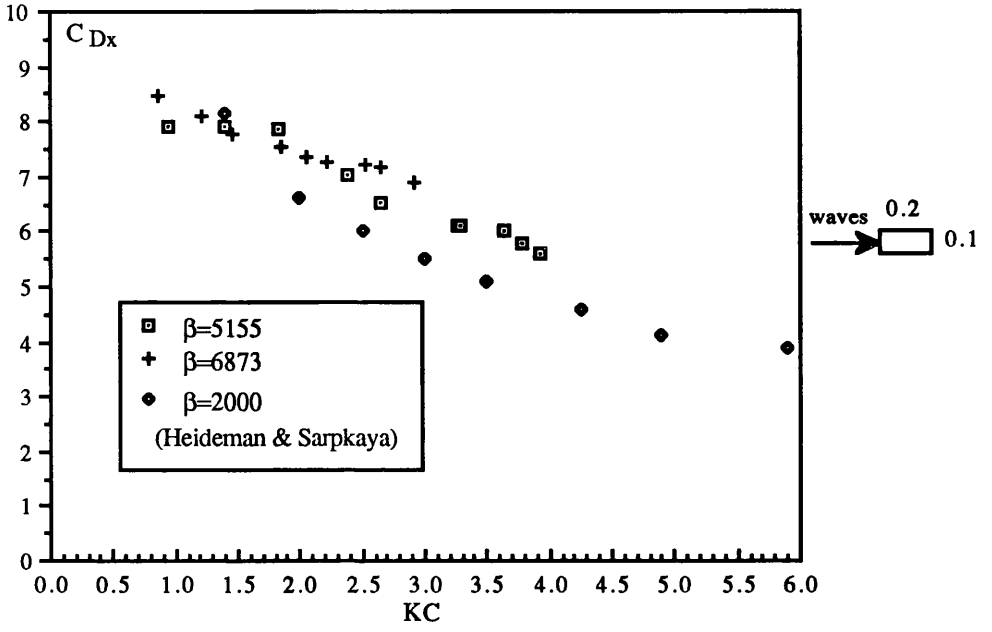

Fig. 4.75 C_{Dx} versus KC for a horizontal cylinder wih d/D=2 in waves

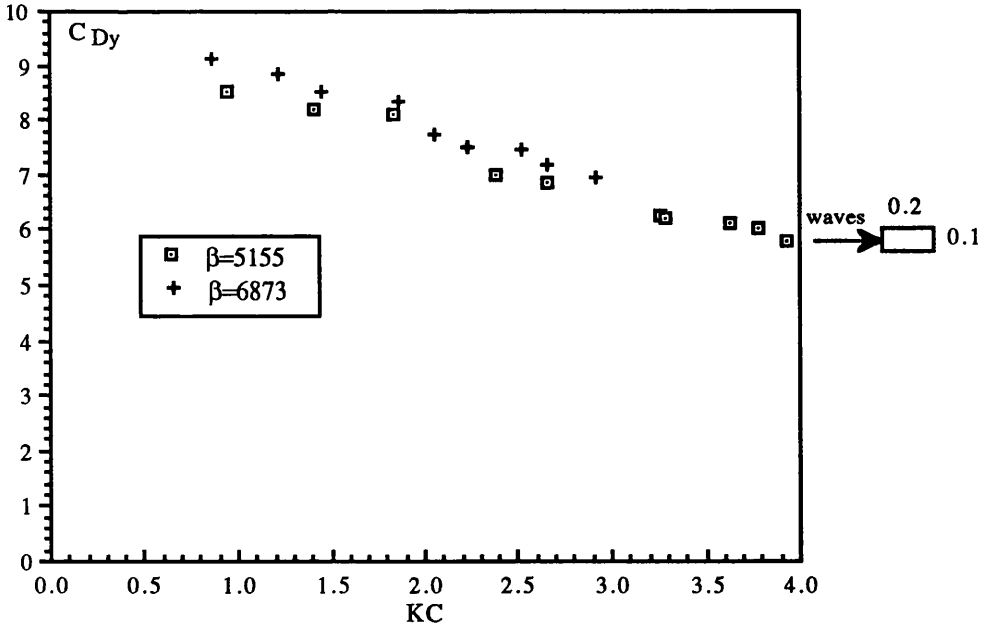

Fig. 4.76 C_{Dy} versus KC for a horizontal cylinder wih d/D=2 in waves

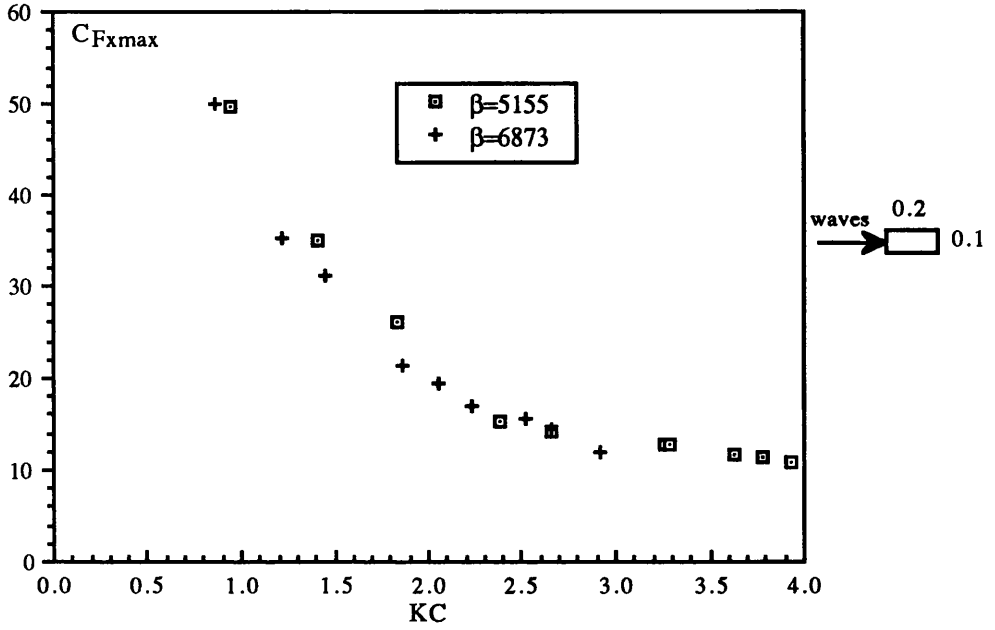

Fig. 4.77 C_{Fxmax} versus KC for a horizontal cylinder wih d/D=2 in waves

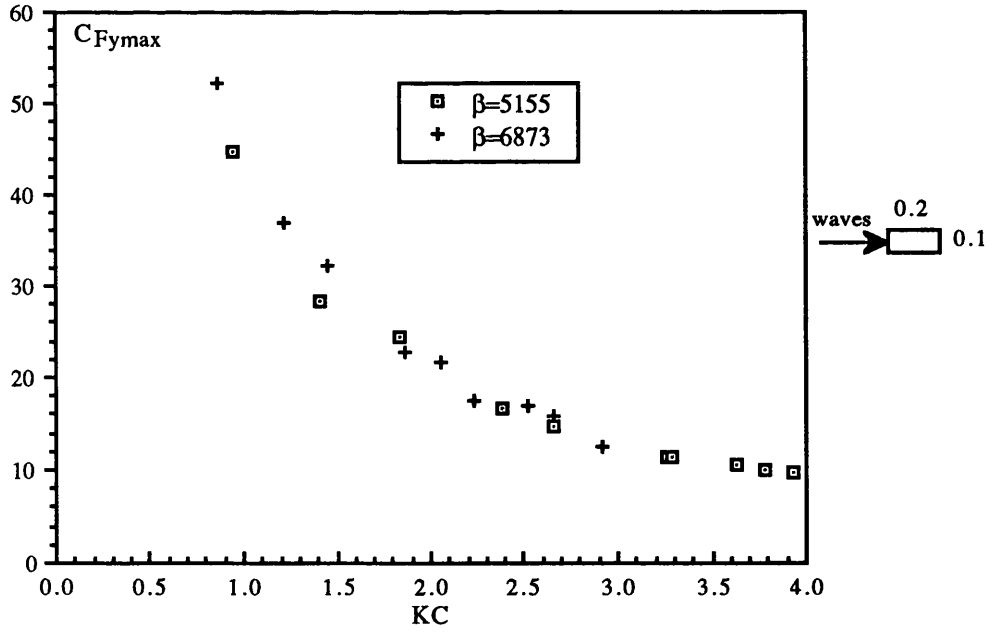

Fig. 4.78 C_{Fymax} versus KC for a horizontal cylinder wih d/D=2 in waves

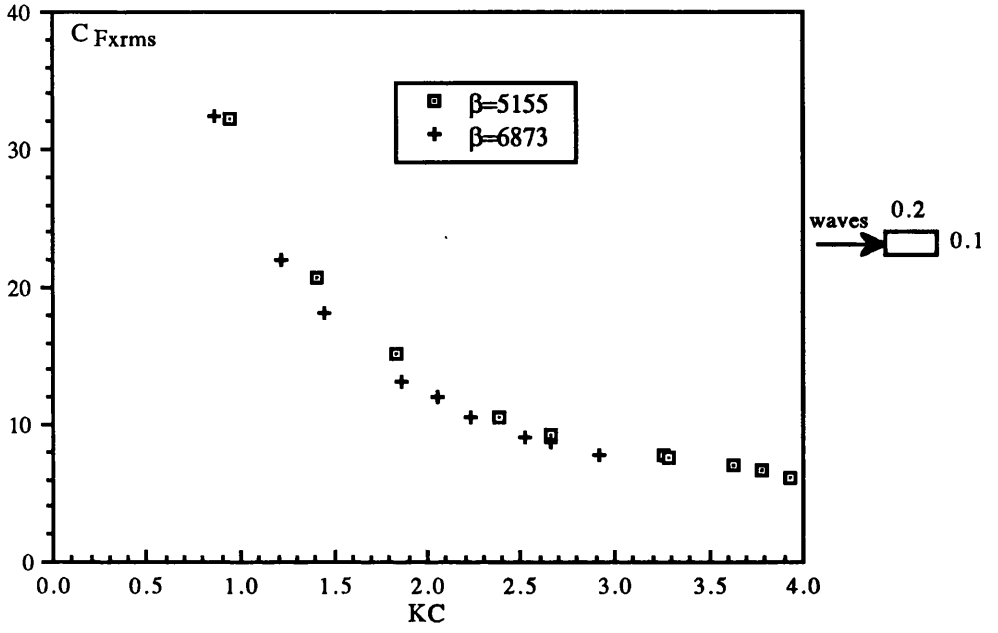

Fig. 4.79 C_{Fxrms} versus KC for a horizontal cylinder wih d/D=2 in waves

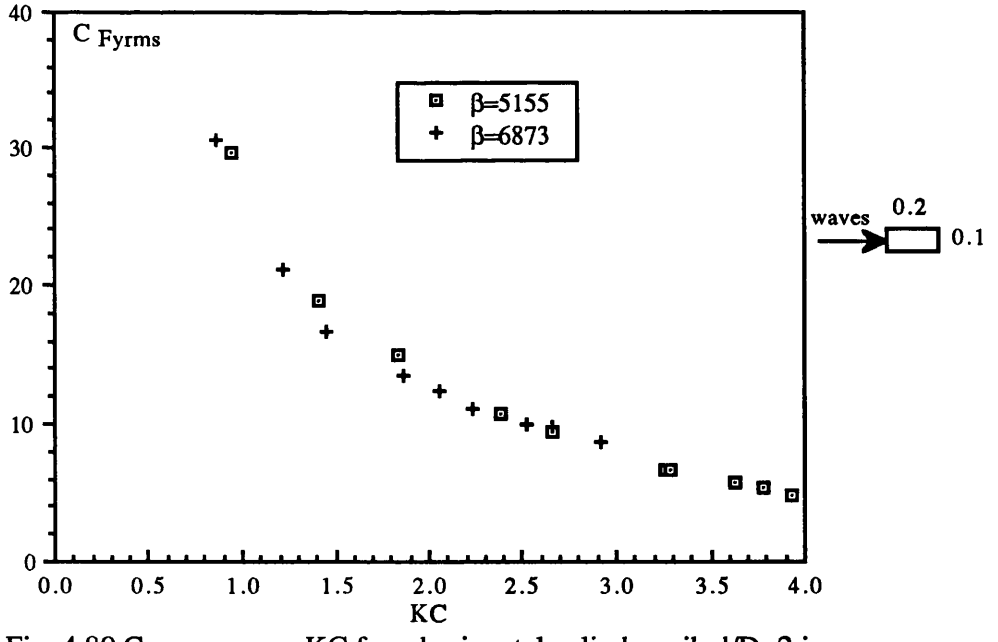

Fig. 4.80 C_{Fyrms} versus KC for a horizontal cylinder wih d/D=2 in waves

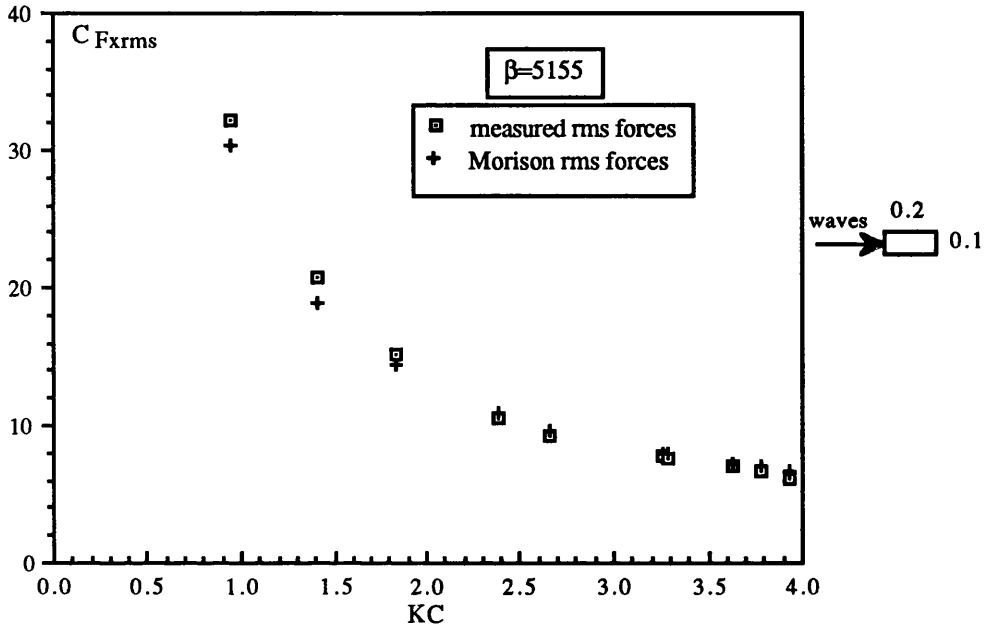

Fig. 4.81 C_{Fxrms} versus KC for a horizontal cylinder wih d/D=2 in waves

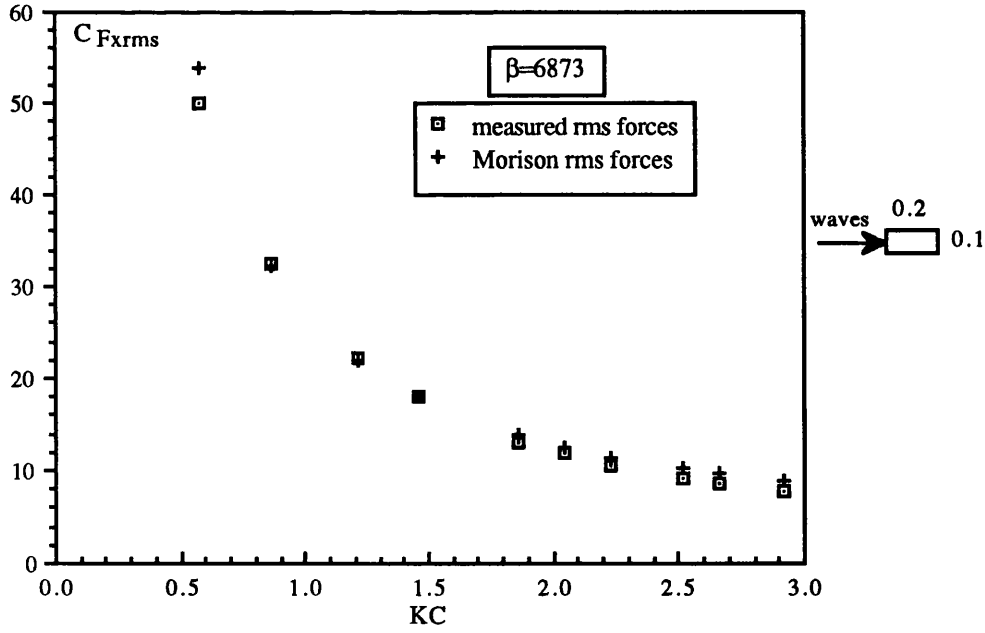

Fig. 4.82 C_{Fxrms} versus KC for a horizontal cylinder wih d/D=2 in waves

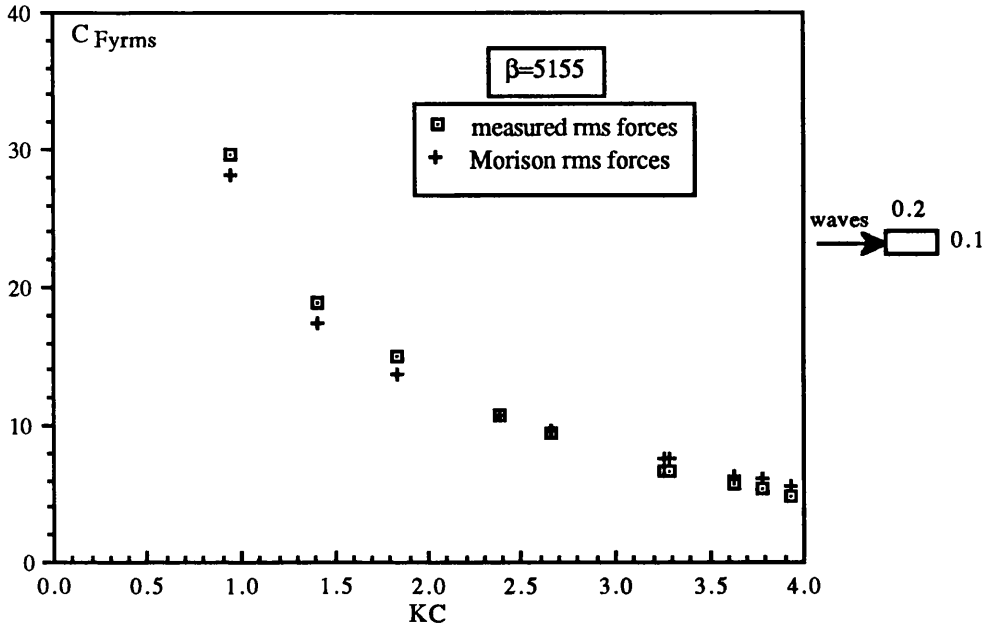

Fig. 4.83 C_{Fyrms} versus KC for a horizontal cylinder wih d/D=2 in waves

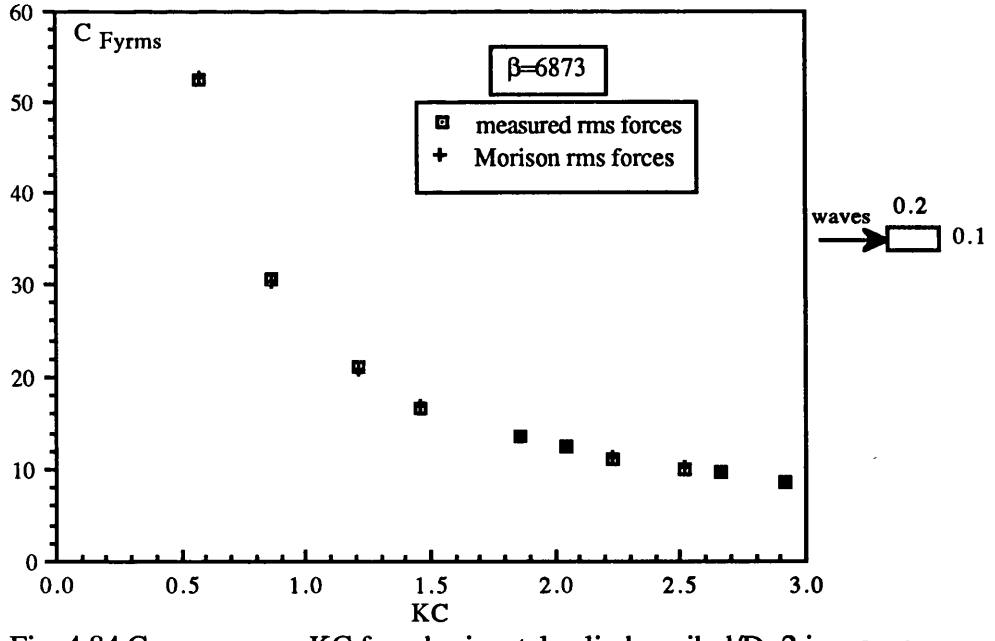

Fig. 4.84 C_{Fyrms} versus KC for a horizontal cylinder wih d/D=2 in waves

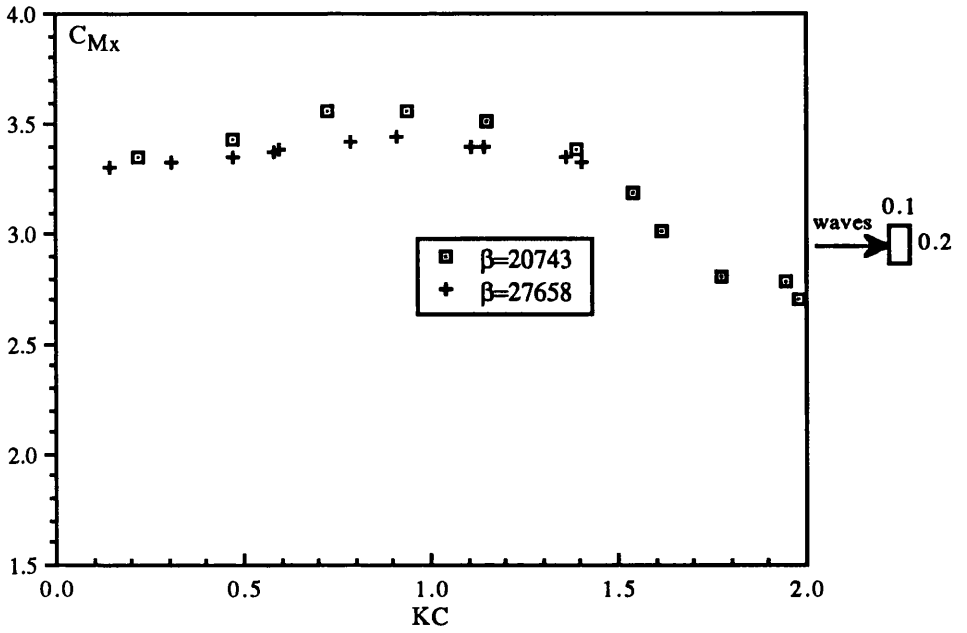

Fig. 4.85 C_{Mx} versus KC for a horizontal cylinder with d/D=0.5 in waves

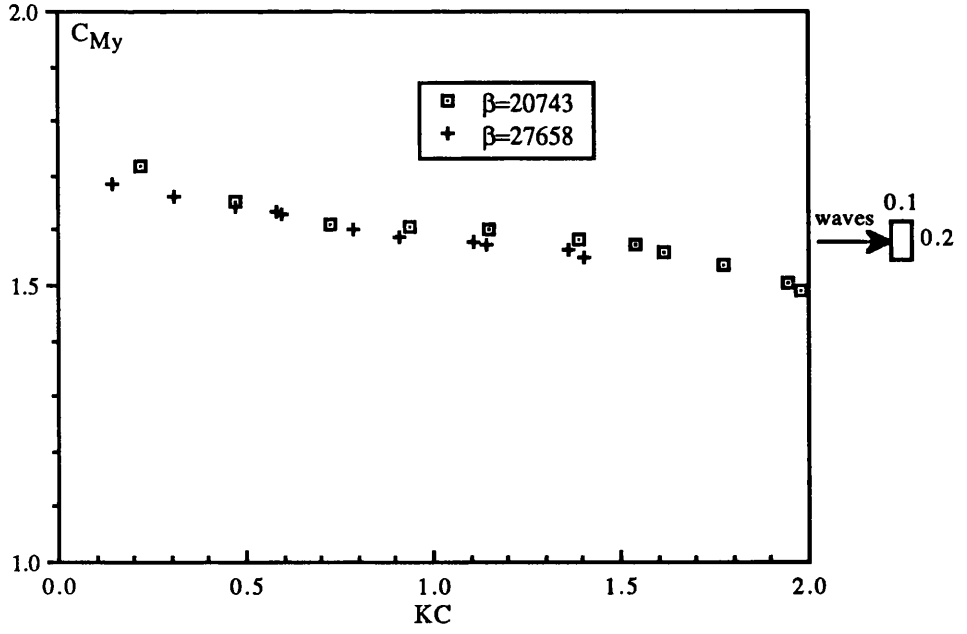

Fig. 4.86 C_{My} versus KC for a horizontal cylinder with d/D=0.5 in waves

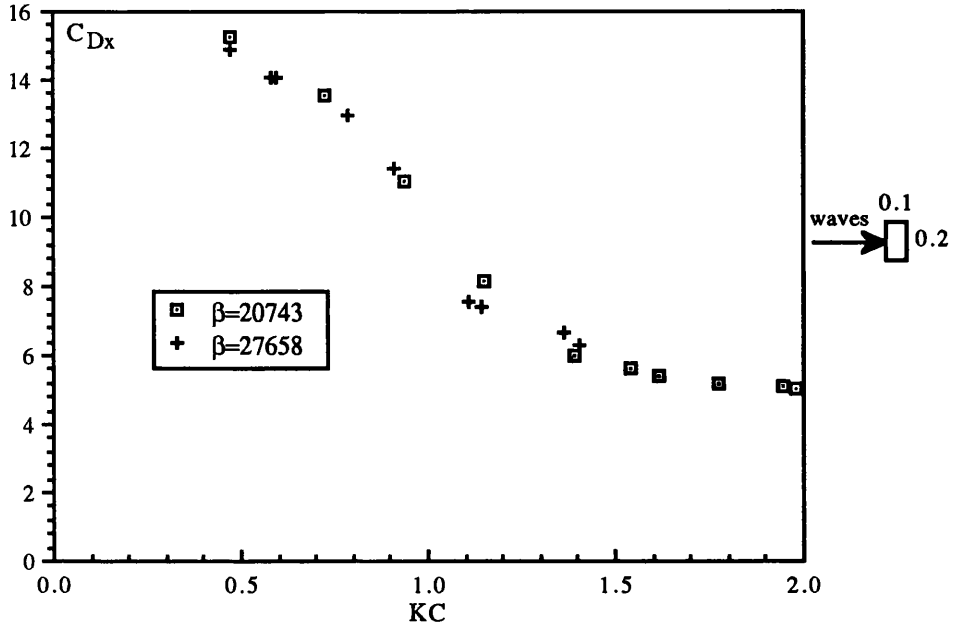

Fig. 4.87 C_{Dx} versus KC for a horizontal cylinder with d/D=0.5 in waves

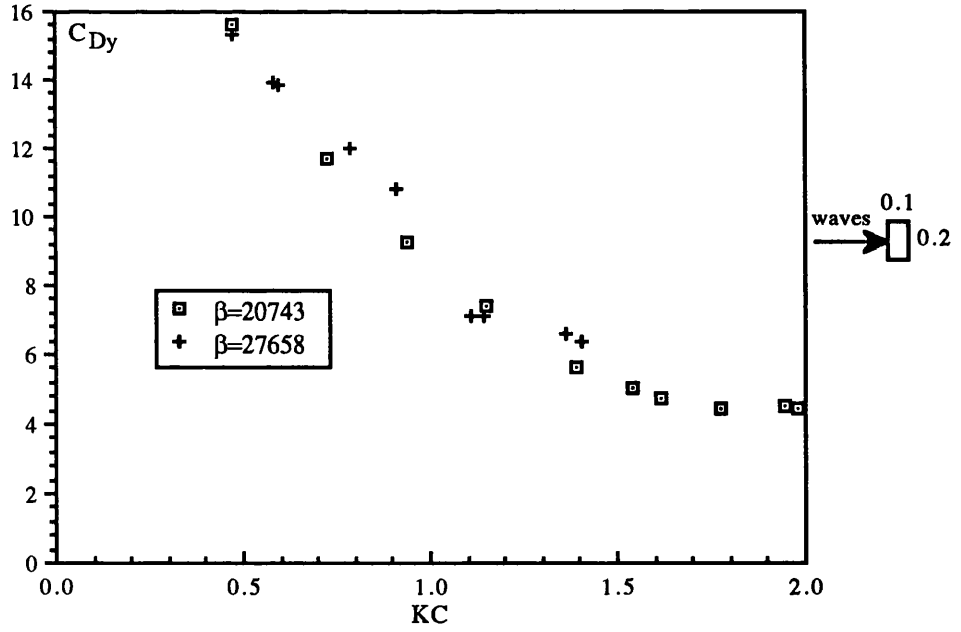

Fig. 4.88 C_{Dy} versus KC for a horizontal cylinder with d/D=0.5 in waves

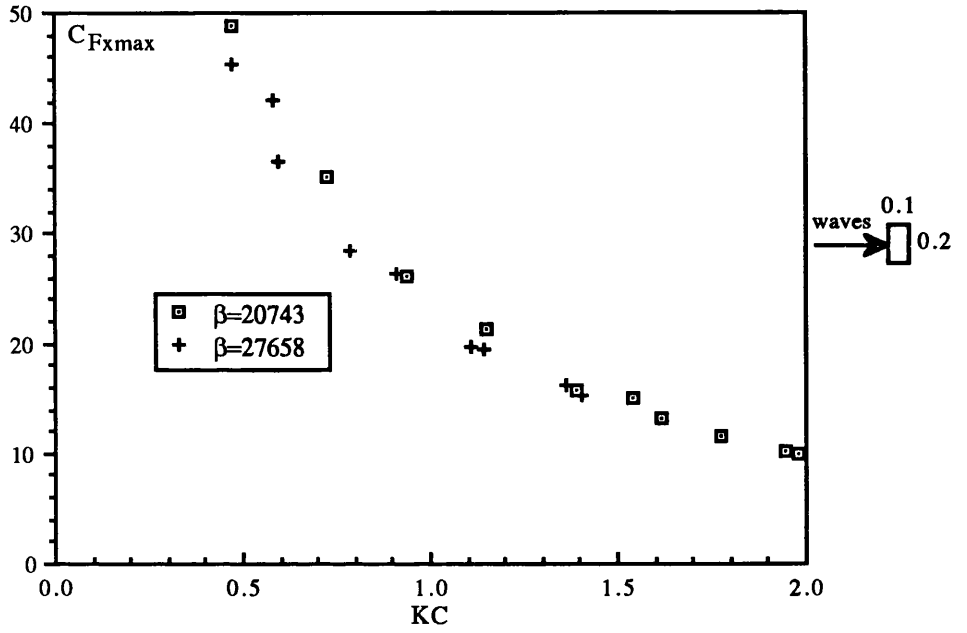

Fig. 4.89 C_{Fxmax} versus KC for a horizontal cylinder with d/D=0.5 in waves

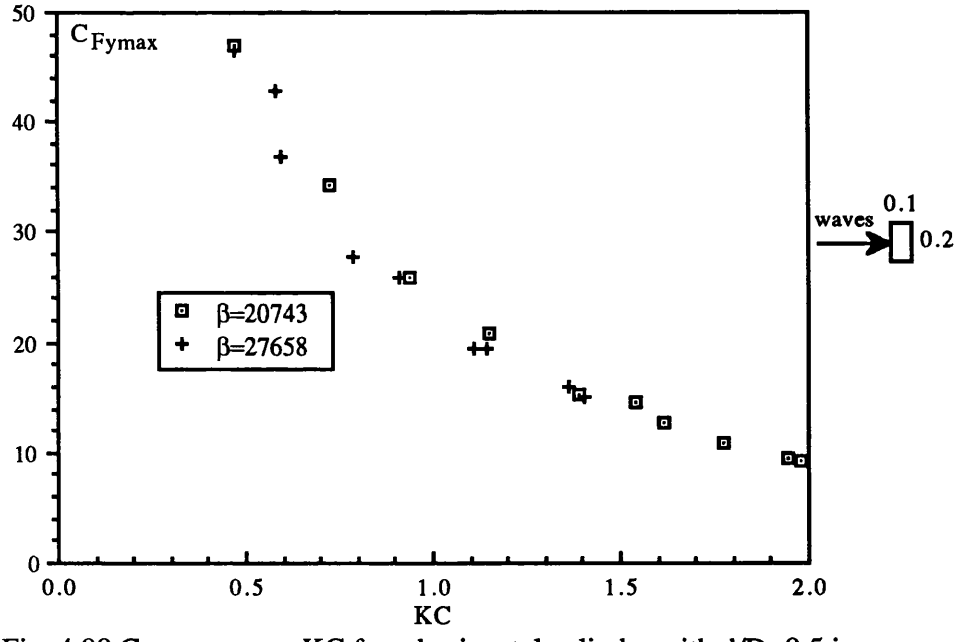

Fig. 4.90 C_{Fymax} versus KC for a horizontal cylinder with d/D=0.5 in waves

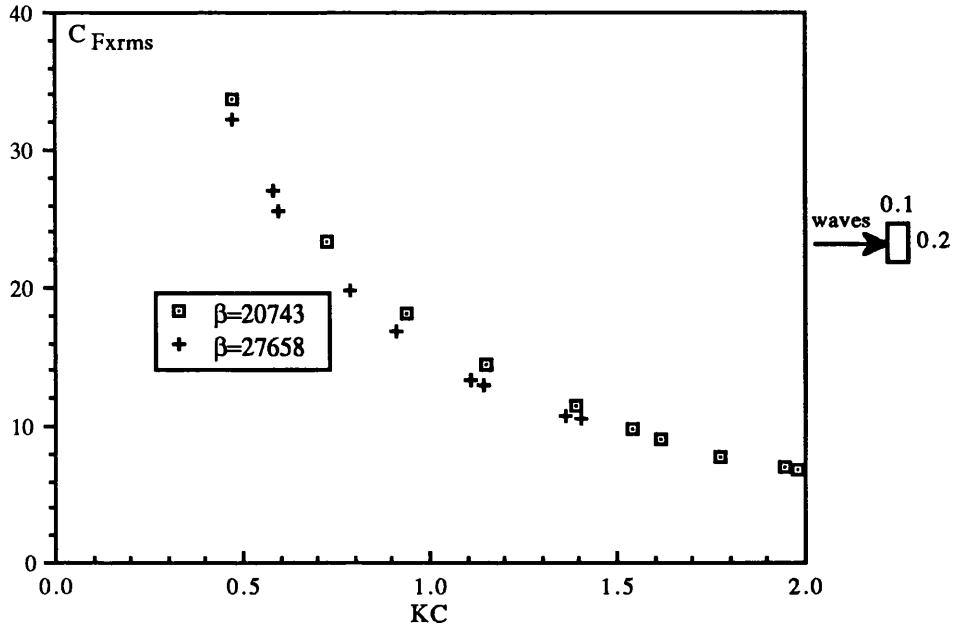

Fig. 4.91 C_{Fxrms} versus KC for a horizontal cylinder with d/D=0.5 in waves

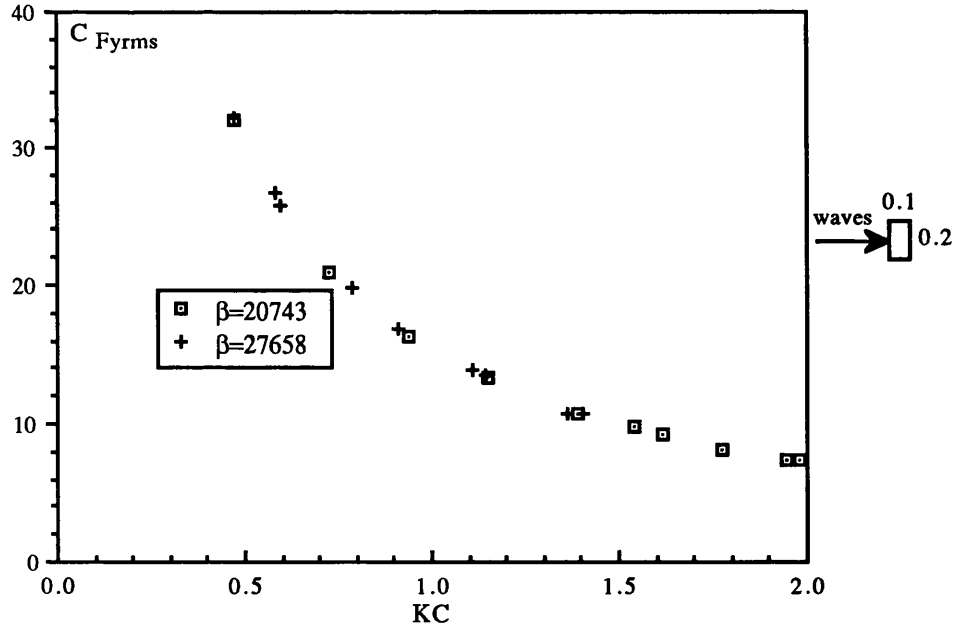

Fig. 4.92 C_{Fyrms} versus KC for a horizontal cylinder with d/D=0.5 in waves

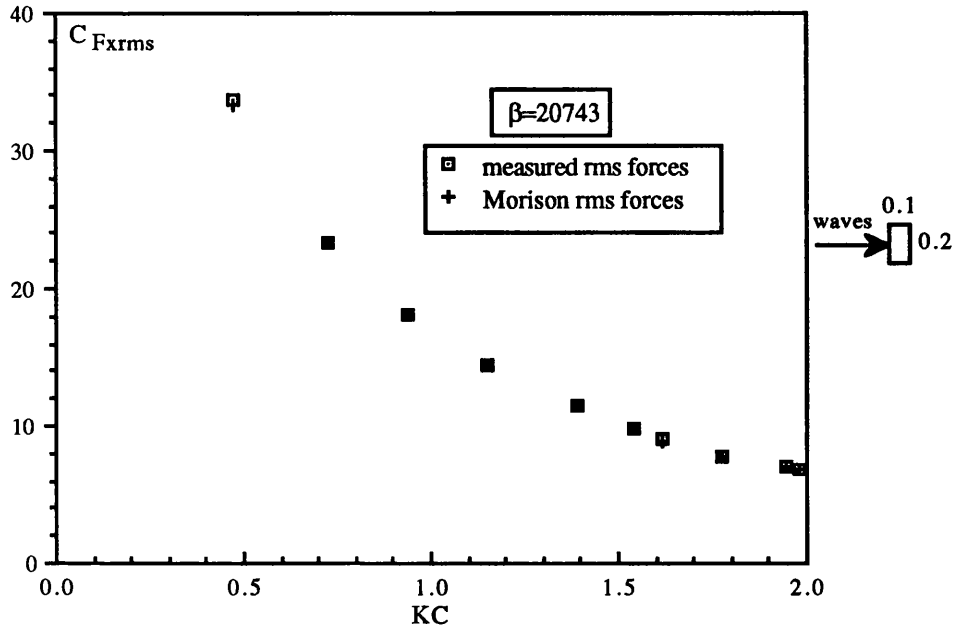

Fig. 4.93 C_{Fxrms} versus KC for a horizontal cylinder with d/D=0.5 in waves

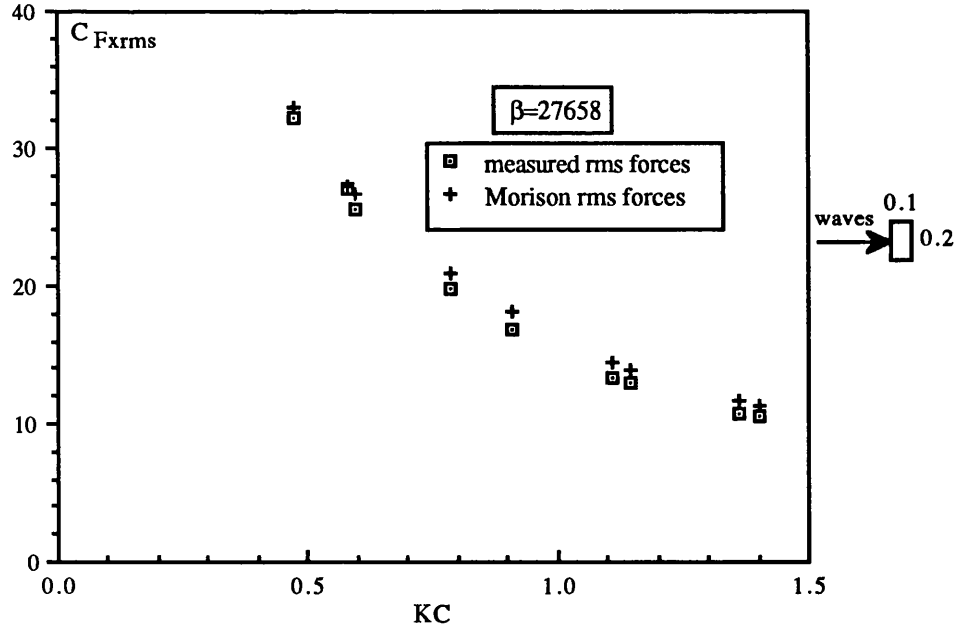

Fig. 4.94 C_{Fxrms} versus KC for a horizontal cylinder with d/D=0.5 in waves

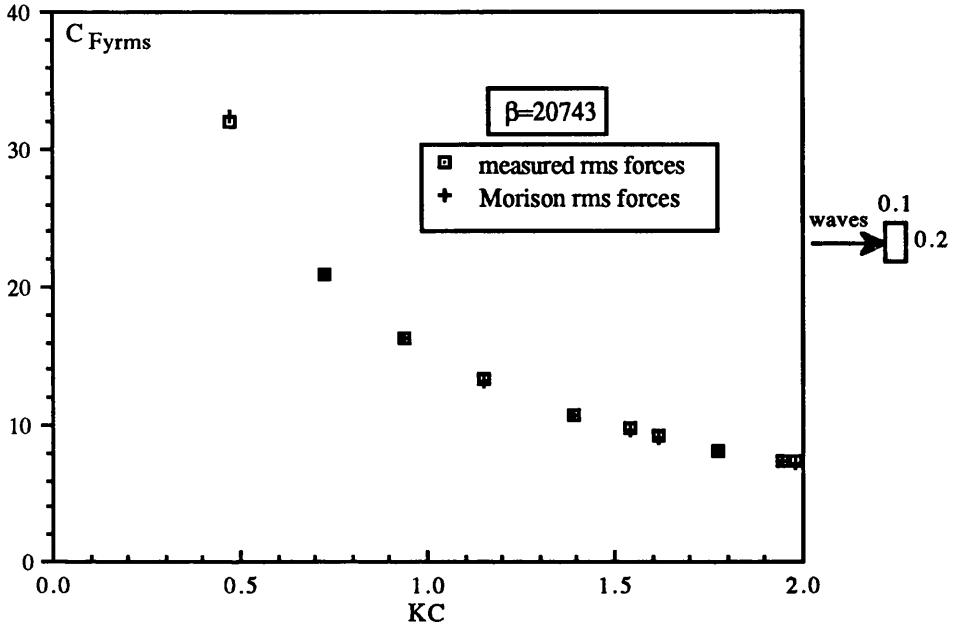

Fig. 4.95 C_{Fyrms} versus KC for a horizontal cylinder with d/D=0.5 in waves

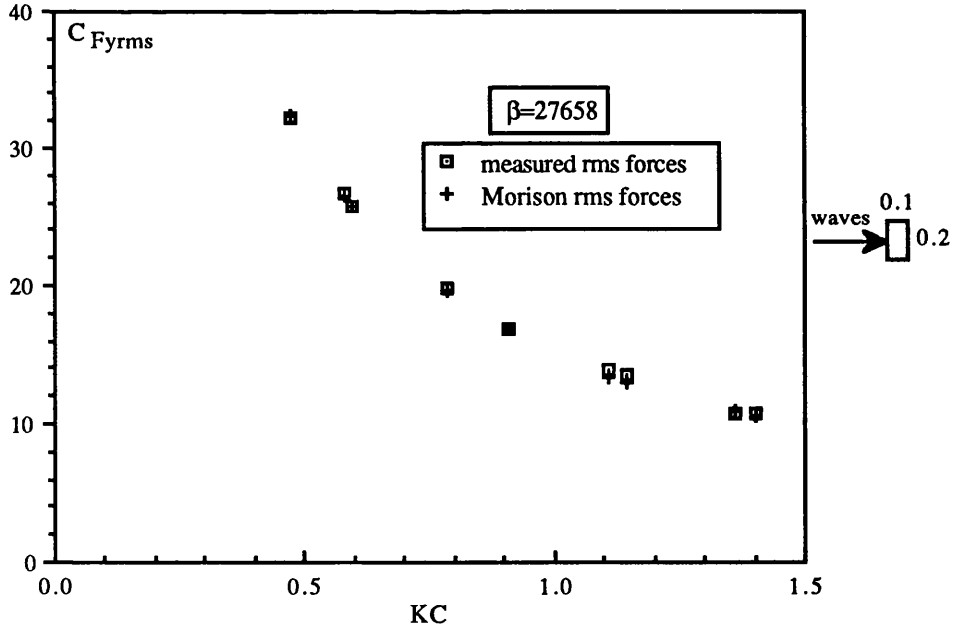

Fig. 4.96 C_{Fyrms} versus KC for a horizontal cylinder with d/D=0.5 in waves

With regard to the cylinder with an aspect ratio of 2, at a low KC number of about 1.3, the in-line C_M coefficient decreased by 26% but C_D coefficient increased by 20% (compare Figures 4.40, 4.41 with 4.73, 4.75) when the orientation of this cylinder was changed from vertical to horizontal. At a higher KC number approaching 3, the in-line C_M coefficient decreased by 34% and C_D coefficient increased by 11%. At a KC number of about 1.3, the in-line C_{Fmax} and C_{Frms} coefficients decreased by 8% and 21% respectively when the orientation of this cylinder was changed from vertical to horizontal (compare Figures 4.42, 4.43 with 4.77, 4.79). At a higher KC number of about 3, the in-line C_{Fmax} and C_{Frms} coefficients decreased by 21% and 28% respectively.

When the orientation of the cylinder with the smallest aspect ratio of 0.5 was changed from vertical to horizontal at KC=0.5, the in-line C_M and C_D coefficients remained almost unchanged (compare Figures 4.46, 4.47 with 4.85, 4.87). However, at a higher KC number approaching 2, the in-line C_M and C_D coefficients decreased by 13% and 8% respectively. Accordingly, at KC=0.5, the in-line C_{Fmax} and C_{Frms} coefficients did not vary much due to the change in the cylinder's orientation (compare Figures 4.48, 4.49 with 4.89, 4.91). At a KC number of about 2, however, C_{Fmax} and C_{Frms} coefficients decreased by 25% and 13% respectively.

4.3.4 COMPARISON OF FOURIER AND LEAST SQUARES METHODS

The drag coefficients determined using the Fourier averaging technique were compared with those obtained using the least squares method.

The C_D coefficients for the different vertical and horizontal cylinders determined from Fourier averaging technique were found in general to be up to 6% higher than those determined using the least squares method.

It is deemed in this study that such a difference could be induced by experimental errors and therefore, it is concluded that both methods give a drag coefficient with the same order of magnitude.

4.4 COMBINED WAVY AND STEADY FLOWS

The three cylinders tested in regular waves at moderate KC numbers were also tested in combined wavy and steady flows to simulate current effects.

The co-existing flow fields in a laboratory can be created in a number of ways to study hydrodynamic forces on marine structures in waves and current. They are:

(1) Simultaneous generation of waves and current, to which a cylinder is subject.

(2) Oscillating a cylinder periodically in a uniform flow.

(3) Generating a flow characterised by $Vc+u_m\cos\theta$ in a water tunnel.

(4) Translating a cylinder in an oscillating flow.

(5) Moving a cylinder with constant velocity while oscillating it in the desired direction.

(6) Towing a cylinder with uniform speed in a wave field.

The first method is an ideal way to study this subject. But it is very difficult, if not impossible, to generate a current, that simulates even approximately the field conditions, and laboratory waves simultaneously over a broad range of governing parameters. The second, third and fourth techniques simulate current superimposed on planar oscillatory flow, where the vertical component of the water particle velocity in the case of horizontal cylinders is neglected. Furthermore, the second method is subject to the effects of ambient turbulence and boundary layer and with the fourth method there are certain limitations, the constancy of the frequency of flow oscillation and the limitations imposed on the distance over which the cylinder may be moved tend to reduce the range of VR for given KC and Reynolds numbers. The fourth method was used for example by Sarpkaya et al. (1984) and Sarpkaya and Storm (1985) using a U-shaped water oscillating tank. The fifth technique may be difficult because of vibrations involved.

The last technique was chosen because of the large size of the tank available where VR could be varied over a wide range, and because it takes into account the orbital motion of the water particles and it simulates well the linear superposition principle for considering waves plus current. It is also convenient to maintain β constant while varying the KC number and the reduced velocity VR. This enables one to assess the role of current (i.e. VR) on the hydrodynamic coefficients for given KC and Reynolds numbers.

Therefore, the cylinders were towed along the middle of the tank at constant forward

speeds through oncoming regular waves. Each cylinder was tested for three different speeds and two different frequency parameters. For each cylinder the effects of the presence of a current were studied by measuring for each current velocity the different force coefficients and comparing them with those measured in regular waves tests. These cylinders were also tested vertically as surface piercing and horizontally submerged with their axes parallel to wave crests. The forces were measured using the same force measuring system as in the regular waves tests. Again, the force coefficients presented here were obtained by averaging the force coefficients measured for different wave cycles.

When a current coexists with waves, the Keulegan-Carpenter number may be defined in different ways. Sarpkaya et al. (1984) and Sarpkaya and Storm (1985) gave a partial list of possible KC numbers and Reynolds numbers defined as

$$KC=u_mT/D,\ Re=u_mD/\nu \tag{4.1}$$

$$K^+=KC(1+|V^*|),\ Re^+=Re(1+|V^*|) \tag{4.2}$$

$$K_S=KC\int_{\theta_0}^{\pi}|V^*-\cos\theta|d\theta,\ \text{for}\ V^*\le 1,\ Re_S=K_S(D^2/\nu T) \tag{4.3}$$

$$K_m=KC(1+|V^*|)^2,\ Re_m=Re(1+|V^*|)^2 \tag{4.4}$$

where $V^*=V_C/u_m$ (V_C is current velocity).

Equation 4.3 expresses the Keulegan-Carpenter number in terms of the relative displacement of the fluid about the cylinder, and equation 4.4 represents the ratio of the maximum convective acceleration to the maximum local acceleration.

In this study, the different force coefficients are plotted only against the KC number as defined in the case of wavy flow (eq. 4.1). The frequency parameter $\beta=D^2/\nu T$ appearing in the results takes into account the undisturbed wave period T (no current) and not the encounter period for the sake of comparing the force coefficients obtained with waves tests with those obtained from the waves with forward speeds. The current velocity is represented in the results in terms of the non dimensionalised reduced velocity $VR=V_CT/D$. Results of regular waves only are represented by VR=0 (since $V_C=0$).

The results obtained are expressed in terms of inertia C_M, and drag C_D coefficients as well as in terms of the maximum and r.m.s. force coefficients C_{Fmax} and C_{Frms}. The transverse forces are represented in terms of the lift C_L (C_{Lmax}, C_{Lrms}) coefficients. The equations defining these coefficients are given in Chapter 3.

4.4.1 VERTICAL CYLINDERS

The different force coefficients of vertical cylinders are plotted against the Keulegan-Carpenter KC number for constant values of the frequency parameter β and various values of the reduced velocity VR. The results are shown in Figures 4.97 through 4.132.

4.4.1.1 In-line force coefficients

Figures 4.97 through 4.100 show the variations of C_M and C_D coefficients with the KC number for the square cross-sectional cylinder.

The presence of a current was found to have a significant effect on the force coefficients. The C_M coefficient was found to decrease when a current was present. For the range of the reduced velocity considered, C_M coefficient decreased as VR increased. For example, at KC=0.5 and β=5249 (Figure 4.97), C_M coefficient in the no-current case (VR=0) decreased by 3% for VR=4, by 20% for VR=6 and by 35% for VR=9. For the same β number and at KC=3.5, C_M coefficient in the no-current case decreased by 15% for VR=4, by 16% for VR=6 and by 40% for VR=9. For a higher β number of 6999 and at KC=0.6 (Figure 4.98), C_M coefficient in the no-current case decreased by 5% for VR=4, by 20% for VR=6 and by 43% for VR=8. At a higher KC number of 2.5 and for the same β number, C_M coefficient in the no-current case decreased by 24% for VR=4, by 31% for VR=6 and by 50% for VR=8.

The C_D coefficient was also found to decrease when a current was present, and the effect of the current was found to be more significant at the lower end of the KC number. For example, at a KC number of 1 and for β=5249 (Figure 4.99), C_D coefficient in the no-current case (VR=0) decreased by 53% for VR=4, by 78% for VR=6 and by 79% for VR=9. For the same β number and at KC=3.5, C_D coefficient in the no-current case decreased by 44% for VR=4, by 61% for VR=6 and by 63% for VR=9. For a higher β number of 6999 and at KC=1 (Figure 4.100), C_D coefficient in the no-current case decreased by 71% for VR=4, by 80% for VR=6 and by 81% for VR=8. At a higher KC number of 2.5 and for the same β number, C_D coefficient in the no-current case decreased by 56% for VR=4, by 67% for VR=6 and by 70% for VR=8.

The variations of C_{Fmax} and C_{Frms} coefficients with the KC number for the square cylinder are shown in Figures 4.101 through 4.104. As with the drag coefficient, they

were found to be much smaller than those in the no-current case. Because of the large difference between the values of these coefficients obtained under no-current and those obtained with a steady flow presence, they were plotted on their own to reduce the scale. For the range of KC numbers and VR considered, C_{Fmax} and C_{Frms} decreased as VR increased. For example, at KC=3 and β=5249 (Figure 4.101), C_{Fmax} in the no-current case decreased by 78% for VR=4, by 82% for VR=6 and by 87% for VR=9. At the same KC and β numbers (Figure 4.103), C_{Frms} in the no-current case decreased by 79% for VR=4, by 84% for VR=6 and by 87% for VR=9.

Figures 4.109 through 4.112 show the variations of C_M and C_D coefficients with the KC number for the cylinder with an aspect ratio of 2.

As with the square cylinder, C_M coefficient was found to decrease when a steady flow was present but the effect of increasing the value of the reduced velocity VR on C_M coefficient was small and unlike the square cylinder, increasing the value of VR did not decrease C_M coefficient further. At very low KC numbers, i.e. KC<0.5, the effect of current on C_M coefficient was very small. At a higher KC number of 1.3 and β=5455 (Figure 4.109), C_M coefficient in the no-current case decreased by 14% for VR=4, by 13% for VR=6 and by 15% for VR=9. For the same β number and at KC number of about 4, C_M coefficient in the no-current case decreased by 20% for VR varying between 4 and 9. For a higher β number of 7273 and at KC=1.3 (Figure 4.110), C_M coefficient in the no-current case decreased by 13% for VR varying between 4 and 8. At higher a KC number of 3 and for the same β number, C_M coefficient in the no-current case decreased by 17% for VR=4, by 19% for VR=6 and by 18% for VR=8.

As with the square cylinder, C_D coefficient decreased when a current was present, and the decrease was found to be more significant at the lower end of the KC number. For this cylinder, and as with the inertia coefficient, increasing VR above a certain value did not decrease C_D coefficient further particularly at higher KC numbers. For example, at KC=1.3 and for β=5455 (Figure 4.111), C_D coefficient in the no-current case decreased by 53% for VR=4, by 59% for VR=6 and by 65% for VR=9. For the same β number and at a KC number of about 4, C_D coefficient in the no-current case decreased by 38% for VR=4, by 59% for VR=6 and by 41% for VR=9. For a higher β number of 7273 and at KC=1.3 (Figure 4.112), C_D coefficient in the no-current case decreased by 65% for VR=4, by 84% for VR=6 and by 68% for VR=8. At a higher KC number of 3 and for the same β number, C_D coefficient in the no-current case decreased by 54% for VR=4, by 74% for VR=6 and by 63% for VR=8.

The variations of C_{Fmax} and C_{Frms} with the KC number for this cylinder are shown in Figures 4.113 through 4.116. As with the square cylinder, the presence of a steady flow reduced the values of these coefficients. Again for the range of KC and β numbers considered, C_{Fmax} and C_{Frms} decreased for increasing VR. For example, at KC=3 and β=5455 (Figure 4.113), C_{Fmax} in the no-current case decreased by 79% for VR=4, by 83% for VR=6 and by 85% for VR=9. At the same KC and β numbers (Figure 4.115), C_{Frms} in the no-current case decreased by 81% for VR=4, by 86% for VR=6 and by 88% for VR=9.

The variations of C_M and C_D coefficients with the KC number for the cylinder with the smallest aspect ratio of 0.5 are shown in Figures 4.121 through 4.124.

As with other cylinders, the presence of a steady flow decreased C_M coefficient. For example, at KC=0.5 and β=21239 (Figure 4.121), C_M coefficient in the no-current case decreased by 1.5% for VR=2, by 12% for VR=3 and by 23% for VR=4. For the same β number and at a KC number of about 2, C_M coefficient in the no-current case decreased by 8% for VR=2, and by 24% and 25% for VR of 3 and 4 respectively. For a higher β number of 28319 and at KC=0.5 (Figure 4.122), C_M coefficient in the no-current case decreased by 2% for VR=2, and by 12% and 14% for VR of 3 and 4 respectively. At a higher KC number of about 1.4 and for the same β number, C_M coefficient in the no-current case decreased by 5% for VR=2, and by 11% and 13% for VR of 3 and 4 respectively.

The presence of a steady flow was also found for this cylinder to decrease C_D coefficient and particularly at very low KC numbers. For example, at KC=0.5 and for β=21239 (Figure 4.123), C_D coefficient in the no-current case decreased by 85% for VR=2, and by 86% and 83% for VR of 3 and 4 respectively. For the same β number and at a KC number of about 2, C_D coefficient in the no-current case decreased by 46% for VR=2, and by 57% and 62% for VR of 3 and 4 respectively. For a higher β number of 28319 and at KC=0.5 (Figure 4.124), C_D coefficient in the no-current case decreased by 81% for VR=2, and by 80% and 90% for VR of 3 and 4 respectively. At a higher KC number of about 1.4 and for the same β number, C_D coefficient in the no-current case decreased by 64% for VR=2, and by 70% for VR varying between 3 and 4.

Figures 4.125 through 4.128 show the variations of C_{Fmax} and C_{Frms} coefficients with the KC number for this cylinder. As with other cylinders, these coefficients decreased when a steady flow was present. For example at a KC number approaching 2

and β=21239 (Figure 4.125), C_{Fmax} in the no-current case decreased by 75% for VR=2, by 81% for VR=3 and by 84% for VR=4. At the same KC and β numbers (Figure 4.127), C_{Frms} in the no-current case decreased by 77% for VR=2, by 84% for VR=3 and by 86% for VR=4.

4.4.1.2 Transverse (lift) force coefficients

The lift coefficients are expressed in terms of the maximum C_{Lmax} and the root mean square C_{Lrms} of the measured force non dimensionalised using the square of the sum of the wave particle maximum velocity and the steady flow velocity (equations 3.41 and 3.42).

The variations of C_{Lmax} and C_{Lrms} coefficients with the KC number for the square cross-sectional cylinder are shown in Figures 4.105 through 4.108.
As with C_{Fmax} and C_{Frms}, these coefficients decreased when a steady flow was present. They were plotted on their own in order to reduce the scale. Unlike the in-line force coefficients C_{Fmax} and C_{Frms}, these coefficients decreased when VR increased up to a certain value and then started to increase. This shows that there was a critical value of the reduced velocity above which C_{Lmax} and C_{Lrms} coefficients increased for increasing VR. For example, at KC=3 and β=5249 (Figure 4.105), C_{Lmax} in the no-current case decreased by 83% for VR=4, by 89% for VR=6 and by a lower percentage of 69% for VR=9. At the same KC and β numbers (Figure 4.107), C_{Lrms} in the no-current case decreased by 82% for VR=4, by 87% for VR=6 and by 66% for VR=9.

Figures 4.117 through 4.120 show the variations of C_{Lmax} and C_{Lrms} coefficients with the KC number for the cylinder with an aspect ratio of 2.
As with the square cylinder, these coefficients decreased when a steady flow was present. They were found to decrease for increasing VR up to a critical value and to increase thereafter. For example, at KC=3 and β=5455 (Figure 4.117), C_{Lmax} in the no-current case decreased by 48% for VR=4, by 72% for VR=6 and by 67% for VR=9. At the same KC and β numbers (Figure 4.119), C_{Lrms} in the no-current case decreased by 52% for VR=4, by 73% for VR=6 and by 65% for VR=9.

The variations of C_{Lmax} and C_{Lrms} coefficients with the KC number for the cylinder with the smallest aspect ratio of 0.5 are shown in Figures 4.129 through 4.132. As with the other cylinders, the presence of a steady flow reduced the values of these coefficients. For example at a KC number of about 2 and β=21239 (Figure 4.129), C_{Lmax} in the no-current case decreased by 65% for VR varying between 2 and 3 and

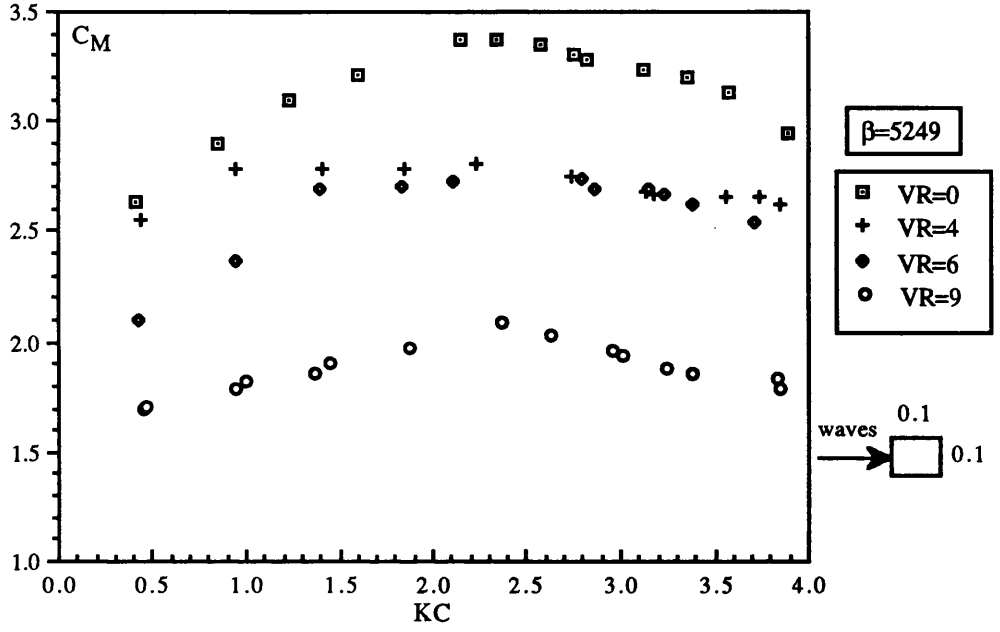

Fig. 4.97 C_M versus KC for a vertical cylinder with d/D=1 in waves and currents

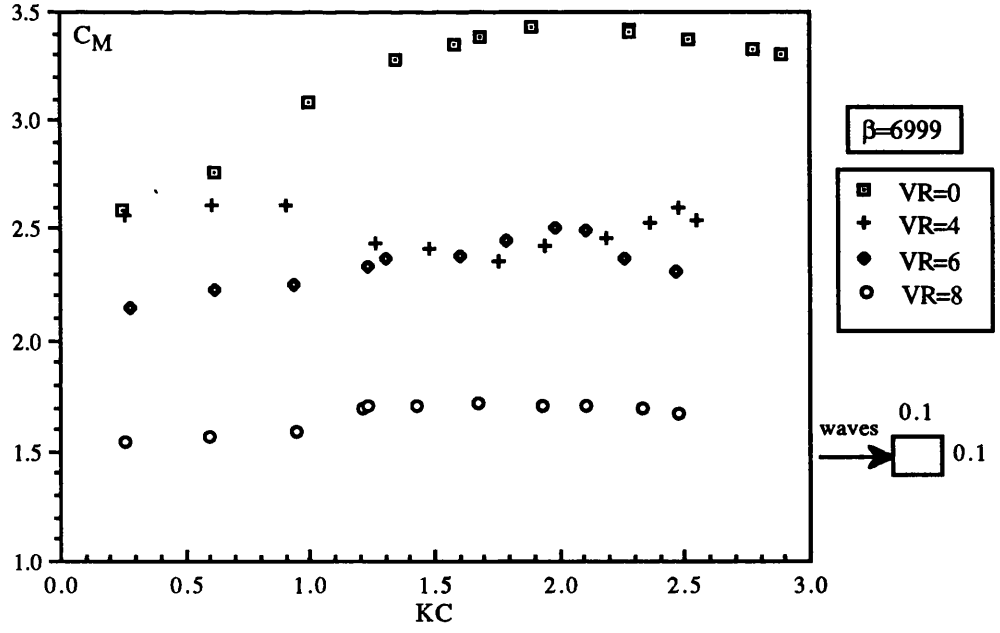

Fig. 4.98 C_M versus KC for a vertical cylinder with d/D=1 in waves and currents

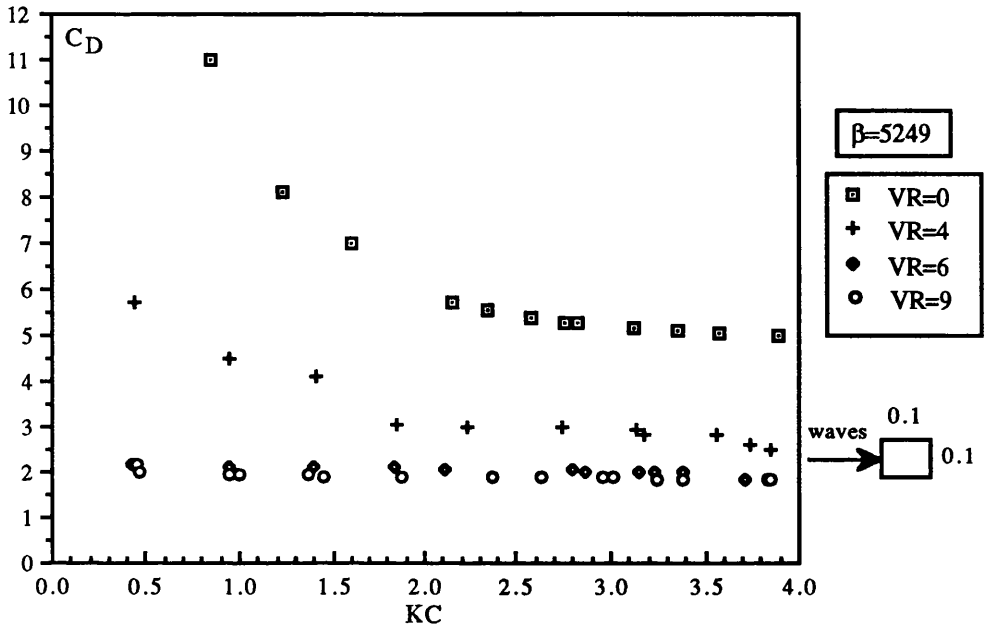

Fig. 4.99 C_D versus KC for a vertical cylinder with d/D=1 in waves and currents

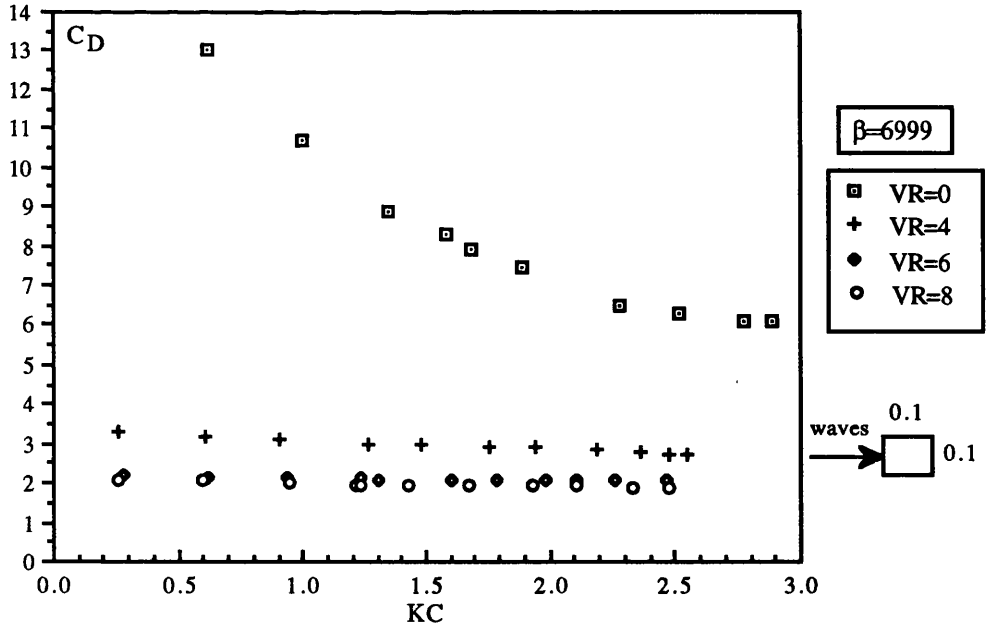

Fig. 4.100 C_D versus KC for a vertical cylinder with d/D=1 in waves and currents

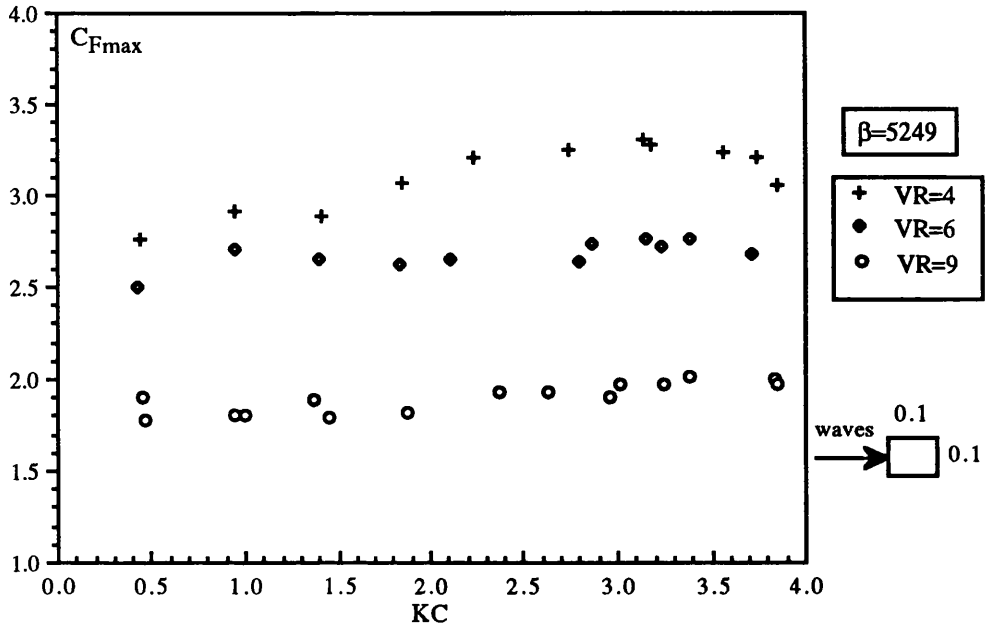

Fig. 4.101 C_{Fmax} versus KC for a vertical cylinder with d/D=1 in waves and currents

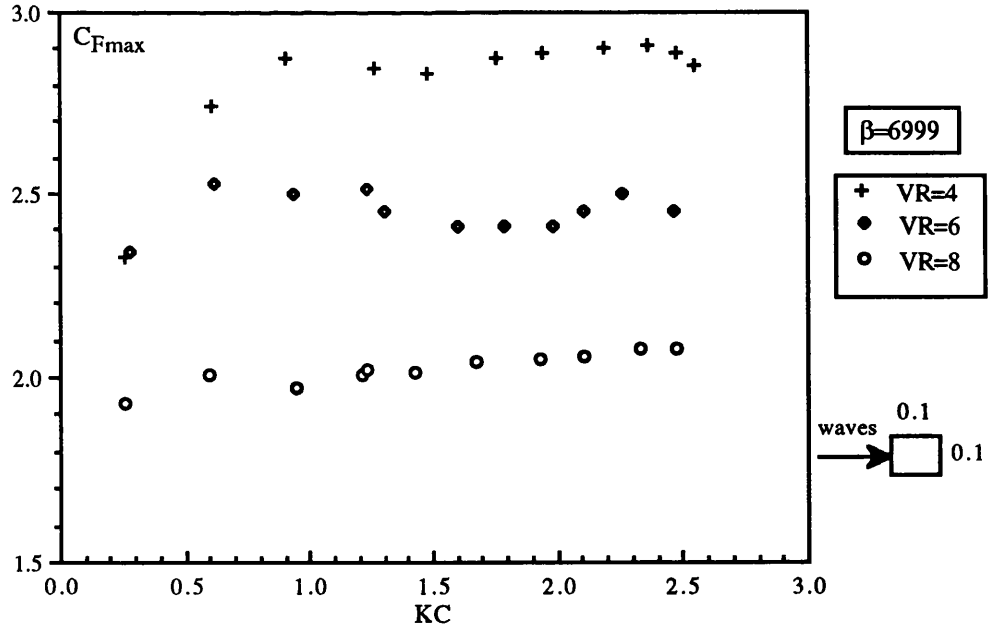

Fig. 4.102 C_{Fmax} versus KC for a vertical cylinder with d/D=1 in waves and currents

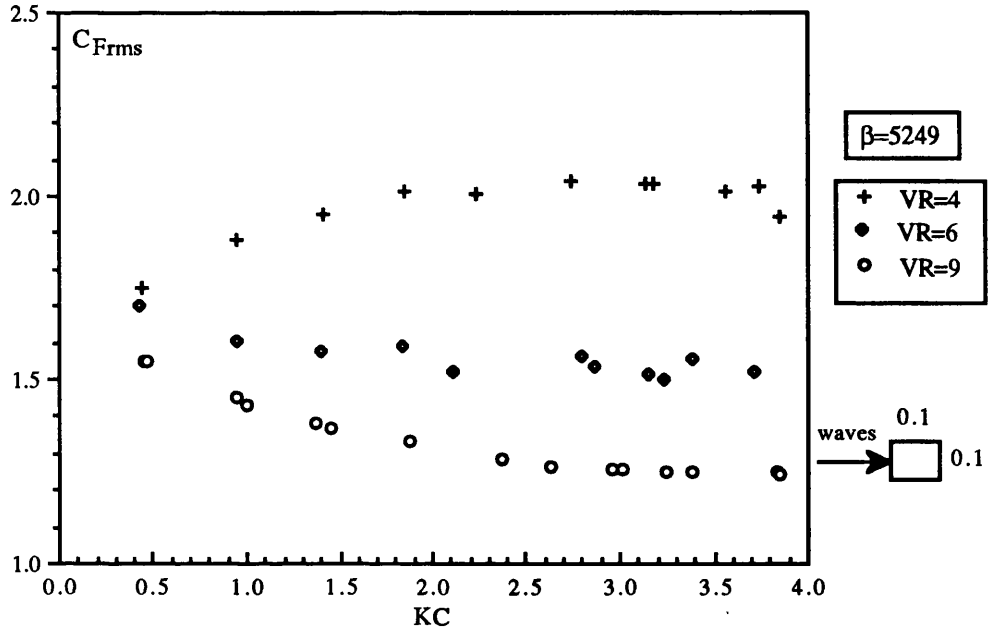

Fig. 4.103 C_{Frms} versus KC for a vertical cylinder with d/D=1 in waves and currents

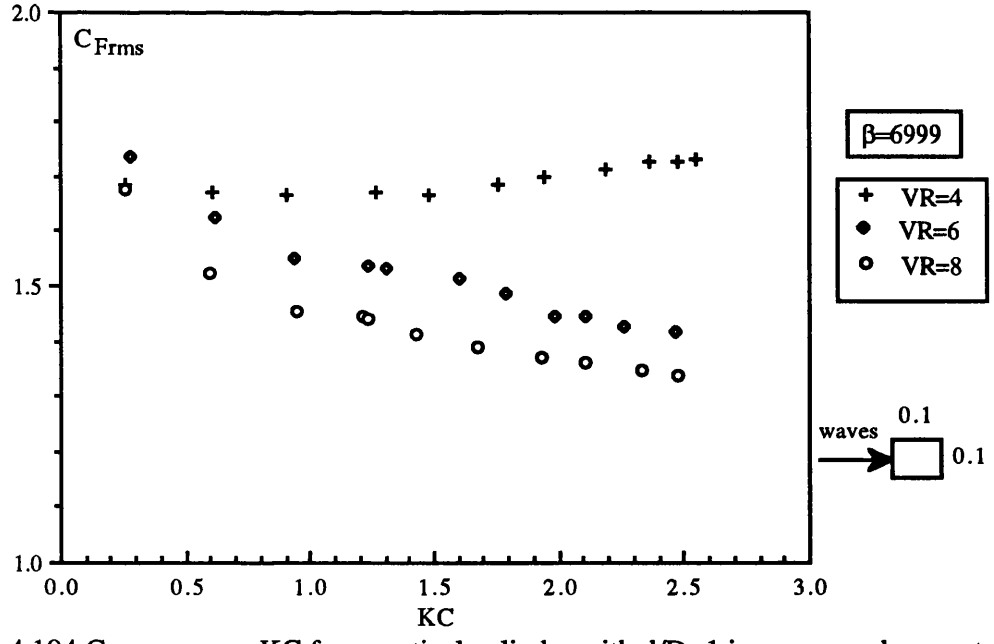

Fig. 4.104 C_{Frms} versus KC for a vertical cylinder with d/D=1 in waves and currents

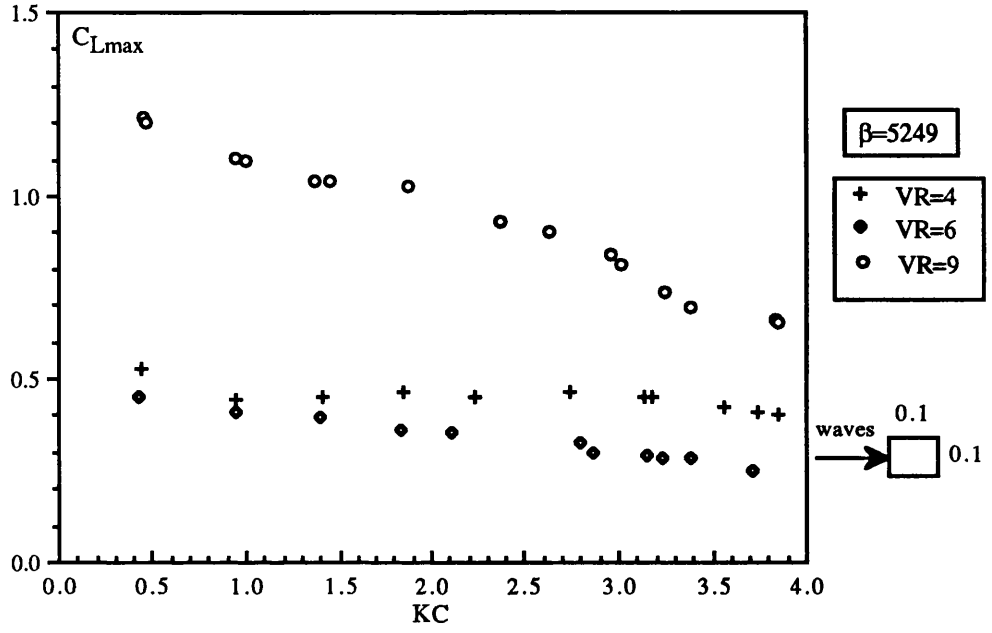

Fig. 4.105 C_{Lmax} versus KC for a vertical cylinder with d/D=1 in waves and currents

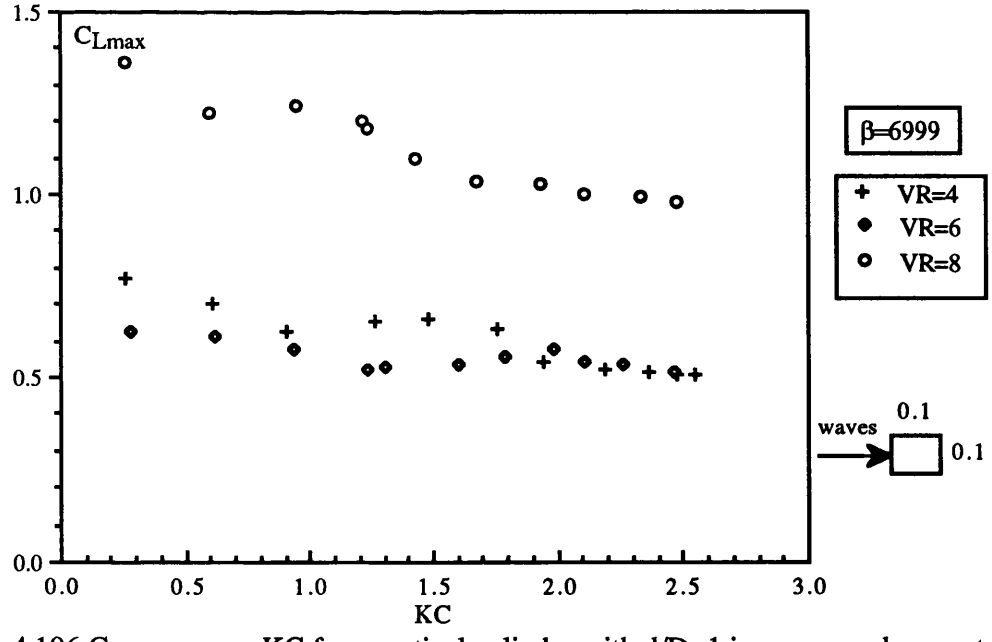

Fig. 4.106 C_{Lmax} versus KC for a vertical cylinder with d/D=1 in waves and currents

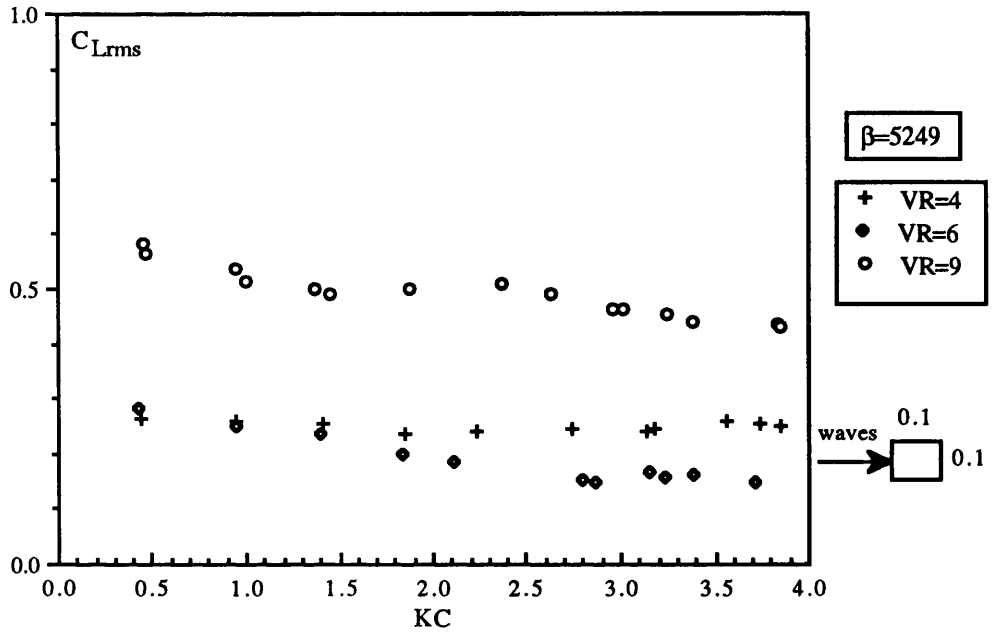

Fig. 4.107 C_{Lrms} versus KC for a vertical cylinder with d/D=1 in waves and currents

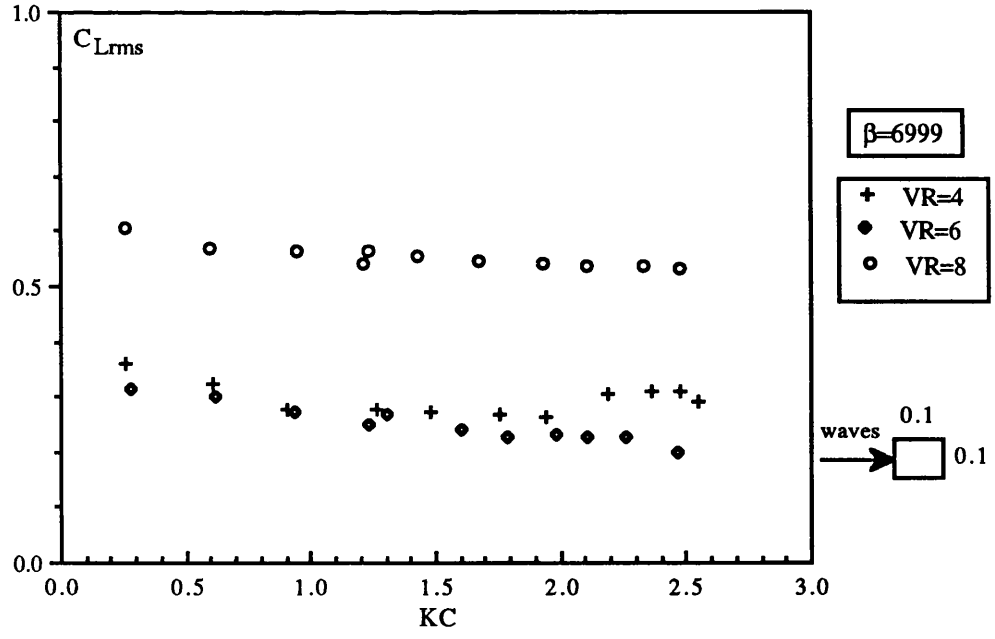

Fig. 4.108 C_{Lrms} versus KC for a vertical cylinder with d/D=1 in waves and currents

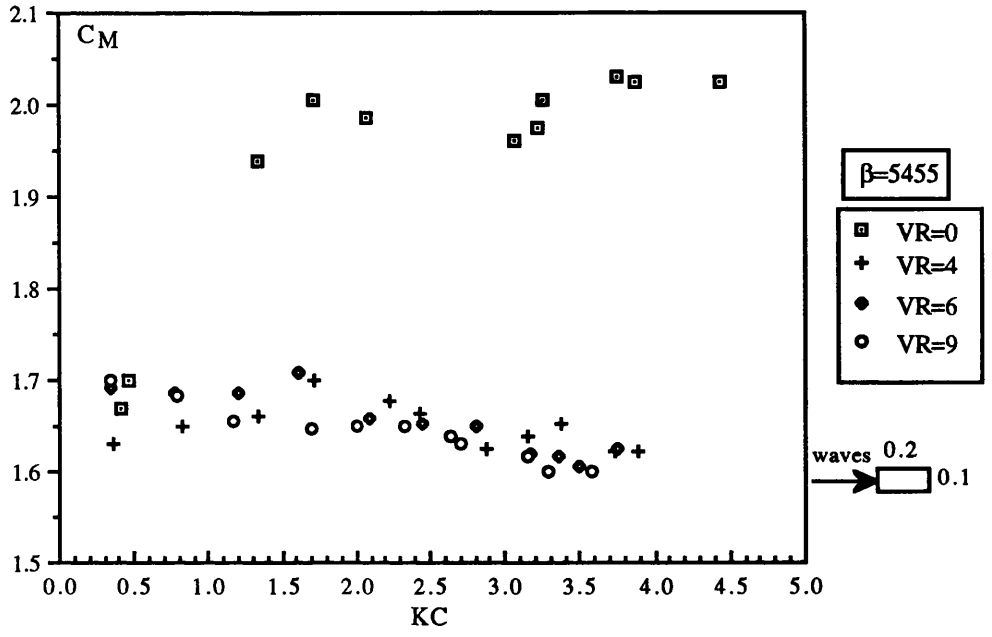

Fig. 4.109 C_M versus KC for a vertical cylinder wih d/D=2 in waves and currents

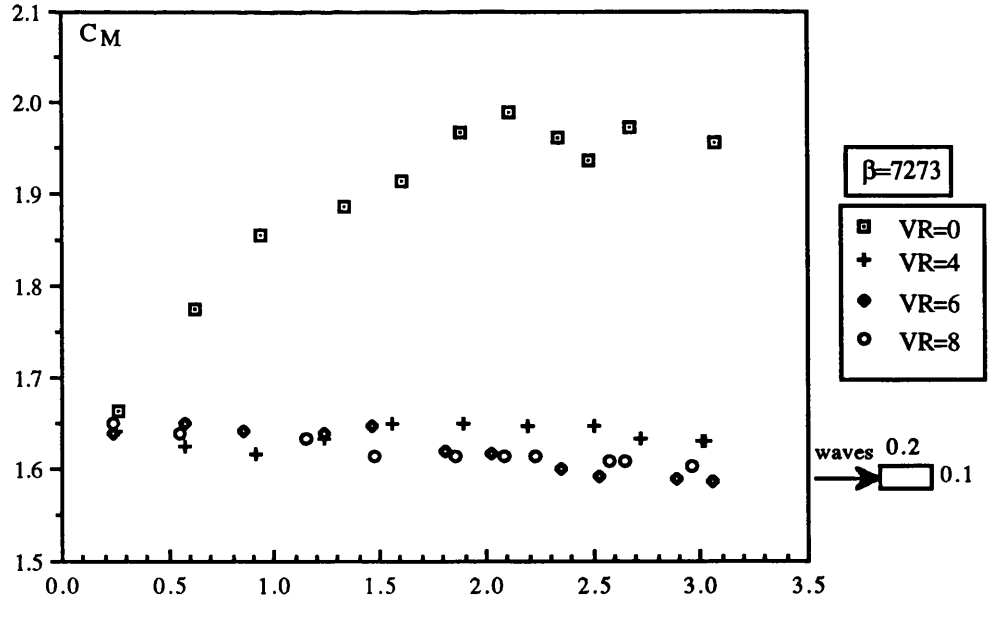

Fig. 4.110 C_M versus KC for a vertical cylinder wih d/D=2 in waves and currents

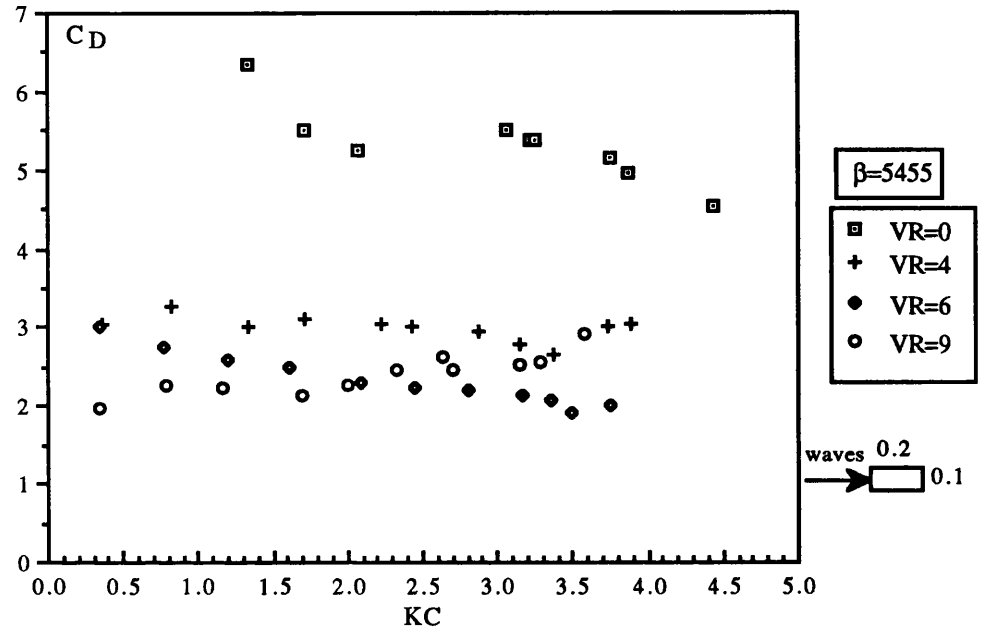

Fig. 4.111 C $_D$versus KC for a vertical cylinder wih d/D=2 in waves and currents

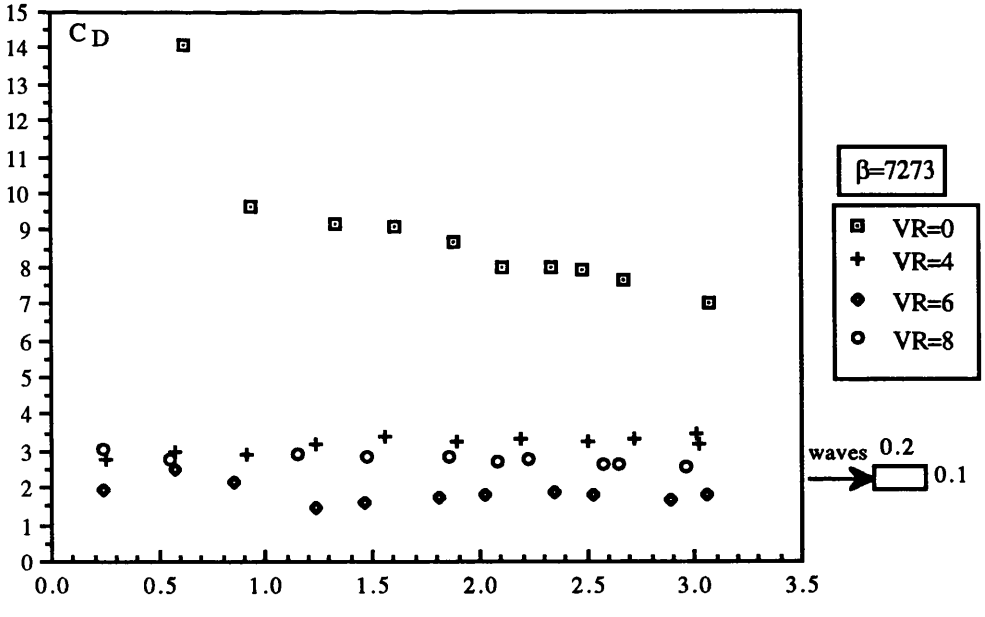

Fig. 4.112 C $_D$versus KC for a vertical cylinder wih d/D=2 in waves and currents

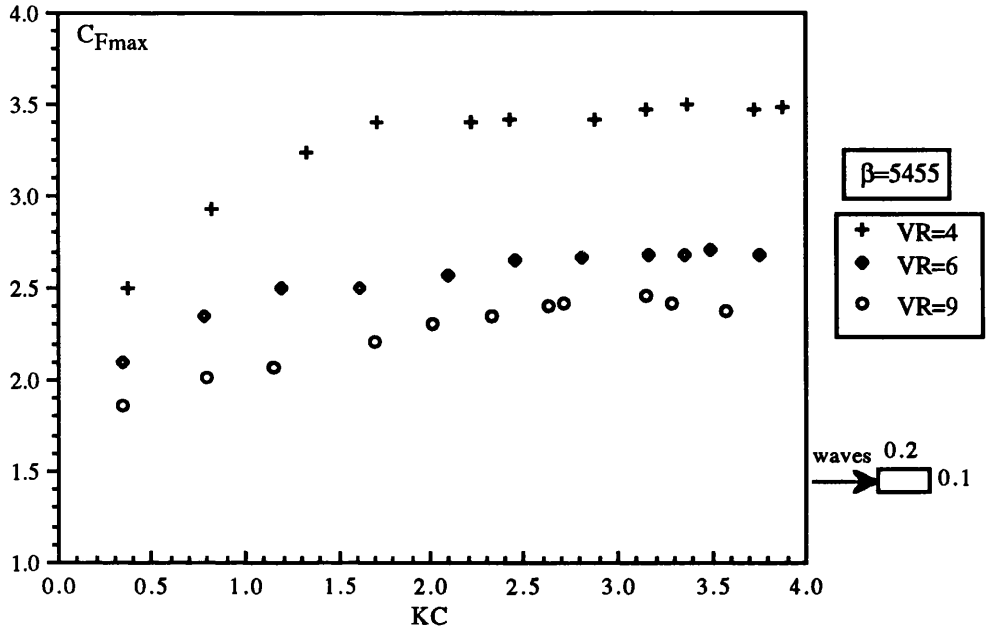

Fig. 4.113 C_{Fmax} versus KC for a vertical cylinder wih d/D=2 in waves and currents

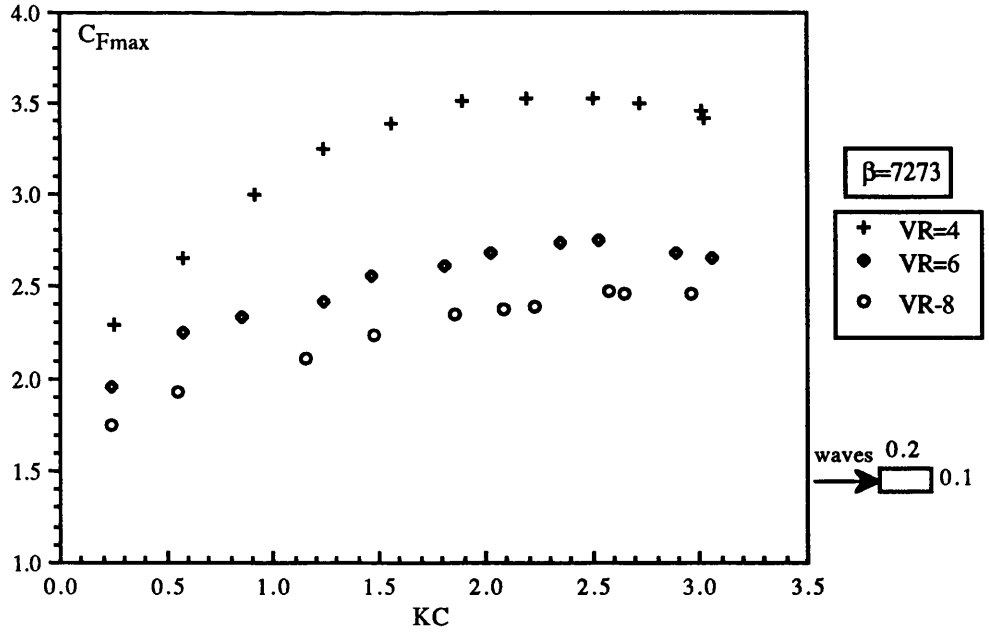

Fig. 4.114 C_{Fmax} versus KC for a vertical cylinder wih d/D=2 in waves and currents

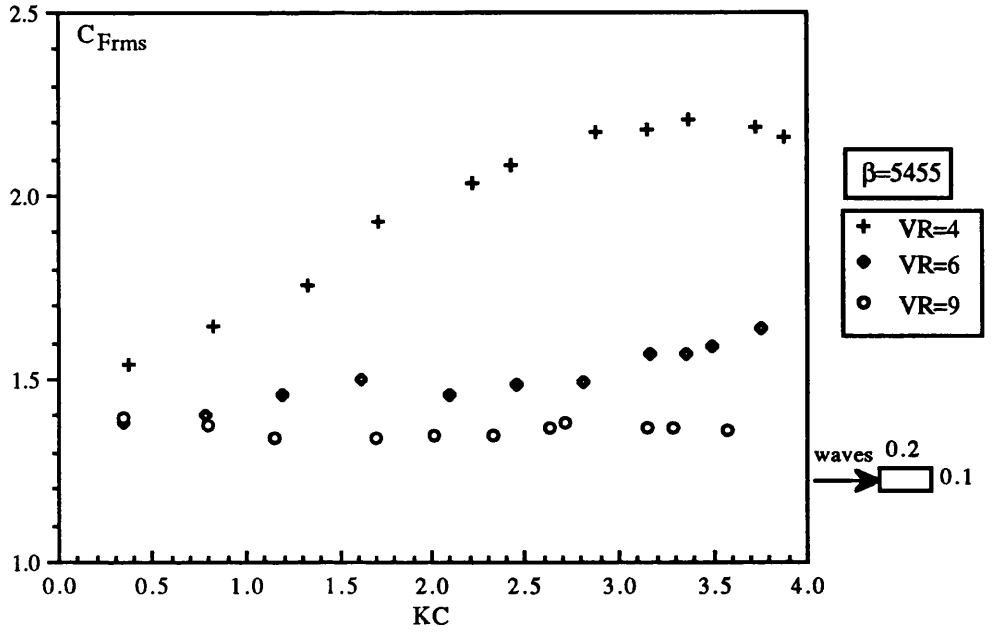

Fig. 4.115 C_{Frms} versus KC for a vertical cylinder wih d/D=2 in waves and currents

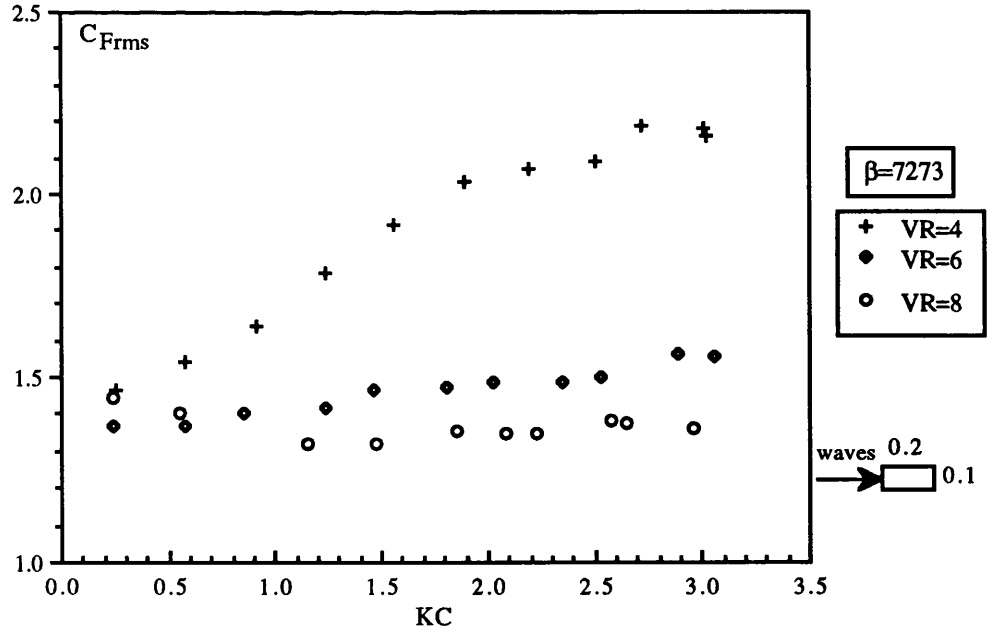

Fig. 4.116 C_{Frms} versus KC for a vertical cylinder wih d/D=2 in waves and currents

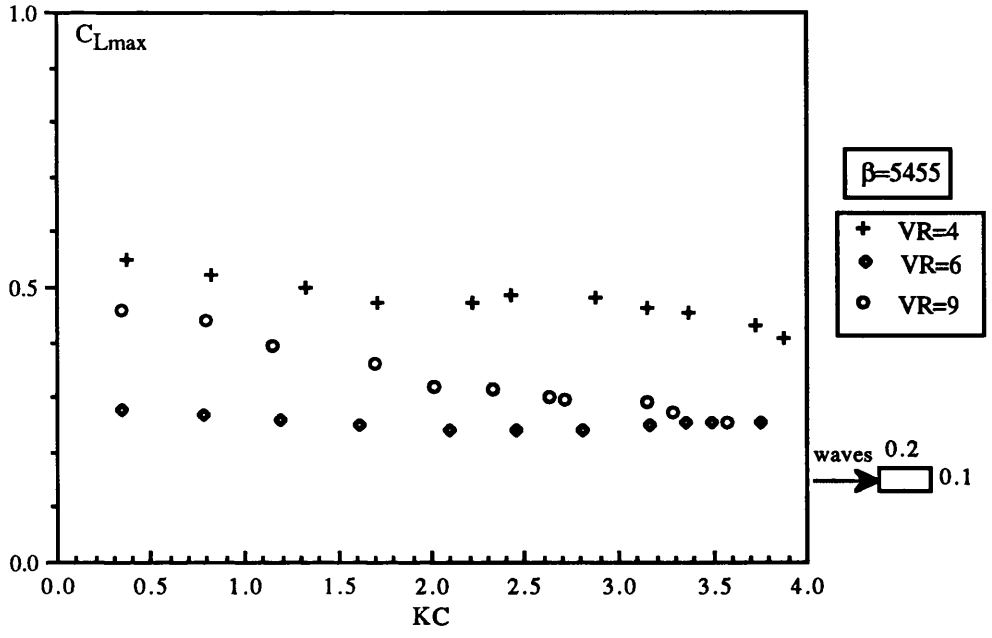

Fig. 4.117 C_{Lmax} versus KC for a vertical cylinder wih d/D=2 in waves and currents

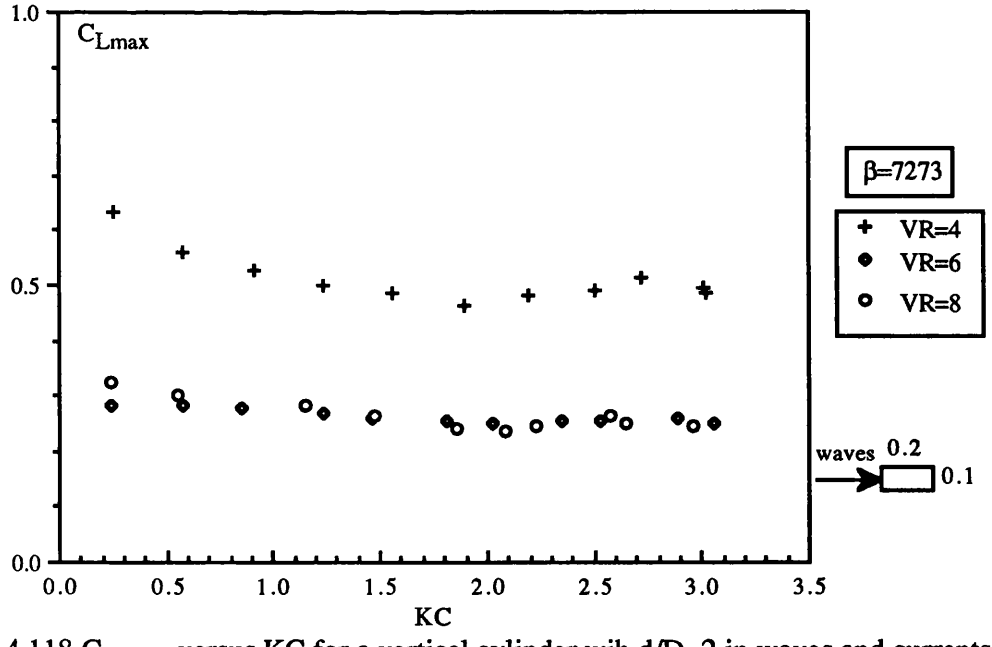

Fig. 4.118 C_{Lmax} versus KC for a vertical cylinder wih d/D=2 in waves and currents

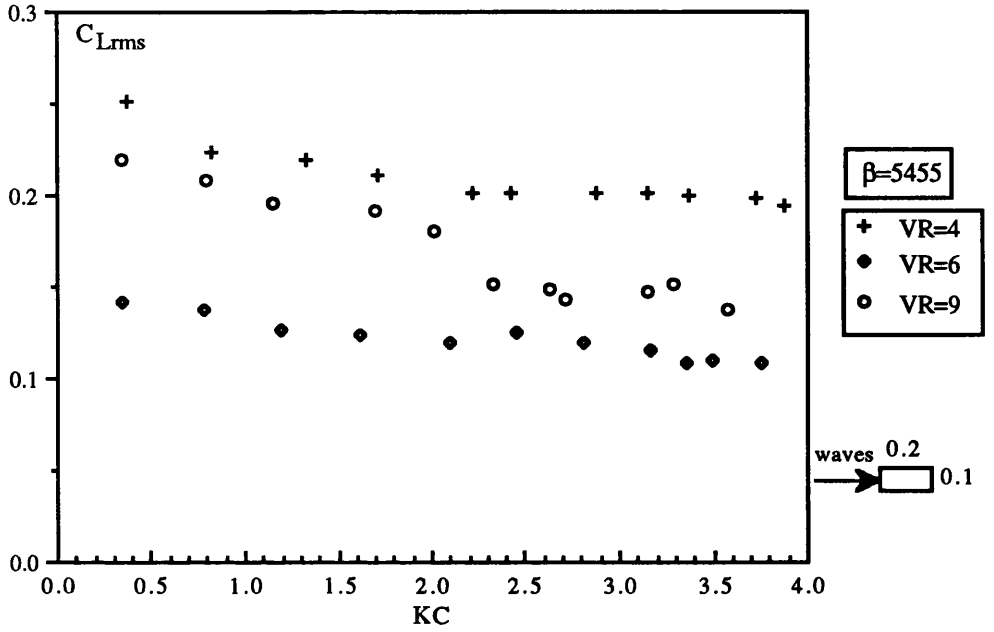

Fig. 4.119 C_{Lrms} versus KC for a vertical cylinder wih d/D=2 in waves and currents

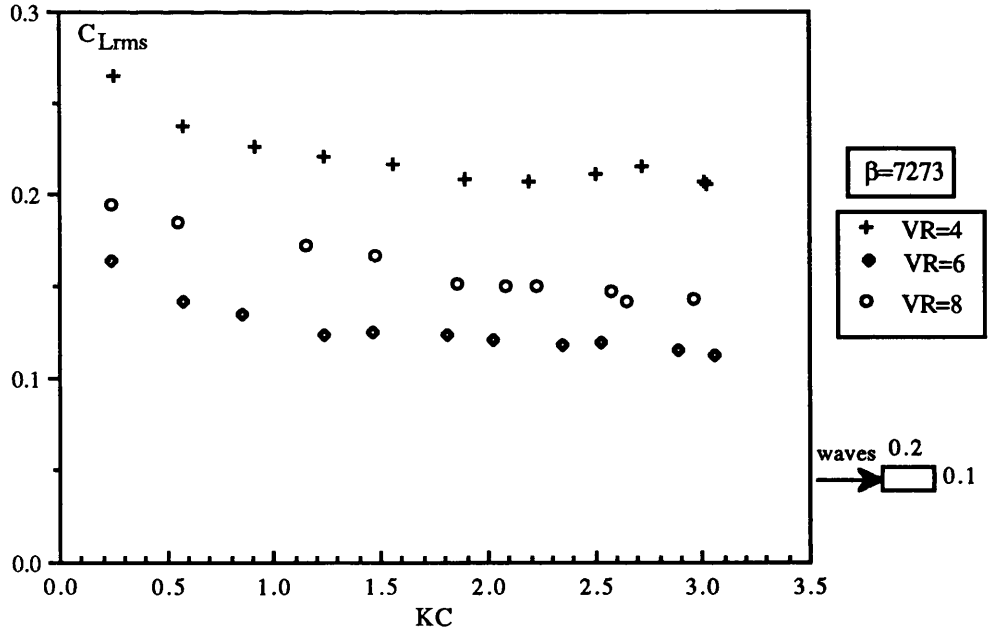

Fig. 4.120 C_{Lrms} versus KC for a vertical cylinder wih d/D=2 in waves and currents

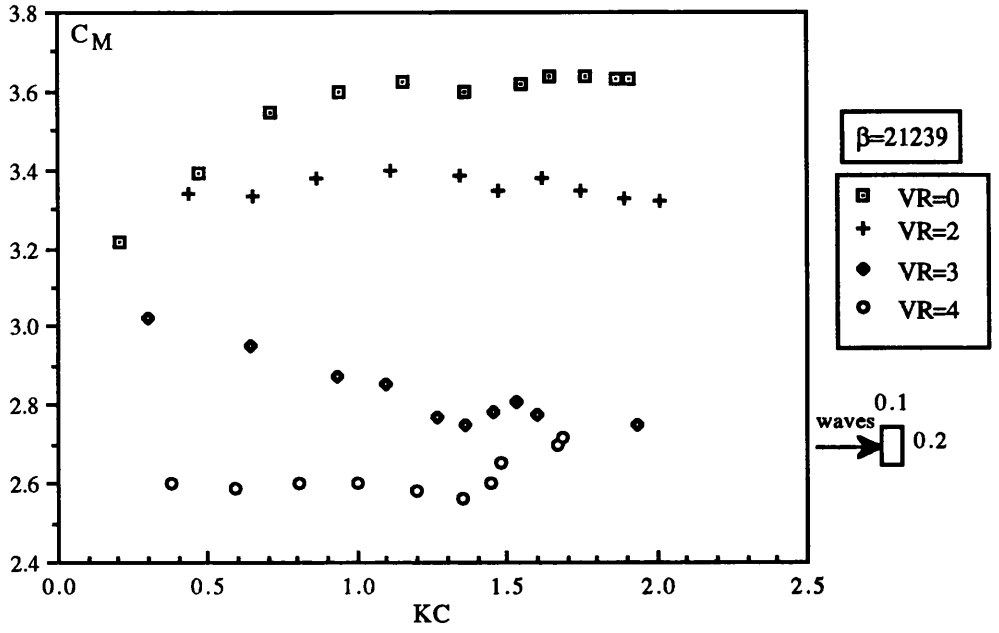

Fig. 4.121 C_M versus KC for a vertical cylinder with d/D=0.5 in waves and currents

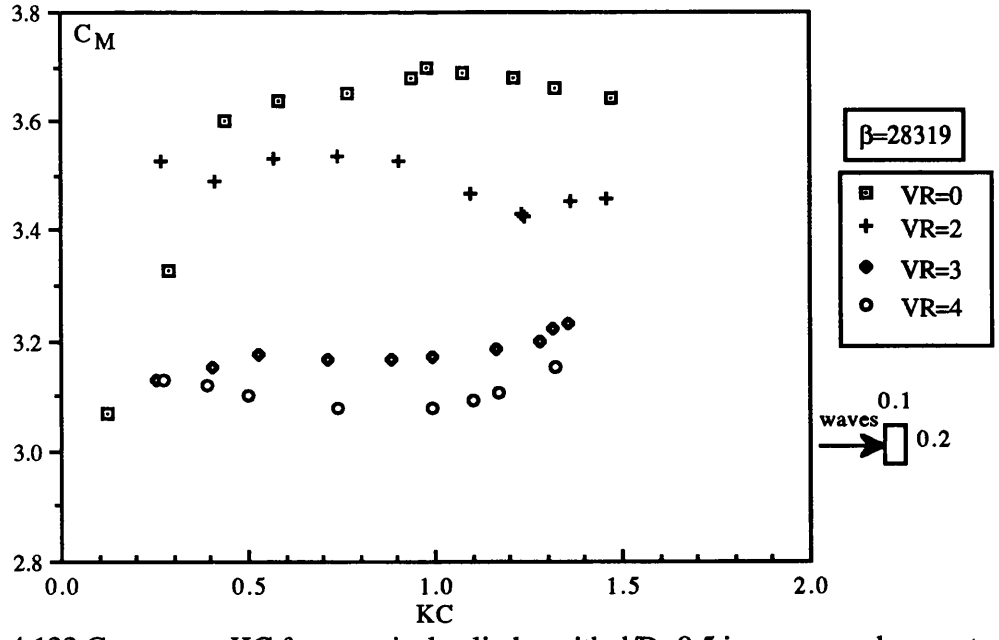

Fig. 4.122 C_M versus KC for a vertical cylinder with d/D=0.5 in waves and currents

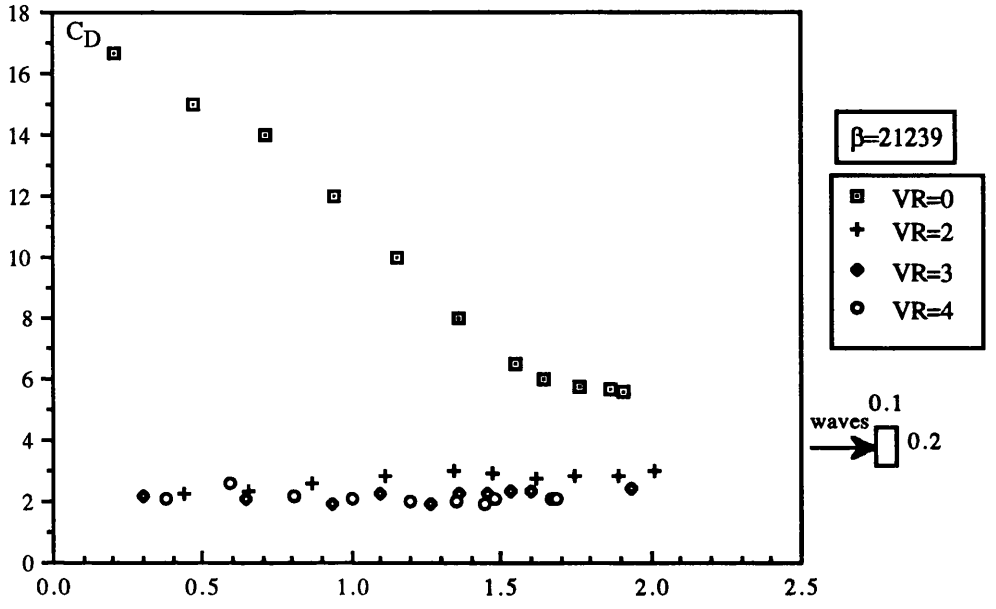

Fig. 4.123 C_D versus KC for a vertical cylinder with d/D=0.5 in waves and currents

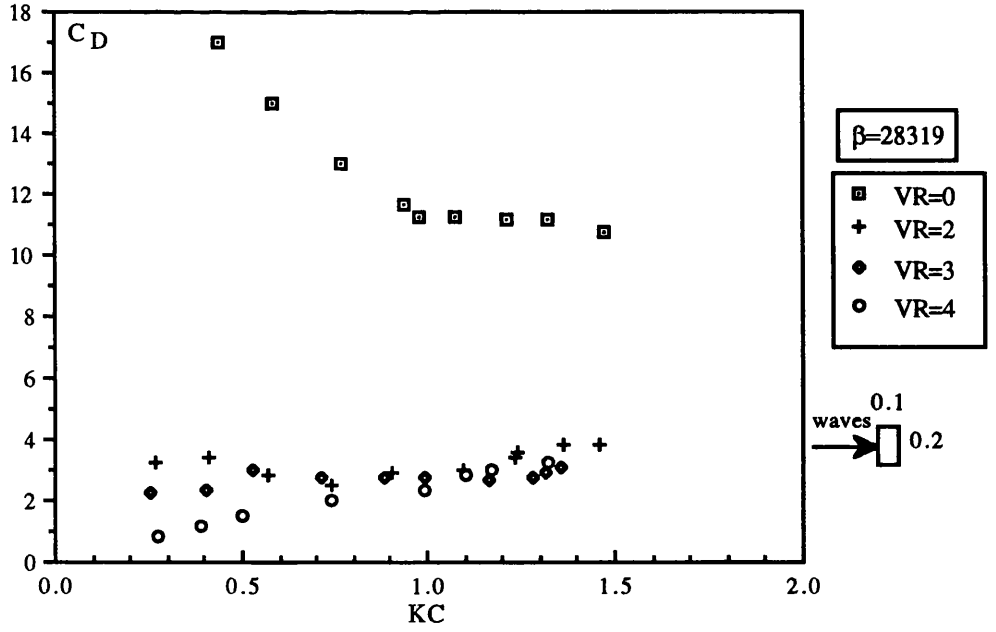

Fig. 4.124 C_D versus KC for a vertical cylinder with d/D=0.5 in waves and currents

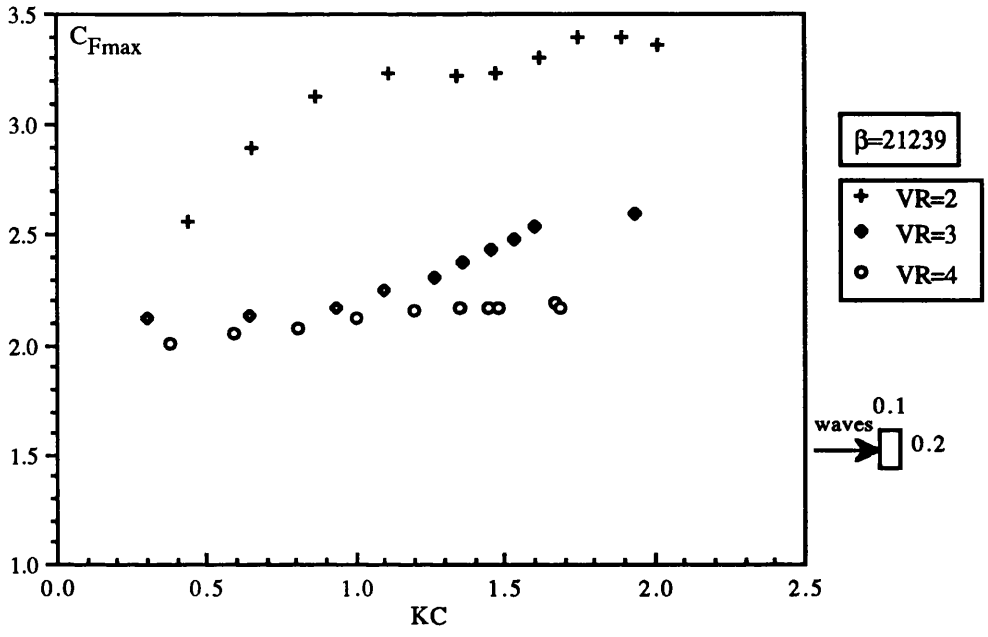

Fig. 4.125 C_{Fmax} versus KC for a vertical cylinder with d/D=0.5 in waves and currents

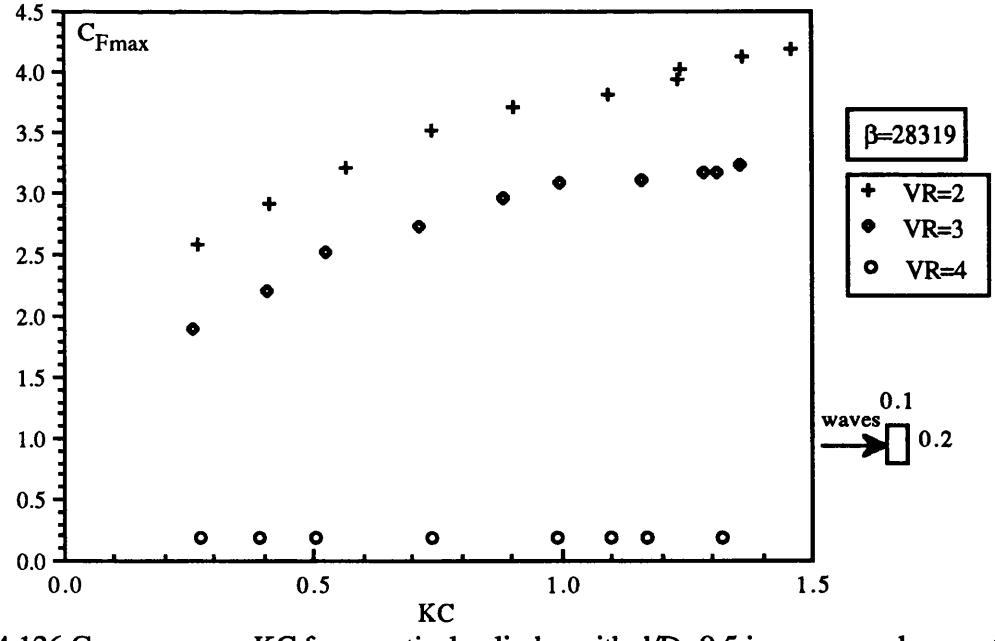

Fig. 4.126 C_{Fmax} versus KC for a vertical cylinder with d/D=0.5 in waves and currents

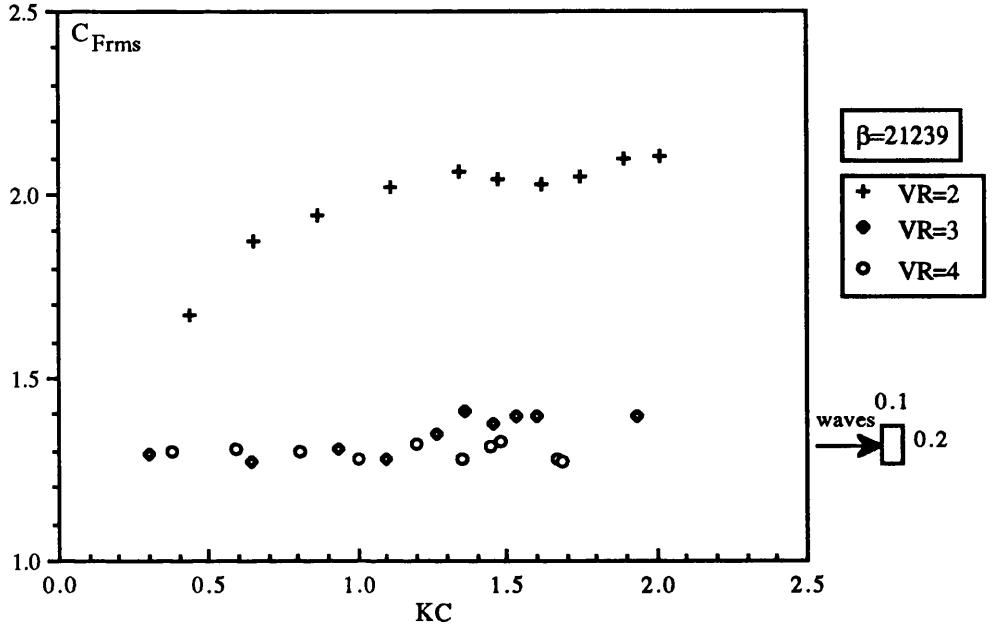

Fig. 4.127 C_{Frms} versus KC for a vertical cylinder with d/D=0.5 in waves and currents

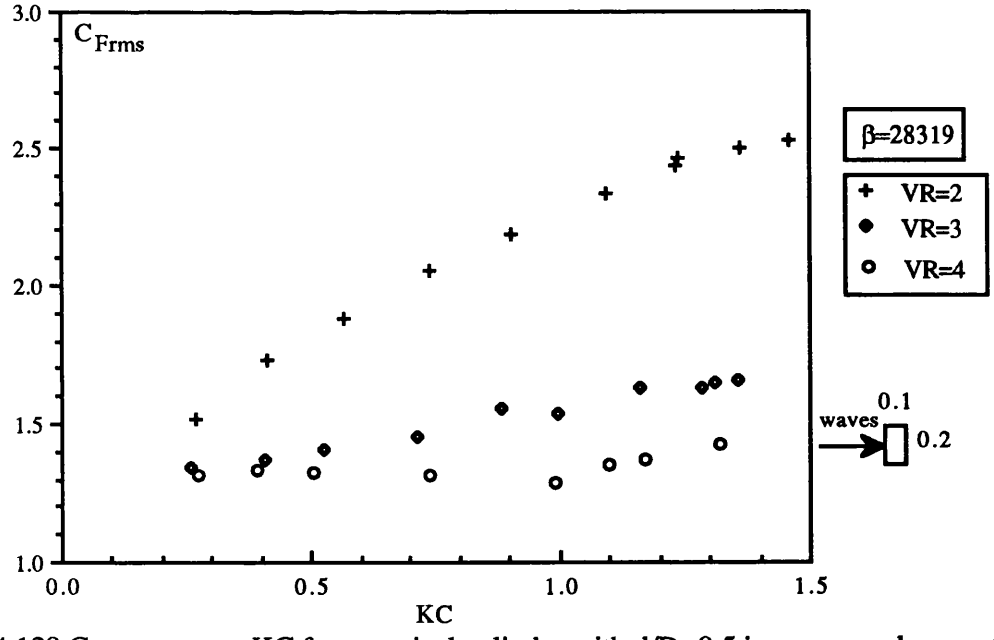

Fig. 4.128 C_{Frms} versus KC for a vertical cylinder with d/D=0.5 in waves and currents

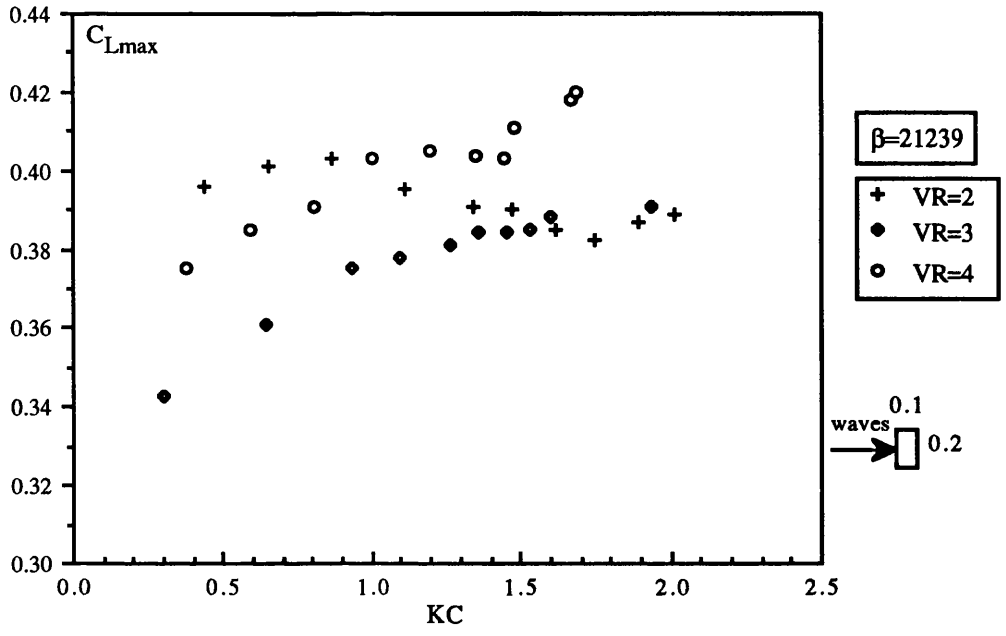

Fig. 4.129 C_{Lmax} versus KC for a vertical cylinder with d/D=0.5 in waves and currents

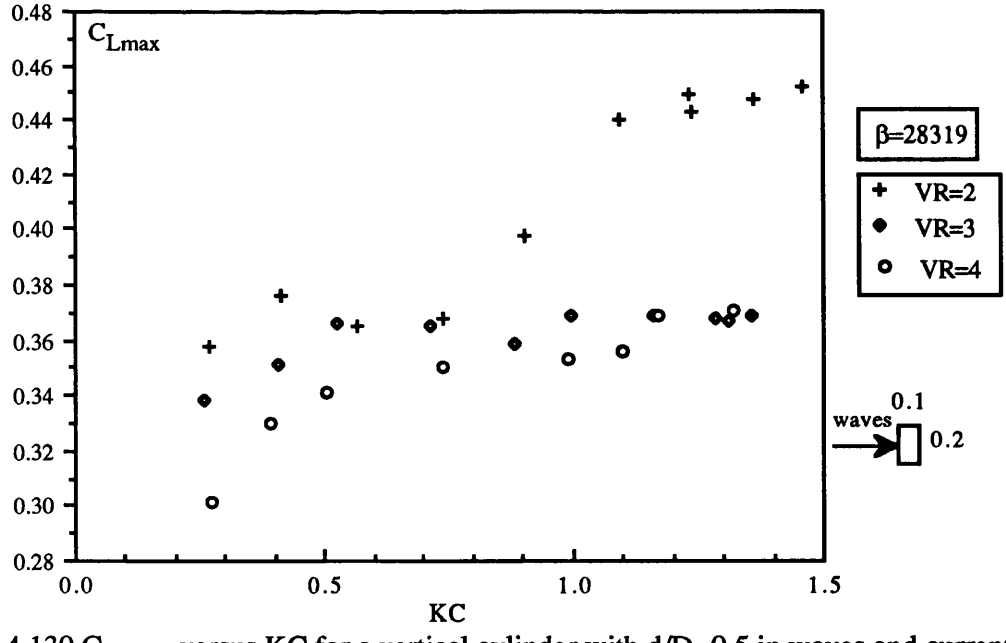

Fig. 4.130 C_{Lmax} versus KC for a vertical cylinder with d/D=0.5 in waves and currents

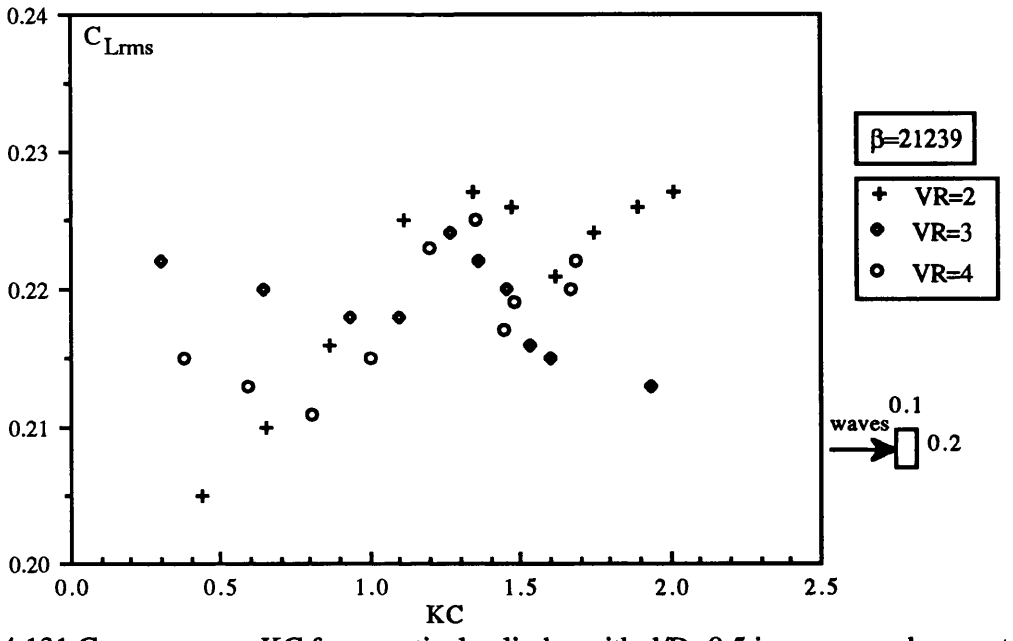

Fig. 4.131 C_{Lrms} versus KC for a vertical cylinder with d/D=0.5 in waves and currents

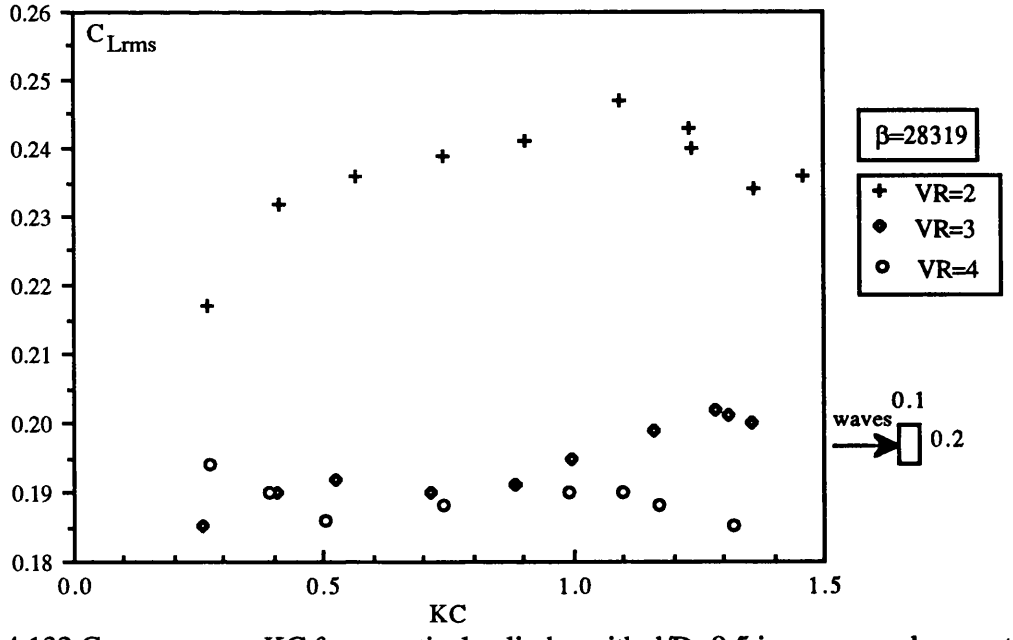

Fig. 4.132 C_{Lrms} versus KC for a vertical cylinder with d/D=0.5 in waves and currents

by 62% for VR=4. At the same KC and β numbers (Figure 4.131), C_{Lrms} in the no-current case decreased by 72% for VR varying between 2 and 4.

4.4.2 HORIZONTAL CYLINDERS

The different in-line force coefficients in terms of C_{Mx}, C_{Dx}, C_{Fxmax} and C_{Fxrms} were also measured for the cylinders tested horizontally and submerged with their axes parallel to wave crests in combined wavy and steady flows. They are plotted against the Keulegan-Carpenter KC number for constant values of the frequency parameter β and for various values of the reduced velocity VR. They are shown in Figures 4.133 through 4.156.

Figures 4.133 through 4.136 show the variations of C_{Mx} and C_{Dx} coefficients with the KC number for the square cross-sectional cylinder.

As in the case with the vertical square cylinder, the presence of a steady flow was found to have significant effects on the inertia coefficient. At KC numbers below about 2.5, C_{Mx} coefficient was found to decrease when a steady flow was present and the reduction was found to be more significant at the lower end of KC numbers. For β number of 5128 and above a KC number of 2.5 a current of higher reduced velocity of 9 was found to have the opposite effect of increasing C_M coefficient (Figure 4.133). For a higher β number of 6838 (Figure 4.134), the KC number at which C_M coefficient started to increase with the presence of a steady flow of relatively high reduced velocity was found to be less (KC number of about 2). These opposite effects of the current on the inertia coefficient suggest that there was a critical value of VR above which C_M coefficient did not decrease with VR. For example, at KC=0.4 and β=5128 (Figure 4.133), C_{Mx} coefficient in the no-current case (VR=0) decreased by 17% for VR=4, by 49% for VR=6 and by 56% for VR=9. For the same β number and at KC=1.7, C_{Mx} coefficient in the no-current case decreased by 8% for VR=4, by 23% for VR=6 and by 25% for VR=9. Again for the same β number and at a higher KC number of about 3, C_{Mx} coefficient in the no-current case decreased by 11% for VR=4, but increased by 3% and 12% for reduced velocities VR of 6 and 9 respectively. For a higher β number of 6838 and at KC=0.5 (Figure 4.134), C_{Mx} coefficient in the no-current case decreased by 22% for VR=4, by 35% for VR=6 and by 32% for VR=8. At KC=1.2 and for the same β number, C_{Mx} coefficient in the no-current case decreased by 15%

for VR=4, and by 11% for VR varying between 6 and 8. Again for the same β number and At KC=1.8, C_{Mx} coefficient in the no-current case decreased by 7% for VR=4, by 2% for VR=6 but increased by 14% for VR=8.

As with the vertical cylinder, the presence of a steady flow had a significant effect of reducing the values of the drag coefficient, particularly at the lower end of KC numbers. For example, at KC=0.4 and β=5128 (Figure 4.135), C_{Dx} coefficient in the no-current case decreased by 82% for VR=4, by 87% for VR=6 and by 90% for VR=9. For the same β number and at a KC number approaching 3, C_{Dx} coefficient in the no-current case decreased by 51% for VR=4, by 47% for VR=6 and by 42% for VR=9. For a higher β number of 6838 and at KC=0.5 (Figure 4.136), C_{Dx} coefficient in the no-current case decreased by 82% for VR=4, by 85% for VR=6 and by 88% for VR=8. For the same β number and at KC=1.8, C_{Dx} coefficient in the no-current case decreased by 60% for VR=4 and by 64% for VR varying between 6 and 8.

The variations of C_{Fxmax} and C_{Fxrms} with the KC number for the square cylinder are shown in Figures 4.137 through 4.140. As in the case of the vertical square cylinder, these coefficients decreased when a steady flow was present. For example at a KC number of about 3 and β=5128 (Figure 4.137), C_{Fxmax} of no-current case decreased by 72% for VR varying between 4 and 6 and by 73% for VR=9. At the same KC and β numbers (Figures 4.139), C_{Fxrms} of no-current case decreased by 77% for VR=4, by 75% for VR=6 and by 73% for VR=9.

The variations of of C_{Mx} and C_{Dx} coefficients with the KC number for the cylinder with an aspect ratio of 2 are shown in Figures 4.141 through 4.144.

For this particular cylinder, the presence of a steady flow did influence less the values of C_{Mx} coefficient compared to the square cross-sectional cylinder, particularly at KC numbers above about 1.5 where the current influence was found to be small as shown in Figures 4.141 and 4.142. However, at lower KC numbers the presence of a steady flow was found to reduce the inertia coefficient. For example, at KC=1 and β=5155 (Figure 4.141) C_{Mx} coefficient in the no-current case (VR=0) decreased by 6% for VR=4, by 11% for VR=6 and by 14% for VR=9. At a lower KC number of 0.5 and β=6873 (Figure 4.142) C_{Mx} coefficient in the no-current case decreased by 11% for VR=4 and by 12% for VR varying between 6 and 9.

As with the square cylinder, the drag coefficient decreased significantly when a steady flow was present, particularly at very low KC numbers. For example, at a KC number of about 1 and β=5155 (Figure 4.143), C_{Dx} coefficient in the no-current case decreased

by 63% for VR=4, by 73% for VR=6 and by 71% for VR=9. For the same β number and at a KC number of about 3.5, C_{Dx} coefficient in the no-current case decreased by 58% for VR=4, by 68% for VR=6 and by 55% for VR=9. At KC=1 and for a higher β number of 6873 (Figure 4.144), C_{Dx} coefficient in the no-current case decreased by 64% for VR=4, and by 71% for VR varying between 6 and 8. For the same β number and at a KC number approaching 2, C_{Dx} coefficient in the no-current case decreased by 63% for VR=4, by 71% for VR=6 and by 66% for VR=8.

The variations of C_{Fxmax} and C_{Fxrms} coefficients with the KC number for this cylinder are shown in Figures 4.145 through 4.148. As with the square cylinder, the presence of a steady flow had the effect of reducing these coefficients. For example at a KC number of about 3 and β=5155 (Figure 4.145), C_{Fxmax} of no-current case decreased by 67% for VR=4, by 74% for VR=6 and by 71% for VR=9. At the same KC and β numbers (Figures 4.147), C_{Fxrms} of no-current case decreased by 74% for VR=4, by 78% for VR=6 and by 76% for VR=9.

The variations of C_{Mx} and C_{Dx} coefficients with the KC number for the cylinder with the smallest aspect ratio of 0.5 are shown in Figures 4.149 through 4.152.

As with other cylinders, the presence of a steady flow had a significant effect in reducing the inertia coefficient. For example, at KC=0.5 and β=20743 (Figure 4.149), C_{Mx} coefficient in the no-current case decreased by 25% for VR varying between 2 and 3 and by 37% for VR=4. For the same β number and at KC=1.6, C_{Mx} coefficient in the no-current case decreased by 19% for VR varying between 2 and 3 and by 26% for VR=4. For a higher β number of 27658 and at a low KC number of 0.3 (Figure 4.150), C_{Mx} coefficient in the no-current case decreased by 17% for VR varying between 2 and 3 and by 31% for VR=4. For the same β number and at a KC number of about 1, C_{Mx} coefficient in the no-current case decreased by 14% for VR=2, by 12% for VR=3 and by 27% for VR=4.

The presence of a steady flow for this cylinder was also found to significantly reduce the drag coefficient, particularly at very low KC numbers. For example, at KC=0.5 and β=20743 (Figure 4.151), C_{Dx} coefficient in the no-current case decreased by 81% for VR=2, and by 84% for VR varying between 3 and 4. For the same β number and at KC=1.6, C_{Dx} coefficient in the no-current case decreased by 52% for VR=2, by 59% for VR=3 and by 64% for VR=4. At a very low KC number of 0.3 and for a higher β number of 27658 (Figure 4.152), C_{Dx} coefficient of the no-current case decreased by

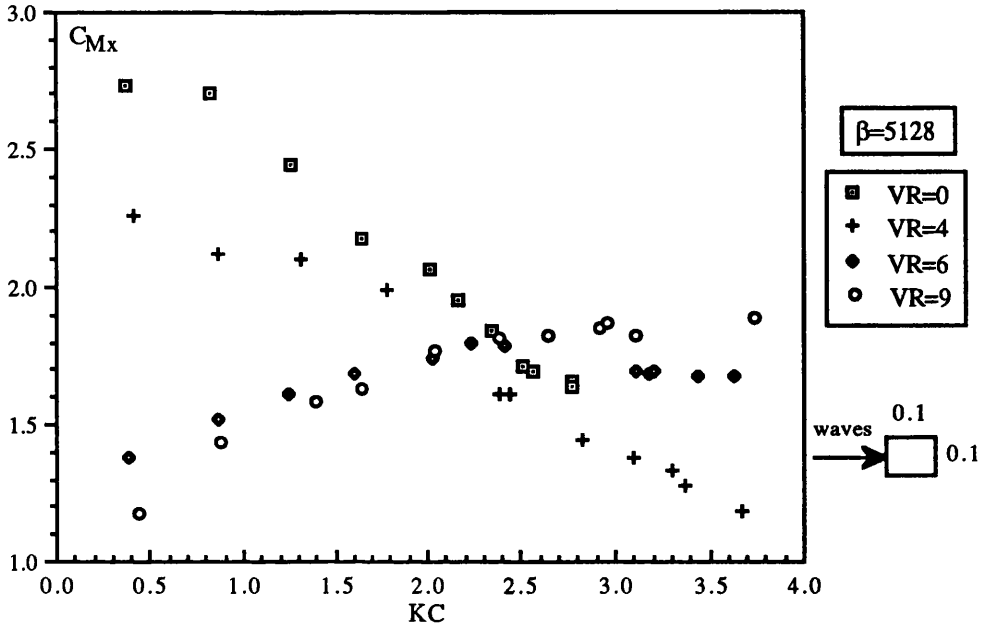

Fig. 4.133 C_{Mx}versus KC for a horizontal cylinder with d/D=1 in waves and currents

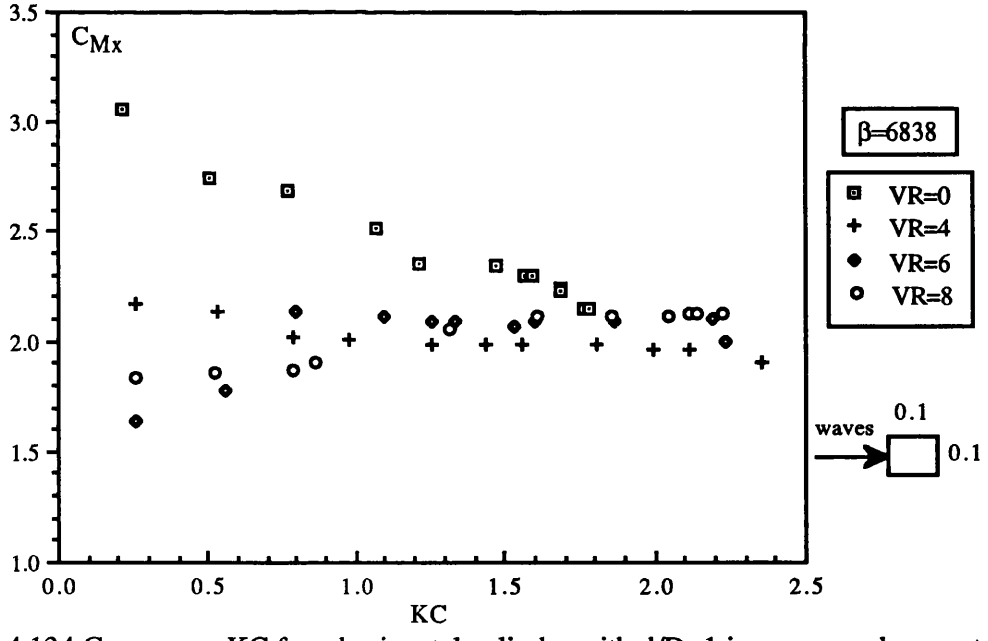

Fig. 4.134 C_{Mx}versus KC for a horizontal cylinder with d/D=1 in waves and currents

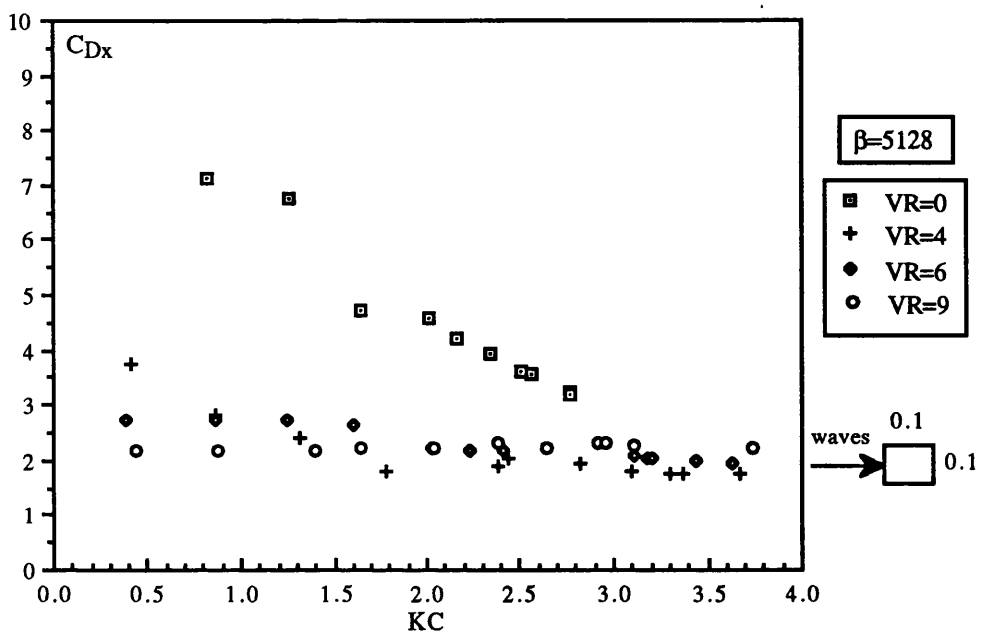

Fig. 4.135 C_{Dx} versus KC for a horizontal cylinder with d/D=1 in waves and currents

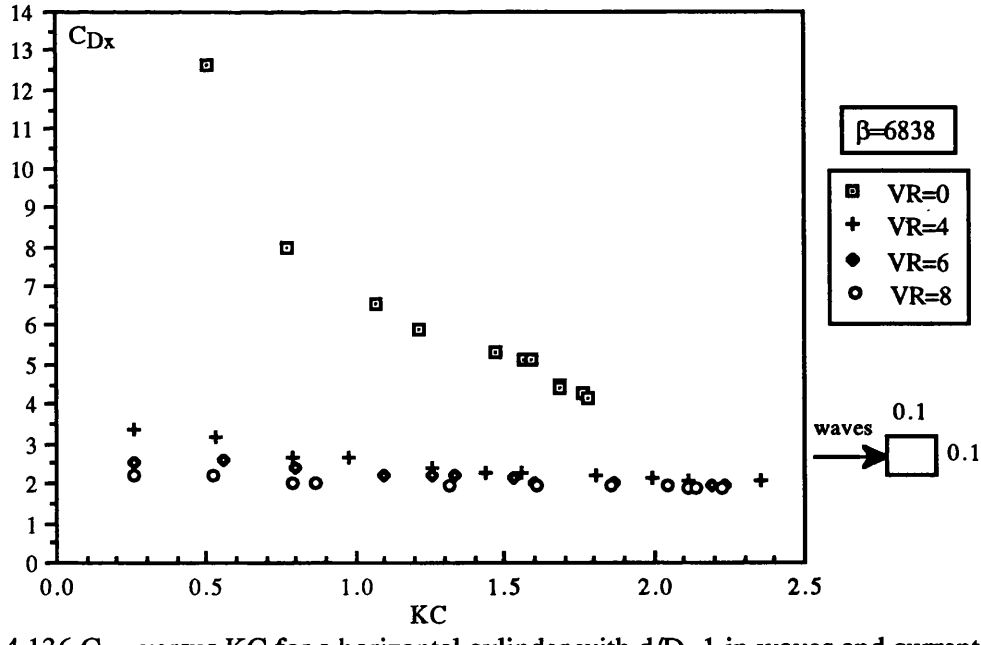

Fig. 4.136 C_{Dx} versus KC for a horizontal cylinder with d/D=1 in waves and currents

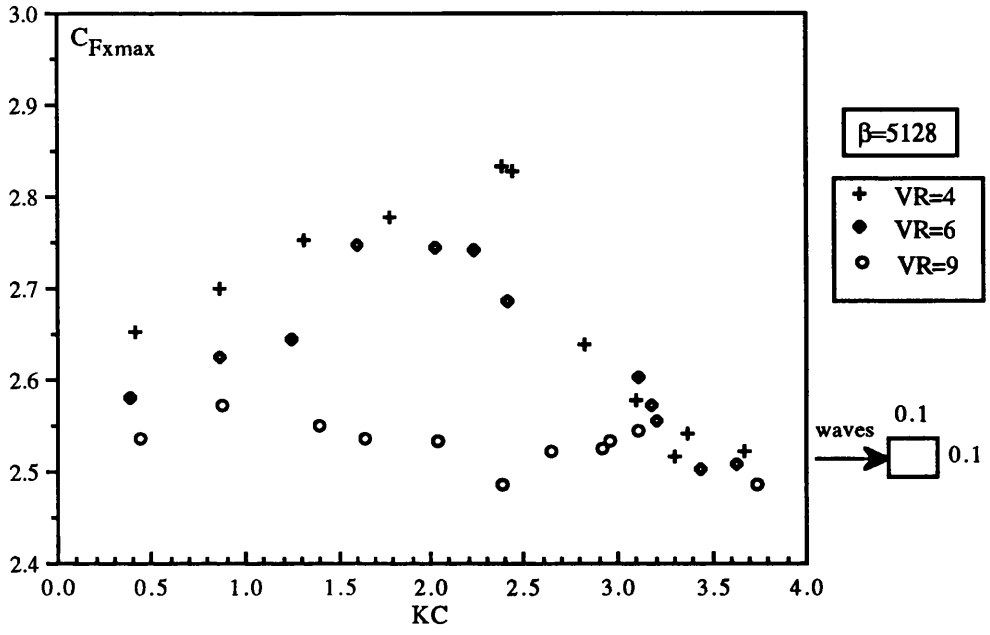

Fig. 4.137 C_{Fxmax} versus KC for a horizontal cylinder with d/D=1 in waves and currents

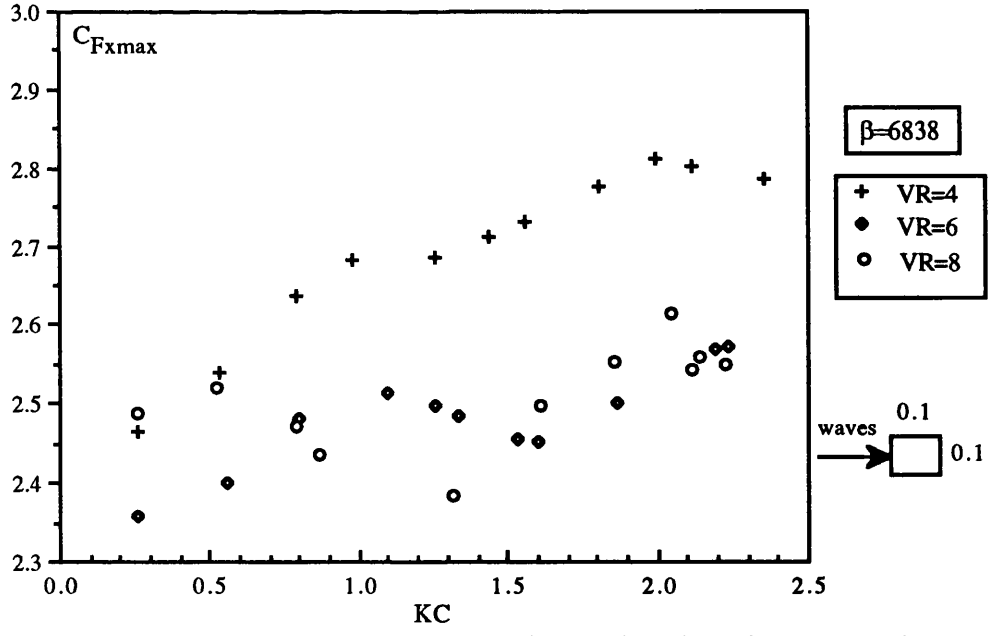

Fig. 4.138 C_{Fxmax} versus KC for a horizontal cylinder with d/D=1 in waves and currents

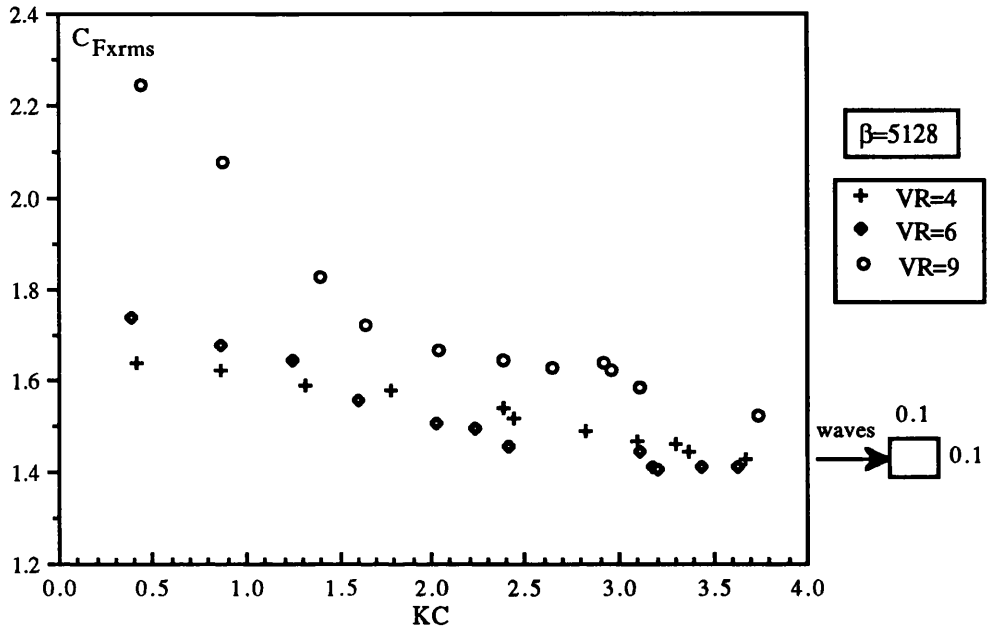

Fig. 4.139 C_{Fxrms} versus KC for a horizontal cylinder with d/D=1 in waves and currents

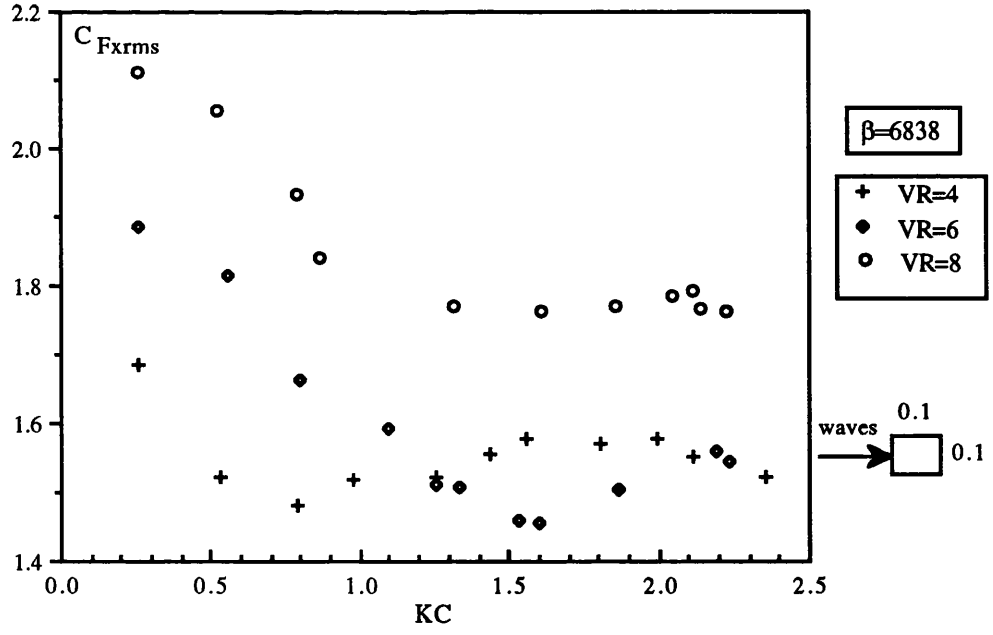

Fig. 4.140 C_{Fxrms} versus KC for a horizontal cylinder with d/D=1 in waves and currents

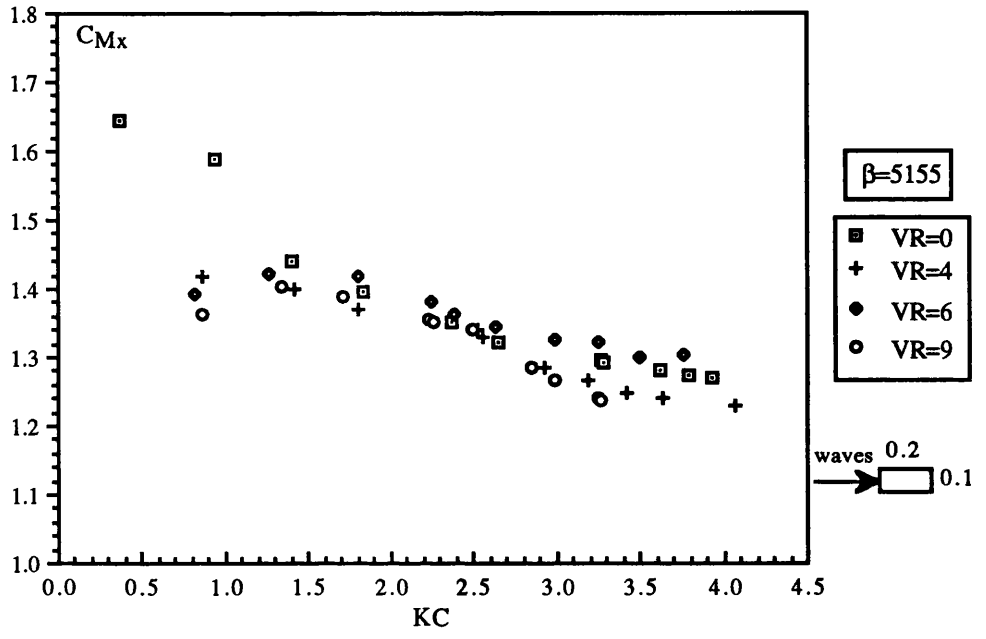

Fig. 4.141 C_{Mx} versus KC for a horizontal cylinder wih d/D=2 in waves and currents

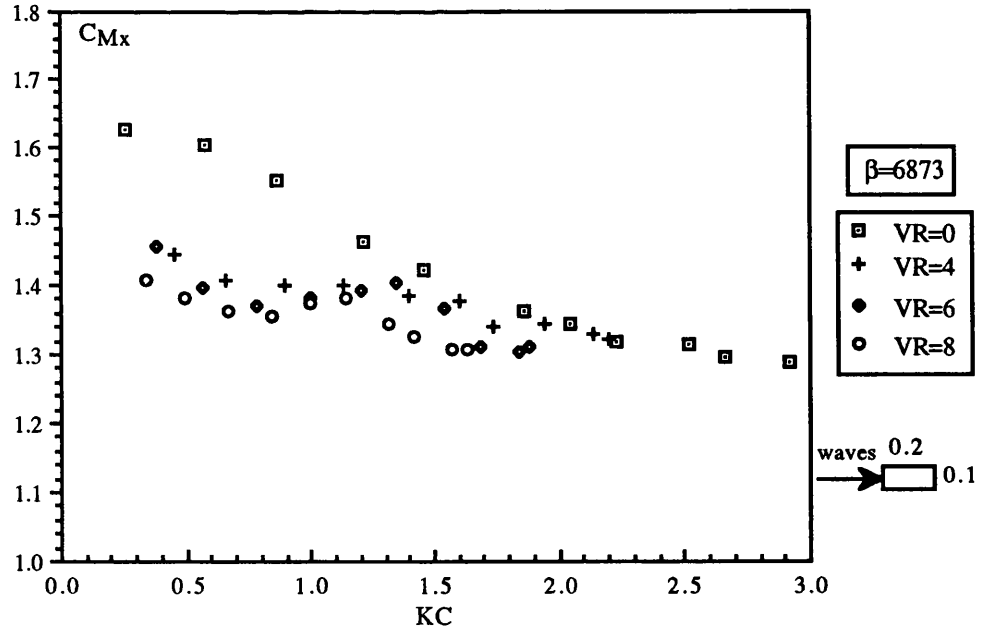

Fig. 4.142 C_{Mx} versus KC for a horizontal cylinder wih d/D=2 in waves and currents

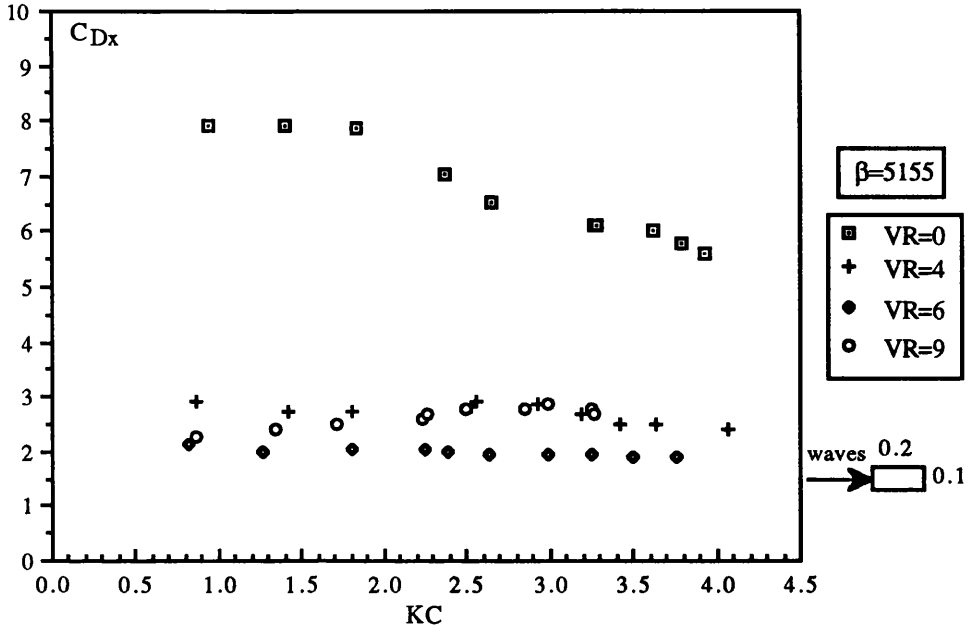

Fig. 4.143 C_{Dx} versus KC for a horizontal cylinder wih d/D=2 in waves and currents

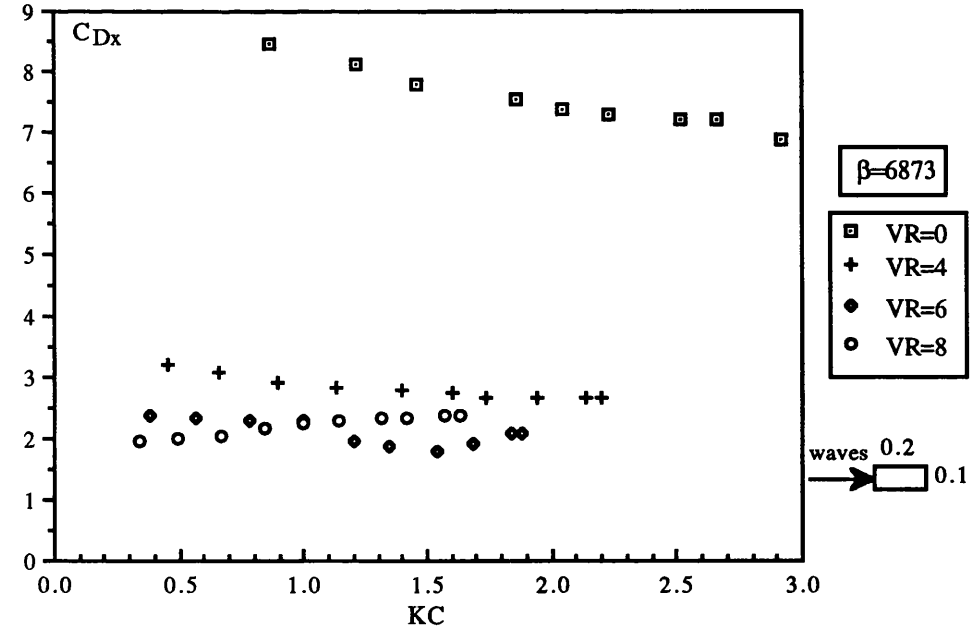

Fig. 4.144 C_{Dx} versus KC for a horizontal cylinder wih d/D=2 in waves and currents

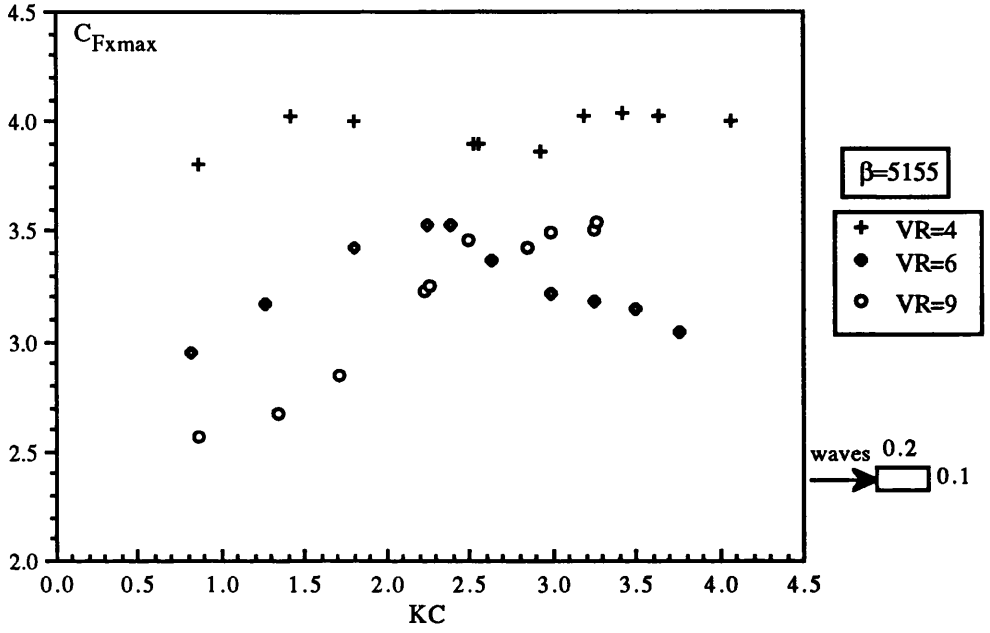

Fig. 4.145 C_{Fxmax} versus KC for a horizontal cylinder wih d/D=2 in waves and currents

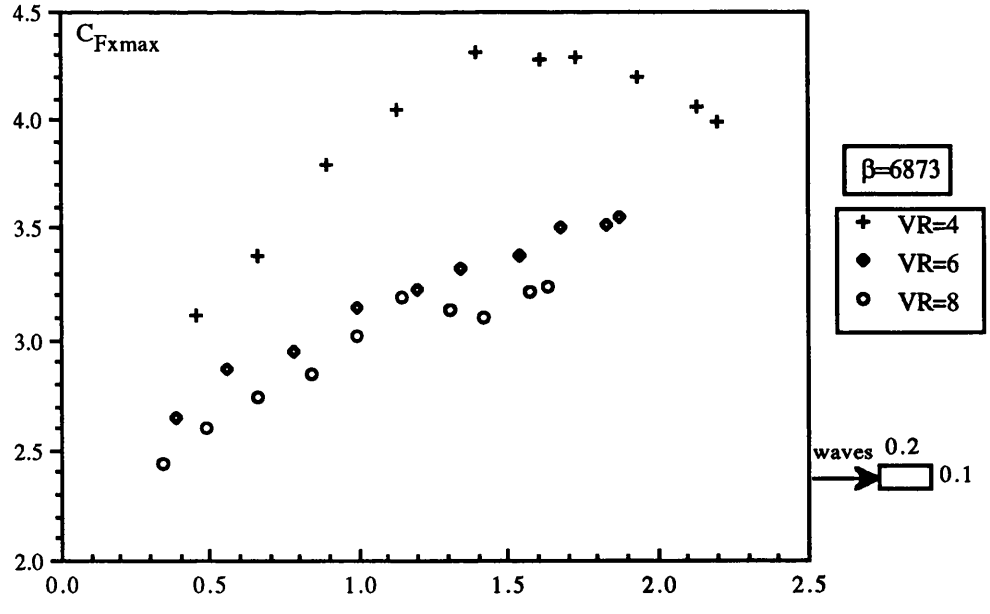

Fig. 4.146 C_{Fxmax} versus KC for a horizontal cylinder wih d/D=2 in waves and currents

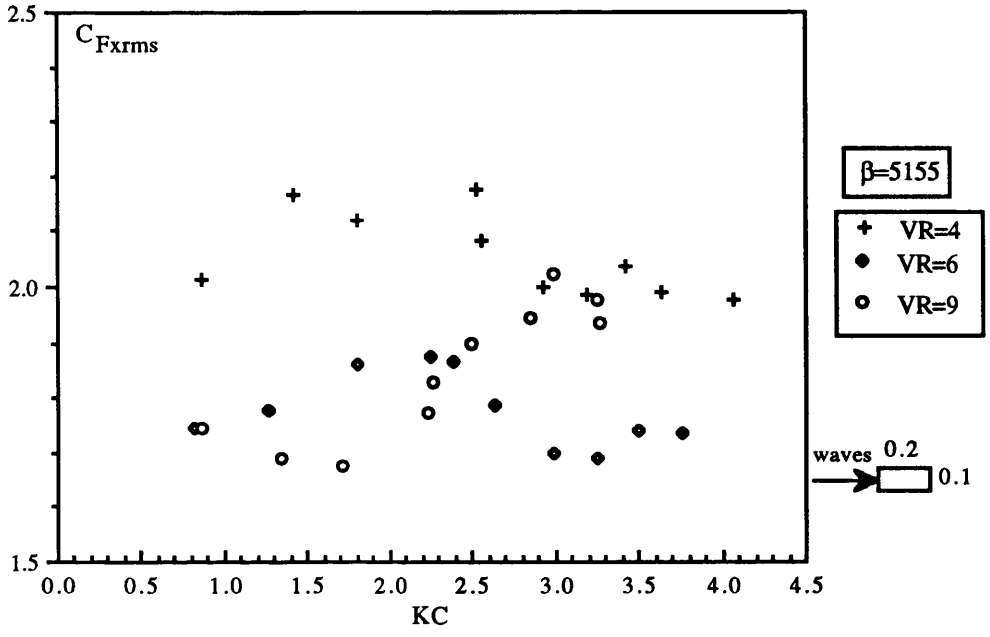

Fig. 4.147 C_{Fxrms} versus KC for a horizontal cylinder wih d/D=2 in waves and currents

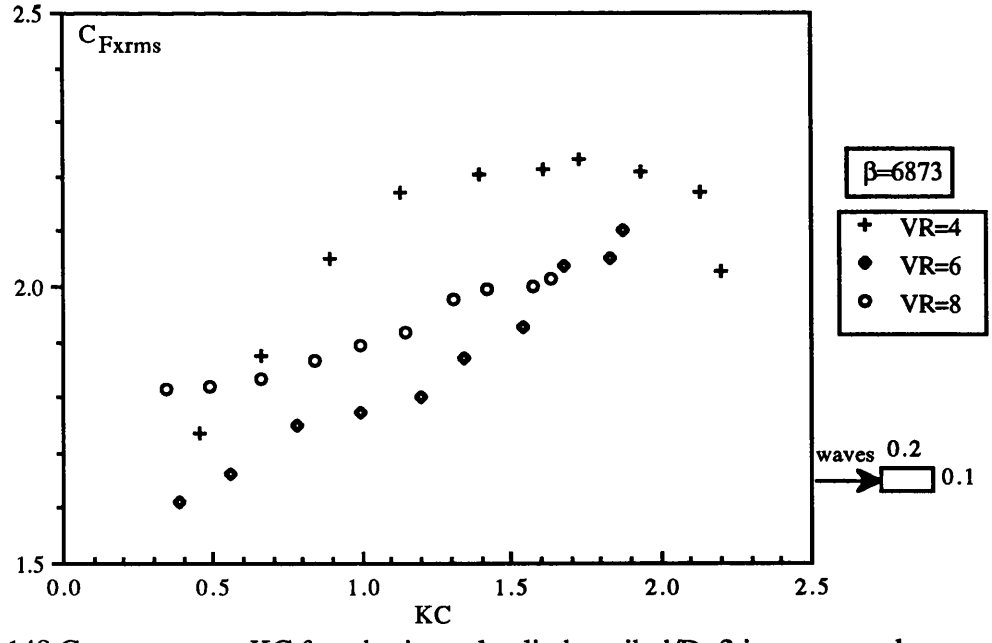

Fig. 4.148 C_{Fxrms} versus KC for a horizontal cylinder wih d/D=2 in waves and currents

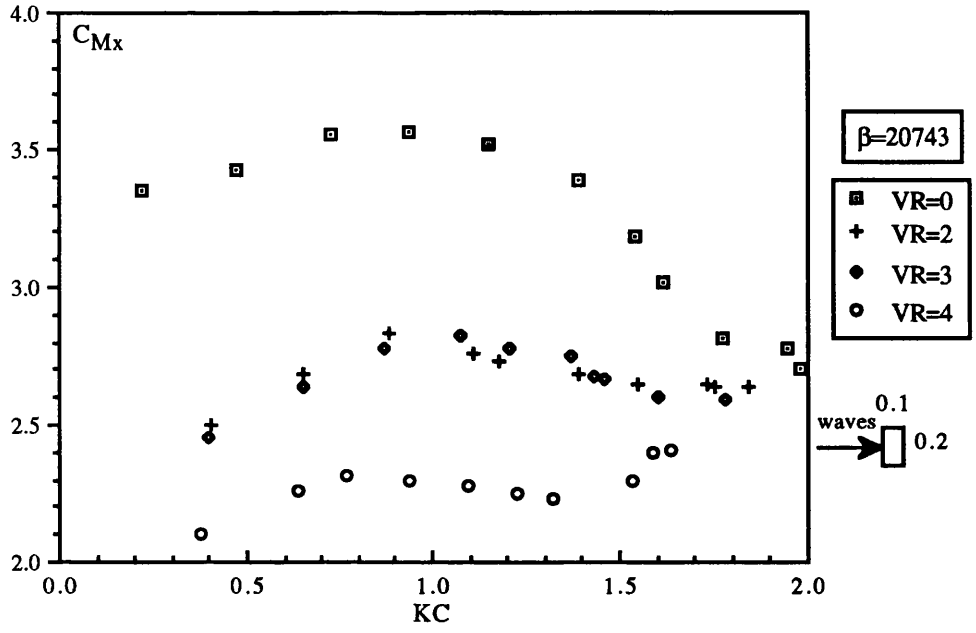

Fig. 4.149 C_{Mx} versus KC for a horizontal cylinder with d/D=0.5 in waves and currents

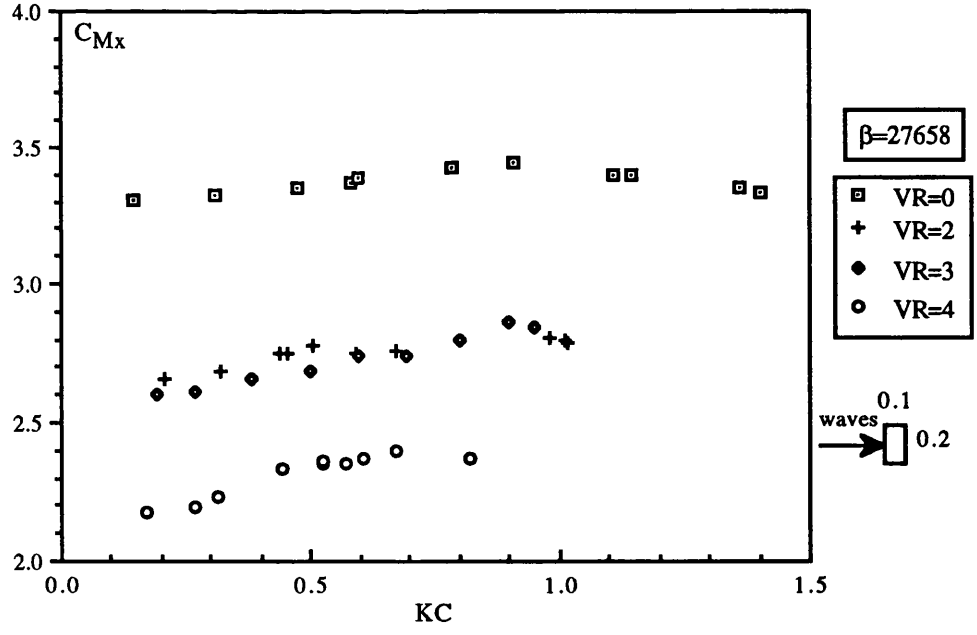

Fig. 4.150 C_{Mx} versus KC for a horizontal cylinder with d/D=0.5 in waves and currents

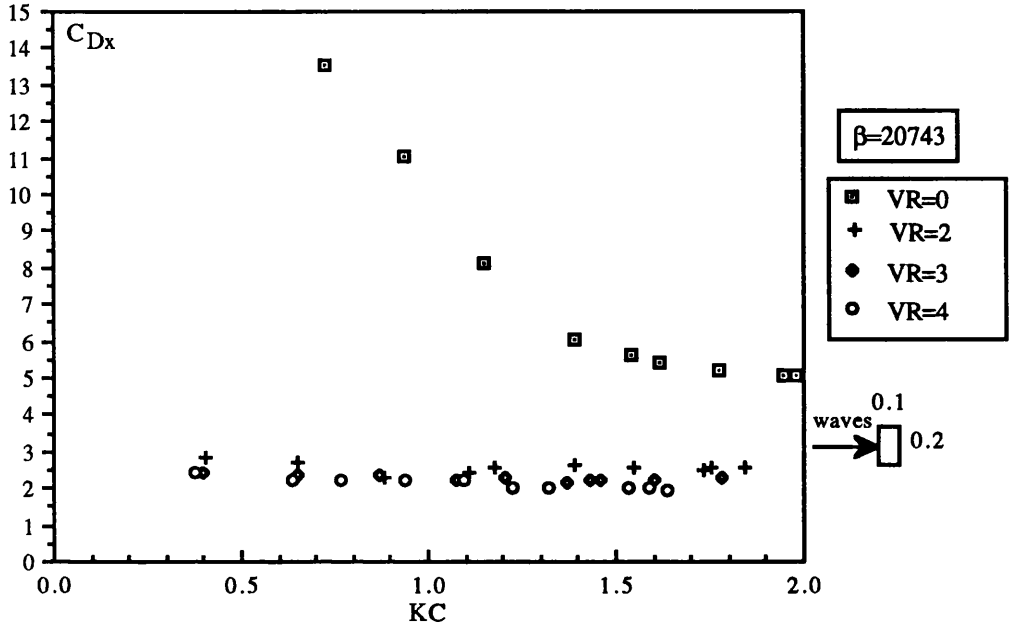

Fig. 4.151 C_{Dx} versus KC for a horizontal cylinder with d/D=0.5 in waves and currents

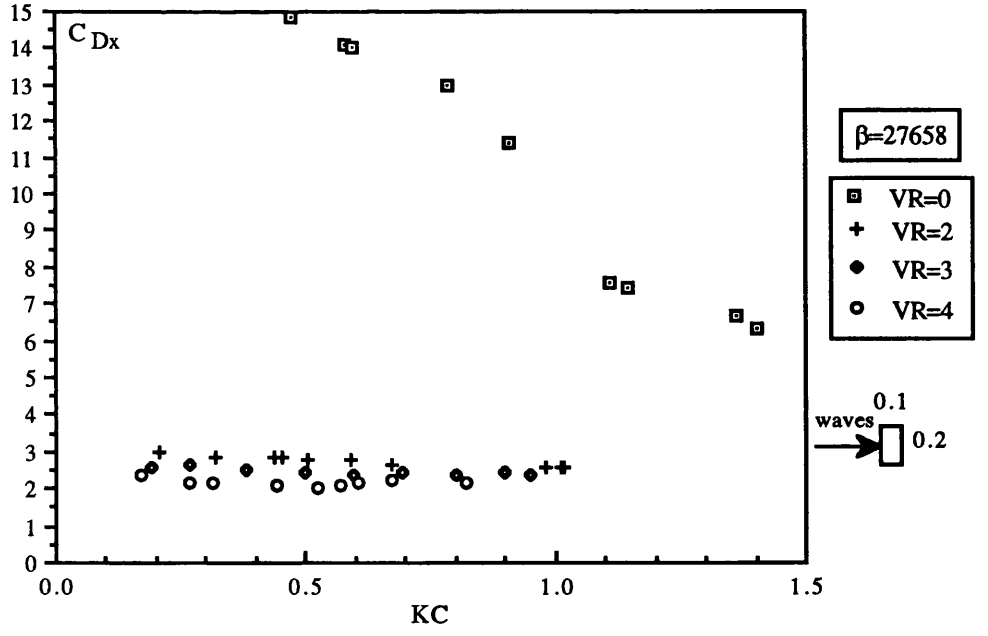

Fig. 4.152 C_{Dx} versus KC for a horizontal cylinder with d/D=0.5 in waves and currents

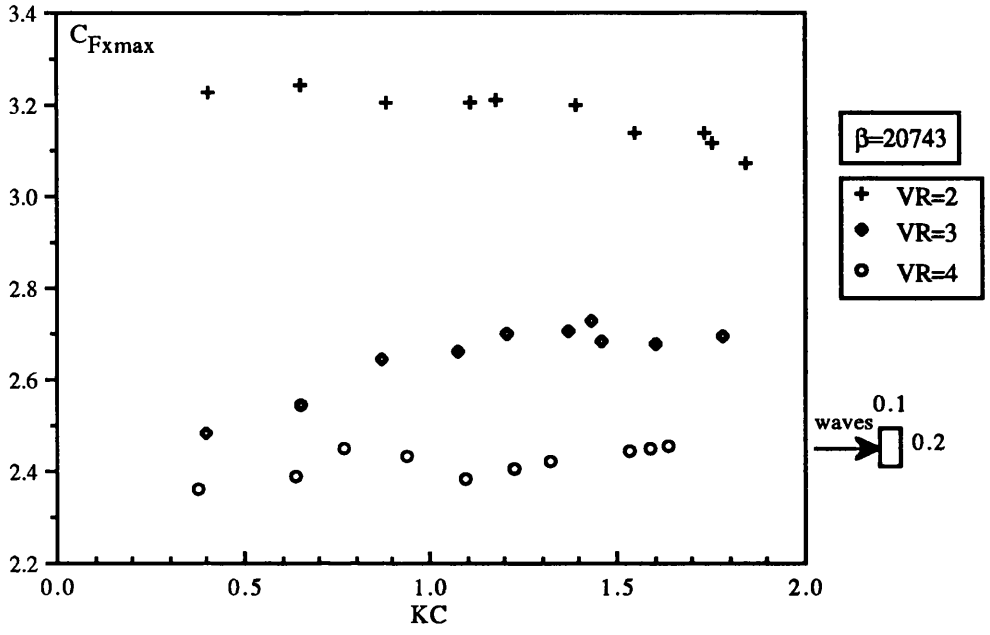

Fig. 4.153 C_{Fxmax} versus KC for a horizontal cylinder with d/D=0.5 in waves and currents

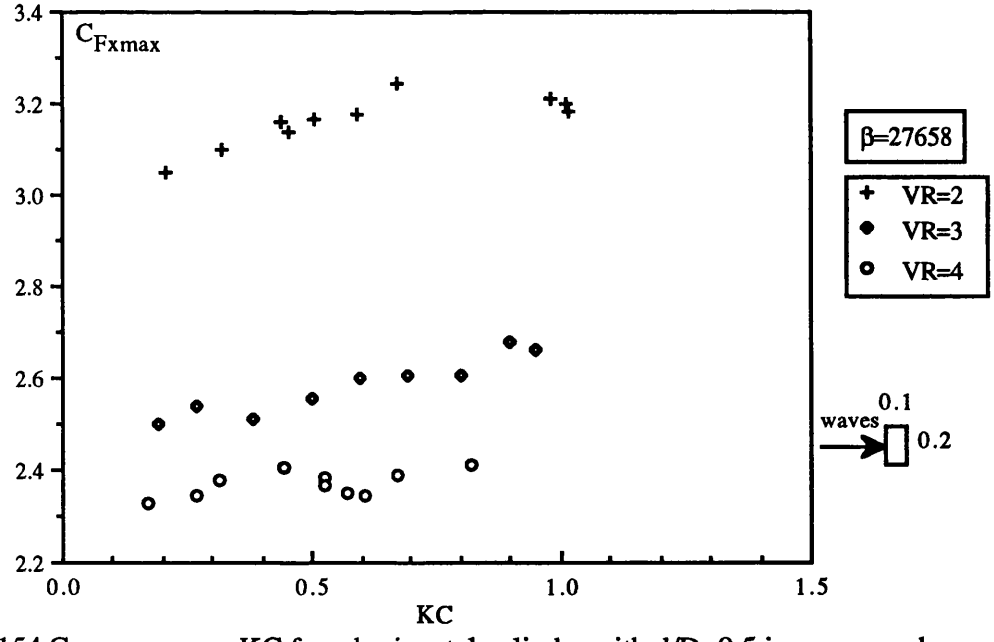

Fig. 4.154 C_{Fxmax} versus KC for a horizontal cylinder with d/D=0.5 in waves and currents

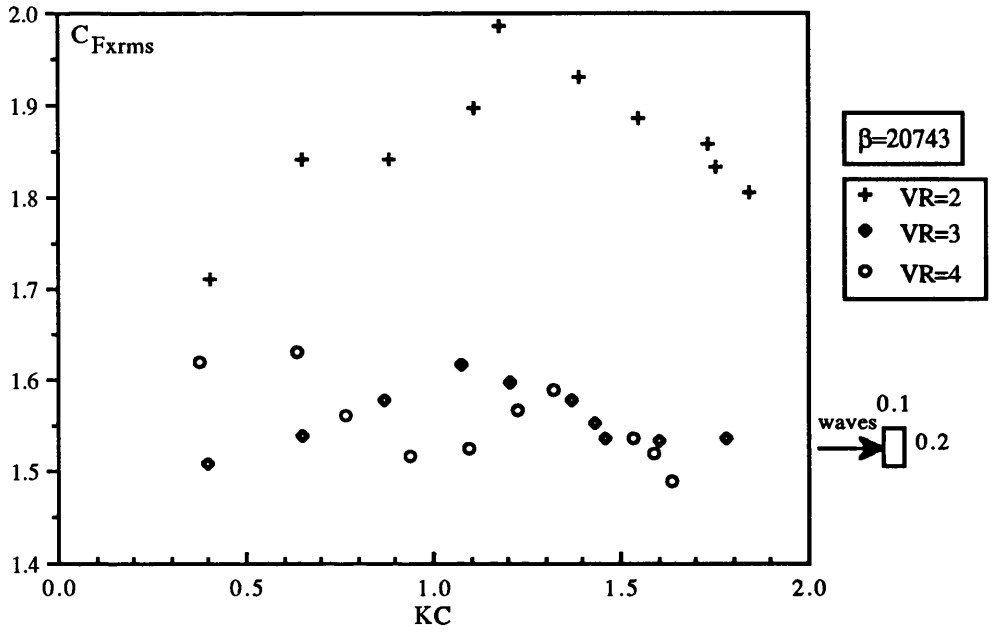

Fig. 4.155 C_{Fxrms} versus KC for a horizontal cylinder with d/D=0.5 in waves and currents

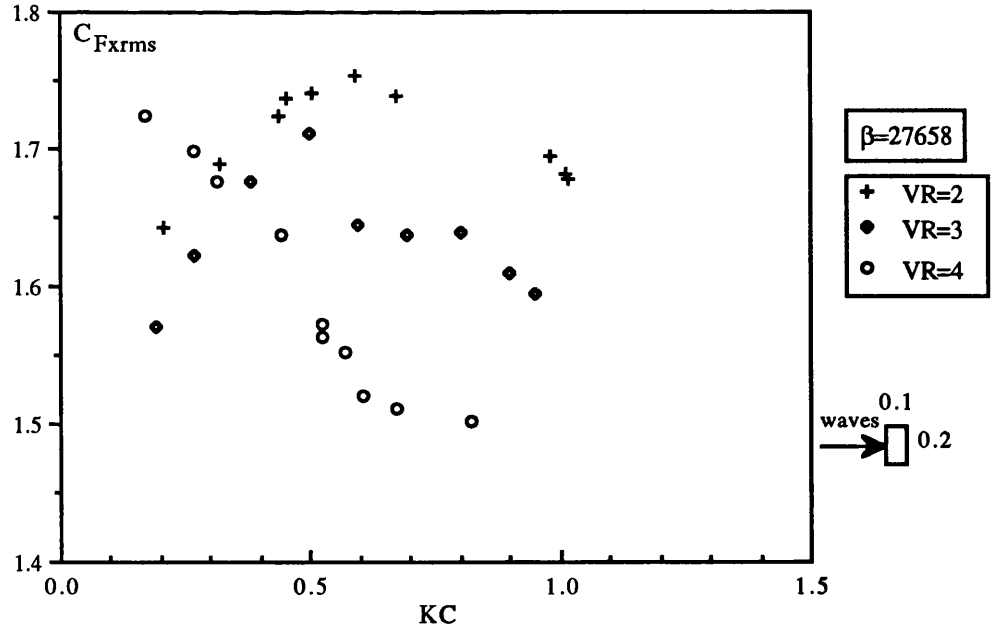

Fig. 4.156 C_{Fxrms} versus KC for a horizontal cylinder with d/D=0.5 in waves and currents

83% for VR varying between 2 and 3 and by 87% for VR=4. For the same β number and at KC=1, C_{Dx} coefficient in the no-current case decreased by 65% for VR=2, by 68% for VR=3 and by 71% for VR=4.

The variations of C_{Fxmax} and C_{Fxrms} coefficients with the KC number for this cylinder are shown in Figures 4.153 through 4.156. As with other cylinders, these coefficients decreased when a steady flow was present. For example at a KC number of about 2 and β=20743 (Figure 4.153), C_{Fxmax} of no-current case decreased by 69% for VR=2, by 73% for VR=3 and by 75% for VR=4. At the same KC and β numbers (Figures 4.155), C_{Fxrms} of no-current case decreased by 77% for VR=2, by 80% for VR=3 and by 83% for VR=4.

Finally, Figure 4.157 shows a record of data of wave profile, in-line and transverse forces measured simultaneously (the time series are shown for 2 wave cycles). It can be clearly seen that the peak of the horizontal force occurs when the wave crosses the mean water level. It is also interesting to see that the lift force, despite the fact that it is random in nature, attains its peak value (in absolute value) when the horizontal force approaches its positive peak . This behaviour was observed not only for the figure shown below but for all other runs and for the entire recorded time series.

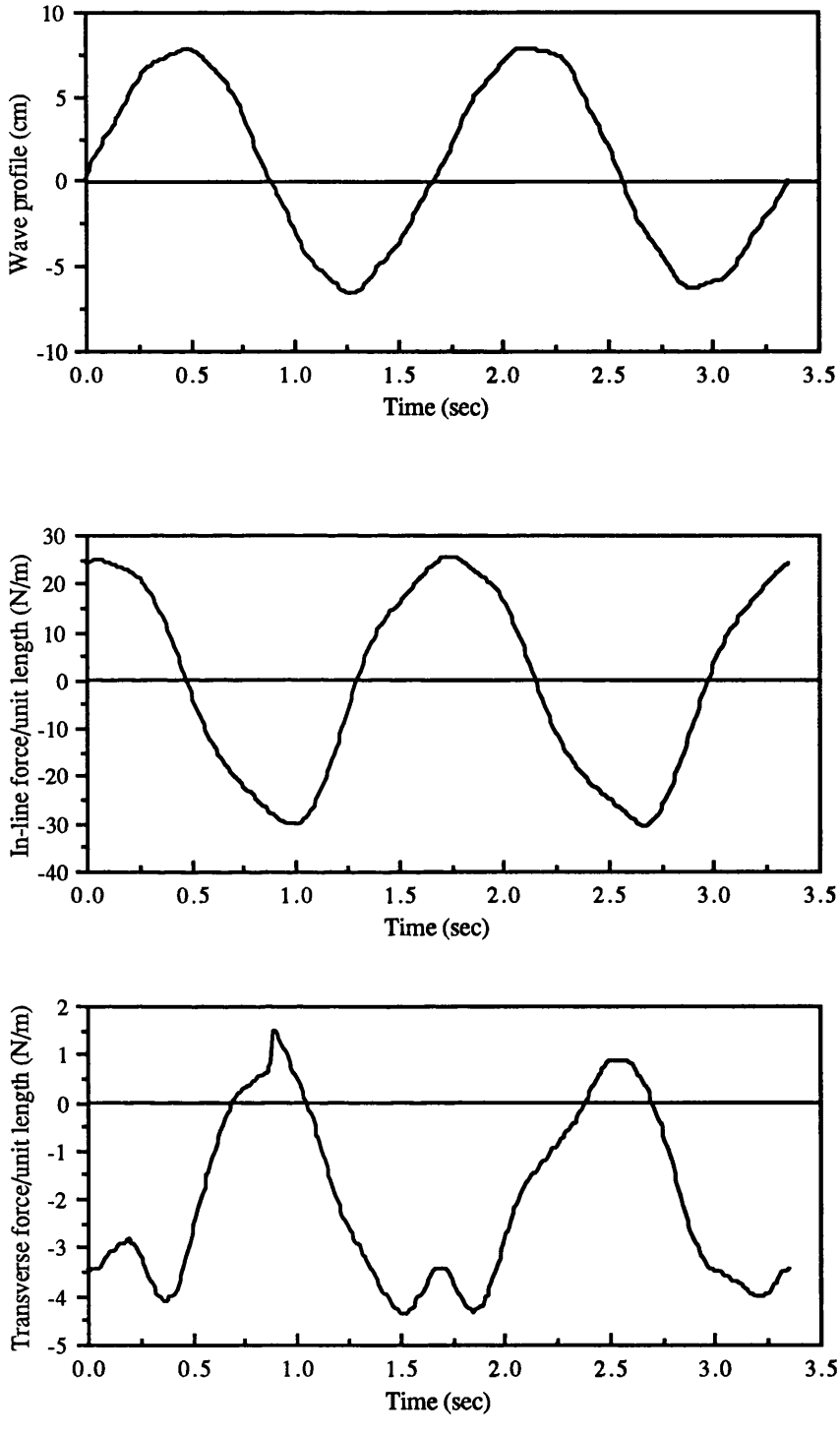

Fig. 4.157 Example of measured wave height, in-line and transverse forces on a vertical square cylinder in waves (β=5249, KC=3.121)

CHAPTER 5

FLOW VISUALISATION

One of the most useful techniques for understanding flow-body interaction is flow visualisation. This technique allows us to comprehend how vortices after flow separation are shed from the body and develop during the stages of a flow cycle. These vortex motions are extremely important in determining both the in-line and transverse forces experienced by bodies immersed in a stream of a flow.

In steady flow, several researchers carried out flow visualisations on rectangular cylinders of various aspect ratios mostly in wind tunnels to understand formation and shedding of vortices and their consequences on the value of the drag force. In wavy flow, however, very few flow visualisations have been carried out on rectangular cylinders with varying aspect ratios. The only exceptions are the square cross-sectional cylinder and flat plates on which the flow was visualised mostly in planar oscillatory flow using U-shaped water oscillating tunnel.

The pattern of formation and shedding of vortices around rectangular cylinders in waves and the effects of changing the afterbody length (effect of the aspect ratio) on the flow separation and vortex shedding are still unexplored. One would expect that the effects of the aspect ratio on the pattern of vortex formation and shedding in steady flow might be similar to those in wavy flow at high KC numbers.

5.1 REVIEW Of FLOW VISUALISATION

In addition to the literature review given in Chapter 1, below are summaries of some flow visualisations conducted by other researchers in steady flow and in periodic flow.

5.1.1 STEADY FLOW

Bearman and Trueman (1972) investigating a flow around rectangular cylinders with different aspect ratios argued that the base pressure cannot be continuously decreased with increasing d/D because at some critical block depth, the path of the separating shear layer would be impeded by the downstream corner during part of the

shedding cycle. Further, the fluid which is entrained into the initial part of the shear layers must be balanced by a return of fluid between the shear layers and the downstream corners. The flow cannot reattach on the side faces because if it did the bubble formed would be immediately cut off from the region of low pressure behind the body and the shear layer itself could not support the low pressure required. This sets an upper limit on the curvature of the free shear layers and on the value of the negative base pressure coefficient. To satisfy these conditions the flow has to readjust to give less shear layer curvature with a higher base pressure and a longer distance to vortex formation.

Bearman and Trueman conducted some flow visualisations in a water tunnel using dye filament. With a rectangular cylinder with an aspect ratio d/D of 0.2, the separated cavity behind the body appeared comparatively large. When the aspect ratio d/D increased to 0.6 (near the critical section), the vortices were seen to form very close to the base, leaving a small separated region. With a cylinder with an aspect ratio d/D of 1 (square cylinder), the flow had a larger base cavity. Nakaguchi et al. (1968) reported earlier similar flow patterns and showed how the vortex formation position moved close to the rear face for the critical section. Bearman and Trueman found that the square cylinder and the flat plate of d/D of 0.2 had almost identical base pressure and drag coefficients. However, the flow visualisation revealed a major difference between the flow fields around the two cylinders namely the distance from the separation points to the position of vortex formation was considerably longer on the square cylinder. Therefore, the shear layers would diffuse more and would be thicker at the position of vortex formation.

Okajima et al. (1983) carried out a flow visualisation on rectangular cylinders in a wind tunnel using the smoke-wire technique to correlate the flow pattern with the discontinuities of the Strouhal number discussed in Chapter 1. They visualised the flow below and above the critical Reynolds numbers where the curve of the Strouhal number versus the Reynolds number showed an abrupt change for different d/D ratios. With a cylinder with d/D of 1.5, a vortex street in regular arrangement with a narrow wake width was seen at a low Reynolds number of 450. At Re=700, a streamwise distance of the vortex street spread out and that corresponded to a reduction of the Strouhal number. With cylinders with d/D of 2 and 3, at a low Reynolds number of 450, vortex streets were orientated in a regular arrangement whereas over the critical Reynolds number at 1.8×10^3 the flow-patterns transformed to a wide wake width. With a cylinder with d/D

of 3, the flow was seen to have a regular vortex street at $Re=0.6x10^3$ corresponding to a high value of the Strouhal number. At $Re=2x10^3$ the regular vortex street disappeared and the wake with a wide width showed a slow oscillation corresponding to a low Strouhal number. At $Re=6x10^3$ the flow pattern was similar to that at $Re=0.6x10^3$ and that explained the good agreement between their values of the Strouhal number.

Sakamoto and Arie (1983) carried out a flow visualisation in a wind tunnel using the smoke-wire technique on square cylinders of different length to width ratios L/D to correlate the flow patterns with the discontinuities found in the Strouhal number. They found that for cylinders with L/D<2, the wake vortices shed behind the cylinders were of the so-called arch-type vortex in which a pair of vortices were arranged symmetrically and for cylinders with L/D>2 the vortices were of Kármán vortex street type in which a pair of vortices were arranged asymmetrically. This change of flow patterns was found to coincide with a change in the variation of the Strouhal number in the vicinity of L/D=2. Sakamoto and Arie observed alternate formation of the two types of vortices when L/D approached 2. They suggested that the reason for this change was that when the length of the square cylinder was larger than the width, the flow separations from both sides were so much stronger than those from the top that the wake behind the cylinder was almost controlled by the flows from the sides. Consequently, the flows separating from both sides formed the Kármán-type vortex street. With an increase in the width of the cylinder, the flow separating from the top end of the cylinder increased in strength and as a result the flow from the top end joined the flows from the sides, forming an entity in the arch-type vortex shed behind the cylinder. Moreover, when the vortices were of the arch-type vortex, the width of the wake was observed to be much smaller than in the case of the Kármán-type vortex street.

Laneville and Yong (1983) summarised the general features of the flow around rectangular cylinders which are the distribution of the vorticity from the point of separation, the growth of a separation bubble and the formation of the wake vortex (Figure 5.1). At the point of separation, the boundary layer from the upstream face separates and part of its vorticity is absorbed by a growing separation bubble near the leading edge. The unabsorbed part of vorticity, c, continues in the shear layer in a proportion controlled by the cylinder afterbody length, d/D. The vorticity and fluid contained in this shear layer feed, according to the time of the cycle, either the opposite vortex or the adjacent vortex while they are forming. As the adjacent wake vortex forms, the separation bubble assumes different sizes and can be considered as a buffer

region filling itself with fluid and vorticity and then releasing them at maturity. When the adjacent vortex has just been shed, the separation bubble shrinks to its minimum size. At the end of its growth, the bubble exhausts its vorticity and the fluid either in the forming wake vortex (d/D <3) or in patches of vorticity in the case of cylinders experiencing reattachment (d/D>3). For cylinders with d/D<3, the side wall is not long enough to trap the bubble, so that the bubble at the end of its growth vents its portion d of fluid and vorticity directly into the adjacent rolling vortex. Portion c of the shear layer rolls as well in the forming vortex. In its formation, the adjacent vortex is also supplied with fluid from the wake (portion e) and the opposite shear layer (portion f). As the vortex reaches its final size with the bubble venting, part of the opposite shear layer is drawn across the wake, the fluid supply from the shear layer (portion c) is cut off, the wake vortex is then released and the separation bubble has shrunk to its minimum size. As this vortex is shed, the opposite vortex starts to form.

The effect of the afterbody length, d/D, on the process is critical in the sense of the distribution of the initial vorticity (or the bubble minimum size and vorticity) and the interaction between the separation bubble and the forming vortex.

For cylinders with d/D>3, the separation bubble is trapped and cannot exhaust directly in the wake vortex. As previously, the separation bubble grows during the periodic cycle till it reaches its minimum size and then vents by releasing a "patch" of fluid and vorticity on the side wall. These released "patches" of fluid marching downstream (d/D=5), form a secondary region in the mean. As they are entrained by the mean external flow, the released "patches" of fluid diffuse.

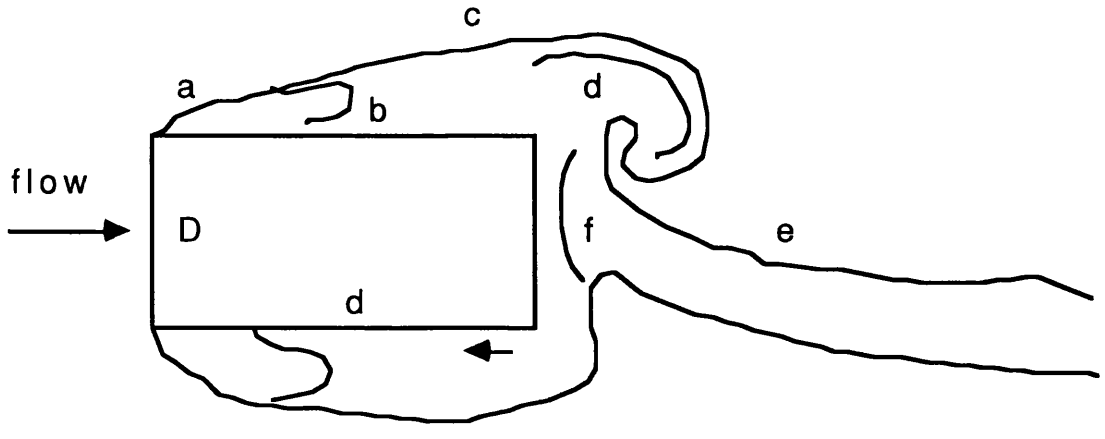

Figure 5.1 Flow separation around a rectangular cylinder

5.1.2 PERIODIC FLOW

The problem of drag forces due to vortex shedding in oscillatory flow and to some extent in wavy flow has been treated both experimentally and theoretically by several researchers.

Keulegan and Carpenter (1958) carried a flow visualisation on circular cylinders and flat plates placed in a node of a standing wave by introducing a jet of coloured liquid on one side of the immersed bodies. At a small KC number number of 1, vortices were forming almost simultaneously at the upper and lower edges of the flat plates. At smaller KC numbers, the vortices were seen to concentrate nearer the edges of the plates. Using a smaller flat plate to increase the KC number up to 15, Keulegan and Carpenter observed that the vortex formation was no longer symmetrical. The separation was seen to occur first at the upper edge of the plate followed by a vortex formed at the lower edge remaining close to the plate. When increasing the KC number to 110, Kármán vortices were obtained.

Bearman et al. (1978) carried out a flow visualisation on horizontal circular, square and diamond cylinders and a flat plate in planar oscillatory flow. In the case of the sharp edges cylinders, they observed that the flow was dominated by the generation of intense discrete vortices at low KC numbers which sometimes appeared to circle the body. The semblance of a vortex street forming during each half cycle was not observed until the KC number was in excess of 20 or 30. Below the KC number of 15, they observed only two main vortices being formed per half cycle one of which tended to grow more rapidly than the other. At flow reversal, the large vortex passed rapidly over one side of the body where vorticity of opposite sign was being generated. The induced flow of the reversed vortex helped to generate quickly a second large vortex of opposite sign. When the two vortices were nearly of the same strength, the pair moved away from the cylinder. In the meantime, the other shear layer rolled up to form a large vortex ready to initiate a similar process on the other side of the body at the next flow reversal. These vortex motions were observed to be similar for all the three sharp edged cylinders though the KC number for a particular regime varied from body to body. For the square cylinder, the vortices were least distinct and the flow displayed a more turbulent appearance.

Singh (1979) carried out a flow visualisation on horizontal circular, square and diamond cylinders and flat plates in planar oscillatory flow using white polystyrene particles. On

a square cross-sectional cylinder, he observed three regions of flow patterns, a symmetric region for KC<5, an asymmetric region for 5<KC<25 and a pseudo Kármán street for KC>25. In the symmetric region, the flow was observed to separate from the leading edges resulting in recirculating fluid on the upper and and lower surfaces. As the flow reversed, the recirculating fluid on the upper and lower surfaces moved back along these faces creating new vorticity of opposite sign. This resulted in weak local disturbances as the flow between the recirculating region and the growing vortex along the upper and lower surfaces departed rapidly away from the cylinder. As the flow developed further, separation occurred at the trailing edges. No reattachment of the separated shear layers took place and the flow developed as in the previous half cycle. In the asymmetric region and at 5<KC<12, the flow was observed to separate at the leading edges. The shear layers rolled up behind the trailing face, a little interaction took place which resulted in asymmetrical growth of a pair of vortices. As the flow reversed, the vortices moved back over the cylinder and lost most of their vorticity because this movement resulted in vorticity of opposite sign being created. These weaker vortices together with the recirculating flow on the upper and lower surfaces resulted in large velocities in the vicinity of these surfaces. As the flow developed further, shear layers from the trailing edges grew slowly and interacted behind the leading face resulting in the asymmetrical growth of another pair of vortices. At that stage, the disturbance caused earlier by the return of vorticity across the cylinder was observed to die out. The flow then behaved in similar manner during the next half cycle. Singh observed that during one half cycle, the top vortex grew larger than the bottom one, then during the next half cycle the reverse was true. At 12<KC<17, greater interaction between the shear layers took place and the vortices though not completely shed during each half cycle were observed to be stronger than those formed at 5<KC<12. Some of the vorticity contained in the opposite shear layer was observed to be pulled across by the stronger vortex as the flow reversed and these two vortices convected away rapidly from the cylinder and broke down into smaller scale eddies which decayed shortly. At 17<KC<25, the wake was more developed and at least one vortex was completely shed during each half cycle. At this range of the KC number, as the flow reversed the pairing of vortices was more visible and again these also lost their distinct structure and broke down into smaller eddies. The flow was seen more locally disturbed than before. This behaviour occurred on both the upper and lower surfaces but the surface with the larger vortex resulted in a more disturbed flow near that surface. In the pseudo-Kármán street

region and at KC>25, the wake became more developed and a number of vortices of different sign were shed alternately from opposite edges of the cylinder during each half cycle. The wake resembled the usual Kármán vortex street. In this region, the number of vortices formed and shed depended on the KC number and increased with it. As the flow was about to reverse, the velocity field induced by the vortices on each other caused them to be squashed together resulting in considerable distortion of these vortices. As the flow reversed, most of the vortices broke down under this strain field resulting in smaller eddies. Singh observed some evidence of three dimensional motion when the flow was very disturbed during the initial motion in the reversed flow direction. On a flat plate, much larger vortices were formed. At KC<4, the flow was observed to be more or less symmetrical. At 4<KC<8, large vortices were formed but not shed remaining close to the plate. At 8<KC<25, the vortices set up a cyclic motion about the plate.

Ikeda et al. (1988) and Otsuka et al. (1990) using a flow of dye poured into the neighbourhood of horizontal circular cylinders in waves observed a strong circulation of the flow around the cylinders. They observed a much larger scale of vortex shedding occurring in regular waves than in plane oscillatory flow. From flow visualisation, they observed two anti-clockwise vortices being released in one wave cycle. Ikeda et al. also observed a strong circulation round a square cylinder horizontally submerged in regular waves. Four vortices rotating in the opposite direction to the orbital motion of fluid particle were observed one at each corner of the square cylinder. From force measurements, Ikeda et al. reported that the inertia coefficient of the square cylinder rapidly decreased with increasing KC number. This tendency of C_M coefficient was different from that in plane oscillatory flow (e.g. Tanaka et al. (1983) and Bearman et al. (1984, 1985)).

The reduction of wave forces on horizontal circular cylinders at low KC numbers was earlier reported by Chaplin (1984 a,b, 1987) and Inoue et al. (1984) who showed that potential values at comparatively high wave height overestimated these forces. Grass et al. (1984) when measuring hydrodynamic forces acting on a circular cylinder moving with circular or elliptical orbital motion in still water found that wave forces estimated by potential theory may be possibly overestimated when applied to the particular case of horizontal structural members. These earlier findings of Chaplin, Inoue et al. and Grass et al. were summarised in Chapter 1.

Smith and Stansby (1991) using the random vortex method computed two-dimensional

viscous oscillatory flows around circular, square and diamond cylinders at low KC numbers. For the square cylinder at maximum onset velocity, the separation bubbles grew as the KC number increased. At KC=0.5, they remained local to the sharp edges and at KC=1 the flow pattern was fairly repetitive and symmetrical with pairs of vortices shed of which one of the vortices in the downstream pair tended to dominate causing asymmetry. At KC=1.5 the basic structure still persisted but the flow became more asymmetrical and the upstream vortex pair was more prominent. At KC=2, the structure had broken down.

Mara and Sortland carried out a flow visualisation using hydrogen bubble techniques on a square box (a three-dimensional square cylinder) in a U-tube water tank generating a planar oscillatory flow. At small KC numbers, vortices were produced around the sharp edges of the box. At a KC number of about 6, they observed convected vortices of parabolic form. These vortices were observed to be convected in the same plane and therefore were locally two-dimensional. The convected velocity of the vortices at the central part of the box was found to be rather big compared to that from the corners.

5.2 PRESENT FLOW VISUALISATION

In this study an attempt was made to carry out a flow visualisation on rectangular cylinders of different aspect ratios vertically immersed in steady flow and in wavy flow. A video camera was used for the purpose and some still photographs were also taken. Due to there being no special visualisation facilities at the Hydrodynamic Laboratory and to some extent due to the comparatively large scale of the experiments conducted in a large towing tank, it was not possible to carry out a rigorous flow visualisation using the usual techniques of spreading particles such as polystyrene or aluminium powder, or continuously injecting colouring liquid such as fluorescent dye. Such flow visualisations are mostly performed in more contained space such as a U-tube water tank. Therefore, in the present study the formation and shedding of vortices during stages of a wave cycle cannot be described in detail. As said before, detailed flow visualisations of rectangular cylinders with varying aspect ratios in regular waves and in combined waves-current flow are needed to capture the instantaneous flow pattern and hence to understand the complex phenomena of viscous flow.

The flow visualisation was carried out on the large cylinders of the first set in steady flow where the range of the Reynolds number attained was of the order of 10^5.

In wavy flow, cylinders of smaller sizes offering a wider range of KC numbers were used. The video film was played in slow motion during the study of the flow visualisation.

5.2.1 STEADY FLOW

With the cylinder of an aspect ratio d/D=0.5, small eddies were seen to shed on the downstream at the minimum Reynolds number of $6.3x10^4$ obtained with this cylinder. As the Reynolds number increased vortices of increased size were seen to shed in opposite sign from the trailing edges of the cylinder. At $Re>2x10^5$ the wake behind the cylinder expanded considerably and the vortices were seen after shedding to come very close to the downstream face of the cylinder. At Reynolds numbers exceeding $3x10^5$ the flow behind the cylinder became more turbulent with very strong vortices forming behind the trailing edges and rolling up close to the downstream face. At Reynolds numbers beyond $4x10^5$ the water was seen to flow from the streamwise sides of the cylinder in the form of jets of water and the flow at the back of the cylinder was fully turbulent.

With the square cross-sectional cylinder the flow was clearly seen to separate at the leading edges with vortices rolling up behind the cylinder at the minimum Reynolds number of $8.8x10^4$. When the Reynolds number was more than $1x10^5$ stronger vortices were seen to shed behind the cylinder and were swept away in the wake. The wake was seen to expand rapidly as the Reynolds number exceeded $2x10^5$. Turbulence of bubbling water was seen to set up at the streamwise sides of the cylinder at Reynolds numbers in excess of $3x10^5$. As the Reynolds number increased further, this turbulence was seen to move downstream along the streamwise sides of the cylinder with the wake becoming more turbulent behind the cylinder. At a Reynolds number of about $5x10^5$ the turbulence was adjacent to the trailing edges of the cylinder. The wake became fully turbulent with random motion of the flow at $Re>6x10^5$. Throughout the increase of the Reynolds number before turbulence set up vortices were seen to shed symmetrically behind the trailing edges of the cylinder giving a symmetry of the flow in the wake.

With the cylinder of an aspect ratio d/D=2, the flow was seen to separate at the leading edges at the minimum Reynolds number of $2.2x10^4$. Small eddies were clearly visible shedding from the trailing edges of the cylinder. As the Reynolds number increased these eddies increased in size and rolled up from both sides of the trailing

edges in opposite rotations before interfering with each other and then being swept away in the wake formed behind the cylinder. Increasing the Reynolds number made the separated flows detach themselves from the sides, which resulted in a widening of the wake. At a Reynolds number of 7.5×10^4 an asymmetry in the vortex pattern shed behind the cylinder similar to the Kármán-type vortex street was observed. As the Reynolds number increased the vortices were seen to become stronger and the wake behind the cylinder to expand more. Above a Reynolds number of 1×10^5 turbulence of bubbling water on the streamwise sides of the cylinder was seen to grow in intensity and to move gradually downstream as the Reynolds number increased further. At a Reynolds number of 1.9×10^5 this turbulence was seen to move away from the streamwise sides and instead was located just behind the cylinder on both sides of the trailing edges leaving a middle region on the back less turbulent.

5.2.2 WAVY FLOW

With the cylinder of an aspect ratio of 0.5, small eddies concentrated near the four corners of the cylinder were seen at the lowest KC number of 0.12 where the flow around the cylinder seemed to be undisturbed. As the KC number approached 0.3, pairs of discrete vortices were seen to shed during a half wave cycle from the corners of the cylinder in a symmetrical pattern. As the KC number increased these vortices increased in intensity and rolled up in pairs at the front and the back surfaces of the cylinder turning symmetrically and in opposite signs. Throughout the range of KC numbers up to 2, the vortices were seen to come very close to the cylinder's front and back surfaces during a half of the wave cycle before they were swept away in the other half cycle. The flow around the cylinder was seen to be symmetrical.

With the square cylinder, at the lowest KC number of 0.25 small eddies concentrated near the four corners of the cylinder were discernible. As the KC number increased, two discrete vortices of opposite signs were seen to shed symmetrically from each face of the cylinder in a half cycle of the wave before they interacted with each other and with the body and were swept away in the second half of the cycle. At KC numbers in excess of 3, the flow behind the square cylinder appeared somewhat turbulent.

With the cylinder of an aspect ratio of 2, very small eddies concentrated near the four corners of the cylinder were seen at the lowest KC number of 0.26. Up to a KC

number of 0.5, these eddies were still concentrated near the corners and the flow around the cylinder appeared undisturbed. At KC numbers between 0.5 and 0.9, two discrete vortices were seen to shed from the corners of the cylinder on each side in the first half of the wave cycle without interfering with each other. They were seen to remain close to the corners before they were swept away from the cylinder in the second half of the cycle. Above a KC number of 0.9, these vortices increased in intensity and seemed to interfere with each other in the first half cycle of the wave before they were swept away in the second half of the wave cycle. The flow around the cylinder at KC numbers in excess of 1 seemed to be asymmetrical, and the motion of the large vortices was somewhat random. At KC numbers higher than 2, the flow became turbulent and the vortices did not show any distinct vortex structure after being shed. Unlike the cylinder with an aspect ratio of 0.5, the vortices shed by this cylinder did not appear to come closer to the front and back surfaces. This is due to the longer afterbody of this cylinder.

The effect of an afterbody in delaying the interaction between the separated shear layers has been studied in steady flow by using splitter plates. Roshko (1954), Bearman (1965) and Gerrard (1966) have shown that by delaying the interaction between the separated shear layers, vortex formation can be inhibited leading to a reduced base suction and hence to a lower drag. The vortex shedding frequency also drops.

CHAPTER 6

DISCUSSION OF RESULTS

6.1 STEADY FLOW

The drag coefficients of horizontal cylinders in the present study were found to be slightly smaller than those of corresponding vertical cylinders (Figures 6.1 and 6.2). A cylinder immersed either vertically or horizontally in steady flow would experience a similar flow pattern and hence would be subjected to an identical drag force. The reason for the discrepancies between the drag coefficients of vertical cylinders and those of corresponding horizontal cylinders measured in this study is believed to be due to the effect of free surface and three dimensionality of the flow inducing a cross flow. Drag coefficients were found to be smaller than those of earlier investigators discussed in Chapter 1 (Nakaguchi et al. (1968), Bearman and Trueman (1972), Bostock and Mair (1972) and Courchesne and Laneville (1979)) who conducted experiments in a two dimensional flow by using cylinders with a very high length to width L/D ratio spanning the entire height of the wind tunnel and with some of them mounted between end plates (see Figure 1.3). Therefore, it is deemed in this study that the length to width ratio L/D of 5, observed in these experiments, is not high enough to ensure an unbounded two dimensional flow. The results shown in Figure 1.3 illustrate the significant effect of the aspect ratio on the value of the drag coefficient. When the length to width L/D ratio of the cylinders decreases and hence a cross flow is induced, C_D coefficient becomes less affected by the variation of the aspect ratio (ESDU results) as it is the case in this study. The reason for the decrease of C_D coefficient when the cylinder length becomes shorter is that a larger proportion of high pressure fluid leaks past the free ends of the cylinder, due to the three dimensionality of the flow, and forms a pair of vortex sheets. The resulting higher base pressure recovery causes a decrease in C_D coefficient. Therefore, the lower the length to width L/D ratio the greater the drag reduction. However, some effect on C_D coefficient by changing the aspect ratio of the cylinders was found in this study. Except for the cylinder of an aspect ratio of 0.5, cylinders of aspect ratio less than unity had higher C_D coefficients. For example, in the horizontal orientation case cylinders of aspect ratios d/D of 0.25 and 0.75 were found to have the highest drag coefficients. In the case of two dimensional flow, a peak of C_D coefficient was found

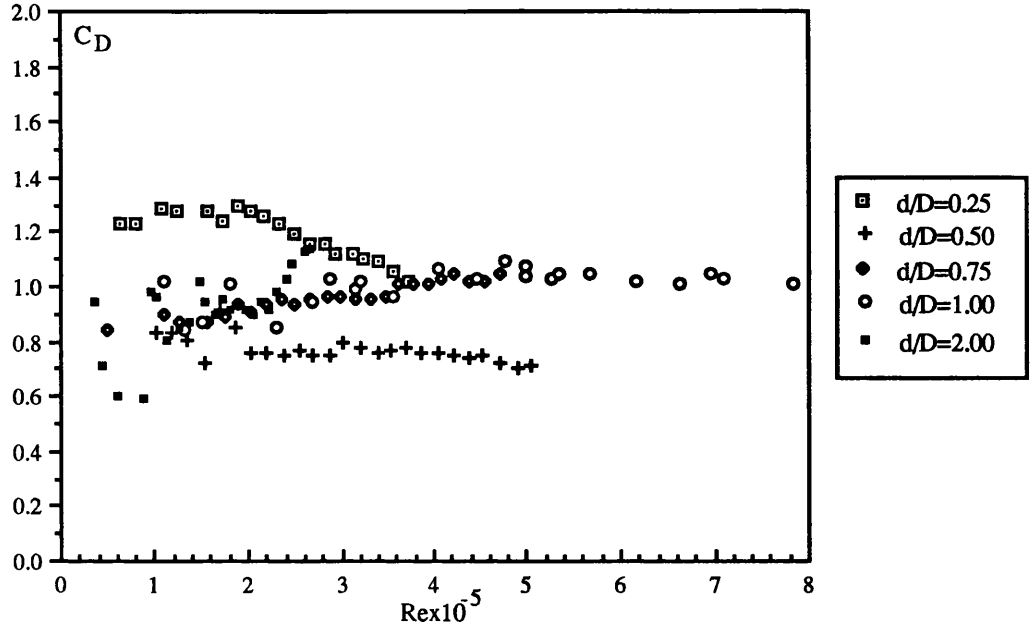

Fig. 6.1 C_D versus Re for different vertical cylinders in steady flow

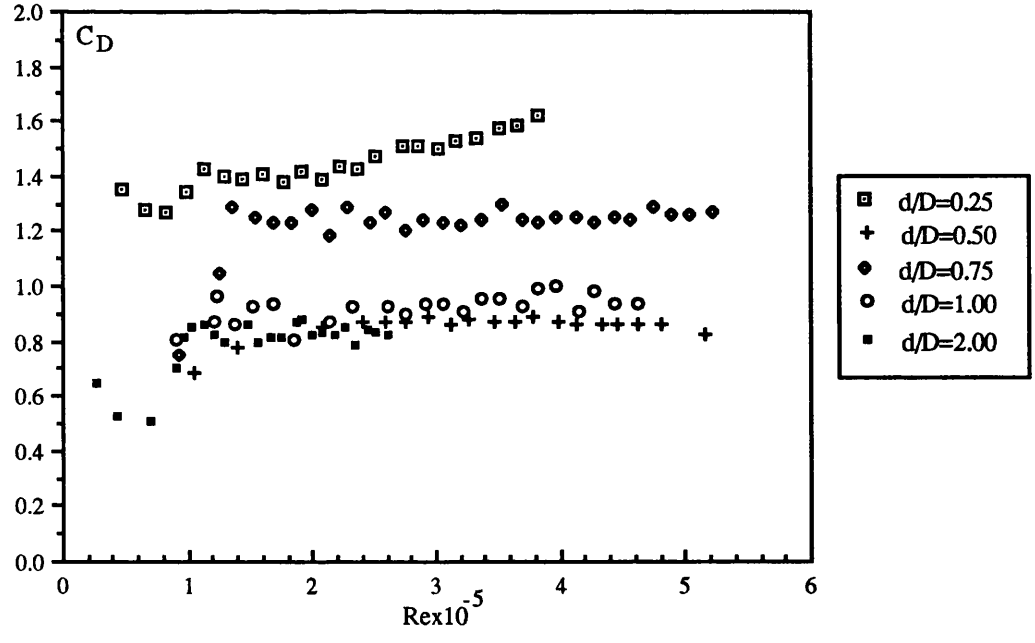

Fig. 6.2 C_D versus Re for different horizontal cylinders in steady flow

when a cylinder had an aspect ratio of 0.67 (see Figure 1.3). When increasing the aspect ratio and hence adding to the cylinder a long afterbody, the drag force was decreased. The reason is that the presence of a long afterbody delays the shear layer interaction which results in weaker vortices being formed and hence a lower drag. The effect of an afterbody in delaying the interaction between the separated shear layers has been studied in steady flow by using splitter plates. Roshko (1954), Bearman (1965) and Gerrard (1966) have shown that by delaying the interaction between the separated shear layers, vortex formation can be inhibited leading to a reduced base suction and hence to a lower drag. The vortex shedding frequency also drops. The smaller wake width results in a smaller drag. If large vortices remain close to the cylinder which is the case with cylinders of small aspect ratios, this results in very low base pressure and hence a large drag.

Since the high drag is a result of regular vortex shedding, then to understand how the increased drag is developed, one must know more about the complex vortex formation region just behind the body. It is known that two free shear layers, free to interact, are basically unstable and roll up to form discrete vortices. During formation the growing vortices (and, to a lesser extent, the shear layers) draw in fluid from the base region and it is suggested that it is this continual entrainment process that sustains the low base pressure. The removal of entrained fluid is balanced by an induced reverse flow into the formation region. The base pressure determines the amount of vorticity that is being shed from each side of the body and this in turn is related in some way to the distance to vortex formation and the strength of the fully formed vortices. Therefore, there is some complex equilibrium set up between the vorticity that is being shed from the body, the distance to vortex formation and the base pressure. Added to this delicate balance is the influence of entrainment, which acts as a form of feedback to stabilise the loop.

It has been shown (e.g. Nakaguchi et al., Bearman and Trueman) that the further the vortices can be persuaded to form away from the body the higher the base pressure and hence the lower drag. It is further known, as mentioned above, that a short splitter plate in the wake delays the interaction between the shear layers and vortices can only form beyond the end of the plate. A splitter plate, therefore, increases the size of the separated region behind the body. Bearman and Trueman suggested that if one supposes that the vortices draw in a similar quantity of fluid, but from an increased base cavity volume, then the entrainment process will not be able to sustain such a low base

pressure. This in turn will decrease the amount of vorticity shed from the body and the vortex formation distance will adjust to some new equilibrium position.

6.2 WAVY FLOW

The inertia coefficient of the cylinders of aspect ratios 1 and 2 horizontally submerged in regular waves (Figure 6.3) decreased rapidly with increasing KC number. This was first reported by Chaplin (1984 a,b) in the case of a circular cylinder horizontally submerged in waves at low KC numbers. He suggested that this is caused by the non-linear effect of oscillatory boundary layer due to viscosity. Later, Chaplin (1988 a), investigating the non linear forces on circular cylinders horizontally submerged in waves at low KC numbers and under circular orbital flow conditions, argued that the reduction of C_M coefficient at low KC numbers was associated with a lift force, caused by the circulation of the flow relative to the cylinder, acting in the opposite direction to the inertia force. Ikeda et al. (1988) also found in the case of a horizontal square cylinder in waves this reduction of the inertia coefficient when the KC number increased at small KC number values. They found that the inertia coefficient rapidly decreased with increasing KC number, reaching a minimum value at a KC number of about 4 and then increasing.

The author believes that the flow circulation created by the rotating separated vortices around the cylinders, such as that observed by Ikeda et al. in the case of a horizontal square cylinder, does induce a reduction of wave forces acting on horizontal members and this could explain the reduction of the inertia coefficient at low KC numbers found in this study. Therefore, the stronger the circulation of the flow around the cylinder the more rapid is the reduction of C_M coefficient at low KC numbers. In the case of the horizontal cylinder with an aspect ratio of 0.5, however, the inertia coefficient was found to vary less with the KC number for the range of KC numbers investigated (up to 2). It is argued that decreasing further the aspect ratio of the cylinder results in weakening the circulating flow around the cylinder and hence the reduction of wave forces which induce a reduction of the inertia coefficient does not take place. It is expected in the case of a flat plate submerged in regular waves at a right angle to the water surface (a cylinder with a very small aspect ratio) that a circulating flow around it hardly occurs and the flow field is similar to that in plane oscillatory flow because vortices are swept away at the moment when incident flow is parallel to the plate. Ikeda

et al. found that the inertia coefficient of a flat plate did not show the same tendency where C_M coefficient rapidly decreased with increasing KC number as in the case of the square cylinder. However, they found that C_M coefficient was different from that in plane oscillatory flow (e.g. Tanaka et al. (1983)). Ikeda et al. observed that the behaviour of vortices around the flat plate was very different from that in plane oscillatory flow. A circulating flow around the flat plate was also observed though not as strong as that of the square cylinder.

With the vertical cylinders, the variation of the inertia coefficient with the KC number showed a different trend (Figure 6.4). The inertia coefficient increased with increasing KC number, reaching a maximum value and remaining more or less constant except for the case of the square cylinder where C_M coefficient decreased after reaching a maximum value at a KC number of about 2. This difference of C_M coefficient of the square cylinder compared with those of the other two cylinders could be associated with the difference in flow pattern. It is known that the square cylinder is particularly sensitive to turbulence and the reduction of C_M coefficient at KC numbers in excess of 2 could be attributed to this turbulence in the same way as the steady flow drag coefficient was found to decrease due to turbulence (Vickery (1966), Laneville et al. (1975)).
The reason for the increase of C_M coefficient at very low KC numbers for the three cylinders is that when a vertical cylinder encounters its own wake, it is likely to experience an increase in the incident velocity rather than a reduction which occurs in the case of a horizontal cylinder.

It is worth mentioning that the inertia coefficients of vertical cylinders were found to be very close to those of corresponding horizontal cylinders when the KC number approached zero. This is not surprising because at very low KC numbers close to zero, there is a tendency towards an attached and an undisturbed flow, as observed from the flow visualisation, with vortex strength tending to zero. Therefore, the inertia coefficient for each cylinder approaches its potential flow value. For example, at the lower end of the KC number range the inertia coefficients of the cylinders with aspect ratios of 0.5 and 2 were found to be close to their theoretical values of 3.25 and 1.70 (Brater, McNown and Stair (1958) from Wiegel (1964)) respectively. The inertia coefficient of the square cylinder at the lowest KC number was found to be little higher than its theoretical value of 2.35 (Brater et al. (1958)). As the KC number increases flow separation becomes important and this results in C_M coefficient departing from its potential flow value.

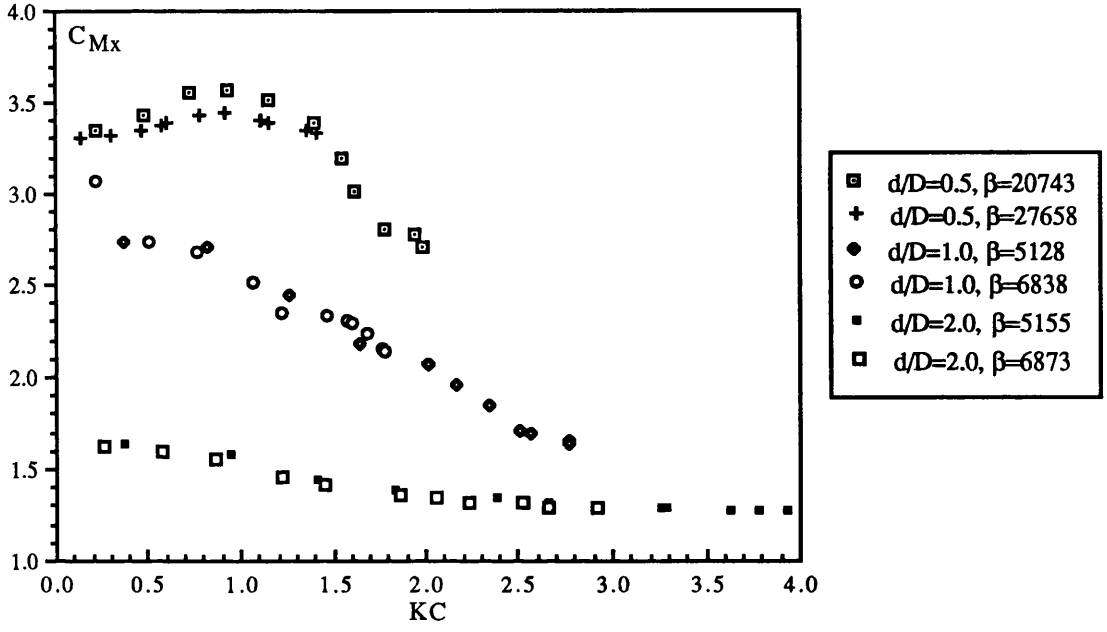

Fig. 6.3 C_{Mx} versus KC for different horizontal cylinders in waves

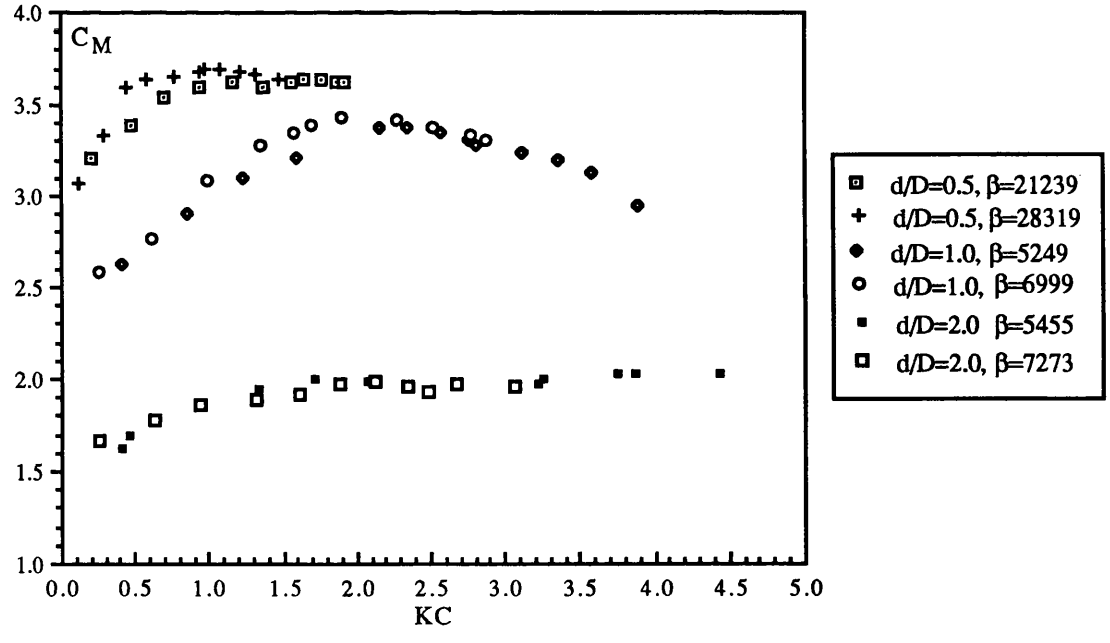

Fig. 6.4 C_M versus KC for different vertical cylinders in waves

With regard to the drag coefficient, its variation with the KC number followed a similar trend for all the cylinders whether tested vertically or horizontally (Figures 6.5 and 6.6). The C_D coefficient decreased rapidly from high values with increasing KC number. The high drag coefficient at low KC numbers is associated with the flow separation and the first appearances of vortices which take place for these sharp-edges cylinders at very early KC numbers. Therefore, the cylinder whose vortices and separated flow are large would be expected to have a higher drag force and hence a high drag coefficient.

The values of C_D coefficient are higher in wavy flow than in steady flow because the wake from one half wave cycle is washed back over the cylinder in the next half cycle (wake re-encounter effects). It is argued in this study that the flow and forces on rectangular cylinders in regular waves are dominated by the effects of wake re-encounter. These effects occur particularly in the flow region where the drag forces are high because the high drag forces are usually associated with the shedding of strong vortices which are prominent in the wake re-encounter. Pearcey (1990) suggests that wake re-encounter introduces strong perturbations to the incident kinematics and hence to stronger shed vortices and therefore introduces a self magnifying mechanism which could be responsible for the high drag when the relative motion is regular, e.g. in regular waves.

The drag coefficient is expected to approach the steady flow value only for very high KC numbers when the returning wake has almost totally decayed. Bearman et al. (1978) found that the drag coefficients of a square, diamond cylinders and a flat plate immersed in planar oscillatory flow approached their steady flow values at a high KC number of about 50 after decreasing from high values at small KC numbers. Heideman and Sarpkaya (1985) found that the drag coefficient of a rectangular cylinder with an aspect ratio of 2 in planar oscillatory flow approached its steady flow value at a much higher KC number of about 150.

The drag coefficients of the different cylinders were not found to vary substantially when changing their orientation from vertical to horizontal as in the case of the steady flow.

The drag coefficient was not found to change dramatically when the aspect ratio varied from 0.5 to 2 in either orientation. However, at very low KC numbers the cylinder of an aspect ratio of 0.5 had the highest drag coefficient though at very different β values. This cylinder which is the bluffer of the three cylinders was seen to shed

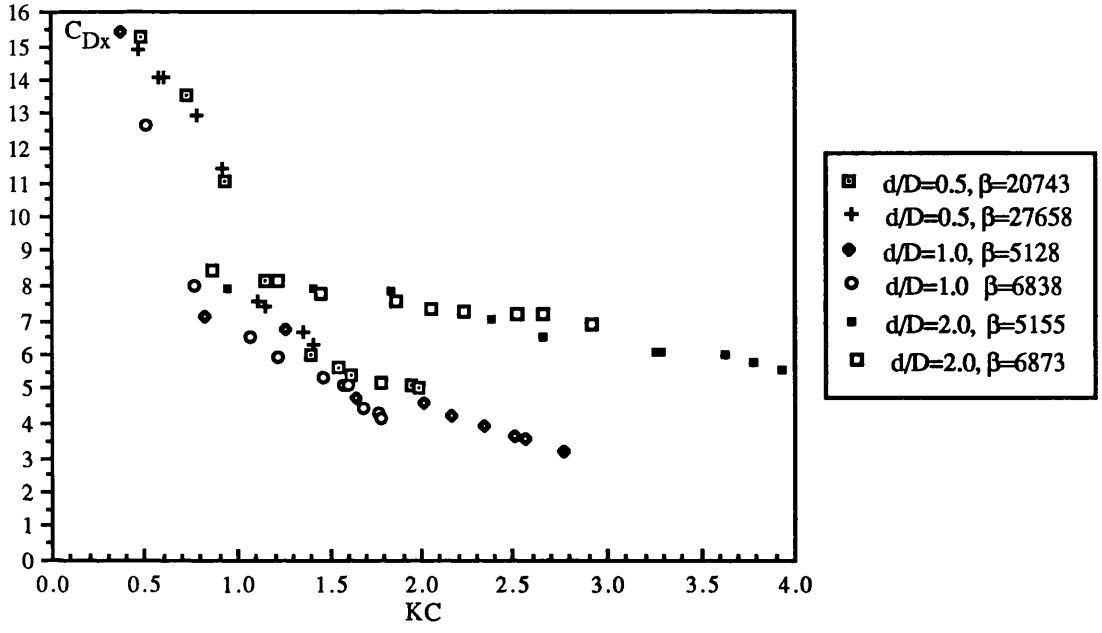

Fig. 6.5 C_{Dx} versus KC for different horizontal cylinders in waves

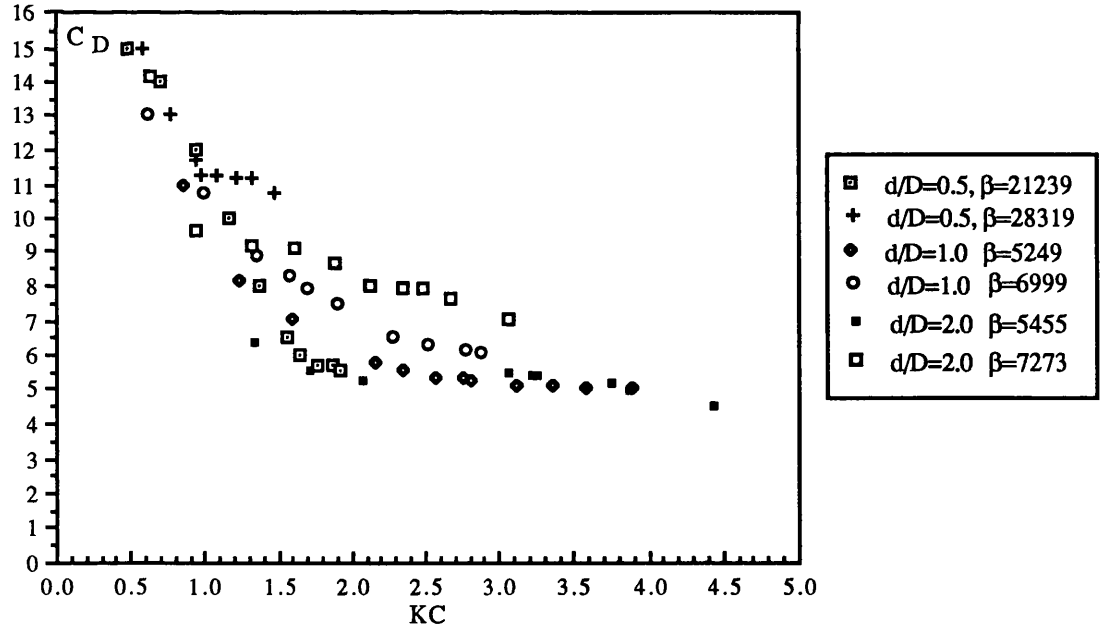

Fig. 6.6 C_D versus KC for different vertical cylinders in waves

vortices at very low KC numbers with a large separated flow. When the aspect ratio is small the vortices shed tend to remain close to the body surface resulting in a low pressure and hence a high drag. Therefore, it is not surprising that this cylinder with the lowest aspect ratio experienced the highest drag.

For the square cylinder, the variations of C_M and C_D coefficients with the KC number were found to be different from those in planar oscillatory flow (Bearman et al. 1984). For example, the drag coefficients measured in waves were found to be higher than those measured under planar oscillatory flow. These differences are attributed to the difference of flow patterns between wavy and planar oscillatory flow. It is natural for example in the case of the drag coefficient to be different from the two flows, since the behaviour of vortex shedding is different between regular waves and plane oscillatory flow. In a U-tube generating planar oscillatory flow, such as that used by Bearman et al., the ratio of the vertical to horizontal wave particle velocities $u_{my}/u_{mx}=0$ whereas in waves under deep condition $u_{my}/u_{mx}=1$. This indicates that the water particle velocities ratio plays a significant role in determining force coefficients for a horizontal cylinder in waves. The inertia coefficients and to some extent the drag coefficients of the horizontal cylinders in waves are smaller than those of the vertical cylinders. This suggests that the presence of the vertical water particle velocity will reduce the hydrodynamic coefficients. Data from Maull and Norman (1978) and Ramberg and Niedzwecki (1979) show that the presence of the vertical velocity will reduce the drag coefficient. For a horizontal cylinder in waves, where u_{my}/u_{mx} is sufficiently large, the wake will move around the cylinder in an elliptic or circular path due to the presence of the vertical velocity. Thus, because of the reduced wake encounter effect, C_D coefficient will be smaller.

The other methods of representing the in-line force are in terms of maximum and root mean square force coefficients which correlate well with the KC number as shown in Figures 6.7 through 6.10. The results show that as the KC number increases, these coefficients tend towards constant values, and as in the case of the drag coefficient they become very large as the KC number approaches zero. This is a consequence of non-dimensionalising these coefficients by $0.5\rho u_m^2 D$, where a finite force at small KC numbers leads to very large values of these coefficients. The figures also show that the square cylinder and the cylinder with an aspect ratio of 2 experience more or less similar forces at equivalent KC numbers, particularly in the vertical case. Among the three cylinders, the one with the lowest aspect ratio 0.5 seems to experience the lowest force.

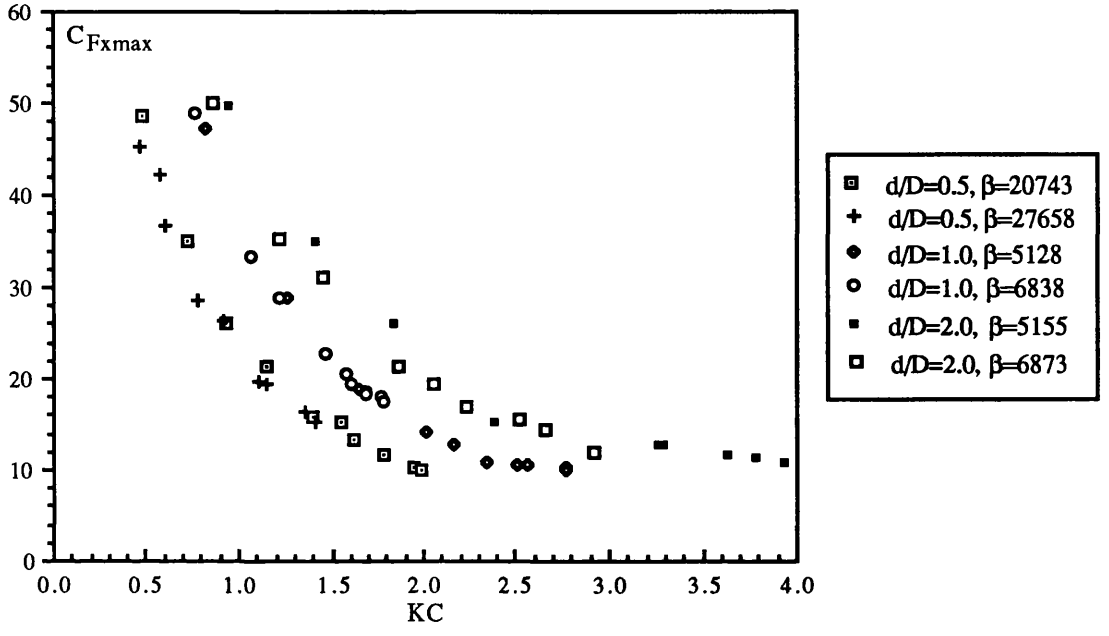

Fig. 6.7 C_{Fxmax} versus KC for different horizontal cylinders in waves

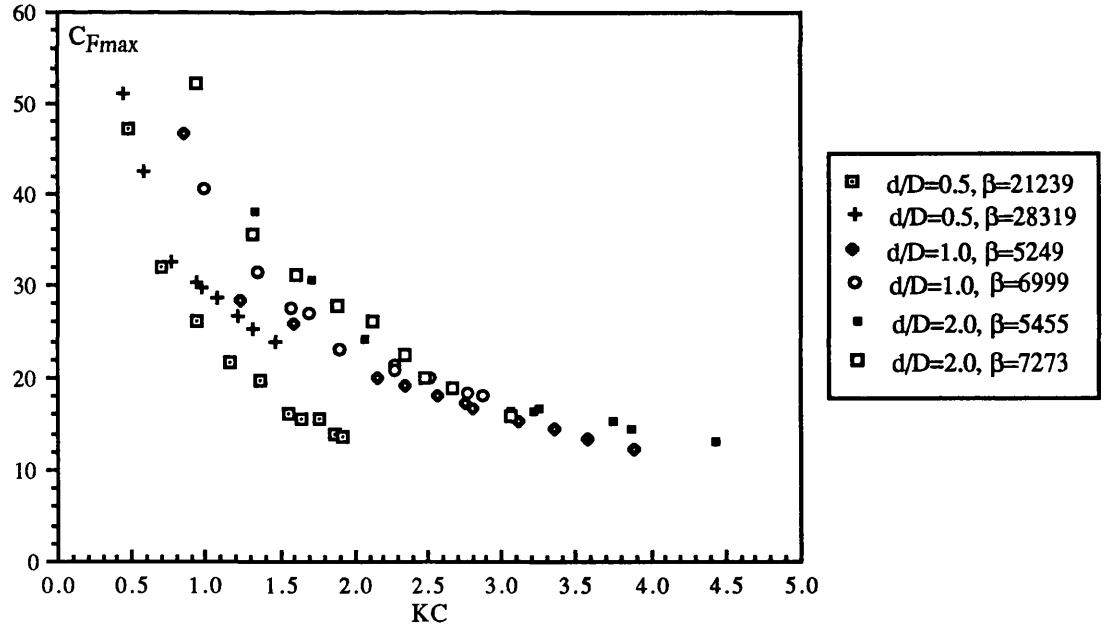

Fig. 6.8 C_{Fmax} versus KC for different vertical cylinders in waves

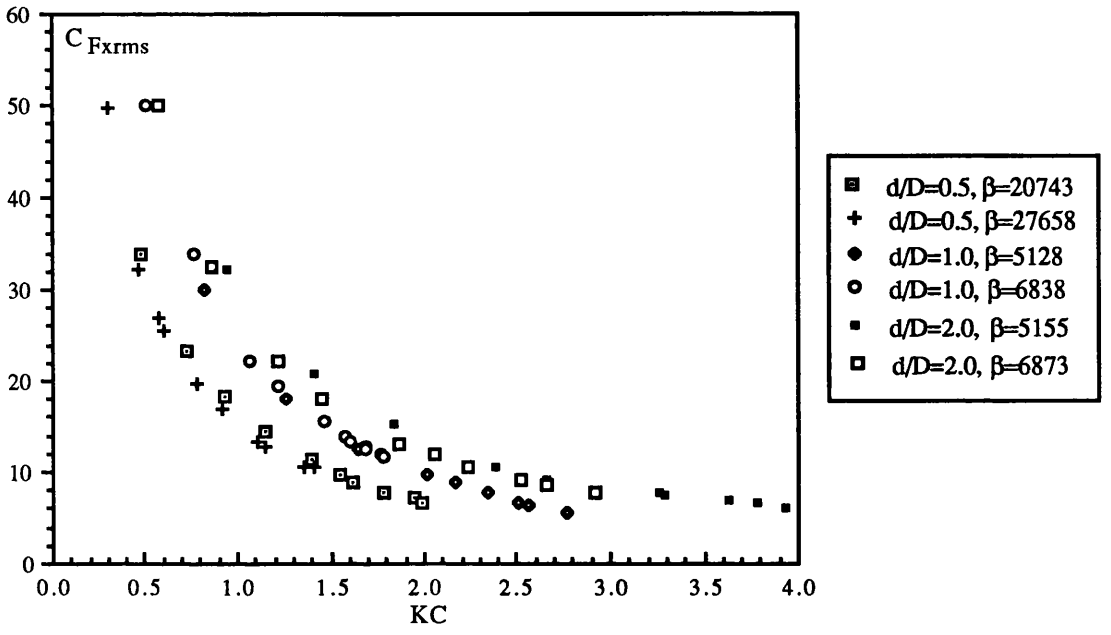

Fig. 6.9 C_{Fxrms} versus KC for different horizontal cylinders in waves

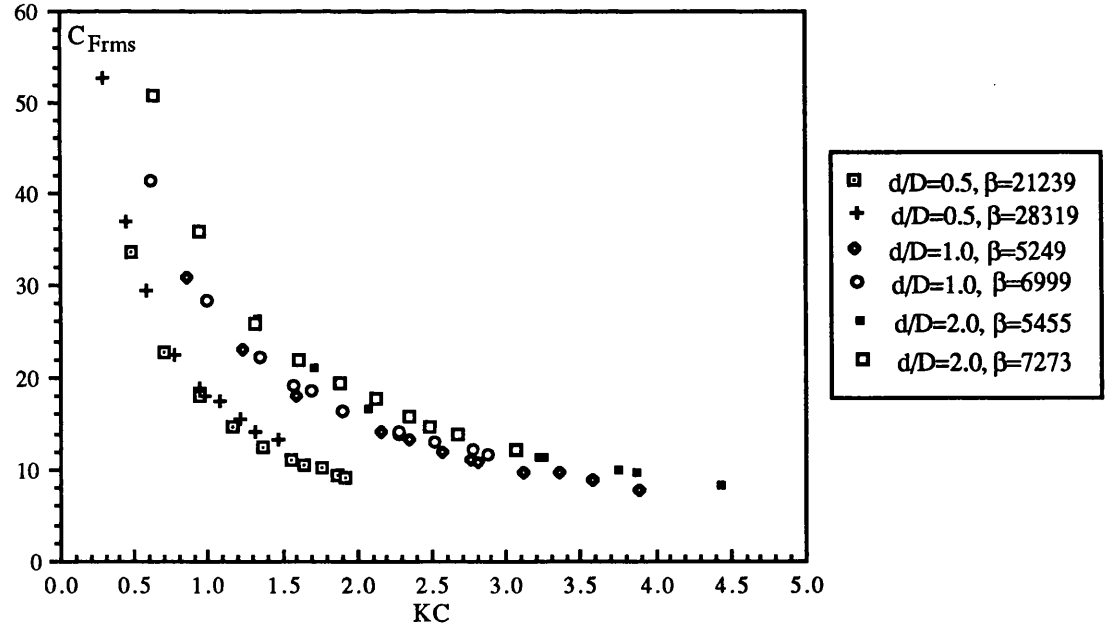

Fig. 6.10 C_{Frms} versus KC for different vertical cylinders in waves

This is in contradiction to the values of the inertia coefficients of this cylinder which were found to be the highest. The reason may emanate from the influence of Reynolds numbers (or β numbers) on the forces. Indeed, comparisons of these force coefficients between the cylinder with an aspect ratio of 0.5 with others were made at much different β numbers, where β numbers of the cylinder with the small aspect ratio were nearly four times those of the two other cylinders.

The figures also show that the wave forces on horizontal cylinders are lower than those on vertical cylinders. The reason, as discussed above, is that the inertia coefficient of horizontal cylinders decrease with increasing KC number and therefore the total wave forces, in which the inertia forces dominates at these low KC numbers, decrease. The drag coefficient, on the other hand, did not vary much when changing the orientation of a cylinder from vertical surface piercing to horizontal fully submerged.

As mentioned in Chapter 1, transverse or lift forces result from the asymmetry in the flow which is produced by the growth and motion of vortices. In a periodic flow, the return of vortices against a body plays an important role in lift generation as growing vortices generate substantial lift as they move back over the body when the flow reverses. These transverse forces are irregular in nature and one way of studying them is by measuring the maximum peak of the lift force during a wave cycle or the root mean square value of the force of the entire record of data. The other way which is more suitable to describe these forces is by studying the data in a statistical approach. However, such an approach requires considerable amount of data to give fairly accurate results. In this study, the transverse force coefficients were expressed in terms of maximum and root mean square force coefficients and as shown in Figures 6.11 through 6.13 they correlate well with the KC number.

As with the maximum and rms values of the in-line force coefficients, these coefficients namely, C_{Lmax}, C_{Lrms} and C_{Lurms} decreased as the KC number increased, and tended to have large values as the KC number approached zero. These coefficients were found to vary from one cylinder to another. This could be explained by the fact that since the sole mechanism responsible for lift generation is the growth and motion of the vortices and since these are very sensitive to changes in the flow conditions, then the lift will be very sensitive to small variations in the flow pattern induced by changing the aspect ratio of the cylinders. For the range of the KC number considered, the square cylinder seemed to experience the largest maximum and rms values of the transverse forces. The author believes that the square cylinder offers a greater area where the

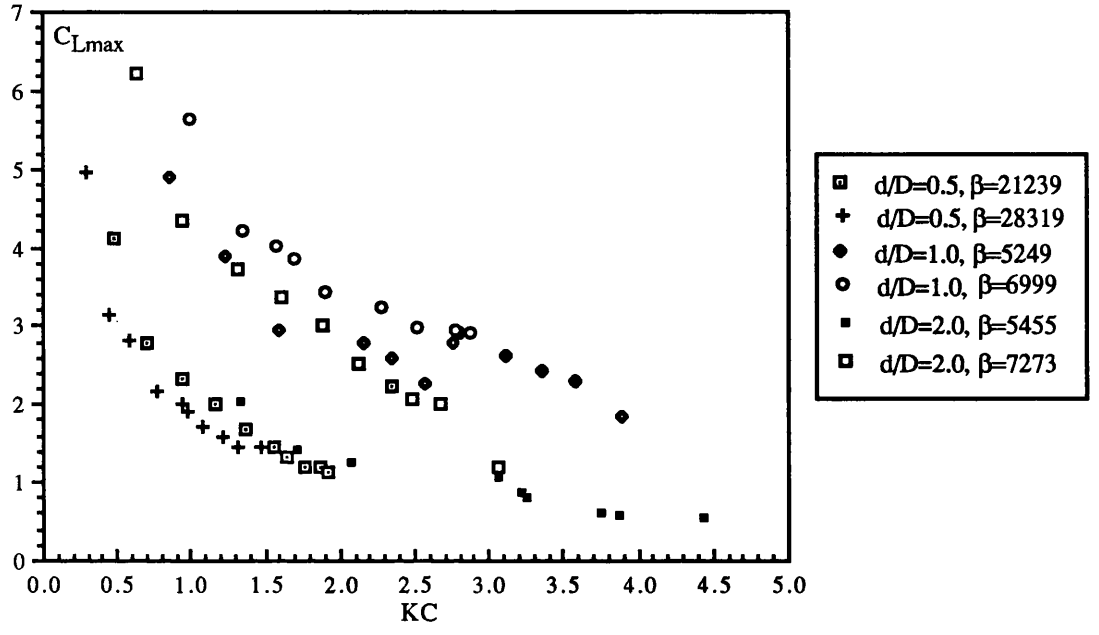

Fig. 6.11 C_{Lmax} versus KC for different vertical cylinders in waves

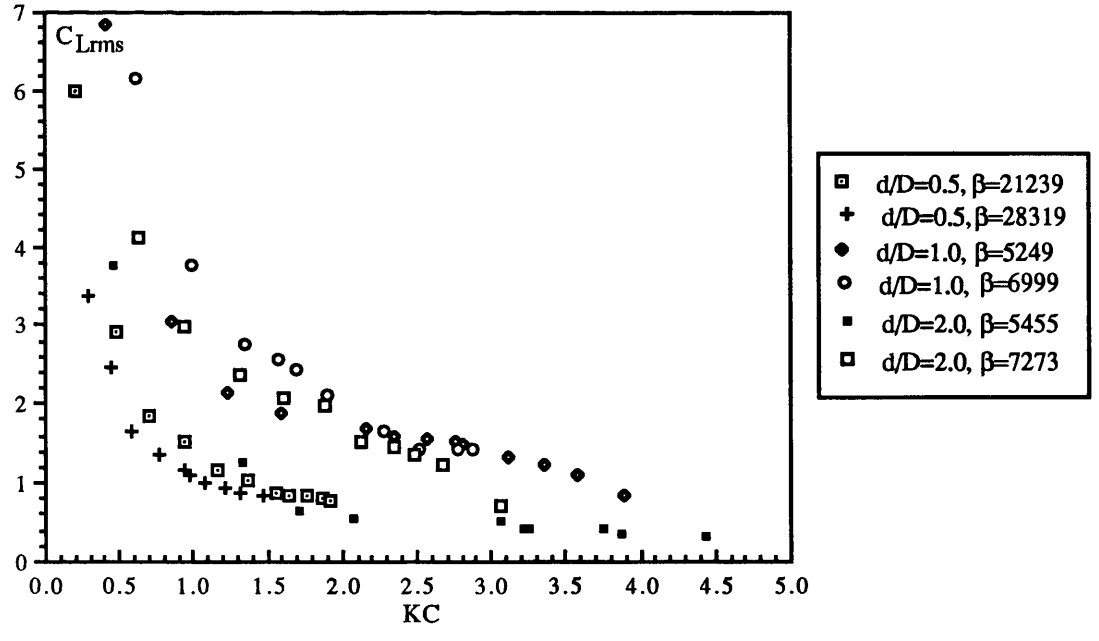

Fig. 6.12 C_{Lrms} versus KC for different vertical cylinders in waves

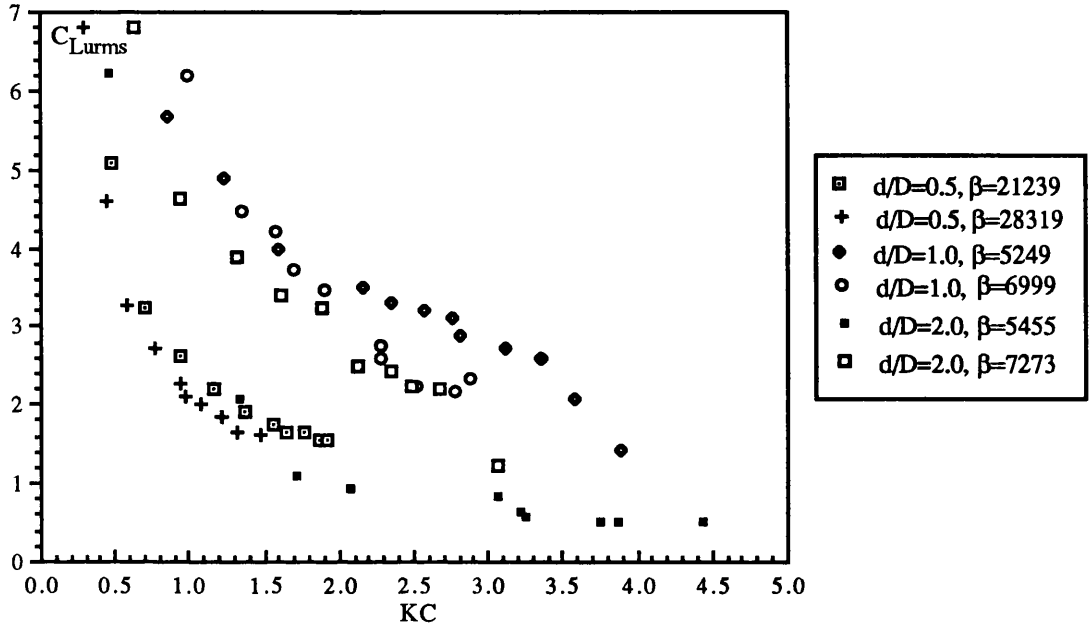

Fig. 6.13 C_{Lurms} versus KC for different vertical cylinders in waves

asymmetry caused by the vortices acts upon it. In other words, a greater area of the square cylinder is in the wake and is therefore subject to larger pressure differences between the surfaces caused by the vortices which give rise to larger lift forces.

Much further work is needed to study the complex flow pattern around rectangular cylinders in regular waves. Detailed flow visualisations are particularly important to understand the formation and shedding of vortices and to study the effects of varying the aspect ratio and orientation of the cylinders on the flow pattern.

Finally, it is worth mentioning that the results in terms of inertia and drag coefficients obtained in wavy flow from the first set of cylinders (cylinders of larger sizes) were found to be different to those obtained from the second set of cylinders. Though the tests on the first and the second set of cylinders were conducted at very different β values, the author does not believe that this is the reason for the discrepancies. One of the reasons is thought to be the different force measuring systems adopted for the two sets as described in Chapter 2. In this type of experiments, the method of measuring the forces is of considerable importance and any alteration of the

measuring system would undoubtedly influence the results.

The second reason is thought to be the influence of the free surface on the results of the first set of cylinders. From the steady flow results, it was confirmed that the free surface effect was important as the drag coefficients measured in this study were found different to those measured earlier by other investigators in two dimensional flows as discussed in Chapters one and four. The free surface effect on the second set of cylinders is believed to be small as the present results in terms of the inertia coefficients were found to be close to their theoretical values at early KC numbers.

6.3 COMBINED WAVY AND STEADY FLOWS

The results of combined wavy and steady flows presented in Chapter 4 show conclusively that the current has significant effects on inertia, drag and lift coefficients, and therefore on the maximum and r.m.s. force coefficients.

Hydrodynamic forces on submerged marine structures are directly related to the kinematics and dynamics of the water particles and are significantly affected by the presence of currents. The existence of currents influence the wave field by changing wave parameters such as wave amplitude, wave number, wave period and wave kinematic field. Hogben and Standing (1975) pointed out that currents have three distinct effects. First, by changing the fluid particle velocity they change the fluid drag forces, as the drag force term is dependent on the current velocity. The second effect is that by changing the wave speed, the wave propagates over a moving rather than a stationary fluid. This may be associated with the wave steepening. The third effect of currents is to make the structure itself generate waves.

For a cylinder under waves and current, there exist a bias to the wake structure because of the mean flow. One can easily imagine how even a small current will transport vortex structures downstream causing different flows and affecting the time dependent forces, and thus the force coefficients. For example, one would expect steady streaming to be less influential. It is argued in this study that the wake biasing resulting from the current decreases both the inertia and drag coefficients at these low KC numbers. Therefore, the force coefficients for waves and current are different from those obtained under rotating flow from waves.

At very low KC numbers, the presence of currents was found to be most important and caused a significant reduction in the drag coefficient. It is argued in this

study that this may be attributed to the fact that the region of small KC numbers corresponds to a region where the effect of the currents on the convection of vortices is most important in such a way that the currents reduce or eliminate the wake re-encounter effects and therefore eliminate or reduce the reinforcement of vortex shedding.

The reduction of the inertia coefficients in the case of horizontal cylinders when currents are present may suggest that as in the case of horizontal cylinders in wavy flow, the viscous effect caused by the circulating flow which reduces the wave force is created when a cylinder moves at a constant speed in waves. This phenomenon was observed by Ikeda et al. (1990) in the case of a horizontal cylinder towed at constant speed in waves. They observed a circulating vortex flow around the horizontal circular cylinder at a low relative current speed of Vc/u_m=0.25 (following sea) as was also observed at zero current speed. In addition, it is known that there is a strong relationship between the vortex shedding and the value of C_M coefficient. Thus one would anticipate that the biasing of the shedding of vortices by the current would cause profound changes in C_M coefficient relative to the no-current value. This was confirmed by Verley and Moe (1979) with circular cylinders oscillating in a current.

The present results obtained in waves and current and above discussion substantiate the fact that inertia and drag coefficients obtained from tests at sea (where there are always some currents) cannot be compared directly with those obtained under laboratory conditions with zero current. For example, the drag coefficients obtained from tests at sea will always be smaller than those obtained under laboratory conditions. Orbital motion of the fluid particles in waves in the absence of current has a similar effect on the drag coefficient. Sarpkaya and Storm (1984) suggest that the current and orbital motion combination is not likely to reverse their individual effects. Therefore, current and orbital motion may be regarded as the primary mitigating effects of the ocean environment as far as C_D coefficient is concerned.

As in the case with rectangular cylinders in regular waves, much more work, including rigorous flow visualisations on cylinders in the waves-current flow field, is needed to fill the gap in the research on this particular aspect of fluid loading.

6.4 LIMITATIONS OF THE POTENTIAL FLOW THEORY

The results obtained with the small cylinders in terms of the inertia coefficients C_M and the maximum forces during a wave period were compared to theoretical results from a computer program developed by Chan (1990) which is based on a potential flow theory.

The computer program uses theoretical formulations where the derivation of the governing equations for the boundary value problem of potential flow leads to linearised radiation and diffraction problems using the perturbation expansion technique. In order to simplify the complex problem of flow-structure interaction, and to render it a possible case of potential flow, the theory assumes that the fluid is homogeneous, incompressible and inviscid.

The computer program was run several times with the different cylinders vertically and horizontally submerged in regular waves. The input data in terms of immersed cylinder dimensions (submerged length in the case of vertical cylinders and depth in the case of horizontal cylinders), aspect ratios and wave frequencies were exactly the same as those observed during the experiments. The computer program gives, among others, the added mass coefficient and the peak of the total wave force per unit wave amplitude during a wave cycle acting on the submerged section of a cylinder.

The theoretical inertia coefficients derived from the added mass and the peak forces were subsequently compared to those measured from the experiments. Since this theory fails to predict the drag effects, the theoretical inertia C_M coefficient is compared to the measured one at its lowest KC number where flow separation and subsequently drag effect are minimum.

6.4.1 VERTICAL CYLINDERS

(i) Comparison of inertia coefficients

The inertia coefficients of the three different cylinders derived from the potential flow theory were compared to the corresponding measured ones. Tables 6.1 through 6.3 give the values of C_M coefficients with the margin error between the measured and theoretical coefficients.

The theoretical inertia coefficients of the square cylinder were found to be up to 16% lower than the measured ones. However, good agreement was found to be between

measured and theoretical C_M coefficients of the cylinders with aspect ratios of 0.5 and 2.

Table 6.1 Comparison of measured and theoretical C_M coefficients for the square cylinder

β	measured C_M	theoretical C_M	margin error (%)
5249	2.629	2.21	-15.9
6999	2.584	2.22	-14.1

Table 6.2 Comparison of measured and theoretical C_M coefficients for the cylinder with d/D=2

β	measured C_M	theoretical C_M	margin error (%)
5455	1.623	1.71	5.4
7273	1.663	1.715	3.1

Table 6.3 Comparison of measured and theoretical C_M coefficients for the cylinder with d/D=0.5

β	measured C_M	theoretical C_M	margin error (%)
21239	3.214	3.11	-3.2
28319	3.068	3.142	2.4

(ii) Comparison of total peak forces

The measured vertical forces acting on the whole submerged length of each vertical cylinder were obtained by using the Morison equation with the measured inertia and drag C_M and C_D coefficients (proper to each cylinder).

The following equations give the method of determining the total peak force acting on the submerged length of a vertical cylinder and the phase angle at which the peak of the force occurs.

The linear wave theory gives the wave particles velocity and acceleration as

$$u=-u_m \cos\omega t, \text{ and} \tag{6.1}$$

$$\dot{u}=u_m \omega \sin\omega t \tag{6.2}$$

where, u_m is the maximum water particle velocity in deep water condition given by

$$u_m=\frac{H}{2}\omega e^{ky}. \tag{6.3}$$

Replacing u_m by its expression, equations 6.1 and 6.2 become

$$u=-\frac{H}{2}\omega e^{ky}\cos\omega t, \text{ and} \tag{6.4}$$

$$\dot{u}=\frac{H}{2}\omega^2 e^{ky}\sin\omega t. \tag{6.5}$$

The total force acting on the immersed vertical cylinder is given by

$$F = F_I + F_D \tag{6.6}$$

where F_I and F_D are inertia and drag forces respectively.

$$F_I=\int_0 \rho D d C_M \dot{u} dy \tag{6.7}$$

$$=\rho D d C_M \frac{H}{2}\omega^2 \sin\omega t \int_0 e^{ky} dy$$

$$=\rho D d C_M \frac{H}{2}\omega^2 \sin\omega t \int_y e^{ky} dy$$

$$=\rho D d C_M \frac{H}{2}\omega^2 \sin\omega t \frac{1}{k}(1-e^{ky}),$$

where y is the depth of the immersed cylinder (in the experiments y=-0.93m, see Fig.2.1b).

Replacing the wave number k by ω^2/g, the inertia force term is found as

$$F_I=\rho D d C_M \frac{H}{2} g (1-e^{ky})\sin\omega t. \tag{6.8}$$

$$F_D=\int_y^0 \frac{1}{2}\rho D C_D|u|u\,dy \tag{6.9}$$

$$=-\frac{1}{2}\rho D C_D \frac{H^2}{4}\omega^2|\cos\omega t|\cos\omega t\int_y^0 e^{2ky}\,dy.$$

Approximating $|\cos\omega t|\cos\omega t$ by $\frac{8}{3\pi}\cos\omega t$, the drag force term becomes

$$F_D=-\frac{1}{2}\rho D C_D \frac{H^2}{4}\omega^2 \frac{8}{3\pi}\cos\omega t\frac{1}{2k}(1-e^{2ky}) \tag{6.10}$$

and replacing again k by ω^2/g, the drag force term is found as

$$F_D=-\frac{1}{2}\rho D C_D \frac{H^2 g}{3\pi}(1-e^{2ky})\cos\omega t. \tag{6.11}$$

The phase angle ωt at which the total force F is maximum is the angle at which the derivative of the total force F' with respect to time t is equal to zero.

$$F' = F_I' + F_D' \tag{6.12}$$

$$F'=(\rho D d C_M \frac{H}{2} g\,(1-e^{ky})\sin\omega t)'-(\frac{1}{2}\rho D C_D \frac{H^2 g}{3\pi}(1-e^{2ky})\cos\omega t)' \tag{6.13}$$

$$F'=\rho D d C_M \frac{H}{2} g\,(1-e^{ky})\omega\cos\omega t+\frac{1}{2}\rho D C_D \frac{H^2 g}{3\pi}(1-e^{2ky})\omega\sin\omega t. \tag{6.14}$$

F'=0, therefore

$$\frac{\sin(\omega t)}{\cos(\omega t)}=\tan(\omega t)=-\frac{3\pi d(1-e^{ky})}{H(1-e^{2ky})}\frac{C_M}{C_D}. \tag{6.15}$$

The phase angle which is the invtan of the above expression is then replaced in the Morison equation (equations 6.8 and 6.11) to obtain the peak of the total forces acting on the submerged length of each vertical cylinder during a wave cycle.

These forces were compared to the theoretical forces obtained from the computer program. The comparisons are shown in Figures 6.14 through 6.19 for the different vertical cylinders and for the two wave frequency parameters β (or wave frequencies). It is worth mentioning that the theoretical forces shown in those figures contain no drag component.

As shown in the figures, the theory was found to underestimate the measured total forces. However, the measured and predicted forces on the cylinders with aspect ratios of 0.5 and 2 were found to be closer than in the case of the square cylinder.

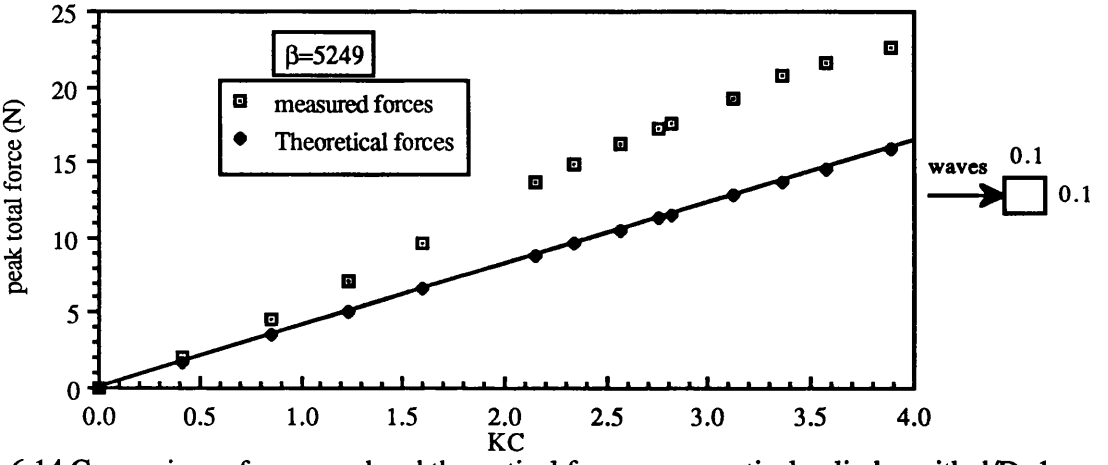

Fig. 6.14 Comparison of measured and theoretical forces on a vertical cylinder with d/D=1

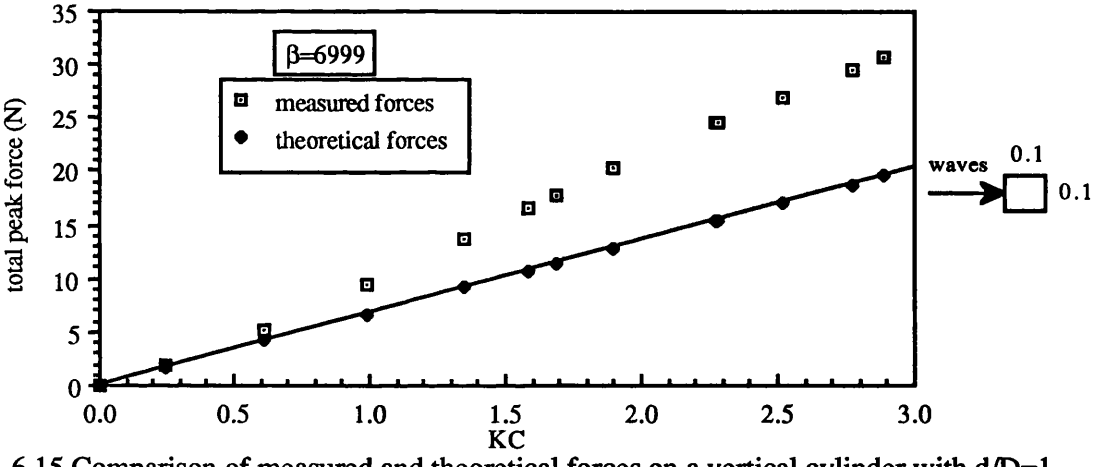

Fig. 6.15 Comparison of measured and theoretical forces on a vertical cylinder with d/D=1

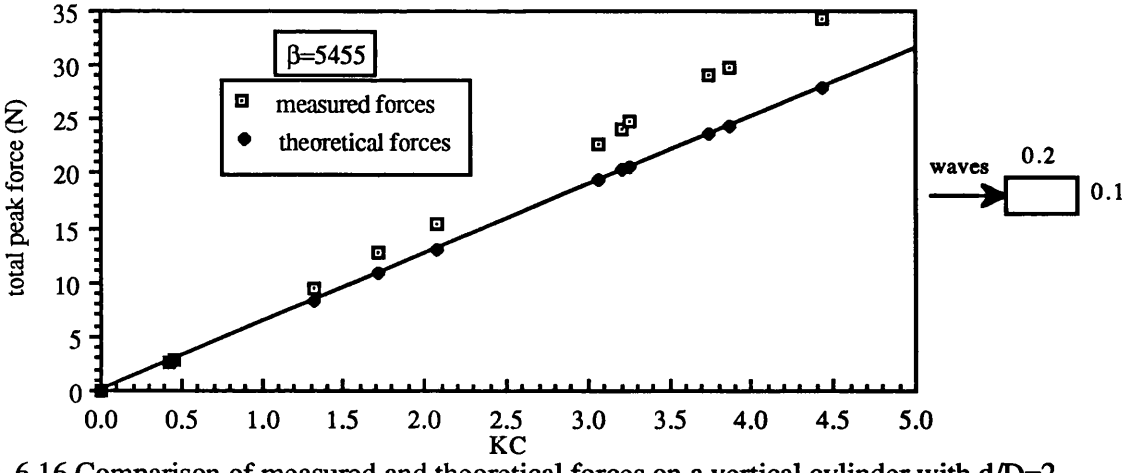

Fig. 6.16 Comparison of measured and theoretical forces on a vertical cylinder with d/D=2

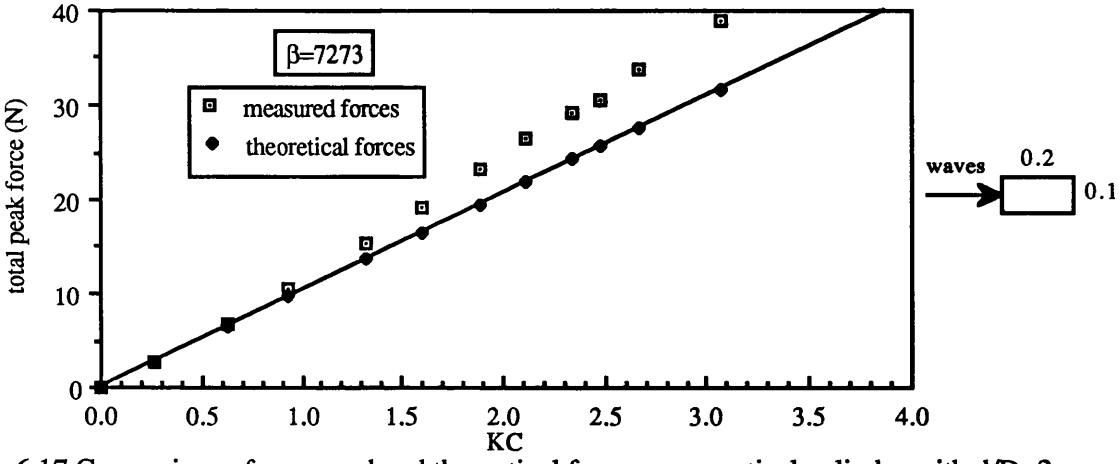

Fig. 6.17 Comparison of measured and theoretical forces on a vertical cylinder with d/D=2

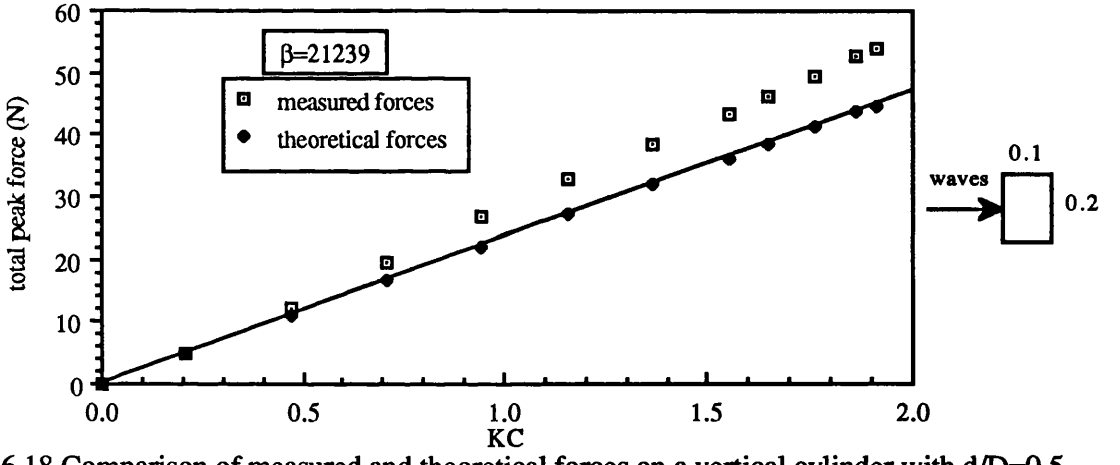

Fig. 6.18 Comparison of measured and theoretical forces on a vertical cylinder with d/D=0.5

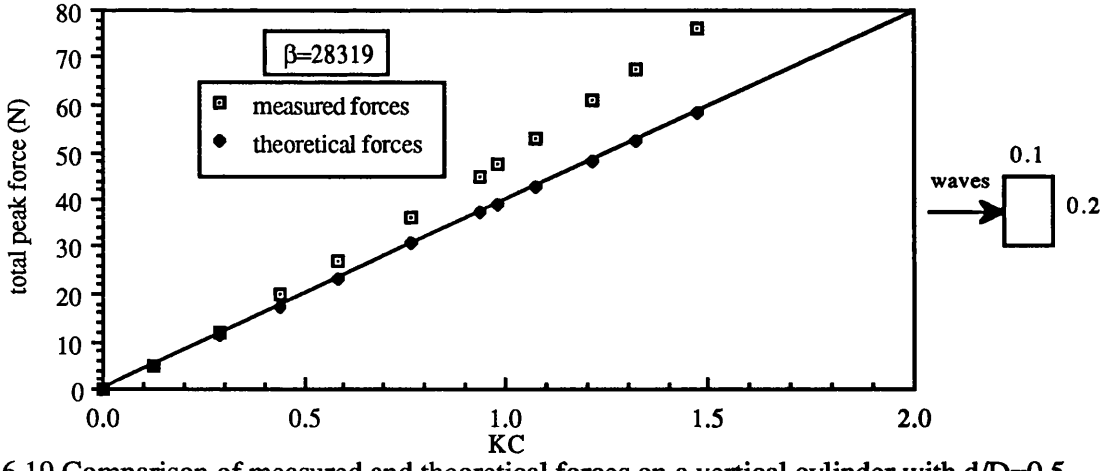

Fig. 6.19 Comparison of measured and theoretical forces on a vertical cylinder with d/D=0.5

6.4.2 HORIZONTAL CYLINDERS

(i) Comparison of inertia coefficients

The comparison and margin errors between the measured inertia coefficients (in-line C_{Mx} and vertical C_{My} coefficients) of the different cylinders and the corresponding ones derived from the potential flow theory are shown in tables 6.4 through 6.6.

As in the case of vertical cylinders, the measured C_M coefficients were found to be higher than their associated theoretical ones with a wider margin error for the square cylinder. Good agreement however was found between the measured and the theoretical C_M coefficients of the cylinders with aspect ratios of 0.5 and 2.

Table 6.4 Comparison of measured and theoretical C_M coefficients for the square cylinder

β	measured C_M (C_{Mx}, C_{My})	theoretical C_M (C_{Mx}, C_{My})	margin error (%)
5128	2.735, 2.678	2.29, 2.30	-16.3, -14.1
6838	3.065, 2.871	2.28, 2.27	-25.6, -20.9

Table 6.5 Comparison of measured and theoretical C_M coefficients for the cylinder with d/D=2

β	measured C_M (C_{Mx}, C_{My})	theoretical C_M (C_{Mx}, C_{My})	margin error (%)
5155	1.645, 3.111	1.776, 3.30	8.0, 6.1
6873	1.625, 3.103	1.76, 3.16	8.3, 1.8

Table 6.6 Comparison of measured and theoretical C_M coefficients for the cylinder with d/D=0.5

β	measured C_M (C_{Mx}, C_{My})	theoretical C_M (C_{Mx}, C_{My})	margin error (%)
20743	3.348, 1.716	3.24, 1.815	-3.2, 5.8
27658	3.303, 1.685	3.196, 1.769	-3.2, 5.0

(ii) Comparison of total peak forces

The measured in-line and vertical forces acting on the whole horizontal submerged length of each cylinder were obtained by using the Morison equation with the measured inertia and drag C_M and C_D coefficients (proper to each cylinder). The phase angle at which the peak of the forces occur was identified as in the case of the vertical cylinders and substituted in the Morison equation. These measured peak forces were then compared to the theoretical forces obtained from the computer program.

The comparisons are shown in Figures 6.20 through 6.31 for the different cylinders and for the two wave frequency parameters β. As in the case of vertical cylinders, it is worth mentioning that the theoretical forces shown in those figures contain no drag component.

As shown in the figures, the theory was found to underestimate the total forces particularly for the square cylinder. However, good agreements were found between the measured and predicted forces on the cylinders with aspect ratios of 0.5 and 2.

The square cylinder whether tested vertically or horizontally presented wider discrepancies in the results between measurement and theory than the other two cylinders. It is argued in this study, that the flow around a square cylinder is less refined than around the other cylinders. It is known that the flow around square cylinders generates, and is particularly sensitive to, turbulence. This was confirmed by Vickery (1966) and Bearman et al. (1978) using flow visualisation techniques.

The above comparisons show clearly that the potential flow theory fails to predict accurately the forces on rectangular bodies. The fact that the theoretical total peak forces were smaller than their associated measured ones is partly a consequence of the lower values of the theoretical C_M coefficients compared to their associated measured ones. The other factor contributing to the discrepancies between measured and predicted results is the drag term in the Morison equation. Therefore, one must not neglect the fact that for these sharp edged cylinders separation occurs at a very early stage and therefore drag forces do contribute to the total forces. Indeed, in the case of sharp edged bodies where separation effects on the body are confined to small regions surrounding each edge, attached viscous and separated inviscid-flow theories would not give an adequate prediction of the inviscid surface velocity, and hence of the boundary-layer thickness. Hence the viscous-force prediction is likely to be considerably in error for these cases as shown above. In this sense the three parts of the force, namely a force due to the inertia of the accelerating outer flow, a force due to the influence of viscous

boundary layers and a force due to separation of these boundary layers leading to the shedding of vortices interact with one another. This aspect of importance in the force generation is missing in the potential flow theories.

Pearcey (1990) investigating the wake re-encounter effect argues that the source of discrepancy between experimental and theoretical results is due to the perturbations in the relative incident velocity which are caused by wake re-encounter.

6.5 THE MORISON EQUATION

In order to evaluate the Morison equation, the measured forces were compared to those predicted by it through the use of the experimentally determined inertia and drag coefficients.

The comparisons are shown in Figures A1 through A60 of appendix 4. In wavy flow and for each vertical and horizontal cylinder, a comparison was made for each β number and for a small and a high KC number. In combined wavy and steady flows and for each vertical and horizontal cylinder, a comparison was made for each reduced velocity VR and each β number.

In wavy flow, as shown in Figures A1 through A24, the prediction of the measured forces by the Morison equation was found good when using the measured C_M and C_D coefficients.

In combined wavy and steady flows (to simulate the presence of a current along with waves), as shown in Figures A25 through A60, the Morison equation using measured C_M and C_D coefficients obtained under these combined flows was found to be adequate to predict the measured forces. However, when the Morison equation was used with C_M and C_D coefficients measured in wavy flow, it was found to overestimate the measured forces.

Therefore, when using the Morison equation to predict forces it is essential to know how the inertia and drag coefficients were obtained before any prediction is made.

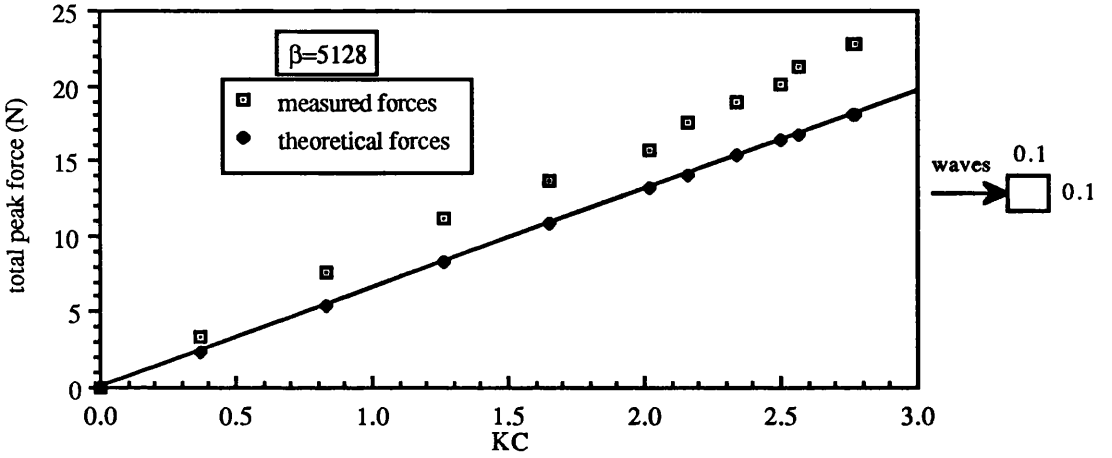

Fig. 6.20 Comparison of measured and theoretical in-line forces on a horizontal cylinder with d/D=1

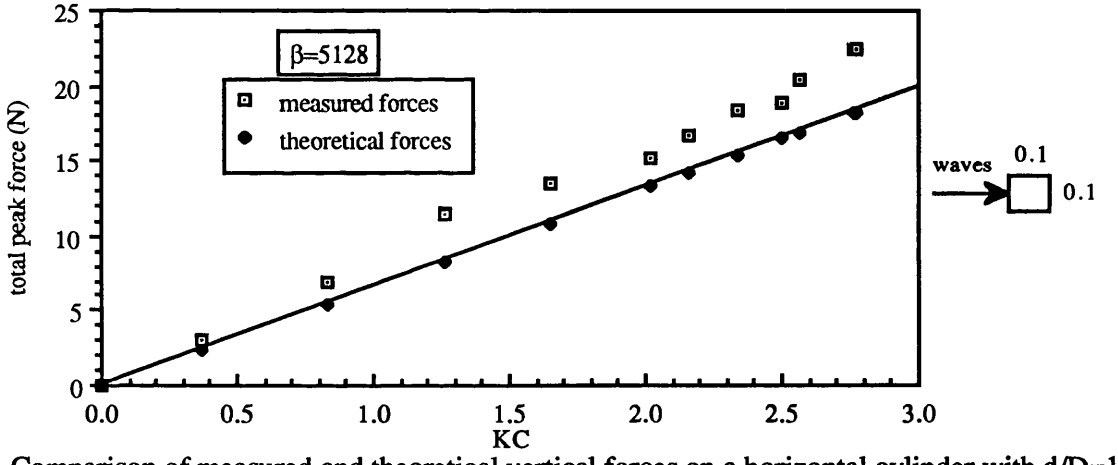

Fig. 6.21 Comparison of measured and theoretical vertical forces on a horizontal cylinder with d/D=1

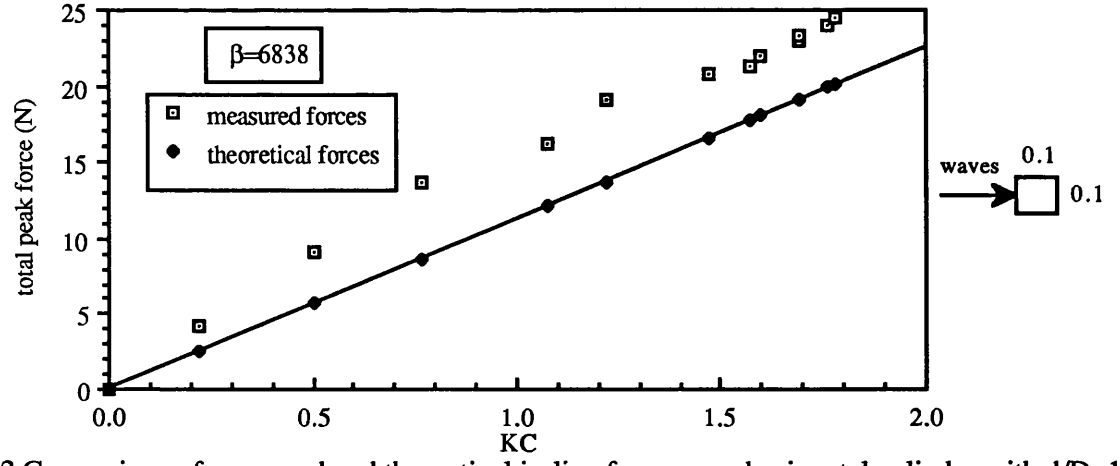

Fig. 6.22 Comparison of measured and theoretical in-line forces on a horizontal cylinder with d/D=1

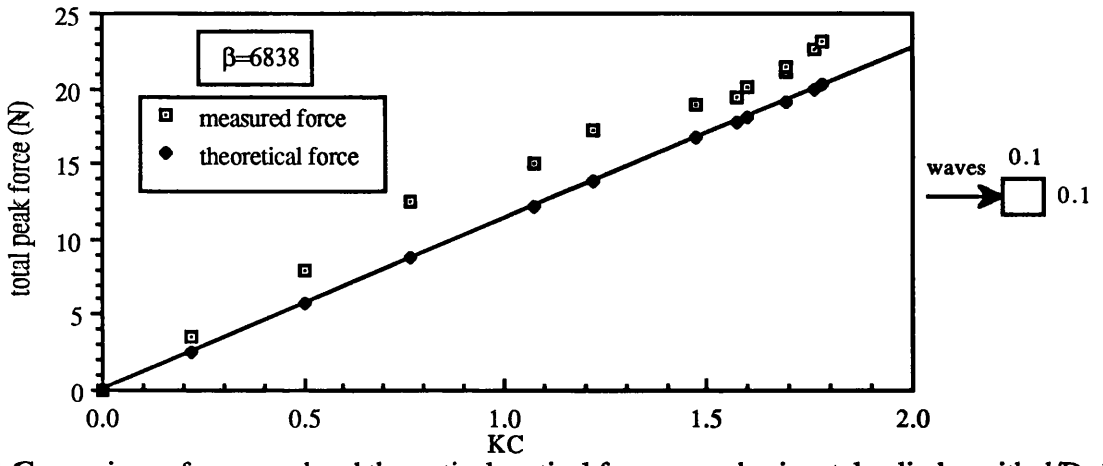

Fig. 6.23 Comparison of measured and theoretical vertical forces on a horizontal cylinder with d/D=1

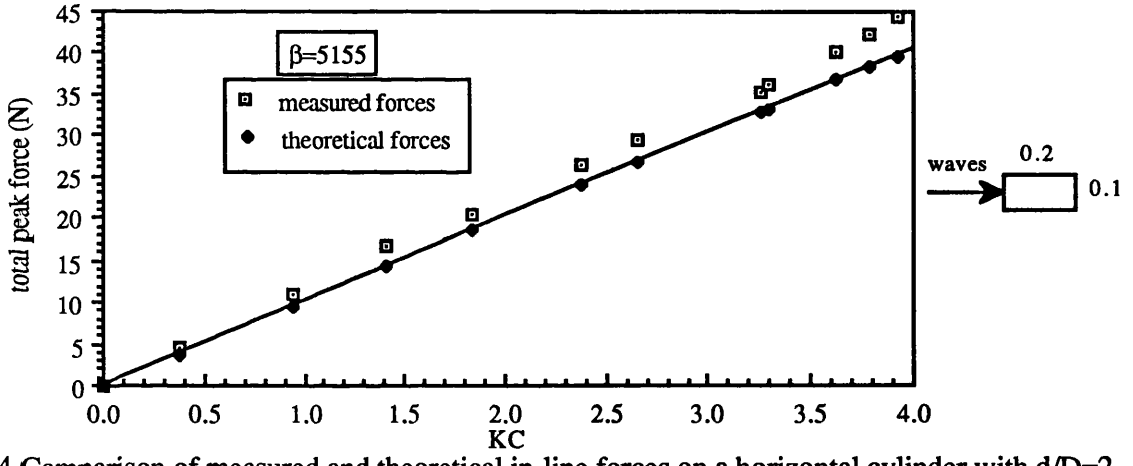

Fig. 6.24 Comparison of measured and theoretical in-line forces on a horizontal cylinder with d/D=2

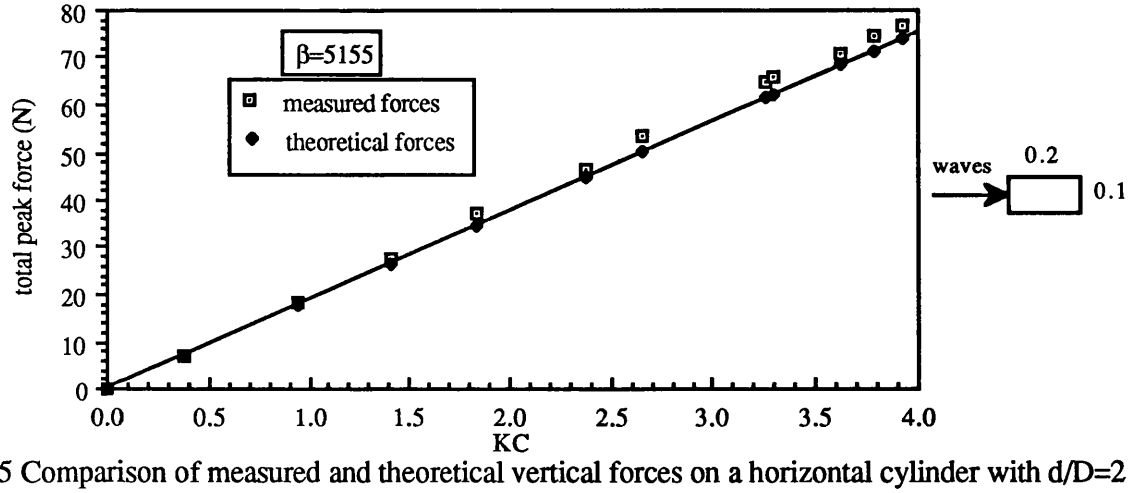

Fig. 6.25 Comparison of measured and theoretical vertical forces on a horizontal cylinder with d/D=2

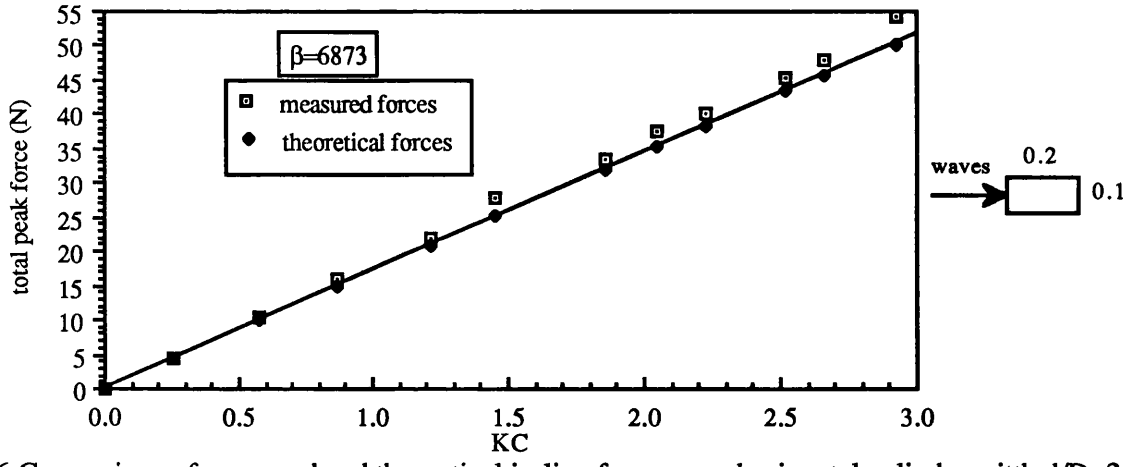

Fig. 6.26 Comparison of measured and theoretical in-line forces on a horizontal cylinder witth d/D=2

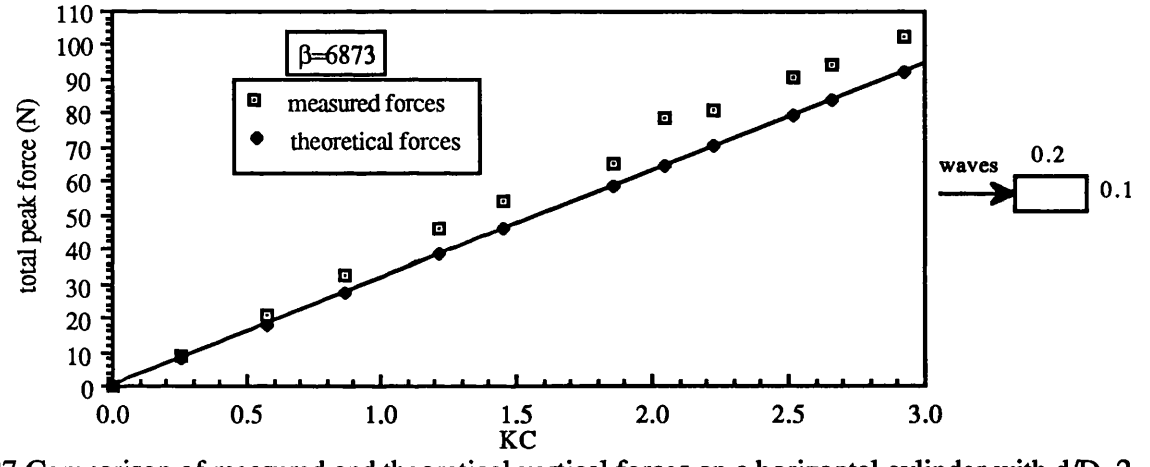

Fig. 6.27 Comparison of measured and theoretical vertical forces on a horizontal cylinder with d/D=2

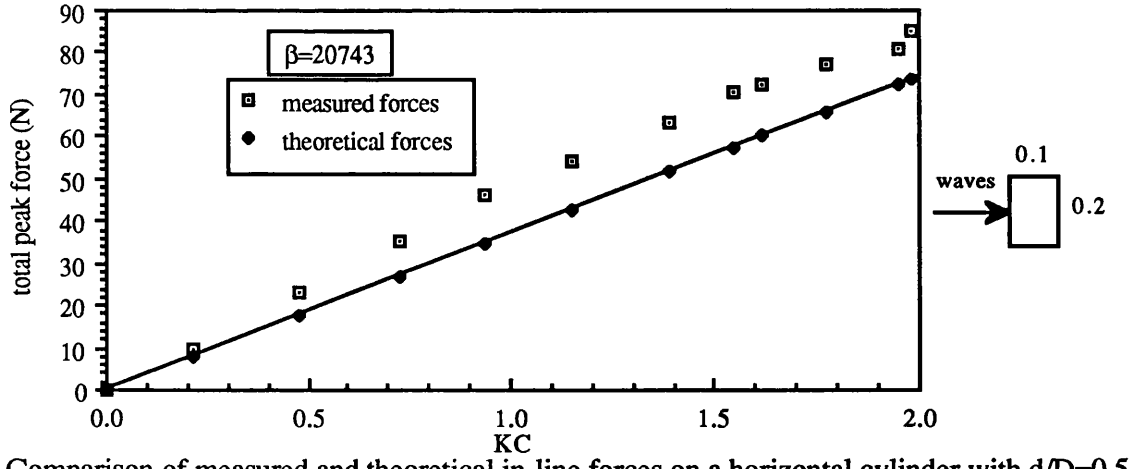

Fig. 6.28 Comparison of measured and theoretical in-line forces on a horizontal cylinder with d/D=0.5

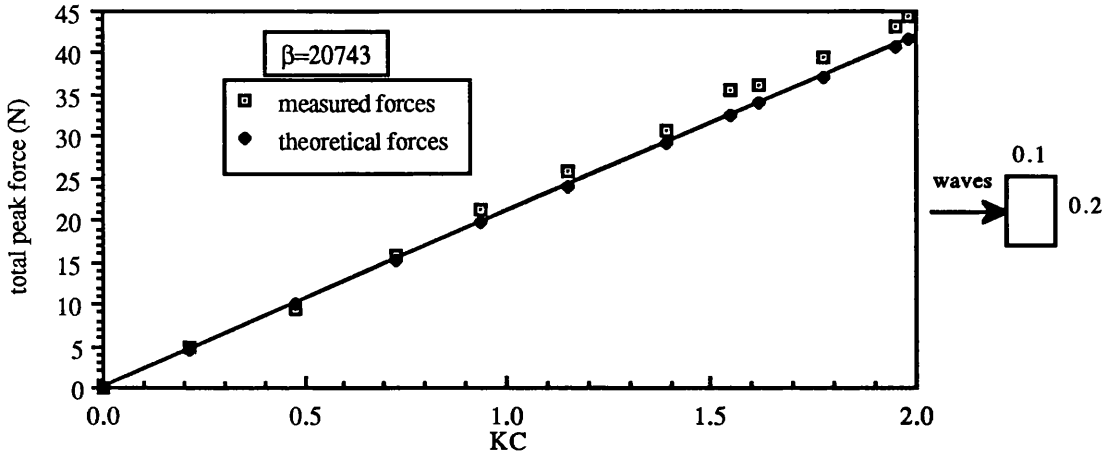

Fig. 6.29 Comparison of measured and theoretical vertical forces on a horizontal cylinder with d/D=0.5

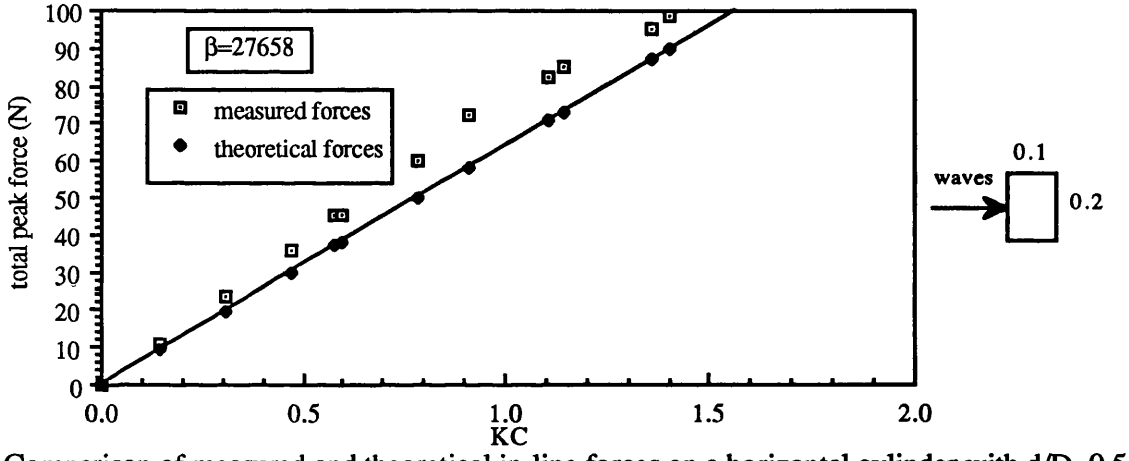

Fig. 6.30 Comparison of measured and theoretical in-line forces on a horizontal cylinder with d/D=0.5

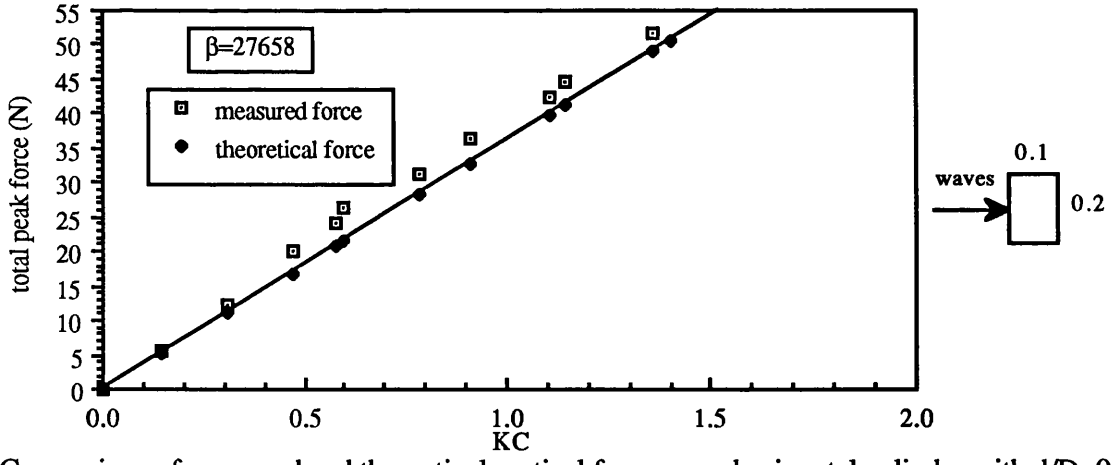

Fig. 6.31 Comparison of measured and theoretical vertical forces on a horizontal cylinder with d/D=0.5

CHAPTER 7

CONCLUSIONS AND RECOMMENDATIONS

7.1 CONCLUSIONS

Experiments were carried out at the Hydrodynamics Laboratory of the Department of Naval Architecture and Ocean Engineering at the University of Glasgow. Rectangular cylinders of various aspect ratios (i.e. cross-sections) were constructed and tested vertically as surface piercing and horizontally with their axes parallel to wave crests in steady flow, wavy flow and the combination of the two flows to simulate a presence of currents along with waves. Force measuring systems were designed and incorporated into the test section of each cylinder.

In-line and transverse forces were measured for the surface piercing vertical cylinders and in-line and vertical forces were measured for the horizontally submerged cylinders. Various hydrodynamic coefficients data base for sharp-edged rectangular cylinders were subsequently generated in terms of inertia C_M, drag C_D and lift C_L coefficients as well as in terms of the maximum C_{Fmax} and the r.m.s. value C_{Frms} of the measured forces.

The following general conclusions were drawn from this research study.

(1) In steady flow, the drag coefficients were found to be smaller than those measured earlier by other investigators mentioned in Chapter 1 who conducted experiments in a two dimensional flow using cylinders with a very high length to width L/D ratio spanning the entire height of the wind tunnel and with some of them mounted between end plates.
It is deemed in this study that the length to width ratio L/D of 5, observed in the first set of cylinders, is not high enough to ensure an unbounded two dimensional flow. When the length to width ratio L/D of a cylinder immersed in a steady flow decreases, a cross flow is induced and C_D coefficient decreases.

(2) The inertia coefficients of the cylinders of aspect ratios 1 and 2 horizontally submerged in regular waves decrease rapidly with increasing KC numbers.

The author believes that the flow circulation created by rotating separated vortices around cylinders of such aspect ratios induces a reduction of wave forces acting on them. In the case of the horizontal cylinder with an aspect ratio of 0.5 the inertia coefficient varied less with the KC number for the range of the KC number investigated (up to 2). It is argued in this study that decreasing the aspect ratio of a horizontal cylinder below 1 results in weakening the circulating flow around the cylinder which lessens or eliminates the reduction of wave forces.

(3) The inertia coefficients of the horizontal cylinders in wavy flow were found to be smaller than those of the vertical cylinders.
The author believes that the presence of the vertical water particle velocity for the horizontal cylinders would reduce the hydrodynamic forces.

(4) The drag coefficients for the different cylinders in wavy flow were found to have high values as the KC number approached zero and to decrease sharply with increasing KC numbers.
It is argued in this study that the high drag coefficients measured at low KC numbers are associated with the flow separation and the first appearances of vortices which take place for these sharp-edges cylinders at very early KC numbers. The effects of wake re-encounter usually associated with the shedding of strong vortices are particularly important at very low KC numbers where high drag coefficients were measured.

(5) The transverse or lift coefficients for the different vertical cylinders in wavy flow were found to have high values as the KC number approached zero and to decrease rapidly as the KC number increased. These coefficients were also found to be affected by the variation of the cylinder's aspect ratio.
For the range of KC numbers considered, the square cross-sectional cylinder had the largest transverse forces. It is believed, that the square cylinder offers a greater area where the asymmetry caused by the vortices acts upon it.

(6) The variations of C_M and C_D coefficients with the KC number in wavy flow were generally found to be different from those in planar oscillatory flow.
These differences are attributed to the difference of flow patterns between wavy and planar oscillatory flow.

(7) The various hydrodynamic force coefficients measured in combined wavy and steady flows (to simulate the presence of currents along with waves) were found to be smaller than those measured in wavy flow.

For a cylinder under waves and current, there exists a bias to the wake structure because of the mean flow. One can easily imagine how even a small current will transport vortex structures downstream causing different flows and affecting the time dependent forces, and thus the force coefficients. It is argued in this study that the wake biasing resulting from the current decreases both the inertia and drag coefficients at low KC numbers.

At very low KC numbers, the presence of currents was found to be most important and caused a significant reduction in the drag coefficient. It is argued in this study that this may be attributed to the fact that the region of small KC numbers corresponds to a region where the effect of the currents on the convection of vortices is most prominent in such a way that the current reduces or eliminates the wake re-encounter effects and therefore eliminates or reduces the reinforcement of vortex shedding.

The reduction of the inertia coefficient in the case of horizontal cylinders when currents are present may suggest that, as in the case of horizontal cylinders in wavy flow, the viscous effect caused by the circulating flow which reduces the wave forces is created when a cylinder moves at a constant speed in waves.

(8) In wavy flow, the Morison equation using measured C_M and C_D coefficients was found to predict the measured forces well. In combined wavy and steady flows, the modified Morison equation using C_M and C_D coefficients measured under these flow conditions was found to predict the measured forces well. However, when using measured C_M and C_D coefficients under wavy flow, the modified Morison equation was found to overestimate the measured forces.

(9) The measured inertia coefficients for the square cross-sectional cylinder were found to be higher than those predicted by the potential flow theory. For the cylinders with aspect ratios of 0.5 and 2, however, the measured inertia coefficients were found to be only slightly higher than those predicted by the potential flow theory. In terms of forces, the theory was found to underestimate the total forces for the square cylinder. However, good agreement was found between the measured and predicted forces on the cylinders with aspect ratios of 0.5 and 2.

7.2 RECOMMENDATIONS

Much more detailed flow visualisations are needed to enable us to comprehend the formation and shedding of vortices and to study the effects of varying the aspect ratio and orientation of sharp-edged cylinders on the flow pattern. These vortex motions are extremely important in determining both the in-line and transverse forces experienced by these bodies immersed in a stream of a flow.

Though such flow visualisation techniques have been amply applied to the circular cylinder, the rectangular cylinder has remained neglected particularly in wavy flow and in combined wavy and steady flows. For example, the pattern of formation and shedding of vortices around rectangular cylinders in wavy flow and the effects of changing the afterbody length (effect of aspect ratio) on the flow separation and vortex shedding are still unexplored.

This present research provides data on the various hydrodynamic coefficients for rectangular cylinders immersed vertically and horizontally in wavy flow and in combined wavy and steady flows for a range of the KC numbers up to a value of 5. Further research is needed at KC numbers beyond 5 where both drag and inertia forces are dominant. It would be interesting for example to investigate the effects of currents on the inertia and drag coefficients at high KC numbers.

In addition, there is a need to determine these hydrodynamic coefficients for rectangular cylinders which are orientated with an angle of incidence to the mean flow and to study the effect of changing the angle of incidence on the forces.

REFERENCES

STEADY FLOW

Bearman, P.W., (1965), "Investigation of the Flow Behind a Two-Dimensional Model with a Blunt Trailing Edge and Fitted with Splitter Plates," J. of Fluid Mech., Vol. 21, pp. 241-255.

Bearman, P.W. and Trueman, D.M., (1972), "An Investigation of the Flow Around Rectangular Cylinders," The Aeronautical Quarterly, Vol. 23, pp. 229-237.

Bostock, B.R. and Mair, W.A., (1972), "Pressure Distributions and Forces on Rectangular and D-Shaped Cylinders," The Aeronautical Quarterly, Vol. 23, pp. 1-6.

Courchesne, J. and Laneville, A., (1979), "A Comparison of Correction Methods Used in the Evaluation of Drag Coefficient Measurements for Two-Dimensional Rectangular Cylinders," Trans. A.S.M.E.: J. of Fluids Engng, Vol. 101, pp. 506-510.

Delany, N.K. and Sorensen, N.E., (1953), "Low-Speed Drag of Cylinders of Various Shapes," NACA TN 3038.

"Fluid Forces, Pressures and Moments on Rectangular Blocks," Engineering Science Data Unit, No. 71016, 1971.

Gerrard, J.H., (1966), "The Mechanics of the Formation Region of Vortices Behind Bluff Bodies," J. of Fluid Mech., Vol. 25, pp. 401-413.

Hamel-Derouich, D., (1991), "Fluid Loading on Rectangular Cylinders in Steady Flow," Proc. Int. Offshore and Polar Engineering, Vol. 3, pp. 258-263.

Laneville, A., Gartshore, I.S. and Parkinson, G.V., (1975), "An Explanation of Some Effects of Turbulence on Bluff Bodies," Proc. 4th Int. Conf. on Wind Effects on Buildings and Structures, London.

Laneville, A. and Yong, L.Z., (1983), "Mean Flow Patterns Around Two-Dimensional Rectangular Cylinders and Their Interpretation," J. of Wind Engineering. and Industrial Aerodynamics, Vol. 14, pp. 387-398.

Lee, B.E., (1975), "The Effect of Turbulence on the Surface Pressure Field of a Square Prism," J. of Fluid Mech., Vol. 69, pp. 263-282.

Miller, B.L. and Davies, M.E., (1982), "Wind Loading on Offshore Structures- A Summary of Wind Tunnel Studies," National Maritime Institute, R136, OT-R-8225.

Nakagushi, H., Hashimoto, K. & Muto, S., (1968), "An Experimental Study Aerodynamic Drag of Rectangular Cylinders," J. of Japan Soc. for Aero and Space Sciences, Vol. 16, pp. 1-5.

Nakamura, Y., Mizota, T., and Yoshimura, K., (1973), "On the Characteristics of the Three Components of Aerodynamic Force and Moment Acting on Rectangular and H-Shaped Sections," Bull. of the Research Institute for Applied Mechanics, Kyushu Univ., Vol. 40, pp. 245-255.

Nakamura, Y. and Mizota, T., (1975a), "Torsional Flutter of Rectangular Prisms," Proc. A.S.C.E.: J. Engng Mech. Div., Vol. 101, pp.125-142.

Nakamura, Y. and Mizota, T., (1975b), "Unsteady Lifts and Wakes of Oscillating Rectangular Prisms," Proc. A.S.C.E.: J. Engng Mech. Div., Vol. 101, pp.855-871.

Nishioka, M. and Sato, H., (1978), "Mechanism of Determination of the Shedding Frequency of Vortices Behind a Cylinder at Lower Reynolds Numbers, J. of Fluid Mech., Vol.89, pp. 49-60.

Novak, M., (1972), "Galloping Oscillation of Prismatic Sructures," Proc. A.S.C.E.: J. Engng Mech. Div., Vol. 98, pp. 27-45.

Okajima, A., (1982), "Strouhal Numbers of Rectangular Cylinders," J. of Fluid Mech., Vol. 123, pp. 379-398.

Okajima, A., Mizota, T. and Tanida, Y., (1983), "Observation of Flow Around Rectangular Cylinders," Proc. 3rd Int. Symp. on Flow Visualisation, Ann Arbor, USA, pp. 381-386.

Otsuki, Y., Washizu, K., Tomizawa, H. and Oya, A., (1974), "A Note on the Aeroelastic Instability of a Prismatic Bar with Square Section," J. Sound Vib., Vol. 34, pp. 233-248.

Parkinson, G.V. and Brooks, N.P.H., (1961), "On the Aeroelastic Instability of Bluff Cylinders," Trans. A.S.M.E.: J. Appl. Mech., Vol. 28, pp. 252-258.

Roshko, A., (1954), "On the Drag and Shedding Frequency of Two-Dimensional Bluff Bodies," U.S. National Advisory Committee for Aeronautics, TN 3169.

Roshko, A., (1955), "On the Wake and Drag of Bluff Bodies," J. of Aeronautical Sciences, pp. 124-132.

Roshko, A., (1961), "Experiments on the Flow Past a Circular Cylinder at Very High Reynolds Number," J. of Fluid Mech., Vol. 10, pp. 345-356.

Roshko, A. and Fiszdon, W., (1969), "On the Persistence of Transition in the Near Wake," Problems of Hydrodynamics and Continuum Mechanics, Soc. of Industrial and Applied Mathematics, Philadelphia, pp. 606-616.

Sakamoto, H. and Arie, M., (1983), "Vortex Shedding From a Rectangular Prism and a Circular Cylinder Placed Vertically in a Turbulent Boundary Layer," J. Fluid Mech., Vol.126, pp. 147-165.

Scruton, C., (1981), "An Introduction to Wind Effects on Structures," Oxford Univerity Press (Design Council).

Taneda, S., (1959), "Downstream Development of the Wakes Behind Cylinders," J. Phys. Soc. Japan, Vol.14, p. 843.

Taneda, S., (1963), "The Stability of Two-Dimensional Laminar Wakes at Low Reynolds Number," J. Phys. Soc. Japan, Vol.18, p. 288.

Vickery, B.J., (1966), "Fluctuating Lift and Drag on a Long Cylinder of Square Cross-Section in a Smooth and in a Turbulent Stream," J. of Fluid Mech., Vol. 25, pp. 481-494.

Xuejian, X., (1985), "Vortex Shedding From Rectangular Cylinders," Proc. Int. Symp. on Refined Flow Modelling and Turbulence Measurements, Iowa City, USA, Vol. 1, pp. D14-1-D14-10.

WAVY AND PLANAR OSCILLATORY FLOWS

Atkins (1979), "Wave Force Investigation at Forties Field Platform FB, Final Report of Results," W. S. Atkins Consultants, Epsom.

Barltrop, N.D.P., Mitchell, G.M. and Atkins, J.B., (1990), "Fluid Loading on Fixed Offshore Structures, Vol.1," Prepared by W. S. Atkins Engineering Sciences for the Dept. of Energy.

Bearman, P.W., Graham, J.M.R. and Singh, S., (1978), "Forces on Cylinders in Harmonically Oscillating Flow," Proc. Symp. on Mechanics of Wave-Induced Forces on Cylinders, Bristol (UK), pp. 437-449.

Bearman, P.W., Graham, J.M.R., Obasaju, E.D. and Drossopoulos, G.M., (1984), "The influence of Corner Radius on the Forces Experienced by Cylindrical Bluff Bodies in Oscillatory Flow," Applied Ocean Research, Vol. 6, pp. 83-89.

Bearman, P.W., Chaplin, J.R., Graham, J.M.R, Kostense, J.K., Hall, P.F. and Klopman, G., (1985a), "The Loading on a Cylinder in Post-Critical Flow Beneath Periodic and Random Waves," Proc. of BOSS Conf., Delft.

Bearman, P.W., Downie, M.J., Graham, J.M.R. and Obasaju E.D., (1985b), "Forces on Cylinders in Viscous Oscillatory Flow at Low Keulegan-Carpenter Numbers," J. Fluid Mech., Vol.154, pp. 337-365.

Bishop, J. R., (1984), "Wave Force Investigation at the Second Christchurch Bay Tower, Summary Report," OT-0-82100, NMI R177.

Bishop, J.R., (1987), "Wave Force Coefficients for Horizontal and Vertical Cylinders with Kelp Fouling, Measured at the Christchurch Bay Tower," O.T.H. 87268, H.M.S.O.

Borgman, L.E. and Yfantis, E., (1979), "Three Dimensional Character of Waves and Forces," Civ. Engng. in the Oceans IV, A.S.C.E., pp. 791-804.

Chakrabarti, S.K., Wolbert, A.L. and Tam, W.A., (1976), "Wave Forces on Vertical Circular Cylinder," J. Waterways Harbors and Coastal Engng Div., Vol. 102, pp. 103-221.

Chakrabarti, S.K., (1980), "In-Line Forces on Fixed Vertical Cylinder in Waves," J. Waterway Port Coastal and Ocean Div., Vol. 106, pp. 145-155.

Chakrabarti, S.K., (1987), "Hydrodynamics of Offshore Structures," Computational Mechanics Publications.

Chan, H.S., (1990), "A Three-Dimensional Technique for Predicting First and Second Order Hydrodynamic Forces on a Marine Vehicle Advancing in Waves," Ph.D. Thesis, Dept. of Naval Architecture and Ocean Engineering, University of Glasgow.

Chaplin, J.R., (1981), "Boudary Layer Separation from a Cylinder in Waves," Proc. Int. Symp. on Hydrodynamics in Ocean Engng., Trondheim, pp. 645-666.

Chaplin, J.R., (1984a), "Mass Transport Around a Horizontal Cylinder Beneath Waves," J. Fluid Mech., Vol. 140, pp. 175-187.

Chaplin, J.R., (1984b), "Nonlinear Forces on a Horizontal Cylinder Beneath Waves," J. Fluid Mech., Vol. 147, pp. 449-464.

Chaplin, J.R., (1985a), "Morison Inertia Coefficients in Orbital Flow," J. Waterway Port Coastal and Ocean Eng. Div., A.S.C.E., Vol. 111, pp. 201-215.

Chaplin, J.R., (1985b), "Loading on a Cylinder in Uniform Elliptical Orbital Flow," Liverpool University, Civil Engng Report, MCE/JUL/85.

Chaplin, J.R., (1987), "Recent Developments in Large Scale wave Loading Experiments in the Morison Regime," Int. Conf. on Mobile Offshore Structures, London (UK), pp. 428-445.

Chaplin, J.R., (1988a), "Non-linear Forces on Horizontal Cylinders in the Inertia Regime in Waves at High Reynolds Numbers," Proc. of BOSS Conf., Vol. 2, pp. 505-518.

Chaplin, J.R., (1988b), "Loading on a Cylinder in Uniform Oscillatory Flow: Part II-Elliptical Orbital Flow," Applied Ocean Research, Vol. 10, pp. 199-206.

Davies, M.J.S., Graham, J.M.R and Bearman, P.W., (1990), "In-Line Forces on Fixed Cylinders in Regular and Random Waves," Soc. for Underwater Technology Conf., Vol. 26, pp. 113-136.

Dawson, T.H., (1984), "In-Line Forces on Vertical Cylinders in Deep Water Waves," Proc. of Offshore Technology Conference, pp. 463-470.

Dean, R.G., (1970), "Relative Validities of Water Wave Theories," J. Waterways and Harbors Div., A.S.C.E., Vol. 96, No. WW1.

Gaston, J.D. and Ohmart, R.D., (1979), "Effects of Surface Roughness on Drag Coefficients," Civil Engng in the Oceans IV, A.S.C.E., pp. 611-621.

Graham, J.M.R., (1978), "Forces on Cylindrical Bodies in Oscillatory Flow at Low Keulegan-Carpenter Numbers," Proc. Symp. on Mechanics of Wave-Induced Forces on Cylinders, Bristol (UK), pp. 461-474.

Graham, J.M.R., (1980), "The Forces on Sharp-Edged Cylinders in Oscillatory Flow at Low Keulegan-Carpenter Numbers," J. Fluid Mech., Vol. 97, pp. 331-346.

Grass, A.J., Simons, E.E. and Cavenagh, N.J., (1984), "Fluid Loading on Horizontal Cylinders in Wave Type Orbital Flow," Proc. Int. Symp. Offshore Mech. and Arctic Engng., A.S.M.E.

Hallam, M.G., Heaf, N.J. and Wootton, L.R., (1978), "Dynamics of Marine Structures: Methods of Calculating the Dynamic Response of Fixed Structures Subject to Wave and Current Action," Atkins Research and Development, Report UR8 (2nd edition), CIRIA Underwater Engineering Group.

Hamel-Derouich, D., (1991), "Wave Forces on Rectangular Cylinders at Low Keulegan-Carpenter Numbers," Proc. of Offshore Technology Conference, pp. 207-216.

Hamel-Derouich, D., (1992), "Forces on Vertical Rectangular Cylinders in Wavy Flow and in Combined Wave and Current Flow at Low KC Numbers," Proc. Int. Symp. Offshore Mech. and Arctic Engng., A.S.M.E., pp. 79-86.

Hamel-Derouich, D., (1993), "Hydrodynamic Forces on Rectangular Cylinders Horizontally Submerged in Waves and Currents at Low KC Numbers," Proc. Int. Offshore and Polar Engineering.

Hara, S. and Sortland, B., "Hydrodynamic Coefficient of Three-Dimensional Bodies with a Low KC Number,".

Heideman J.C., Olsen O.A. and Johannson, P.I., (1979), "Local Wave Force Coefficients," Civ. Engng. in the Oceans IV, A.S.C.E., pp. 684-699.

Heideman J.C. and Sarpkaya, T., (1985), "Hydrodynamic Forces on Dense Arrays of Cylinders," Proc. of Offshore Technology Conference, pp. 421-428.

Hogben, N. and Standing, R.G., (1975), "Experience in Computing Wave Loads on Large Bodies," Proc. of the Offshore Technology Conference, pp. 413-431.

Holmes, P. and Chaplin, J.R., (1978), "Wave loads on Horizontal Cylinders," Proc. 16th Int. Conf. on Coastal Engng., Hamburg, Vol. 3., p. 2449.

Ikeda, Y., Otsuka, K. and Tanaka, N., (1988), "Wave Forces Acting on Horizontally Submerged Cylinders in Regular Waves at Low KC Number," J. of the Soc. of Naval Architects of Japan, Vol.163.

Inoue, R. and Kyozuka, Y., (1984), "On the Nonlinear Wave Forces Acting on Submerged Cylinders," J. of the Soc. of Naval Architects of Japan, Vol. 156, pp. 115-127.

Isaacson, M. de St. Q., (1978a), "Wave Forces on Large Square Cylinders," Proc. Symp. on Mechanics of Wave-Induced Forces on Cylinders, Bristol (UK), pp. 609-622.

Isaacson, M. de St. Q., (1978b), "Vertical Cylinders of Arbitrary Section in Waves," J. Waterways Port and Ocean Div., A.S.C.E., Vol. 104, No. WW4, pp. 309-324.

Isaacson, M. de St. Q., (1979), "Wave Forces on Rectangular Caissons," Proc. Civil Engng. Oceans IV, ASCE, San Francisco, Vol. I, pp. 518-530.

Keulegan, G.H. and Carpenter, L.H., (1958), "Forces on Cylinders and Plates in an Oscillating Fluid," J. of research of the National Bureau of Standards, Vol. 60, pp. 423-440.

Lian, W., (1988), "A Numerical Study of Two-Dimensional Separated Flow Past Bluff Bodies at Moderate KC-Numbers," Applied Ocean Research, Vol. 10, pp. 114-119.

Maull, D.J. and Norman, S.G., (1978), "A Horizontal Circular Cylinder Under Waves," Proc. Symp. on Mechanics of Wave-Induced Forces on Cylinders, Bristol (UK), pp. 359-378.

Morison, J.R., O'Brien, M.P., Johnson, J.W. and Schaaf, S.A., (1950), "The Forces Exerted by Surface Waves on Piles," J. Petrol. Technol. Am. Inst. Mining Engrs, Vol. 189, pp. 149-157.

Myers, J.J., Holm, C.H. and McAllister, R.F., (1969), "Handbook of Ocean and Underwater Engineering," Mc Graw-Hill Book Company.

Ohmart, R.D. and Gratz, R.L., (1979), "Drag Coefficients from Hurricane Wave Data," Civ. Engng. in the Oceans IV, A.S.C.E., pp. 260-272.

Otsuka, K. , Ikeda, Y. and Tanaka, N., (1990), "Viscous Forces Acting on a Horizontal Circular Cylinder in Regular and Irregular Waves," Proc. Int. Symp. Offshore Mech. and Arctic Engng., A.S.M.E.

Paape, A. and Breusers, H.N.C., (1967), "The Influence of Pipe Dimension on Forces Exerted by Waves," 10th Coastal Engng. Conf., A.S.C.E., Chapter 48.

Patel, M.H., (1989), "Dynamics of Offshore Structures," Butterworth and Co. Publishers.

Pearcey, H.H., (1978), "Some Observations on Fundamental Features of Wave-Induced Viscous Flows Past Cylinders", Proc. Symp. on Mechanics of Wave-Induced Forces on Cylinders, Bristol (UK), pp. 1-54.

Pearcey, H.H., (1979), "The Effects of Surface Roughness on the Wave Loading for Cylindrical Members of Circular Cross Section," National Maritime Institute, N.M.I. R65, OT-R-7960.

Pearcey, H.H., Singh, S., Cash, R. and Matten, R., (1985), "Fluid Loading on Roughened Cylindrical Members of Circular Cross Section," BMT Report 191, OT-0-8411.

Pearcey, H.H., (1990), "On the Effects of Wake Re-Encounter for Wave Forces on Cylinders," Soc. for Underwater Technology Conf., Vol. 26, pp. 159-183.

Ramberg, S.E. and Niedzwecki, J.M., (1979), "Some Uncertainties and Errors on Wave Force Computations," Proc. of Offshore Technology Conference, pp. 2091-2101.

Ramberg, S.E., (1981), "Discussion of In-Line Forces on Fixed Vertical Cylinders in Waves," J. Waterway Port Coastal and Ocean Div., Vol. 107, pp. 45-46.

Sarpkaya, T. and Garrison C.J., (1963), "Vortex Formation and Resistance in Unsteady Flow," J. Applied Mech., Vol. 30, pp. 16-24.

Sarpkaya, T., (1976a), "Vortex Shedding and Resistance in Harmonic Flow about Smooth and Rough Circular Cylinders at High Reynolds Numbers," Report No. NPS-59SL76021, Naval Postgraduate School, Monterey, California.

Sarpkaya, T., (1976b), "In Line and Transverse Forces on Smooth and Sand-Roughened Cylinders in Oscillatory Flow at High Reynolds Numbers," Report No. NPS-69SL76062, Naval Postgraduate School, Monterey, California.

Sarpkaya, T. and Isaacson, M., (1981), "Mechanics of Wave Forces on Offshore Structures," Van Nostrand Reinhold Co.

Shankar, N.J., Balendra, T. and Soon, C.E., (1983), "Wave Forces on Large Vertical Cylinders of Square and Rectangular Sections," Trans. Inst. Engrs. Australia Civ. Engng., Vol. CE25, No. 1, pp.36-44.

Singh, S., (1979), "Forces on Bodies in Oscillatory Flow," Ph.D. Thesis, Imperial College, University of London.

Smith, P.A. and Stansby, P.K., (1991), "Viscous Oscillatory Flows Around Cylindrical Bodies at Low Keulegan-Carpenter Numbers Using the Vortex Method," Journal of Fluids and Structures, Vol. 5, pp.339-361

Stansby, P.K., Bullock, G.N. and Short, I., (1983), "Quasi 2-D Forces on a Vertical Cylinder in Waves," J. Waterway Port Coastal and Ocean Div., Vol. 109, pp. 128-132.

Swan, C., (1990), "Wave Kinematics Within the Crest to Trough Region," Soc. for Underwater Technology Conf., Vol. 26, pp. 45-60.

Tanaka, N., Ikeda, Y., Himeno, Y. and Fukutomi, Y., (1980), "Experimental Study on Hydrodynamic Viscous Force Acting on Oscillating Bluff Body," J. of the Kansai Soc. of Naval Architects, Vol. 179, pp.35-43.

Tanaka, N., Ikeda, Y. and Nishino, K., (1982), "Hydrodynamic Viscous Force Acting on Oscillating Cylinders With Various Shapes," Proc. 6th Symp. Marine Technology, Soc. Naval Arch. of Japan.

Wiegel, R.L., Beeb, K.E. and Moon, J., (1957), "Ocean Wave Forces on Circular Cylindrical Piles," Proc. A.S.C.E., Vol. 83, No. HY2.

Wiegel, R.L., (1964), "Oceanographical Engineering," Prentice Hall Inc.

Wolfram, J. and Theophanatos, A., (1985), "The Effects of Marine Fouling on the Fluid Loading of Cylinders- Some Experimental Results," Proc. of the Offshore Technology Conference, pp. 517-526.

PRESENCE OF CURRENTS WITH WAVES

Dalrymple, R.A. and Dean, R.G., (1975), "Waves of Maximum Height on Uniform Currents," J. Waterways and Harbors Div., A.S.C.E., Vol. 101, No. WW3, pp. 317-328.

Hedges, T.S., Anastasiou, K. and Gabriel, D., (1985), "Interaction of Random Waves and Currents," J. Waterway, Port, Coastal and Ocean Engineering, Vol. 111, No.2, pp. 275-288.

Ikeda, Y., Otsuka, K. and Kiku, T., (1990), "Wave Forces Acting on a Horizontal Circular Cylinder Moving at a Constant Speed," Proc. of the first Pacific Asia Offshore Mech. Sym., Seoul, Korea, pp. 79-86.

Ismail, N.M., (1983), "Effects of Wave-Current Interaction on the Design of Marine Structures," Proc. of the Offshore Technology Conference, pp. 307-316.

Kato, M., Abe, T., Tamiya, M. and Kumakiri, T., (1983), "Drag Forces on Oscillating Cylinders in a Uniform Flow," Proc. of the Offshore Technology Conference, pp. 95-102.

Kiku, T., Otsuka, K. and Ikeda, Y., (1991), "Viscous Forces Acting on a Horizontal Circular Cylinder in Waves and Steady Current," J. Kansai Soc. Naval Arch., No. 216, pp. 101-109 (in Japanese).

Li, Y.C and Kang, H.G., (1992), "Wave-Current Forces on Slender Circular Cylinder," Proc. Int. Symp. Offshore Mech. and Arctic Engng., A.S.M.E., pp. 117-125.

Maeda, H., Masuda, K., Maruyama, F. and Kitakouji, Y., (1990), "Research on Separated Flow Around a Submerged Horizontal Cylinder in Water Waves and Currents," J. Soc. Naval Architects of Japan, Vol. 168, No. 2, pp. 195-204 (in Japanese).

Malleswara-Rao, L.V.N. and Narasimham, M.L., (1990), "Estimation of Hydrodynamic Forces and Moments in the Presence of Combined Wave and Current Field," National Seminar on Offshore Structures, Andhra Univ., pp. 194-203.

Moe, G. and Verley, R., (1980), "Hydrodynamic Damping of Offshore Structures in Waves and Currents," Proc. of the Offshore Technology Conference, pp. 37-44.

Sarpkaya, T., (1955), "Oscillatory Gravity Waves in Flowing Water," Trans. A.S.C.E., Vol. 122, pp. 564-586.

Sarpkaya, T., Bakmis, C. and Storm, M.A., (1984), "Hydrodynamics Forces from Combined Wave and Current Flow on Smooth and Rough Circular Cylinders at High Reynolds Numbers," Proc. of the Offshore Technology Conference, pp. 455-462.

Sarpkaya, T. and Storm, M.A., (1985), "In-Line Force on a Cylinder Translating in Oscillatory Flow," Applied Ocean Research, Vol. 7, pp. 188-196.

Teng, C.C. and Nath, J.H., (1985), "Forces on Horizontal Cylinder Towed in Waves, " J. Waterway Port Coastal and Ocean Engng. Div., A.S.C.E., Vol. 111, No. 6, pp. 1022-1040.

APPENDIX 1

METHOD OF DETERMINING THE INERTIA C_M AND DRAG C_D COEFFICIENTS IN WAVY FLOW

This method is based on the Fourier averaging technique in which the total force is assumed to be represented as Fourier series containing drag and inertia terms with a remainder term which when added they equate with the measured force exactly.
The linear wave theory is used in order to compute the water particle kinematics. The sinusoidal velocity and acceleration are given by

$$u = -u_m \cos\theta \tag{A1.1}$$

$$\dot{u} = u_m \frac{2\pi}{T} \sin\theta \tag{A1.2}$$

where $\theta = \frac{2\pi}{T} t$

and where the maximum velocity u_m is given by

$$u_m = \frac{H}{2} \frac{2\pi}{T} e^{-ky}. \tag{A1.3}$$

The in-line force per unit length derived by Morison et al. is given as

$$F = \frac{1}{2} \rho D C_D |u| u + \rho A C_M \dot{u} \tag{A1.4}$$

where A is the cross-sectional area of the cylinder.
Replacing u and $\dot{u}$ by their expressions, F becomes

$$F = -\frac{1}{2} \rho D C_D u_m^2 |\cos\theta| \cos\theta + \rho A C_M \frac{2\pi}{T} u_m \sin\theta \tag{A1.5}$$

By the rule of Fourier

$$|\cos\theta| \cos\theta = \sum_{n=0}^{\infty} \frac{\int_0^{2\pi} |\cos\theta| \cos\theta \cos n\theta \, d\theta}{\int_0^{2\pi} \cos^2 n\theta \, d\theta}$$

$$= a_0 + a_1 \cos\theta + a_2 \cos 2\theta + a_3 \cos 3\theta + \ldots \tag{A1.6}$$

where $a_n = 0$ for n even

and $a_n = (-1)^{\frac{n+1}{2}} \frac{8}{n(n^2-4)\pi}$ for n odd

$\Rightarrow a_1 = \frac{8}{3\pi}$, $a_3 = \frac{8}{15\pi}$,...

ignoring a_3, a_5, etc

$$|\cos\theta|\cos\theta = \frac{8}{3\pi}\cos\theta. \qquad \text{(A1.7)}$$

Therefore

$$F = -\frac{1}{2}\rho D C_D u_m{}^2 \frac{8}{3\pi}\cos\theta + \rho A C_M \frac{2\pi}{T} u_m \sin\theta$$

and

$$\frac{F}{\rho u_m{}^2 D} = -\frac{4}{3\pi} C_D \cos\theta + \frac{2\pi A}{\frac{u_m T}{D} D^2} C_M \sin\theta. \qquad \text{(A1.8)}$$

Multiplying both sides once by $\sin\theta$ and once by $\cos\theta$, and integrating between 0 and 2π, one has

$$\int_0^{2\pi} \frac{F\sin\theta}{\rho u_m{}^2 D} d\theta = -\frac{4}{3\pi} C_D \int_0^{2\pi} \cos\theta\sin\theta d\theta + \frac{2\pi A}{\frac{u_m T}{D} D^2} C_M \int_0^{2\pi} \sin\theta\sin\theta d\theta \qquad \text{(A1.9)}$$

and

$$\int_0^{2\pi} \frac{F\cos\theta}{\rho u_m{}^2 D} d\theta = -\frac{4}{3\pi} C_D \int_0^{2\pi} \cos\theta\cos\theta d\theta + \frac{2\pi A}{\frac{u_m T}{D} D^2} C_M \int_0^{2\pi} \sin\theta\cos\theta d\theta. \qquad \text{(A1.10)}$$

$$\int_0^{2\pi} \cos\theta\sin\theta d\theta = \int_0^{2\pi} \frac{1}{2}\sin 2\theta \, d\theta = -\frac{1}{4}\left[\cos 2\theta\right]_0^{2\pi} = -\frac{1}{4}(1-1) = 0 \qquad \text{(A1.11)}$$

and

$$\int_0^{2\pi} \sin^2\theta\, d\theta = \int_0^{2\pi} \frac{1-\cos 2\theta}{2}\, d\theta = \left[\frac{1}{2}\theta - \frac{1}{4}\sin 2\theta\right]_0^{2\pi} = \pi. \qquad \text{(A1.12)}$$

Therefore

$$\int_0^{2\pi} \frac{F\sin\theta}{\rho u_m{}^2 D} d\theta = \frac{2A\pi^2}{\frac{u_m T}{D} D^2} C_M$$

and

$$C_M = \frac{D^2}{2A\pi^2} \frac{u_m T}{D} \int_0^{2\pi} \frac{F\sin\theta}{\rho u_m{}^2 D} d\theta. \qquad \text{(A1.13)}$$

Similarly

$$\int_0^{2\pi} \sin\theta\cos\theta\, d\theta = 0$$

and

$$\int_0^{2\pi} \cos^2\theta\, d\theta = \int_0^{2\pi} \frac{1+\cos 2\theta}{2} d\theta = \left[\frac{1}{2}\theta + \frac{1}{4}\sin 2\theta\right]_0^{2\pi} = \pi. \qquad \text{(A1.14)}$$

Therefore

$$\int_0^{2\pi} \frac{F\cos\theta}{\rho u_m{}^2 D} d\theta = -\frac{4}{3} C_D$$

and

$$C_D = -\frac{3}{4} \int_0^{2\pi} \frac{F\cos\theta}{\rho u_m{}^2 D} d\theta. \qquad \text{(A1.15)}$$

C_M and C_D are assumed to remain constant during a wave cycle. The fact of ignoring the fourier parameters a_3, a_5, etc in equation (A1.6) makes C_M and C_D independent of θ.

APPENDIX 2

R.M.S. FORCE COEFFICIENT FROM MORISON'S EQUATION

The Morison equation gives the in-line force per unit length as

$$F=\frac{1}{2}\rho DC_D|u|u+\rho AC_M\dot{u} \tag{A2.1}$$

where A=Dxd is the cross-sectional area of the cylinder.

Substituting

$$u = - u_m \cos\theta \tag{A2.2}$$

where

$\theta = 2\pi t/T$

the Morison equation becomes

$$F=-\frac{1}{2}\rho DC_D u_m{}^2|\cos\theta|\cos\theta+\rho A\frac{2\pi}{T}C_M u_m\sin\theta \tag{A2.3}$$

$$=P|\cos\theta|\cos\theta+Q\sin\theta$$

where $P=-\frac{1}{2}\rho DC_D u_m{}^2$ and $Q=\rho A\frac{2\pi}{T}C_M u_m$.

The mean square value of F is

$$\overline{F}^2=\frac{1}{T}\int_0^T(P^2|\cos\theta|^2\cos^2\theta+Q^2\sin^2\theta+2PQ\sin\theta\cos\theta|\cos\theta|)dt \tag{A2.4}$$

or integrating with respect to θ

$$\overline{F}^2=\frac{1}{T}\int_0^{2\pi}(P^2|\cos\theta|^2\cos^2\theta+Q^2\sin^2\theta+2PQ\sin\theta\cos\theta|\cos\theta|)\frac{T}{2\pi}d\theta. \tag{A2.5}$$

$$|\cos\theta|^2\cos^2\theta=\cos^4\theta=\left(\frac{1+\cos2\theta}{2}\right)^2=\frac{1+2\cos2\theta+\frac{1+\cos4\theta}{2}}{4}$$

$$=\frac{4\cos2\theta+\cos4\theta+3}{8} \tag{A2.6}$$

therefore

$$\int_0^{2\pi}\cos^4\theta d\theta=\frac{3}{4}\pi \tag{A2.7}$$

and

$$\sin^2\theta=\frac{1-\cos2\theta}{2}$$

therefore

$$\int_0^{2\theta} \sin^2\theta d\theta = \pi. \qquad \text{(A2.8)}$$

$$2\sin\theta\cos\theta|\cos\theta| = \sin 2\theta|\cos\theta|$$

therefore

$$\int_0^{2\pi} \sin 2\theta|\cos\theta| d\theta = 0. \qquad \text{(A2.9)}$$

Therefore equation (A2.5) can be simplified to

$$\overline{F}^2 = \frac{1}{2\pi}\left(\frac{3}{4}\pi P^2 + \pi Q^2\right)$$

$$= \frac{3}{8}P^2 + \frac{Q^2}{2}. \qquad \text{(A2.10)}$$

Substituting P and Q by their expressions, equation (A2.10) becomes

$$\overline{F}^2 = \frac{3}{8}\frac{1}{4}\rho^2 D^2 C_D{}^2 u_m{}^4 + \frac{1}{2}\rho^2 A^2 \frac{4\pi^2}{T^2} C_M{}^2 u_m{}^2, \qquad \text{(A2.11)}$$

and substituting the cross-section area A by Dxd, equation (A2.11) becomes

$$\overline{F}^2 = \frac{3}{8}\frac{1}{4}\rho^2 D^2 C_D{}^2 u_m{}^4 + \frac{1}{2}\rho^2 d^2 D^2 \frac{4\pi^2}{T^2} C_M{}^2 u_m{}^2$$

$$= \frac{\rho^2 u_m{}^4 D^2}{8}\left(\frac{3}{4}C_D{}^2 + \frac{16 d^2 \pi^2}{u_m{}^2 T^2} C_M{}^2\right). \qquad \text{(A2.12)}$$

Non dimensionalising the mean square value by $\frac{1}{2}\rho u_m{}^2 D$, one obtains

$$\frac{\overline{F}^2}{\left(\frac{1}{2}\rho u_m{}^2 D\right)^2} = (C_{Frms})^2 = \frac{4\rho^2 u_m{}^4 D^2}{8\rho^2 u_m{}^4 D^2}\left(\frac{3}{4}C_D{}^2 + \frac{16 d^2 \pi^2}{u_m{}^2 T^2} C_M{}^2\right)$$

$$= \frac{1}{2}\left(\frac{3}{4}C_D{}^2 + \frac{16 d^2 \pi^2}{u_m{}^2 T^2} C_M{}^2\right). \qquad \text{(A2.13)}$$

Therefore, the non-dimensionalised root mean square value of the in-line Morison force per unit length is given by

$$C_{Frms} = \sqrt{\frac{1}{2}\left(\frac{3}{4}C_D{}^2 + \frac{16 d^2 \pi^2}{u_m{}^2 T^2} C_M{}^2\right)}. \qquad \text{(A2.14)}$$

APPENDIX 3

METHOD OF DETERMINING THE INERTIA C_M AND DRAG C_D COEFFICIENTS IN COMBINED WAVY AND STEADY FLOWS

The linear wave theory gives the sinusoidal velocity and acceleration as

$$u = -u_m \cos\theta \tag{A3.1}$$

$$\dot{u} = u_m \frac{2\pi}{T} \sin\theta \tag{A3.2}$$

where $\theta = \frac{2\pi}{T} t$

and where the maximum velocity u_m is given by

$$u_m = \frac{H}{2} \frac{2\pi}{T} e^{-ky}. \tag{A3.3}$$

Note that these equations are also given in Appendix 1.

The modified Morison equation gives the in-line force per unit length as

$$F = \frac{1}{2}\rho D C_D (V_C + u)|V_C + u| + \rho A C_M \dot{u}, \tag{A3.4}$$

where A=Dxd is the cross-sectional area of the cylinder, and Vc is the current velocity.

Substituting the water particle velocity and acceleration, eq. (A3.4) becomes

$$F = \frac{1}{2}\rho D C_D (Vc - u_m \cos\theta)|Vc - u_m \cos\theta| + \rho A C_M \frac{2\pi}{T} u_m \sin\theta. \tag{A3.5}$$

Using the same Fourier method described in Appendix 1, where both sides of eq. (A3.5) are multiplied once by sinθ and once by cosθ, and integrating between 0 and 2π, one obtains

$$C_M = \frac{\frac{u_m T}{D} D^2}{2\pi A} \frac{1}{\int_0^{2\pi} \sin^2\theta d\theta} \int_0^{2\pi} \frac{F \sin\theta}{\rho u_m^2 D} d\theta, \tag{A3.6}$$

and

$$C_D = \frac{\int_0^{2\pi} F \cos\theta d\theta}{\frac{1}{2}\rho D \int_0^{2\pi} (Vc - u_m \cos\theta)|Vc - u_m \cos\theta| \cos\theta d\theta}. \tag{A3.7}$$

The steps of finding eq. (A3.6) are described in detail in Appendix 1.

Carrying out the integration in eq. (A3.6), the inertia coefficient is found as

$$C_M = \frac{D^2}{2A\pi^2}\frac{u_m T}{D}\int_0^{2\pi}\frac{F\sin\theta}{\rho u_m{}^2 D}d\theta. \qquad \text{(A3.8)}$$

The inertia coefficient is equivalent to that in wavy flow since the current velocity Vc does not appear explicitly in the inertia term of the modified Morison equation.

The eq. (A3.7) may be integrated partially to give

$$C_D = -\frac{1}{\frac{1}{2}\rho D u_m{}^2 R}\int_0^{2\pi} F\cos\theta d\theta, \qquad \text{(A3.9)}$$

where

$$R = 2\pi\frac{Vc}{u_m} \quad \text{for} \frac{Vc}{u_m} \geq 1 \qquad \text{(A3.10)}$$

which is the case in this study, and

$$R = 4\left(\frac{Vc}{u_m}\right)^2 \sin\zeta + 2\frac{Vc}{u_m}(2\zeta - \sin 2\zeta - \pi) + \frac{1}{3}(\sin 3\zeta + 9\sin\zeta) \quad \text{for} \frac{Vc}{u_m} < 1, \qquad \text{(A3.11)}$$

where $\zeta = \cos^{-1}(-\frac{Vc}{u_m})$,

(Sarpkaya et al. (1984), Sarpkaya and Storm (1985) and Chakrabarti (1987)).

The above method assumes that the hydrodynamic coefficients are invariant over a wave cycle.

APPENDIX 4

COMPARISON OF MEASURED AND COMPUTED MORISON FORCES

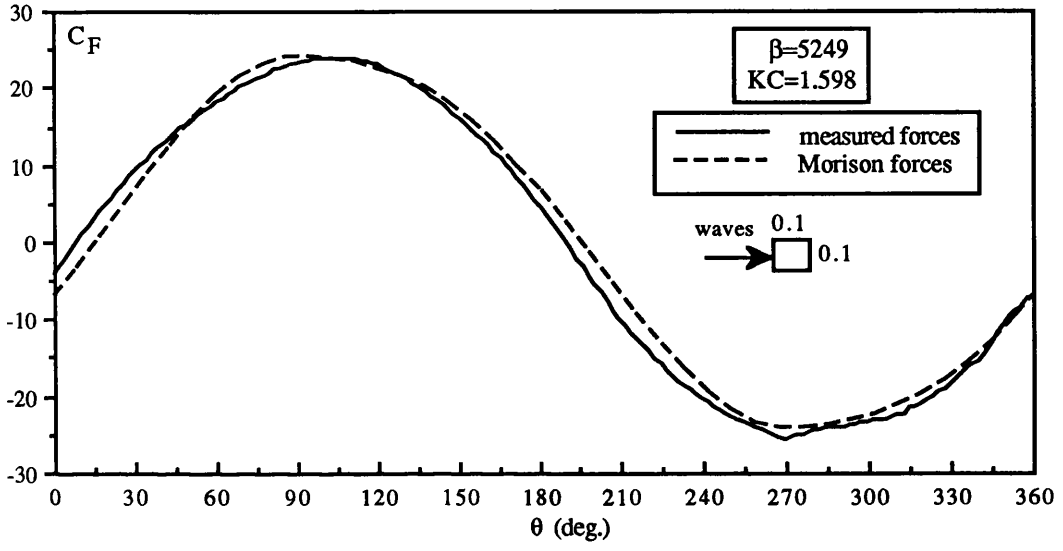

Fig. A1 Comparison of measured and computed forces on a vertical cylinder with d/D=1 in waves

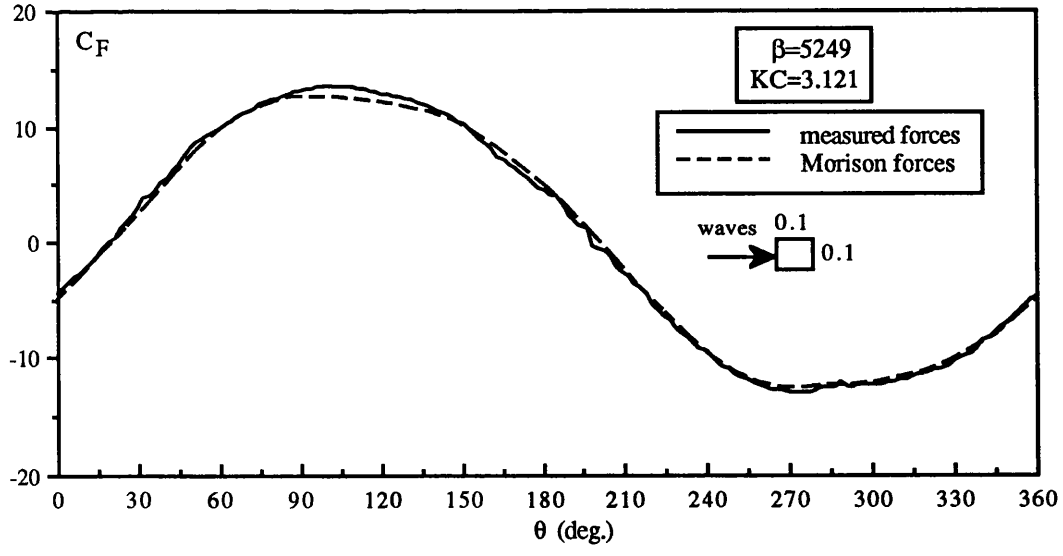

Fig. A2 Comparison of measured and computed forces on a vertical cylinder with d/D=1 in waves

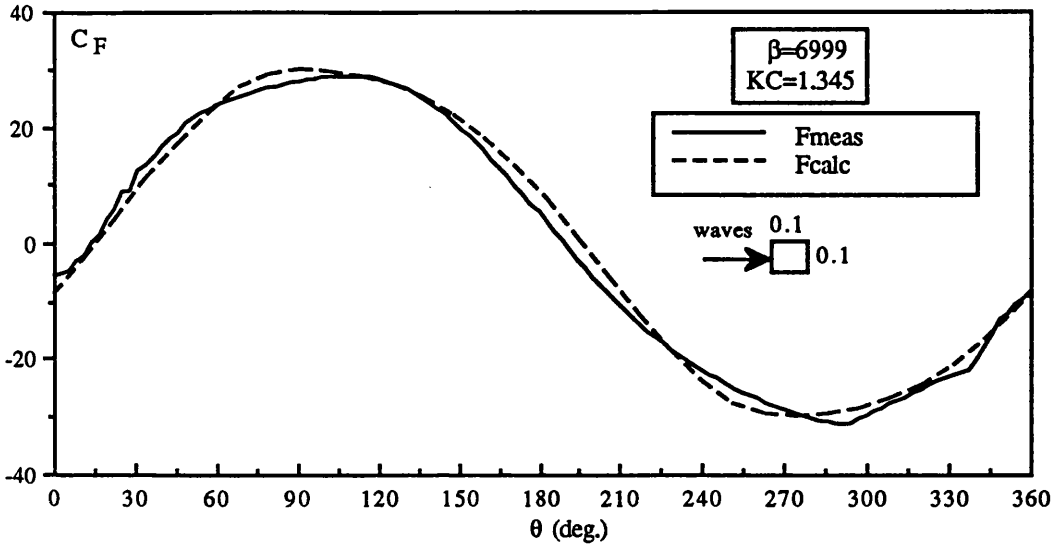

Fig. A3 Comparison of measured and computed forces on a vertical cylinder with d/D=1 in waves

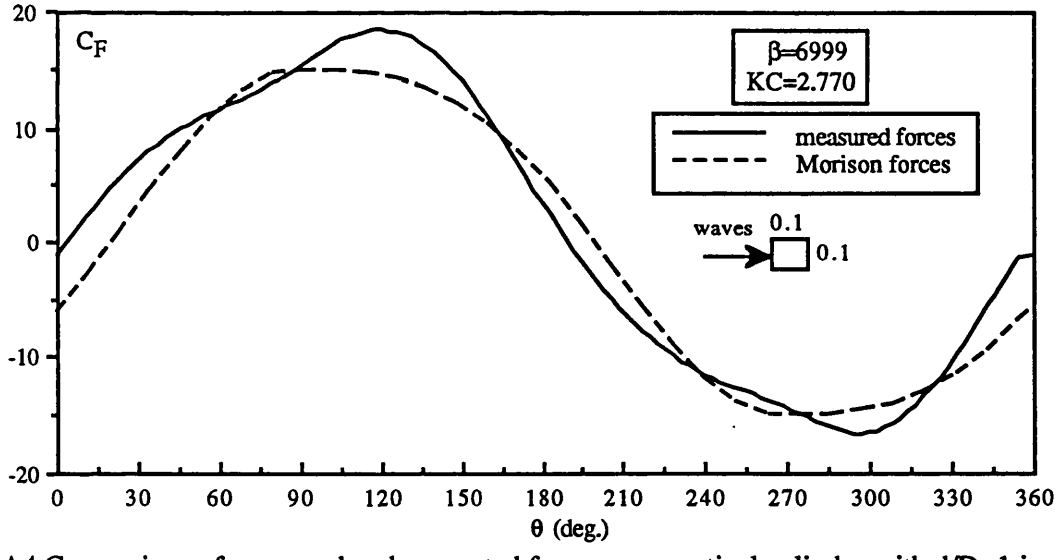

Fig. A4 Comparison of measured and computed forces on a vertical cylinder with d/D=1 in waves

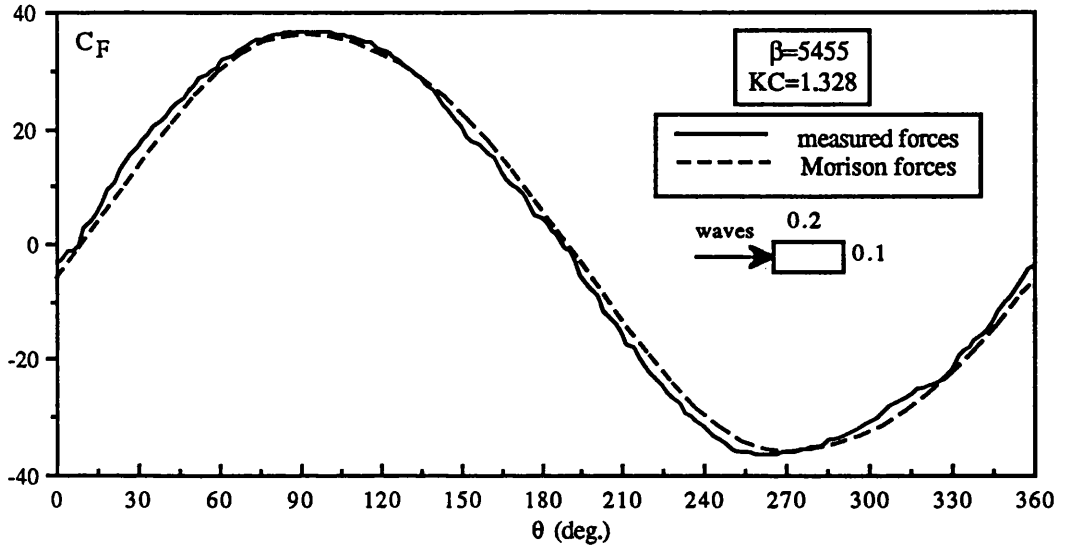

Fig. A5 Comparison of measured and computed forces on a vertical cylinder with d/D=2 in waves

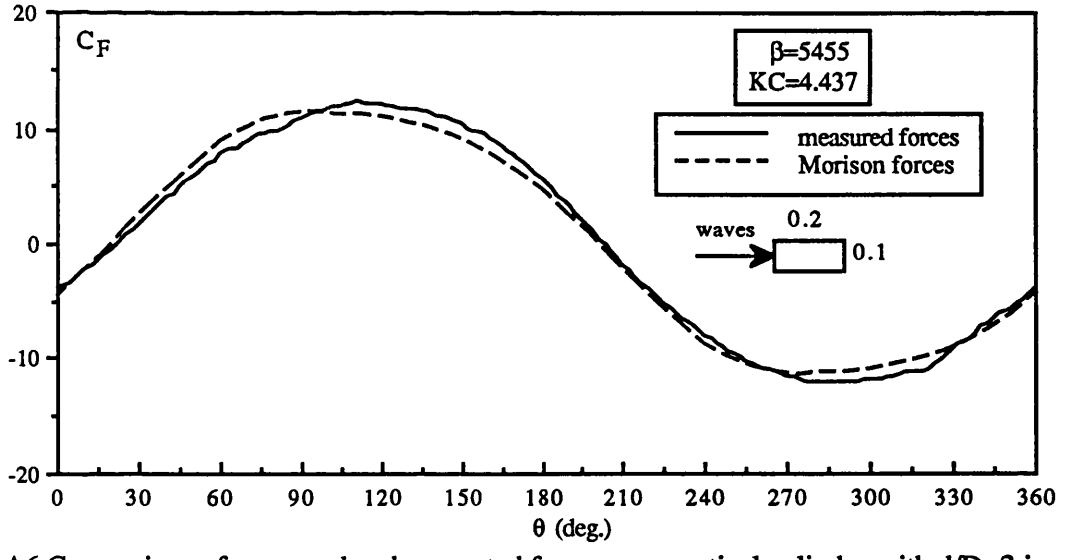

Fig. A6 Comparison of measured and computed forces on a vertical cylinder with d/D=2 in waves

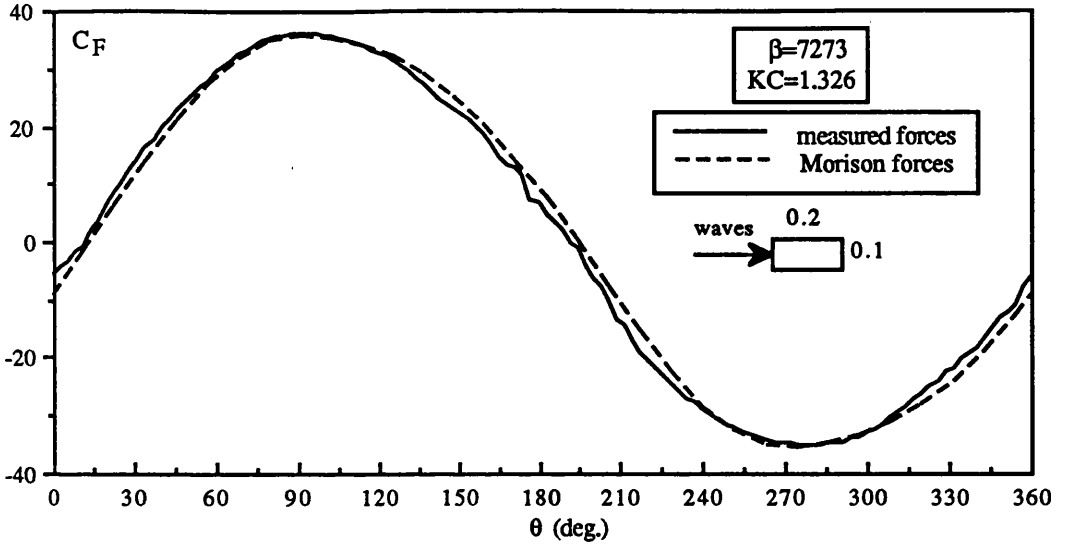

Fig. A7 Comparison of measured and computed forces on a vertical cylinder with d/D=2 in waves

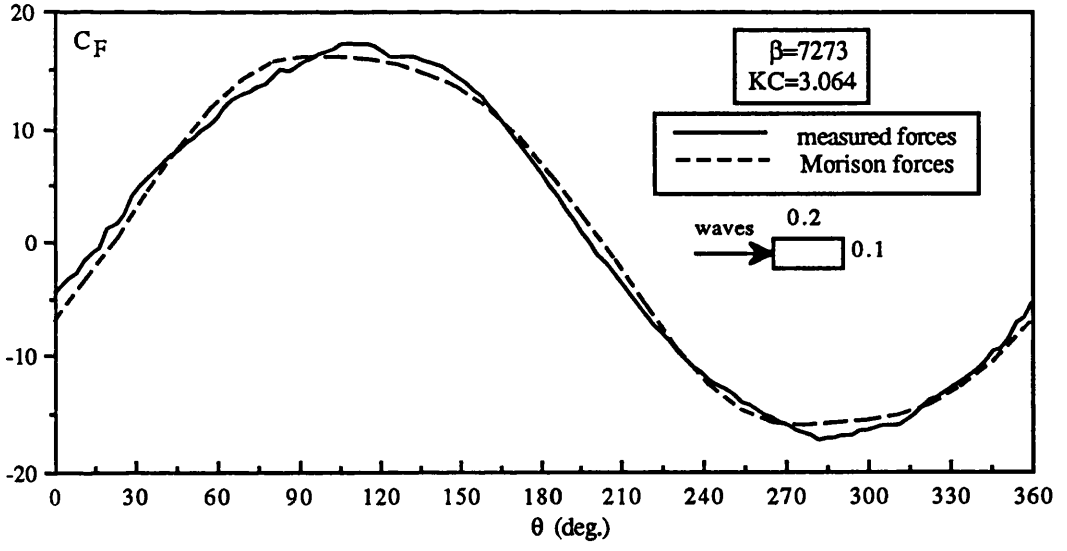

Fig. A8 Comparison of measured and computed forces on a vertical cylinder with d/D=2 in waves

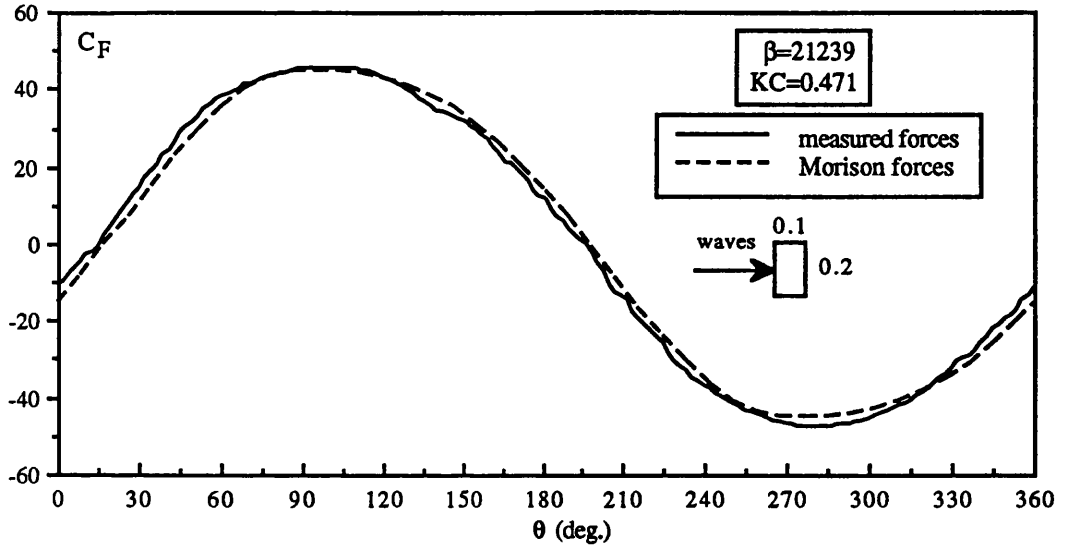

Fig. A9 Comparison of measured and computed forces on a vertical cylinder with d/D=0.5 in waves

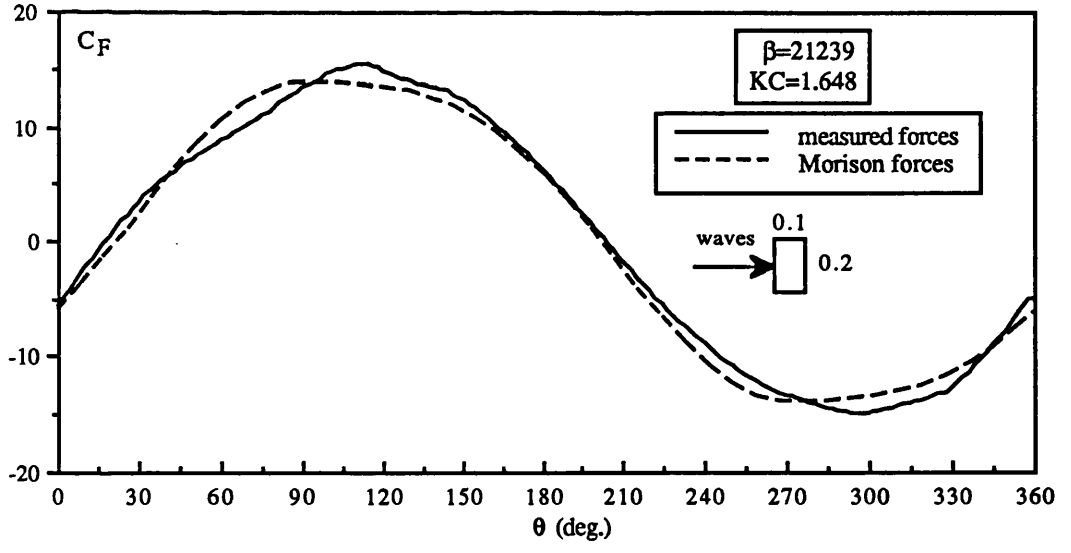

Fig. A10 Comparison of measured and computed forces on a vertical cylinder with d/D=0.5 in waves

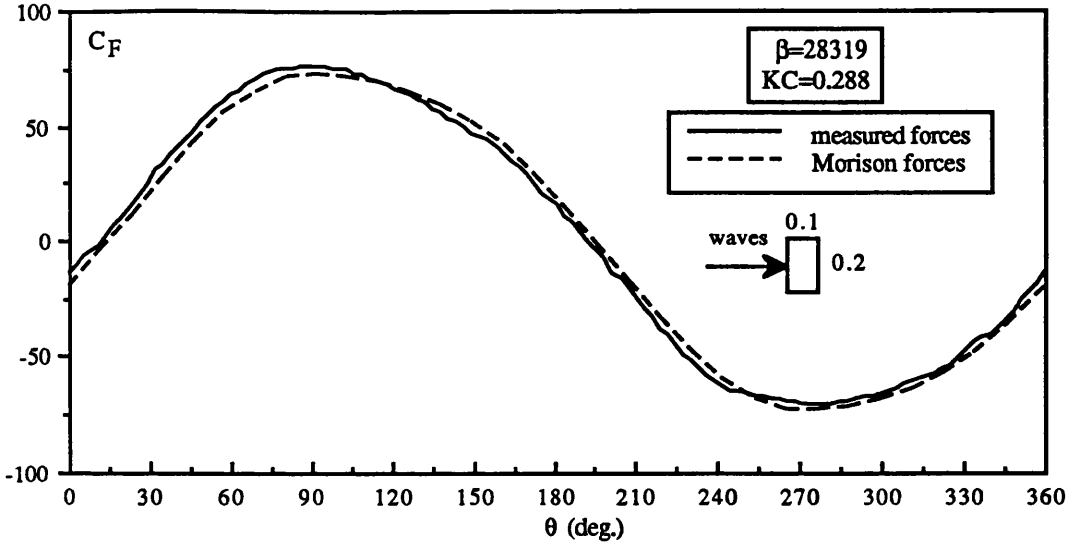

Fig. A11 Comparison of measured and computed forces on a vertical cylinder with d/D=0.5 in waves

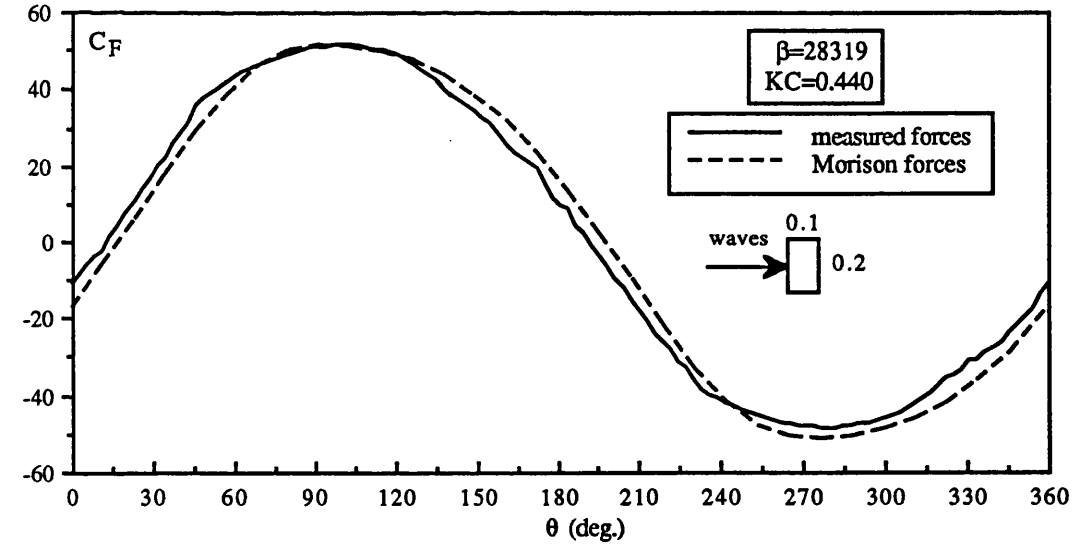

Fig. A12 Comparison of measured and computed forces on a vertical cylinder with d/D=0.5 in waves

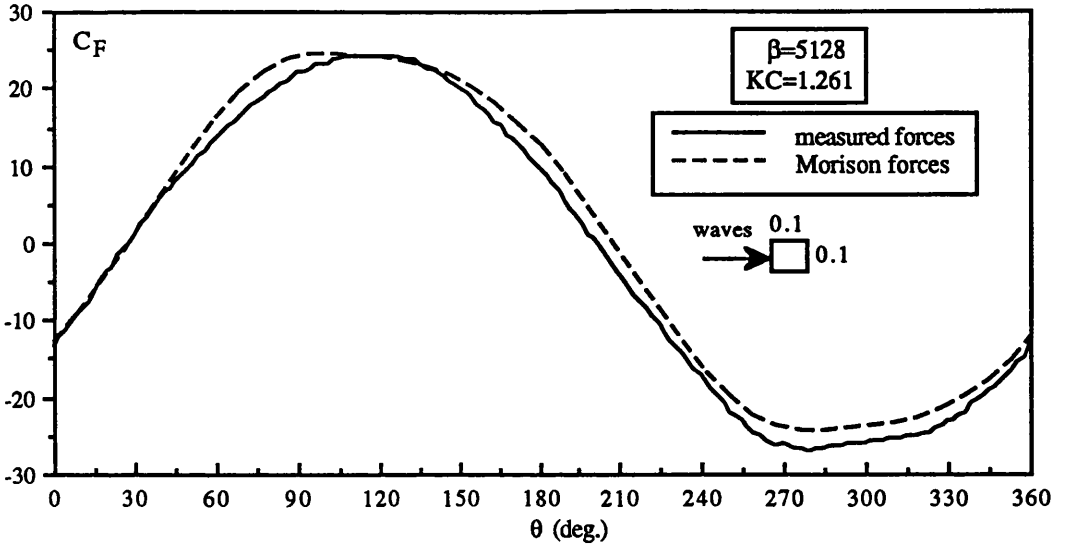

Fig. A13 Comparison of measured and computed in-line forces on a horizontal cylinder with d/D=1 in waves

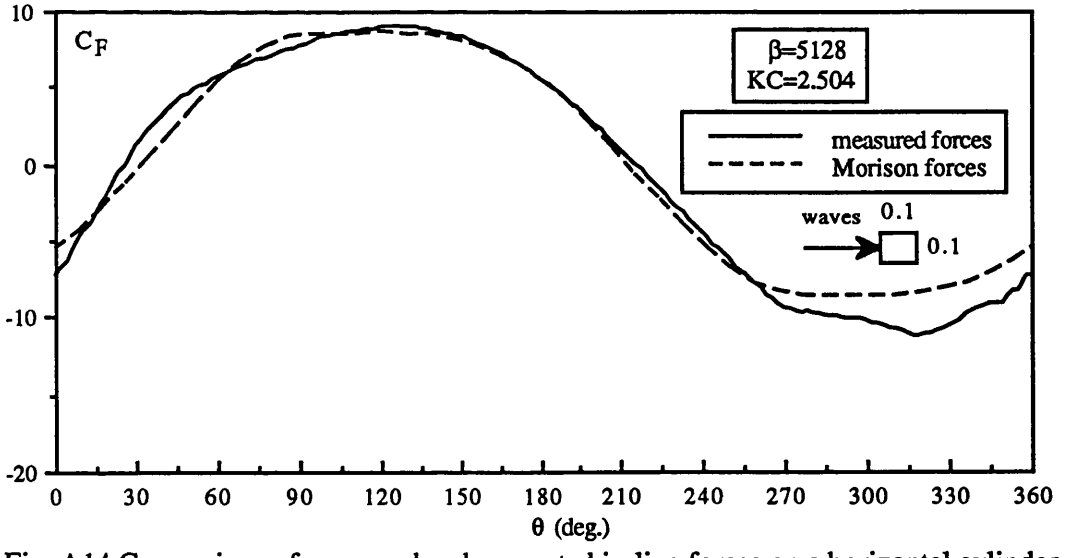

Fig. A14 Comparison of measured and computed in-line forces on a horizontal cylinder with d/D=1 in waves

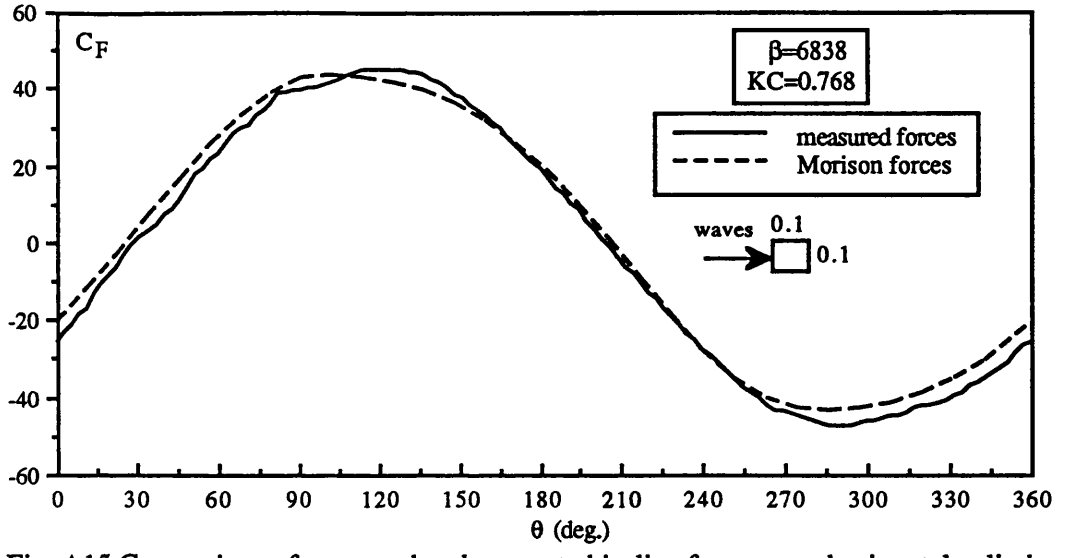

Fig. A15 Comparison of measured and computed in-line forces on a horizontal cylinder with d/D=1 in waves

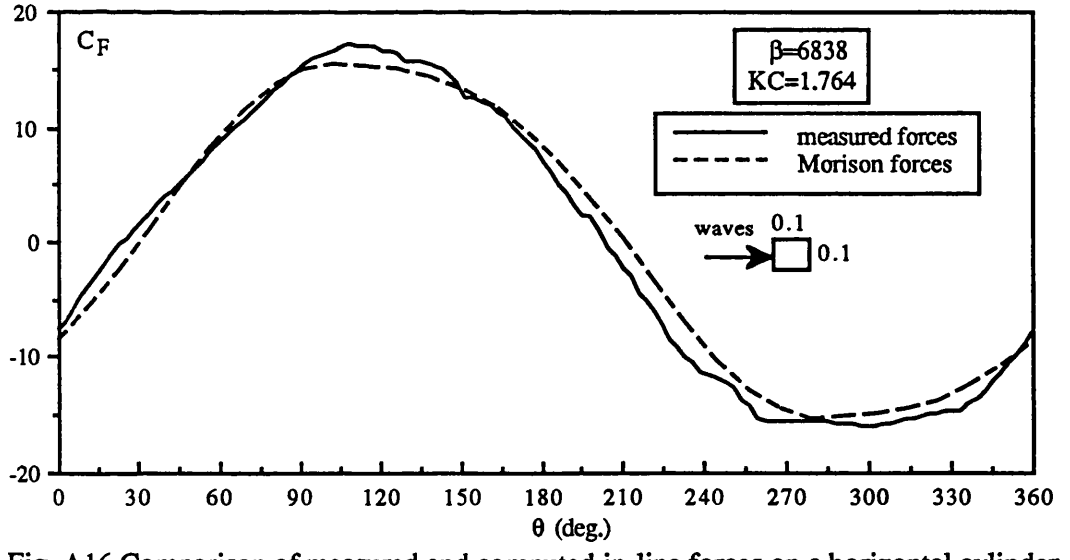

Fig. A16 Comparison of measured and computed in-line forces on a horizontal cylinder with d/D=1 in waves

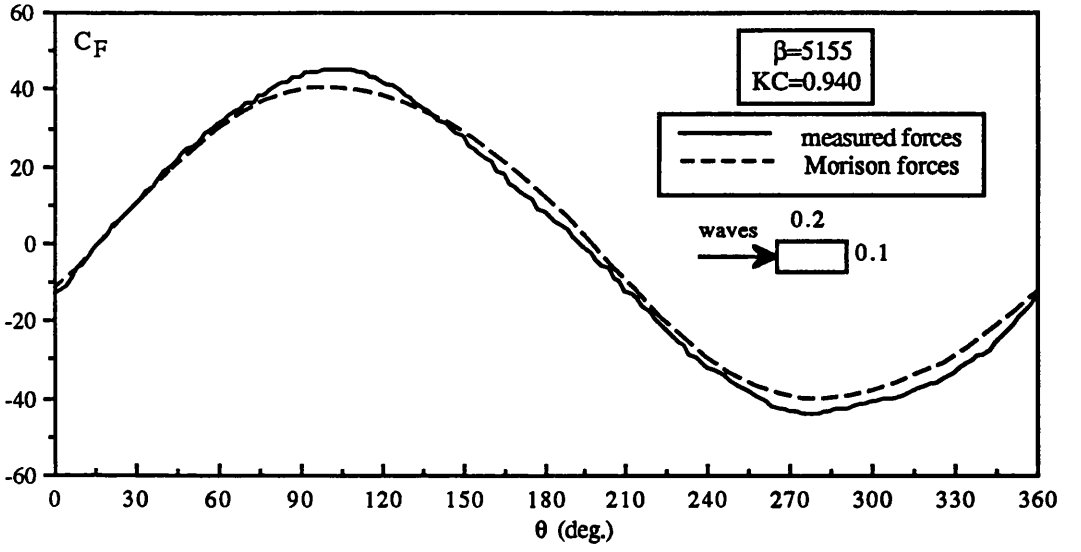

Fig. A17 Comparison of measured and computed in-line forces on a horizontal cylinder with d/D=2 in waves

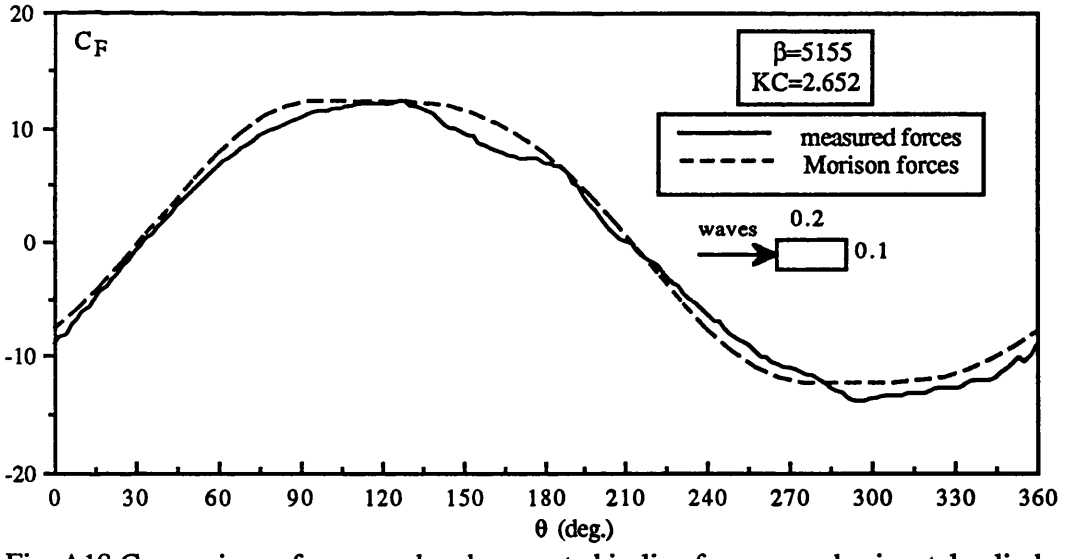

Fig. A18 Comparison of measured and computed in-line forces on a horizontal cylinder with d/D=2 in waves

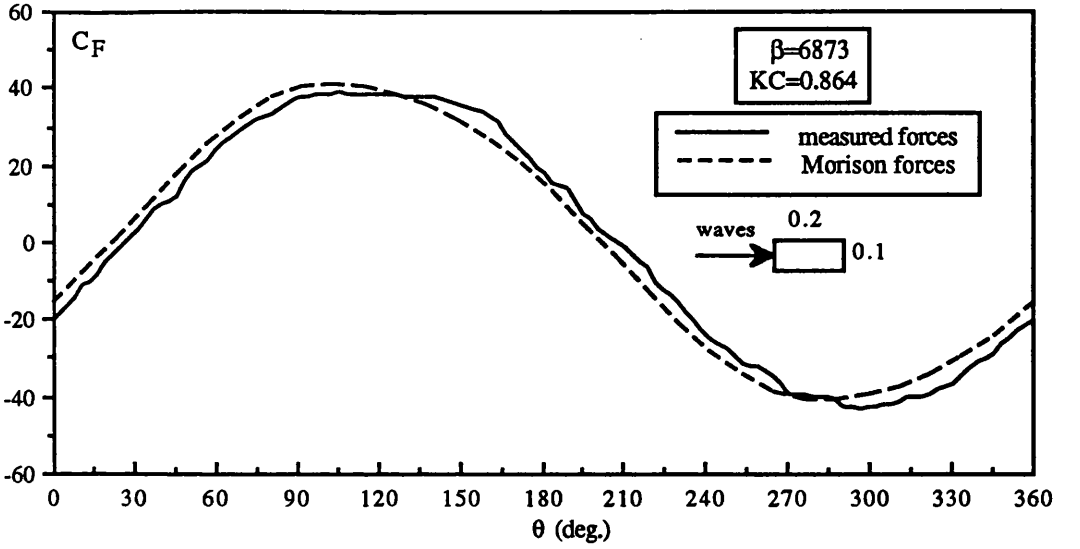

Fig. A19 Comparison of measured and computed in-line forces on a horizontal cylinder with d/D=2 in waves

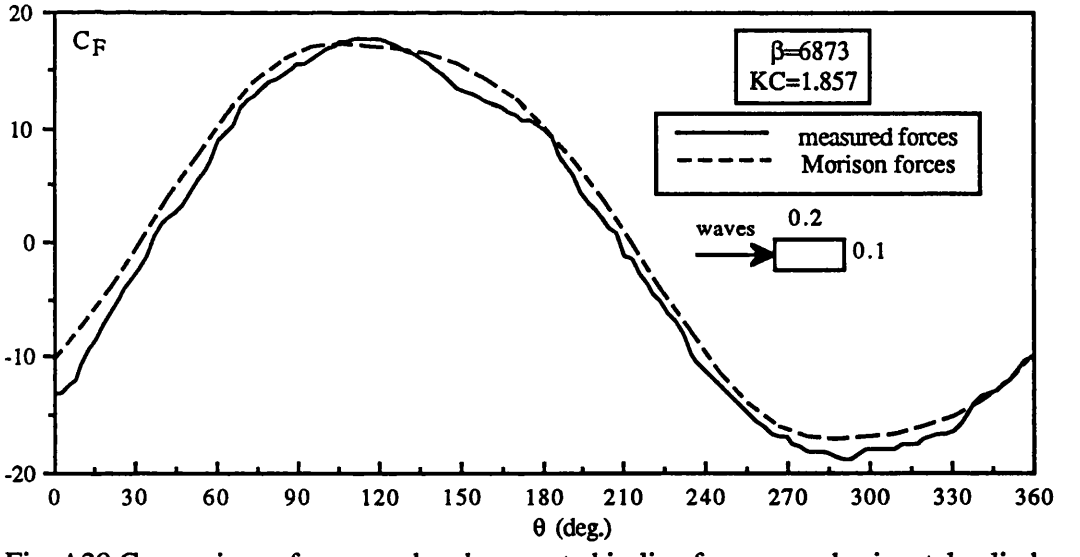

Fig. A20 Comparison of measured and computed in-line forces on a horizontal cylinder with d/D=2 in waves

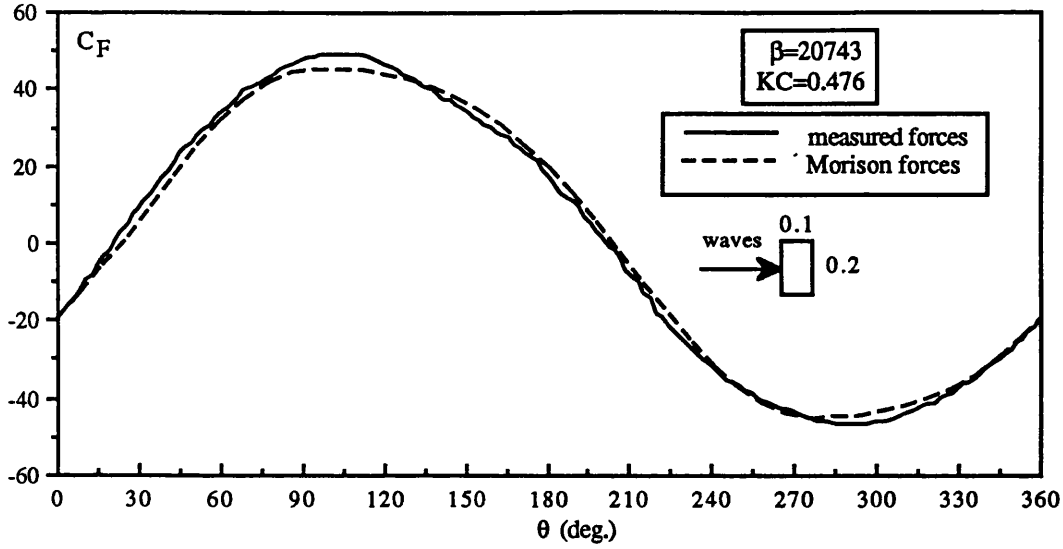

Fig. A21 Comparison of measured and computed in-line forces on a horizontal cylinder with d/D=0.5 in waves

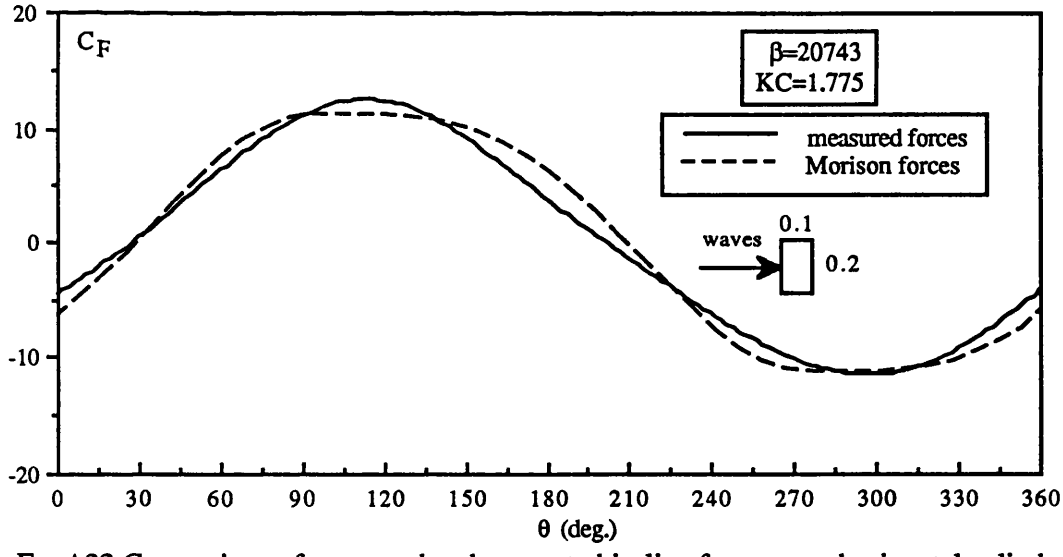

Fg. A22 Comparison of measured and computed in-line forces on a horizontal cylinder with d/D=0.5 in waves

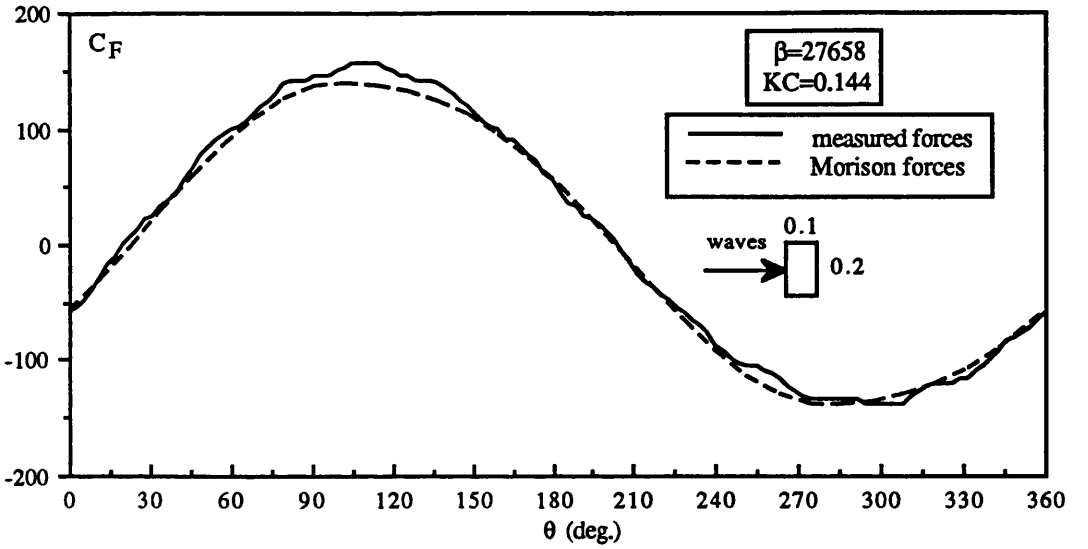

Fig. A23 Comparison of measured and computed in-line forces on a horizontal cylinder with d/D=0.5 in waves

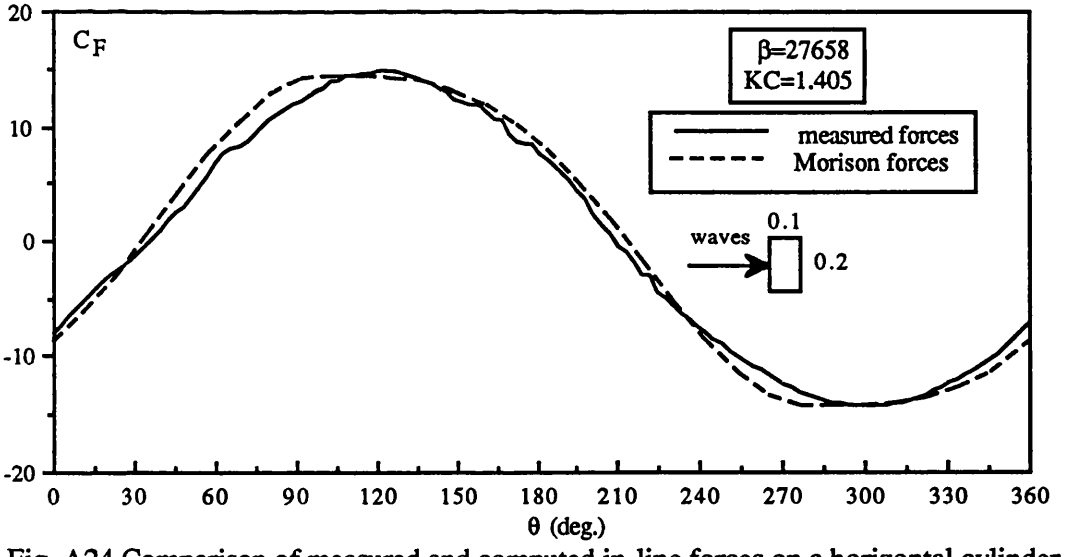

Fig. A24 Comparison of measured and computed in-line forces on a horizontal cylinder wih d/D=0.5 in waves

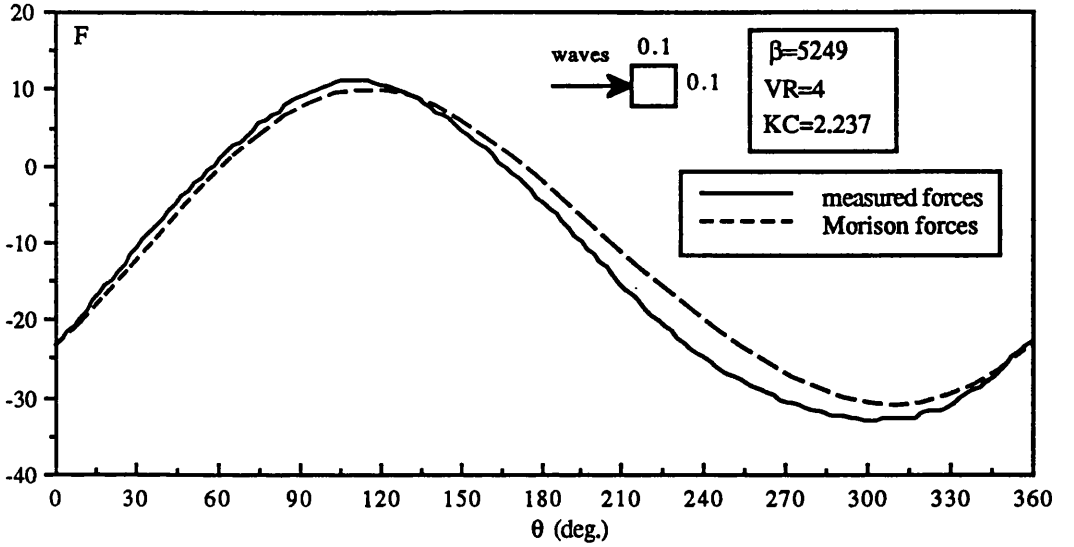

Fig. A25 Comparison of measured and computed forces on a vertical cylinder with d/D=1 in waves and current

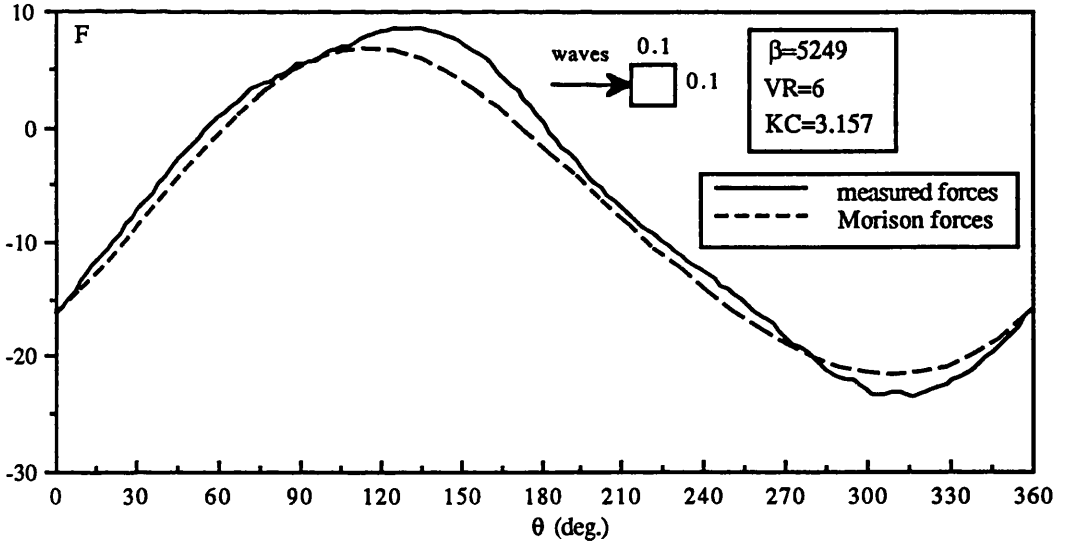

Fig. A26 Comparison of measured and computed forces on a vertical cylinder with d/D=1 in waves and current

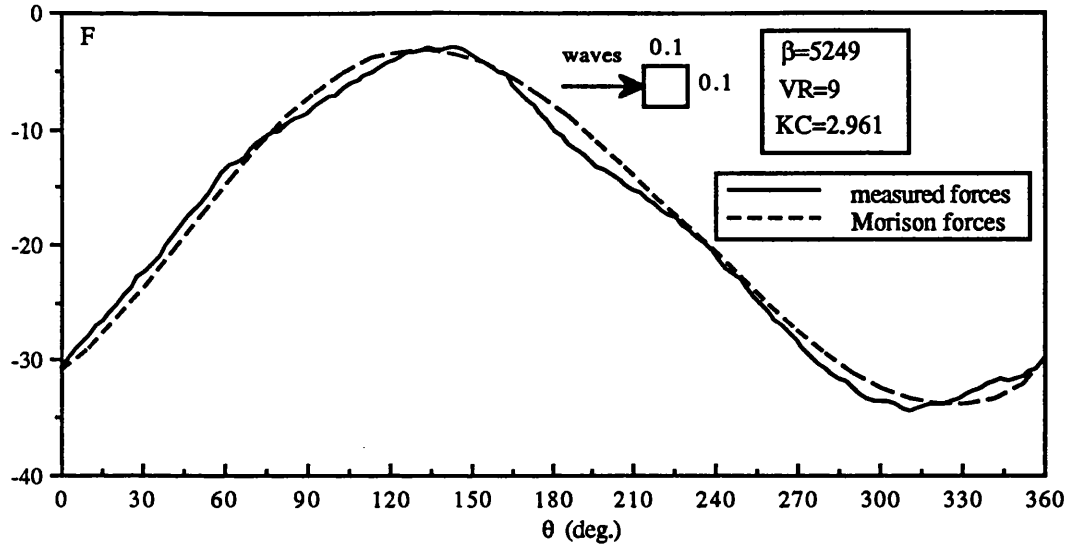

Fig. A27 Comparison of measured and computed forces on a vertical cylinder with d/D=1 in waves and current

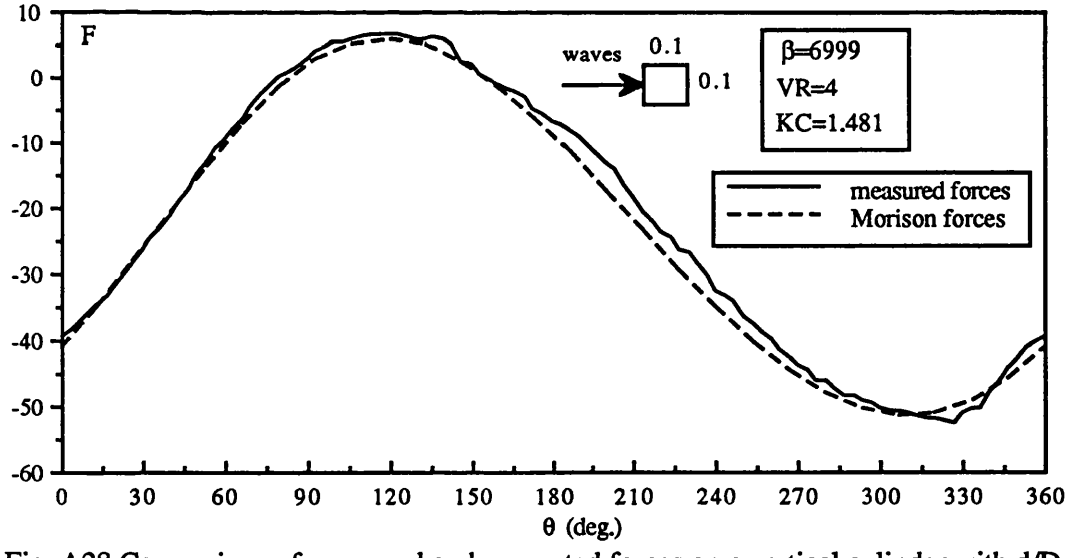

Fig. A28 Comparison of measured and computed forces on a vertical cylinder with d/D=1 in waves and current

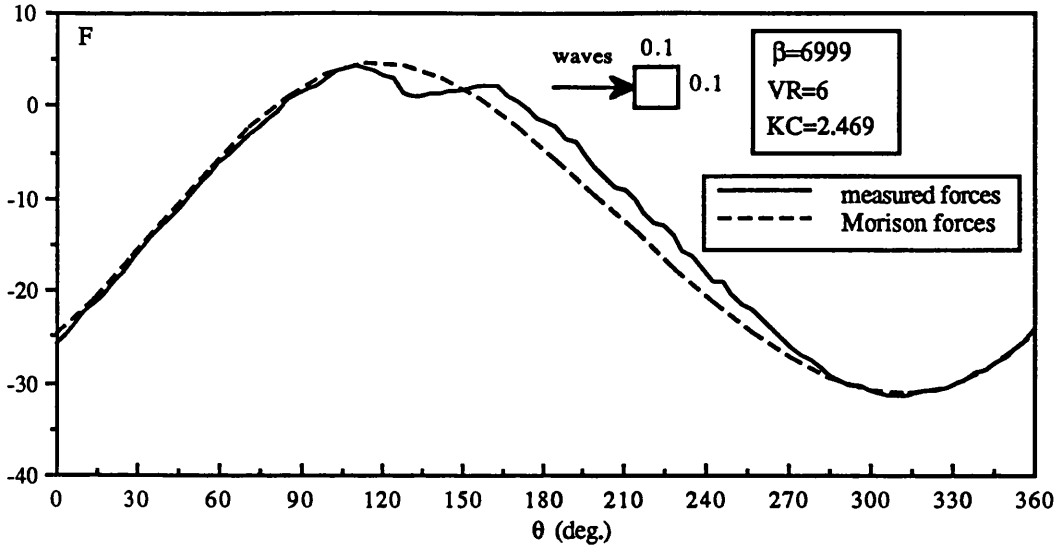

Fig. A29 Comparison of measured and computed forces on a vertical cylinder with d/D=1 in waves and current

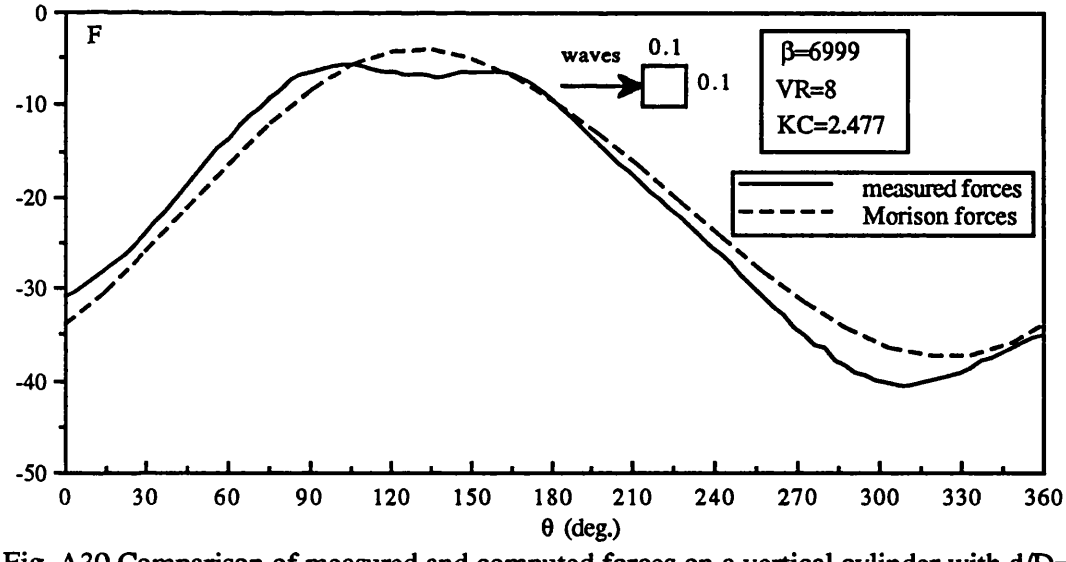

Fig. A30 Comparison of measured and computed forces on a vertical cylinder with d/D=1 in waves and current

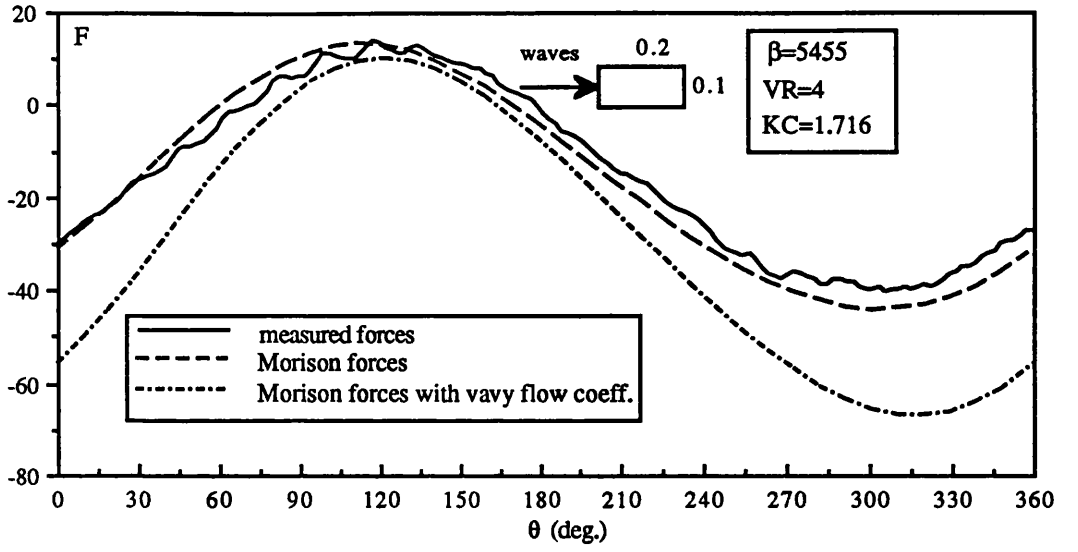

Fig. A31 Comparison of measured and computed forces on a vertical cylinder with d/D=2 in waves and current

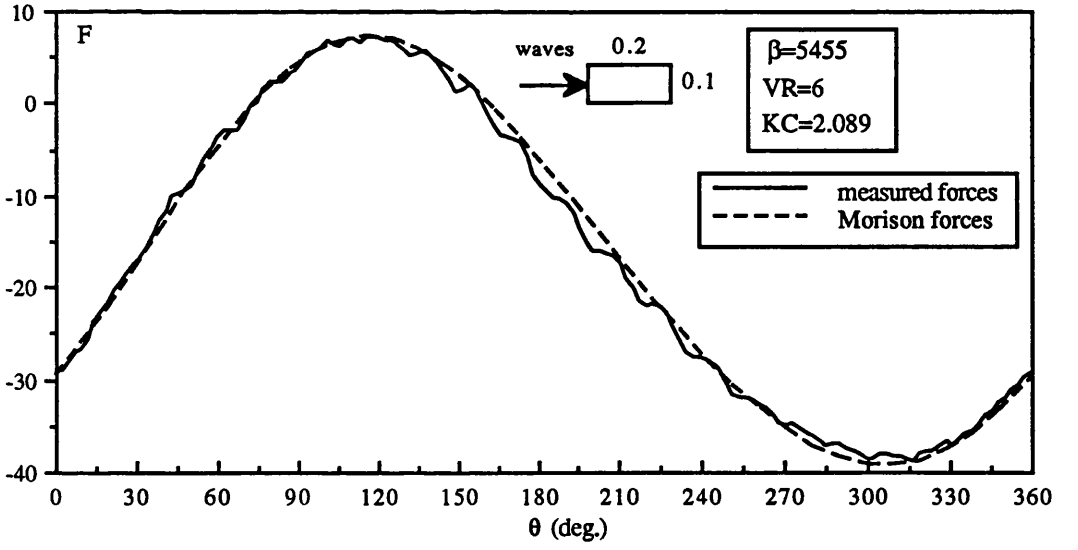

Fig. A32 Comparison of measured and computed forces on a vertical cylinder with d/D=2 in waves and current

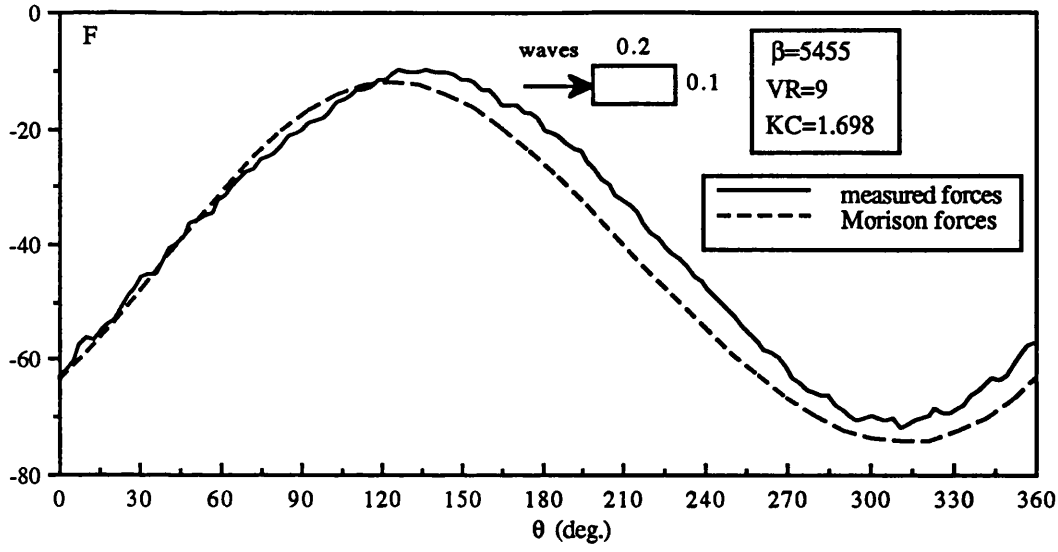

Fig. A33 Comparison of measured and computed forces on a vertical cylinder with d/D=2 in waves and current

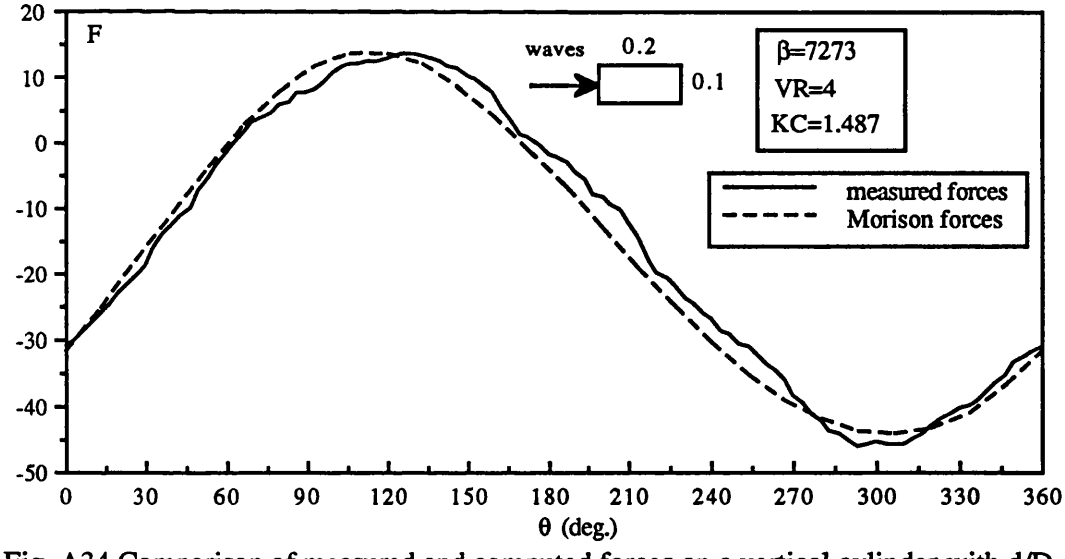

Fig. A34 Comparison of measured and computed forces on a vertical cylinder with d/D=2 in waves and current

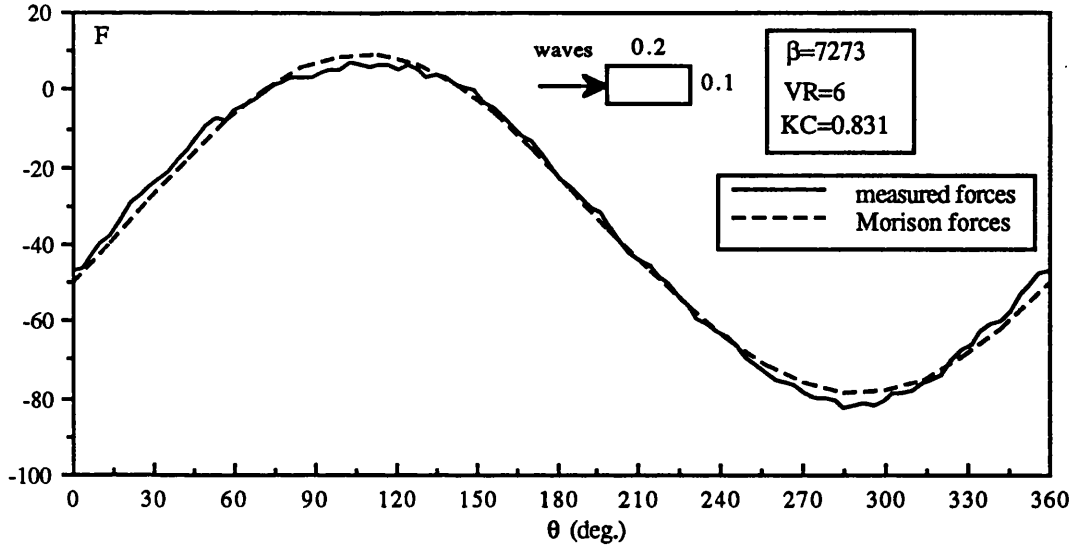

Fig. A35 Comparison of measured and computed forces on a vertical cylinder with d/D=2 in waves and current

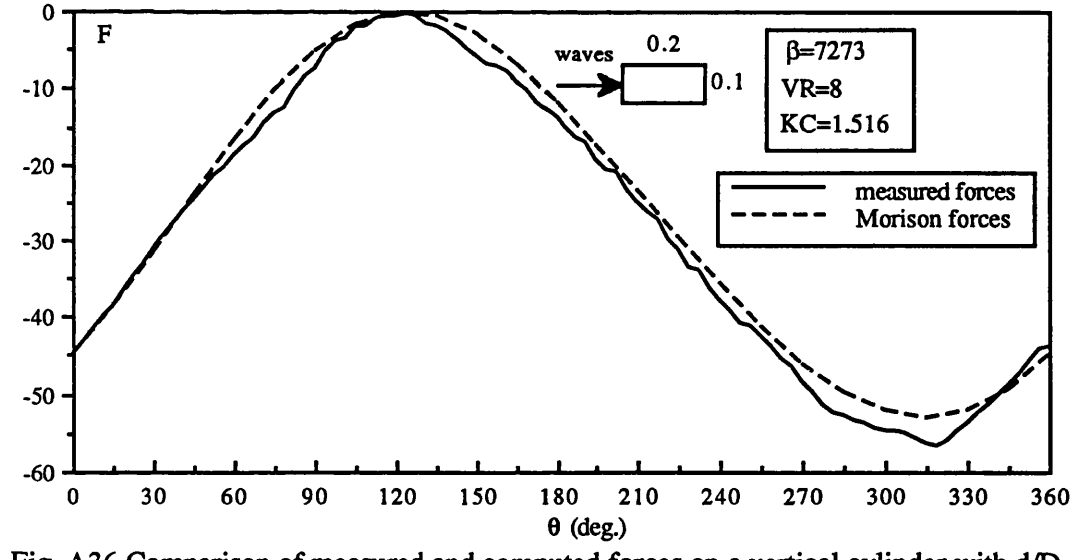

Fig. A36 Comparison of measured and computed forces on a vertical cylinder with d/D=2 in waves and current

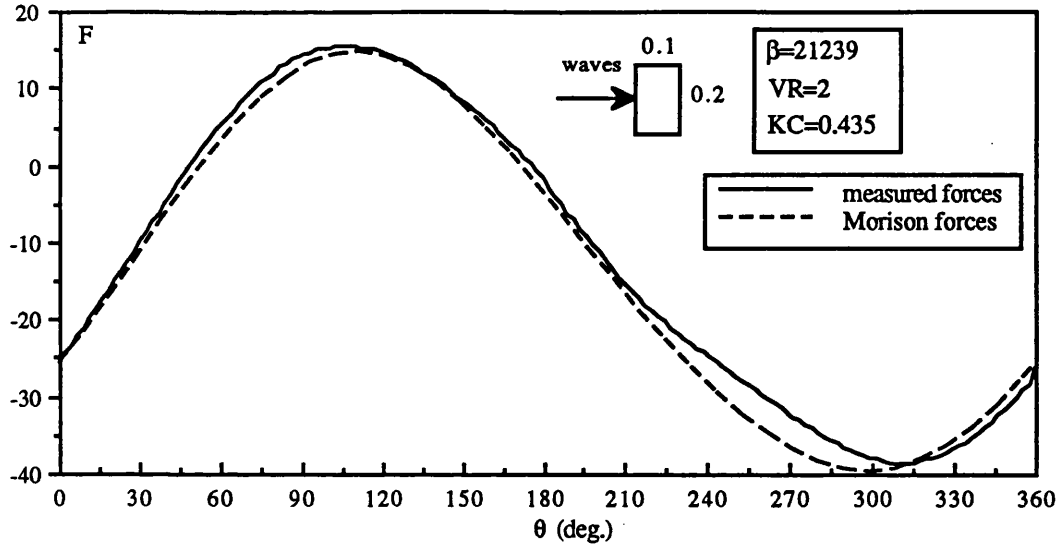

Fig. A37 Comparison of measured and computed forces on a vertical cylinder wih d/D=0.5 in waves and current

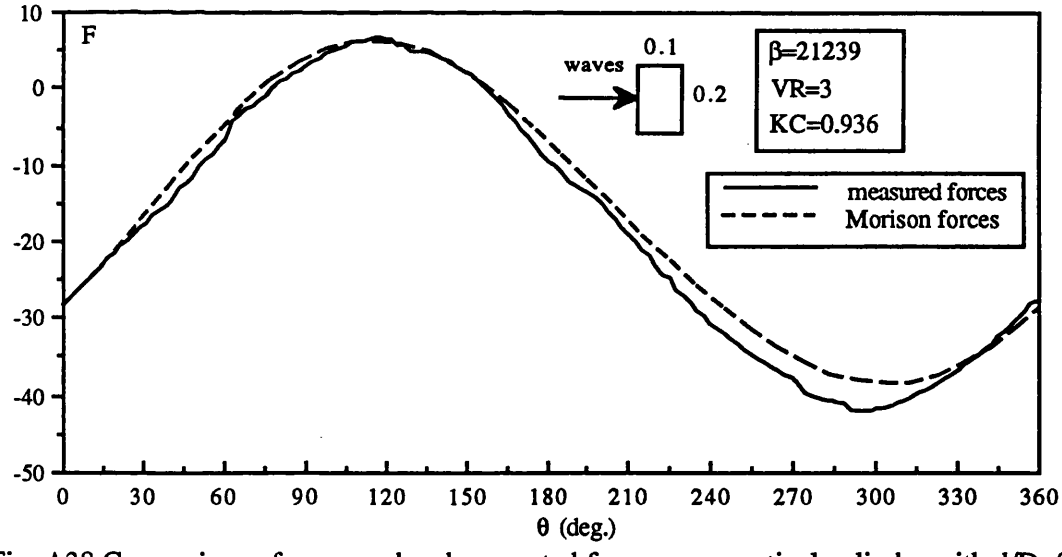

Fig. A38 Comparison of measured and computed forces on a vertical cylinder with d/D=0.5 in waves and current

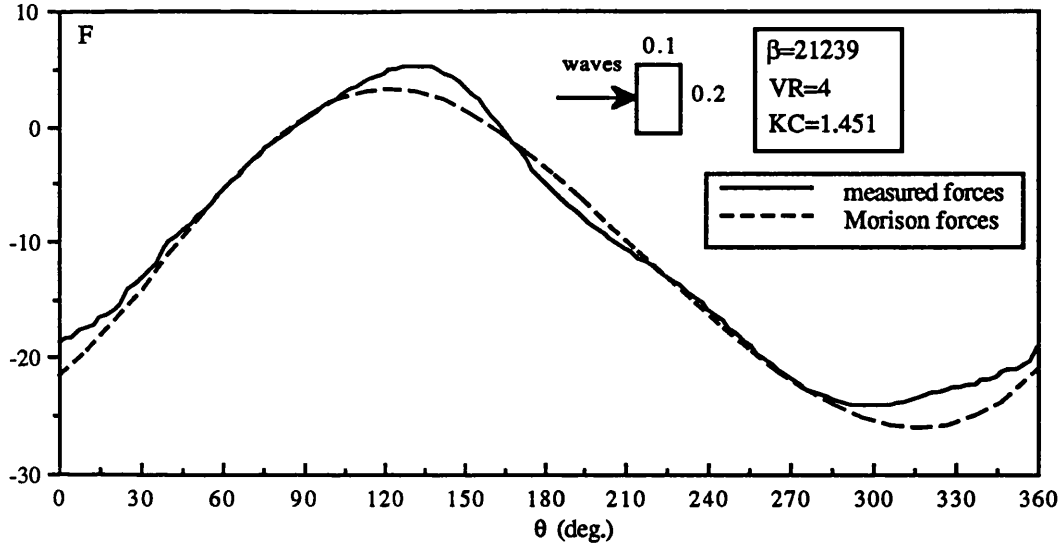

Fig. A39 Comparison of measured and computed forces on a vertical cylinder with d/D=0.5 in waves and current

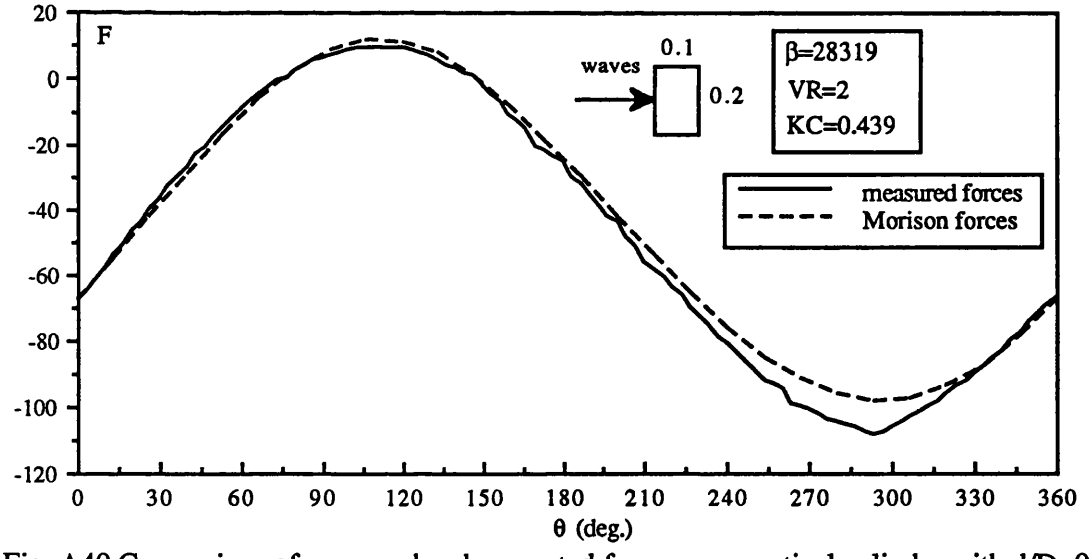

Fig. A40 Comparison of measured and computed forces on a vertical cylinder with d/D=0.5 in waves and current

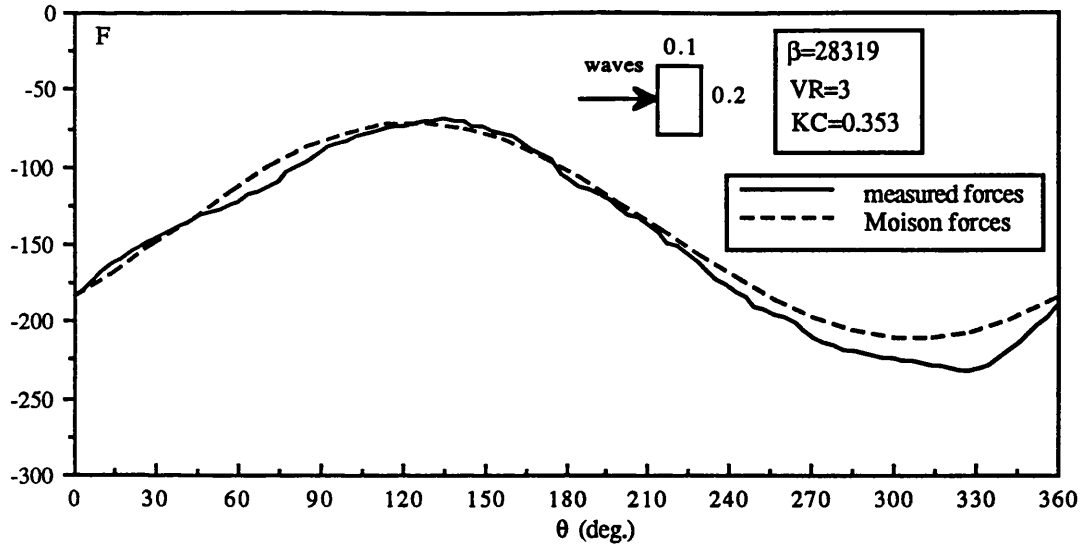

Fig. A41 Comparison of measured anf computed forces on a vertical cylinder with d/D=0.5 in waves and current

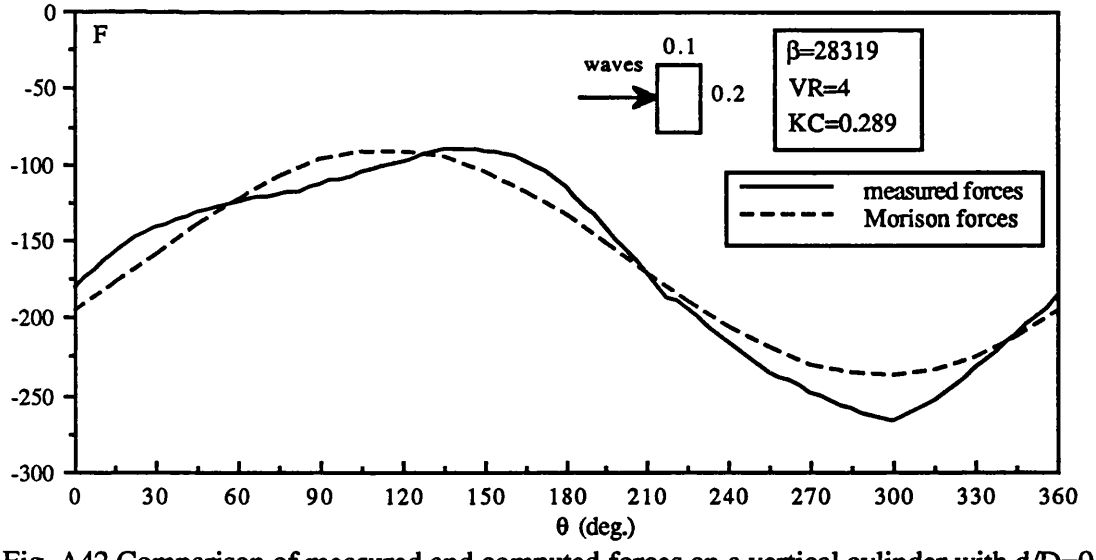

Fig. A42 Comparison of measured and computed forces on a vertical cylinder with d/D=0.5 in waves and current

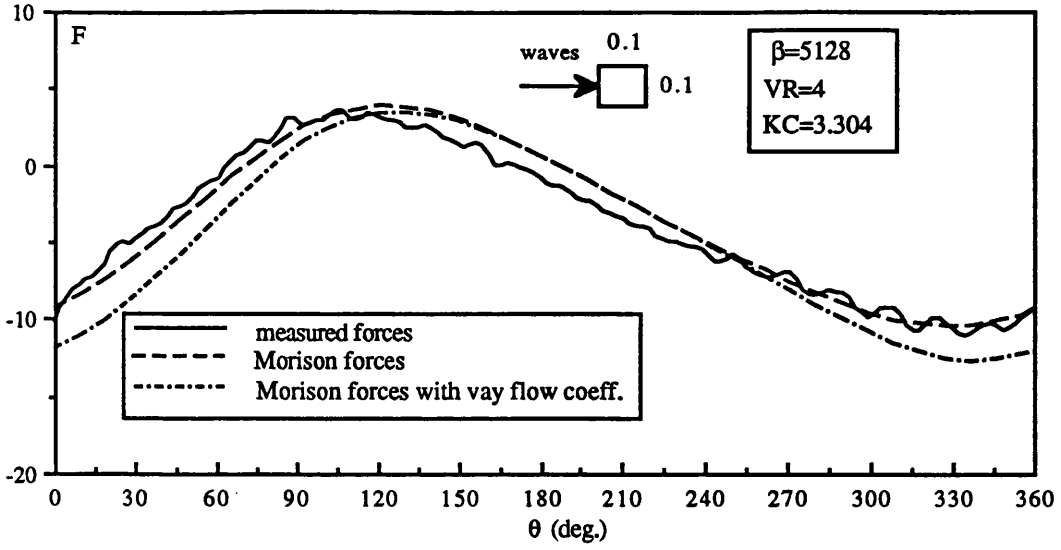

Fig. A43 Comparison of measured and computed in-line forces on a horizontal cylinder with d/D=1 in waves and current

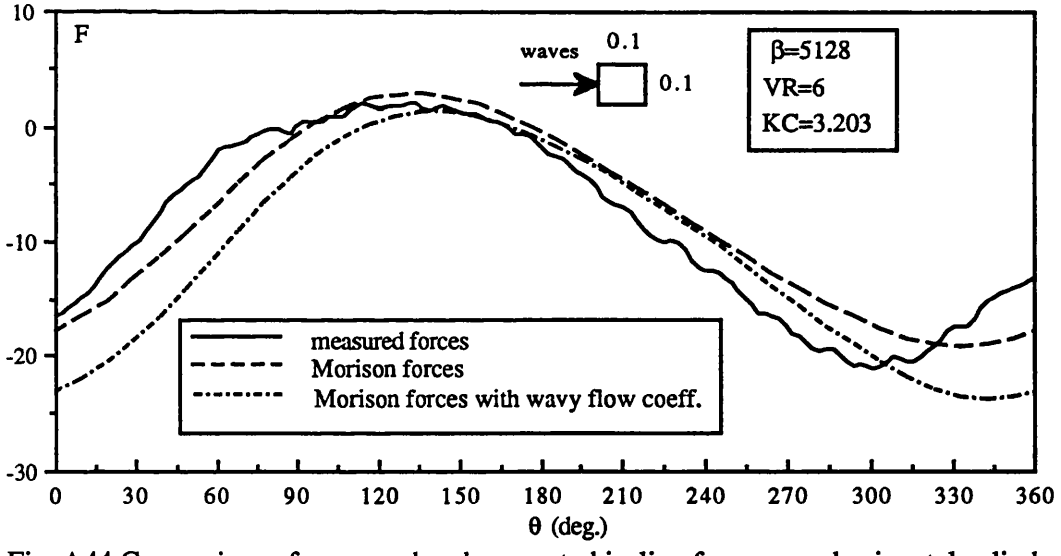

Fig. A44 Comparison of measured and computed in-line forces on a horizontal cylinder with d/D=1 in waves and current

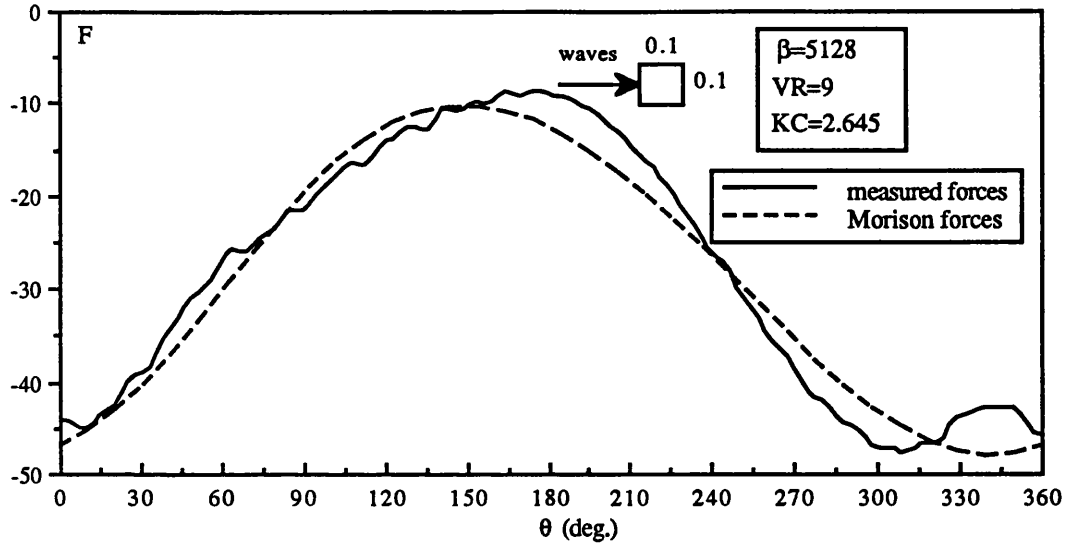

Fig. A45 Comparison of measured and computed in-line forces on a horizontal cylinder with d/D=1 in waves and current

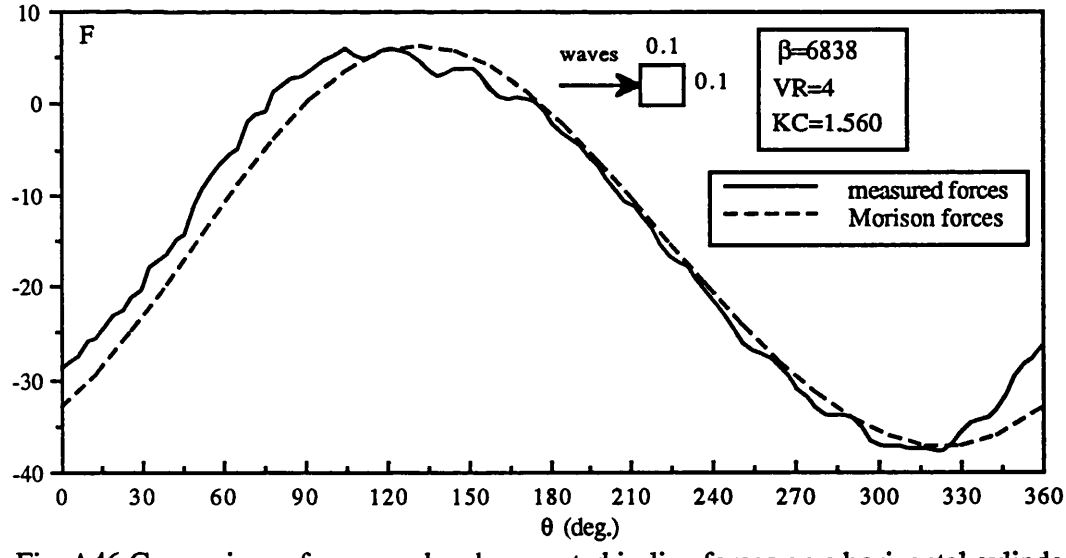

Fig. A46 Comparison of measured and computed in-line forces on a horizontal cylinder with d/D=1 in waves and current

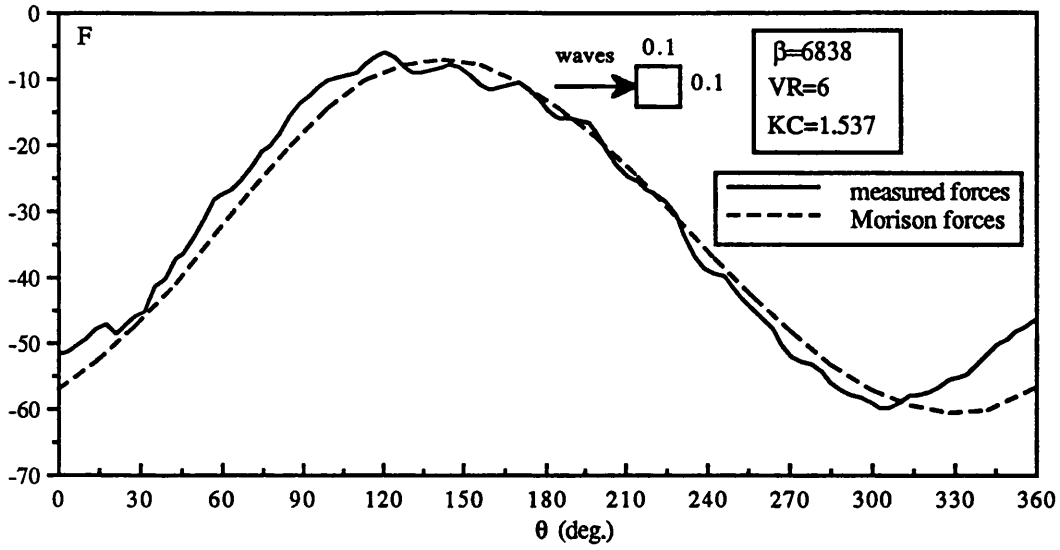

Fig. A47 Comparison of measured and computed in-line forces on a horizontal cylinder with d/D=1 in waves and current

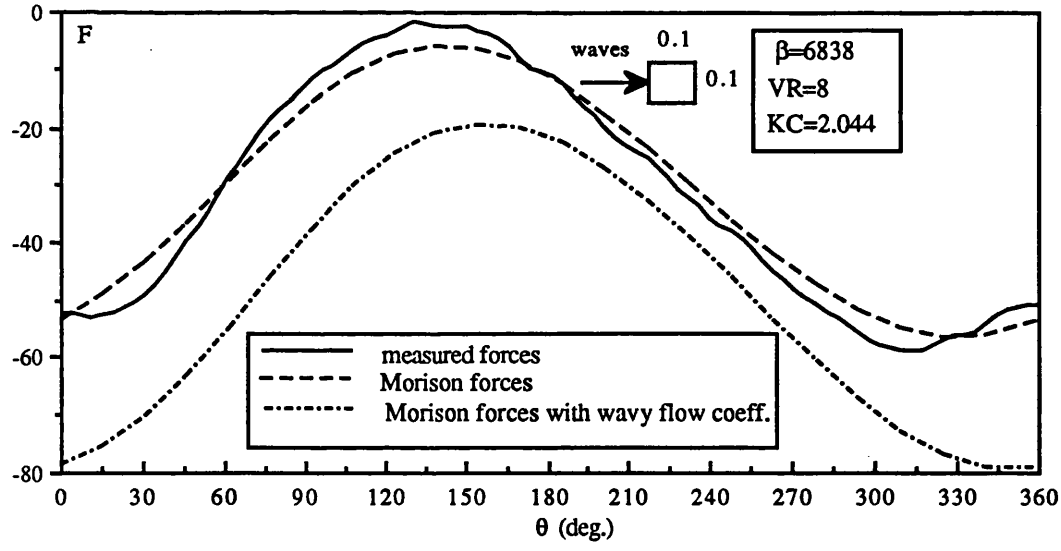

Fig. A48 Comparison of measured and computed in-line forces on a horizontal cylinder wih d/D=1 in waves and current

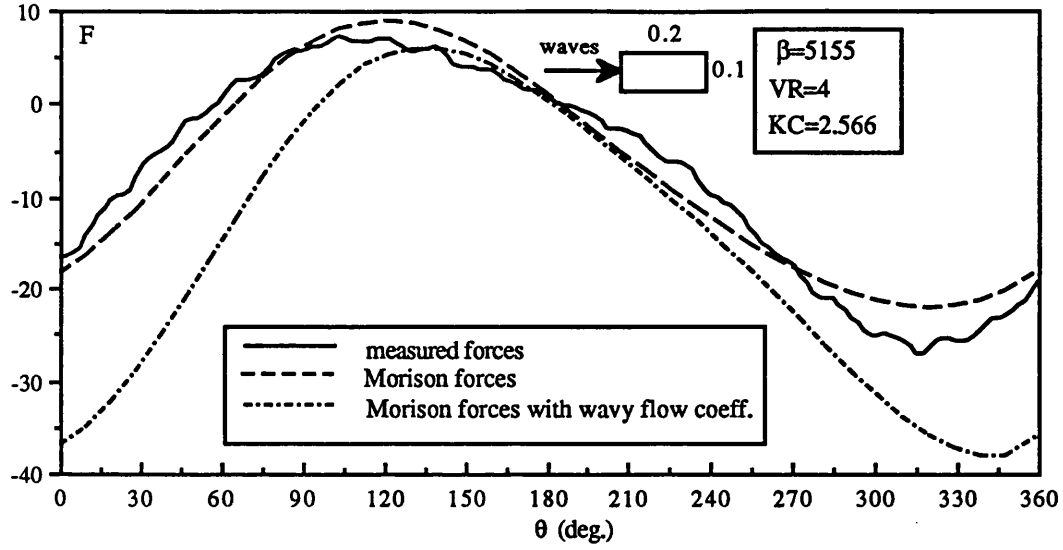

Fig. A49 Comparison of measured and computed in-line forces on a horizontal cylinder with d/D=2 in waves and current

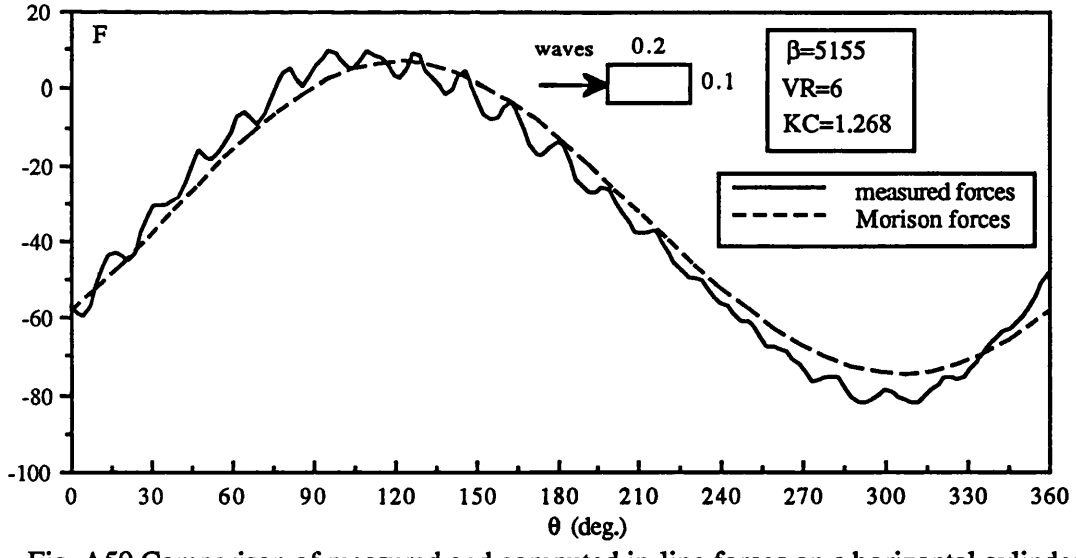

Fig. A50 Comparison of measured and computed in-line forces on a horizontal cylinder with d/D=2 in waves and current

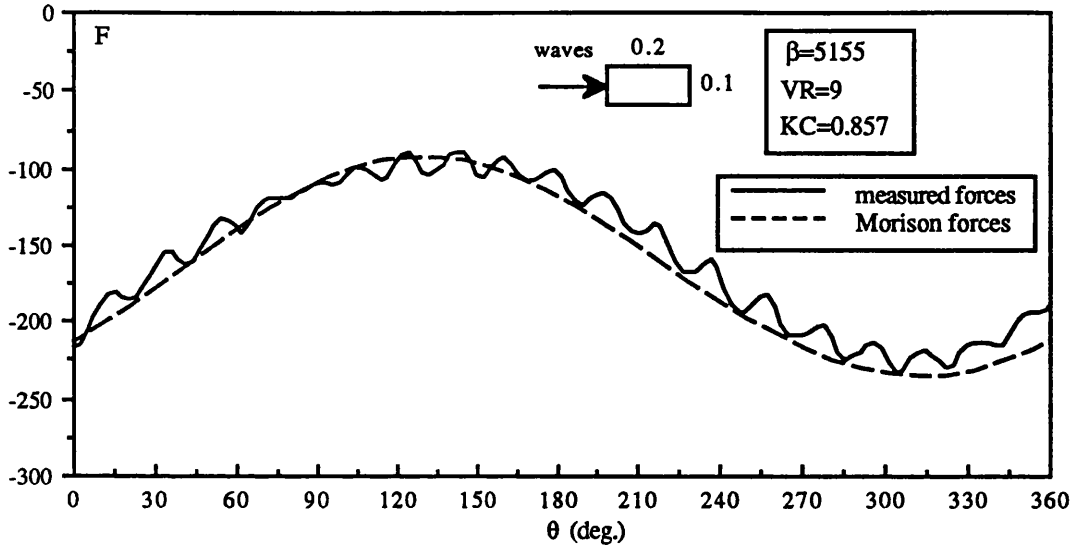

Fig. A51 Comparison of measured and computed in-line forces on a horizontal cylinder wih d/D=2 in waves and current

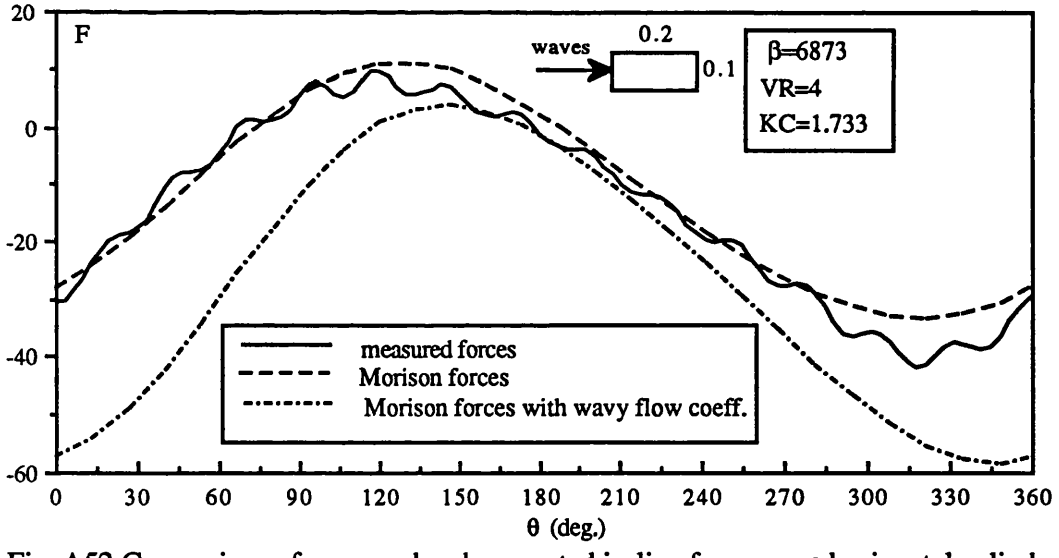

Fig. A52 Comparison of measured and computed in-line forces on a horizontal cylinder with d/D=2 in waves and current

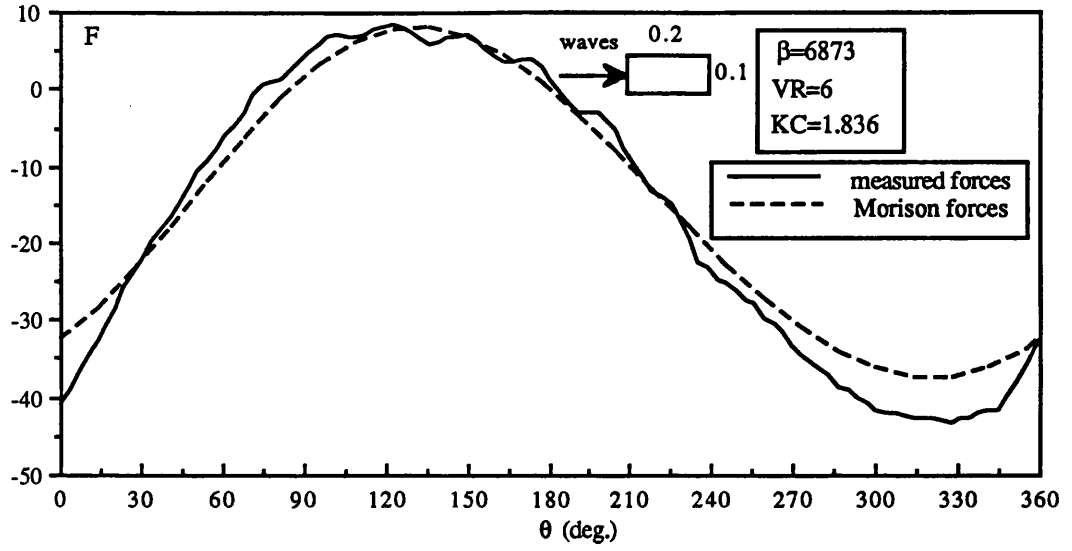

Fig. A53 Comparison of measured and computed in-line forces on a horizontal cylinder with d/D=2 in waves and current

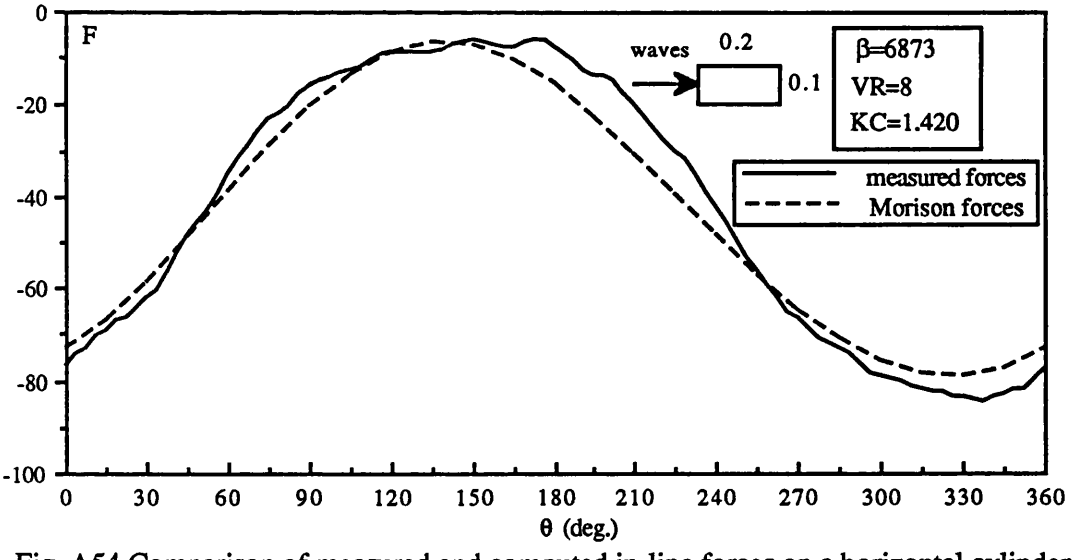

Fig. A54 Comparison of measured and computed in-line forces on a horizontal cylinder with d/D=2 in waves and current

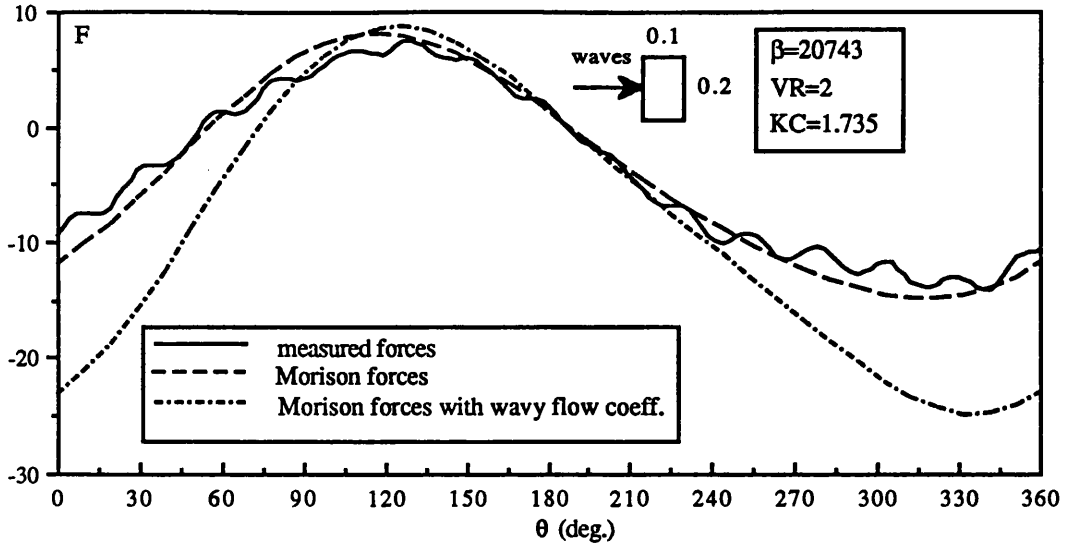

Fig. A55 Comparison of measured and computed in-line forces on a horizontal cylinder with d/D=0.5 in waves and current

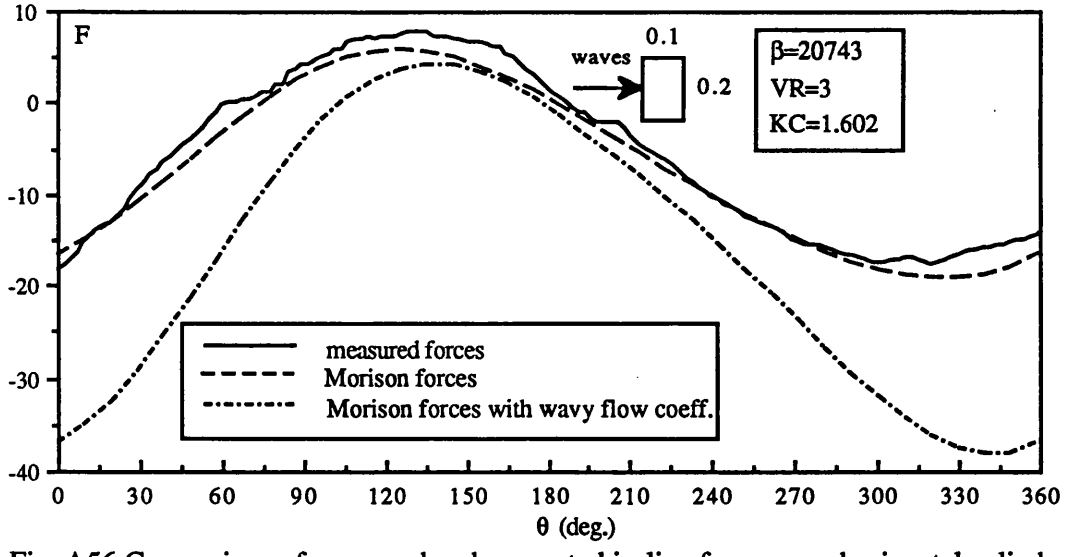

Fig. A56 Comparison of measured and computed in-line forces on a horizontal cylinder with d/D=0.5 in waves and current

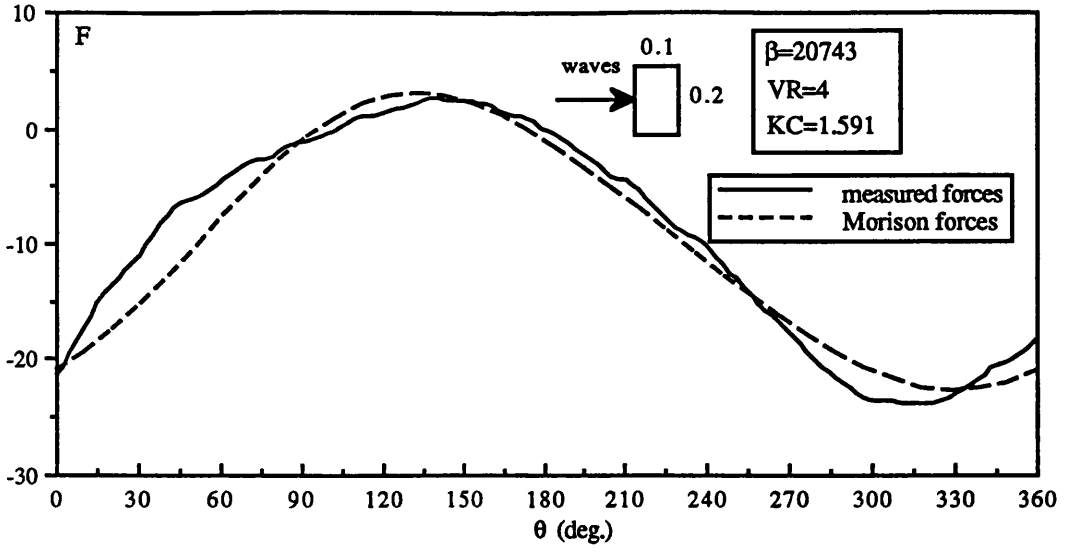

Fig. A57 Comparison of measured and computed in-line forces on a horizontal cylinder with d/D=0.5 in waves and current

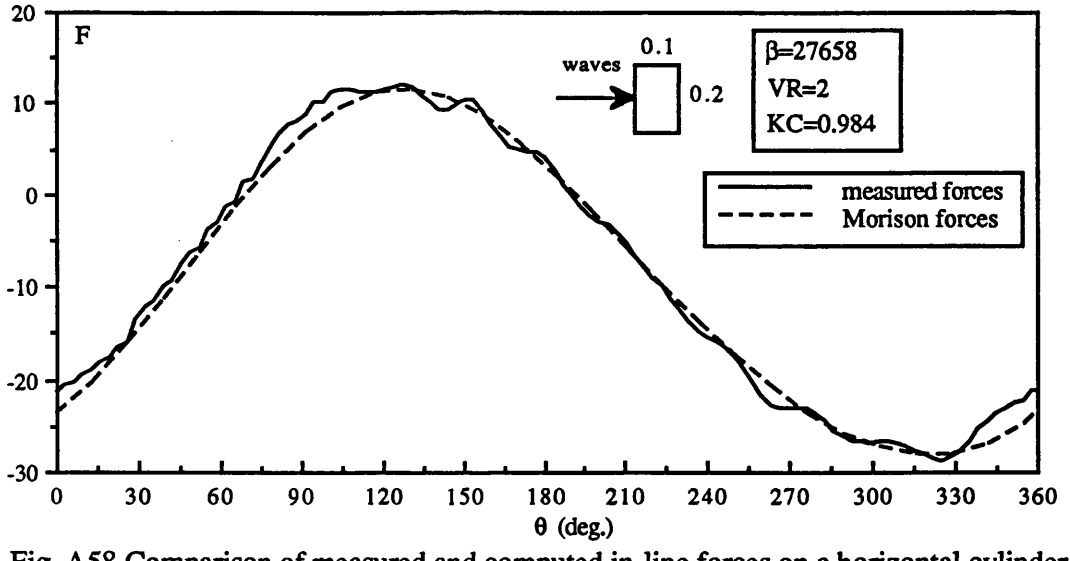

Fig. A58 Comparison of measured and computed in-line forces on a horizontal cylinder with d/D=0.5 in waves and current

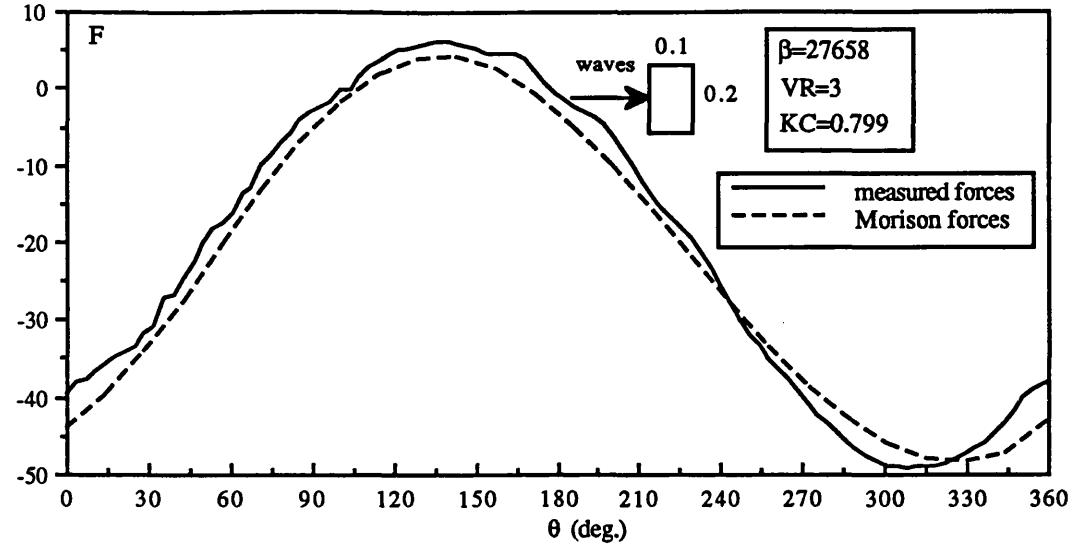

Fig. A59 Comparison of measured and computed in-line forces on a horizontal cylinder with d/D=0.5 in waves and current

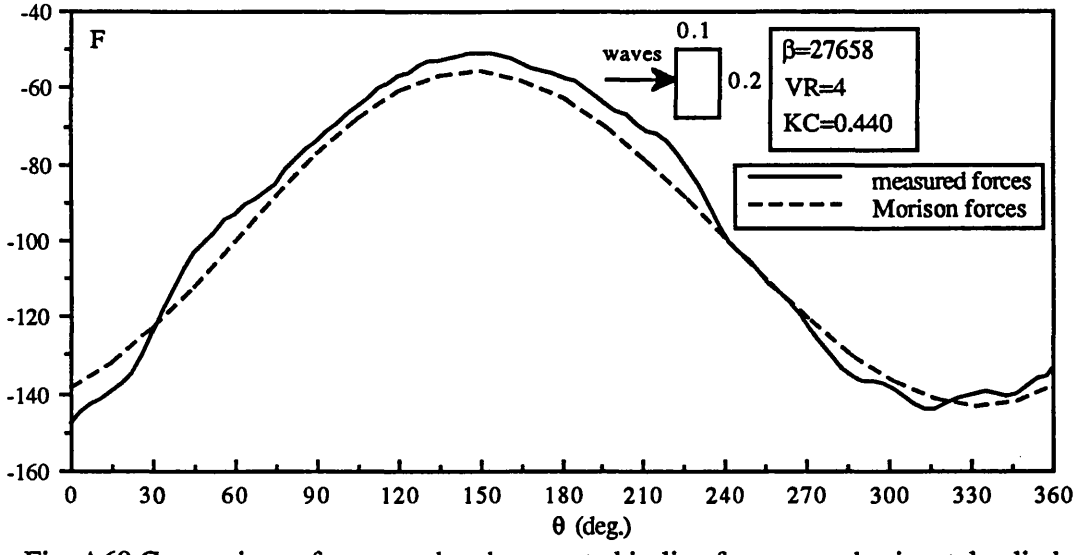

Fig. A60 Comparison of measured and computed in-line forces on a horizontal cylinder with d/D=0.5 in waves and current